Synthesis and Characterisation of Metallic Nanoparticles from Medicinal Plant Extracts and their Application in combating Antibiotic-Resistant Bacterial Pathogens

By

Nemaguvhuni Murunwa Felicia

Student No: 17022786

Dissertation Submitted in the Fulfilment of the Requirements for the Master of Science Degree in Microbiology

To

The Department of Biochemistry and Microbiology

Faculty of Science, Engineering, and Agriculture

University of Venda

Private bag x5050

Thohoyandou

0950

South Africa

Supervisor: Prof A. Samie

Co-supervisors: Prof AN Traore

Dr M Razwinani

Declaration

I, **Murunwa Felicia Nemaguvhuni**, student number **17022786**, affirm that this dissertation reflects my research findings, acknowledges all sources used correctly, and does not contain any material without appropriate recognition. I have not previously submitted this work for any academic qualification at any institution or university. Furthermore, the dissertation does not include any content that has been previously published, authored, or spoken by someone else, except in cases where I explicitly reference them within the text.

Signed (Student):___  ____ Date: 19 April 2024

Dedication

I dedicate this dissertation to the memory of my late father, Mr Isaac Nyadzani Nengovhela.

Acknowledgement

First and foremost, I attribute my gratitude to God Almighty, whose grace and mercy have sustained me through challenges.

I extend my heartfelt gratitude to Prof. A. Samie for his invaluable contributions, inspiration, and insightful suggestions throughout my project.

Special thanks to my co-supervisors, Dr. M. Razwinani and Prof. A.N. Traore, for their dedicated time, advice, and support.

Special thanks to Dr. K Pillay for her valuable assistance and advice.

My appreciation also goes to the Department of Biochemistry and Microbiology at the University of Venda for granting access to necessary equipment and materials.

I thank the Parasitology lab team, Ms. M. Manavhela, Mr. A. Khwathisi, and Mr. I. Moagi, for their constant encouragement and moral support.

I am grateful to individuals like Dr L. Mathomu, Prof. NE Madala, Mrs AT Ramabulana, Dr Tunde, Mr GK Pindihama, Dr R. Mudzielwana, Mrs N Lilimu, Mr S Nemakanga, and Dr Mutshaeni for their dedication and assistance.

My profound gratitude extends to my family and friends for their unwavering support.

Table of Contents

List of abbreviations

AgNO3	Silver nitrate
ABR	Antibiotic-resistant bacteria
Ag	Silver
Au	Gold
CFU	Colony Forming Unit
CO2	Carbon dioxide
DLS	Dynamic Light Scattering
DMEM	Dulbecco's Modified Eagle Media
DMSO	Dimethyl Sulfoxide
DPPH	2,2-diphenyl-1-1-picrylhydrazyl
EMW	Ethyl acetate: Methanol: Water
FeCl3	Ferric chloride
g	Grams
HCl	Hydrochloric acid
IC50	Inhibitory Concentration at 50%
JCPDS	Joint Committee Powder Diffraction Standards
LCMS	Liquid Chromatography-Mass Spectrometry
LPS	Lipopolysaccharide
LSPR	Localised surface plasmon resonance
MEM	Minimum Essential Media
MNP	Metallic nanoparticle
MH	Mueller-Hinton
mg/mL	Milligram per millilitre

mM	Millimolar
min	Minute
m/z	Mass: Charge Ratio
MDR	Multi-Drug Resistant
µl	Microliters
mL	Millilitres
mm	Millimetres
MTT	3-(4,5-dimethylthiazol-2-yl)-2,5-diphenyltetrazolium bromide
NaOH	Sodium hydroxide
NICD	National Institute for Communicable Diseases
nm	Nanometre
NP	Nanoparticles
OD	Optical density
rpm	Rotations per minute
RTI	Respiratory tract infection
ROS	Reactive oxygen species
SPR	Surface plasmon resonance
TEM	Transmission electron microscopy
TLC	Thin layer chromatography
UV-Vis	Ultraviolet-Visible Spectrophotometry
WHO	World Health Organization
XDR	Extensively Drug-Resistant
XRD	X-ray Diffraction
ZP	Zeta Potential

List of Figures

List of Tables

Definitions

Nanoparticles	Are nanoscopic scale particles of different materials and shapes, with sizes ranging from 1 to 100 nanometres (nm) (Zuhrotun et al., 2023).
Green synthesis	Is the eco-friendly production of nanoparticles using natural sources like plants and microorganisms, avoiding hazardous chemicals and toxic solvents (Álvarez-Chimal and Arenas-Alatorre, 2023).
Medicinal plant	A type of plant that possesses compounds within its different parts, which can be utilised for their therapeutic properties or serve as starting materials for the production of beneficial medications (Sofowora et al., 2013).
Antibiotics	Are compounds, whether synthetically produced or occurring naturally, that function to either kill bacteria (bactericidal) or inhibit their growth (bacteriostatic) (Guitor and Wright, 2018).
Antibiotic resistance	Occurs when microorganisms, including bacteria, viruses, fungi, and parasites, develop resistance to antimicrobial agents like antibiotics (Moiketsi et al., 2023).
Bacterial respiratory tract infections	Infections caused by bacteria that affect the upper respiratory tract (rhinitis, sinusitis, pharyngitis, or tracheitis) and/or lower respiratory tract (mostly bronchitis and pneumonia) (Oliva and Terrier, 2021).
Minimum inhibitory concentration	The lowest concentration of drug that inhibit the visible growth of a microorganism after overnight incubation (Andrews, 2001).
Minimum bactericidal concentration	The lowest amount of drug that leads kills 99.9 % of the bacteria being evaluated (Misra and Sahoo,2013).

Abstract

Background: The rise of antibiotic-resistant (ABR) bacterial pathogens is a major global health concern, especially in the case of respiratory tract infections (RTIs), which can make treatment more difficult. According to statistics, more than 2 million lives were lost due to ABR bacterial infections in 2019, highlighting the seriousness of the situation. This study aims to propose a novel approach to combating ABR bacteria by synthesising metallic nanoparticles (MNPs) from medicinal plants. Integrating nanoparticle-based strategies with medicinal plants demonstrates considerable promise in addressing RTIs.

Methodology: The present study investigated the extracts of *Spirostachys africana* (*S. africana*), a medicinal plant traditionally used by healers to treat various infections. Extracts were prepared using methanol, ethanol, acetone, and distilled water. A comprehensive approach was employed to synthesise and characterise silver (SA-AgNPs) and gold (SA-AuNPs) nanoparticles from *S. africana* extracts. Methods of characterisation included Ultraviolet-Visible spectrophotometry (UV-Vis), X-ray diffraction (XRD), Dynamic light scattering (DLS), Transmission electron microscopy (TEM), Fourier-transform infrared spectroscopy (FT-IR), and Liquid chromatography and mass spectroscopy (LC-MS). The antimicrobial activity of the nanoparticles and extracts was tested against the World Health Organization (WHO) ABR priority pathogens using agar well diffusion and microdilution assays. We further, assessed the cytotoxicity, anti-inflammatory, and antioxidant activities using 3-(4,5-dimethylthiazol-2-yl)-2,5-diphenyltetrazolium bromide (MTT), Griess assays, and 2,2-diphenyl-1-picrylhydrazyl (DPPH) method, respectively.

Results: The UV-Vis analysis revealed surface plasmon resonance (SPR) peaks at 480 nm and 541 nm, indicating the formation of SA-AgNPs and SA-AuNPs, respectively. XRD showed face-centred cubic structures with crystalline sizes ranging from 9–19 nm for SA-AgNPs and

9–10 nm for SA-AuNPs. The DLS measurements displayed a polydisperse distribution for SA-AgNPs, while a monodisperse distribution was observed for SA-AuNPs. Most NPs aggregated over time, except for bark-methanol conjugated SA-AgNPs, which exhibited more stability with a zeta potential value of -27 mV. The TEM images showed particle core sizes of 5–49.5 nm for SA-AgNPs, predominantly spherical, and 6–32 nm for SA-AuNPs, mainly spheroidal. The FTIR analysis identified functional groups including hydroxyl, carboxyl, and amine groups in both plant extracts and SA-AgNPs/SA-AuNPs. These fuctional groups are involved in the reduction and capping of Ag^{+} and Au^{+} ions to form SA-AgNPs and SA-AuNPs, respectively. The LCMS technique identified 23 bioactive compounds from *S. africana* extracts, with flavonoids being the most dominant. Antimicrobial assays using agar well diffusion and microdilution methods showed SA-AgNPs were more effective than crude extracts and SA-AuNPs against tested ABR bacteria. Acetone-conjugated SA-AgNPs having the highest zone of inhibition (22 mm) against *P. aeruginosa*. In contrast, methanol/ethanol-conjugated SA-AgNPs displayed potent antimicrobial activity (MIC = 0.05 mg/mL) against *E. coli*, *P. aeruginosa*, and *A. baumannii*, respectively. Additionally, Acetone extracts exhibited selective toxicity against MCF-7 cancer cells, while stimulating MCF-10 cells and RAW 264.7 macrophage cells at concentrations of 0.078 mg/mL. Furthermore, ethanol extracts and ethanol-conjugated SA-AgNPs/SA-AuNPs significantly decreased NO production, indicating their potential as anti-inflammatory agents. Acetone extract exhibited excellent antioxidant activity (IC50 = 0.000335 mg/mL).

Conclusions: The MNPs synthesised from *S. africana* extracts offer a promising solution to combat ABR bacterial pathogens, particularly those causing RTIs. The *S. africana* extracts and MNPs show significant cytotoxic, anti-inflammatory, and antioxidant activities.

Keywords: Antibiotic-resistant bacteria, Respiratory tract infections, *Spirostachys Africana*, Metallic nanoparticles, Antimicrobial activity, Cytotoxicity, Anti-inflammatory activity, Antioxidant activity.

Chapter 1: General Introduction

1.1 Background

The escalating global crisis of antibiotic resistant (ABR) bacterial infections has sparked intense research efforts to explore alternative therapeutic strategies. In this context, synthesising, and characterising nanoparticles (NPs) derived from medicinal plant extracts have emerged as a promising avenue. Nanoparticles (NPs) are tiny particles composed of various materials and shapes, typically measuring between 1 and 100 (nm) in size (Zuhrotun et al., 2023). Nanoparticles (NPs) exhibit unique properties that hold the potential to combat antibiotic-resistant pathogens effectively. Noble MNPs, such as silver nanoparticles (AgNPs) or gold nanoparticles (AuNPs), have attracted considerable interest in recent years due to their distinctive properties. These MNPs possess high stability, biocompatibility, low toxicity, and the capacity to efficiently absorb intense electromagnetic waves through surface plasmon resonance (SPR) within the visible spectrum. Their versatility is further enhanced by the ease of modification, rendering them ideal candidates for various applications (Zuhrotun et al., 2023; Banerjee et al., 2011).

Silver nanoparticles (AgNPs) have demonstrated potent antimicrobial activity, showing multiple modes of inhibitory action against microorganisms (Saratale et al., 2018; Moradi et al., 2020). Notably, their non-toxic nature and heightened potency against viruses and bacteria at lower concentrations without adverse effects make them particularly promising (Adam and Khan, 2021). In parallel, gold nanoparticles (AuNPs) play a pivotal role in nanometal research, particularly regarding antimicrobial properties (Arya et al., 2019). Their determinants of antimicrobial effects, like shape, size, concentration, and coating agent, are extensively studied (Rabiee et al., 2022). Furthermore, AuNPs are more considered due to their electrical and optical properties, with their localised surface plasmon resonance (LSPR) finding utility in

various applications, notably biosensors. They are ideally suited for LSPR biosensors due to their unique property to exhibit a spectral response based on nanoparticle surface location. The LSPR arises from the interaction between electromagnetic radiation and surface electrons of MNPs, leading to strong extinction effects that prove valuable across multiple uses (Venditti, 2019). Both AgNPs and AuNPs find widespread use in various sectors, including medicine and other industries, functioning as antimicrobial agents, carriers for drug delivery, catalysts, sensors, cosmetic components, agents for environmental cleanup, and more. As a result, AgNPs and AuNPs offer promising solutions to addressing the issue of antimicrobial resistance (Pulit-Prociak et al., 2019; Wang et al., 2016).

Various methods used to synthesise AgNPs or AuNPs include chemical, physical, and biological processes. However, chemically synthesised MNPs are toxic. Meanwhile, physical methods are time-consuming and limited to specific requirements, including high temperatures or pressures, making the process more expensive (Samuggam et al., 2021). Nonetheless, a safer, simple, rapid, inexpensive, eco-friendly, and reliable alternative way to synthesise MNPs is via biological methods also known as green synthesis. The green synthesis method includes the production of MNPs using microorganisms and plants. However, the plant-based production method is considered more advantageous due to its wide range of benefits (Patil et al., 2021).

Green synthesis has diverse reducing phytochemicals and is a single-step process for the large-scale synthesis of nanoparticles (Ghaffari-Moghaddam et al., 2014). Green synthesis of AgNPs and AuNPs using medicinal plants has been used successfully in a variety of pharmaceutical and biomedical fields as antimicrobial agents, anticancer agents, anti-inflammatory agents, drug delivery systems, gene therapy, and bio-imaging (Bharadwaj et al., 2021; Muddapur et al., 2022). Moreover, medicinal plants are utilised traditionally to treat infections, including respiratory tract infections (RTIs). Plants are rich in phytochemical compounds with

advantageous therapeutic effects. Among these compounds are coumarins, terpenoids, glycosides, flavonoids, phenols, insecticides, polyphenols, vitamins, and steroids (Al-Snafi, 2015; Dhanasekaran et al., 2019; Shaikh et al., 2022). They play a crucial role in the synthesis of MNPs from metallic ions, functioning as both capping or stabilizing agents and reducing agents (Dada et al., 2019). The current study tested the medicinal plant *Spirostachys africana* (*S. africana*) which contains phytochemical constituents believed to cure many illnesses, including dysentery, diarrhoea, colds, flu, fever, headaches, and nose or gum bleeding infections (Mabogo, 1990; Lennox and Bamford, 2015). Traditional healers also use this plant for the treatment of respiratory diseases (Mabogo, 1990; Singh, 2017).

In 2017, the World Health Organization (WHO) released a list of priority pathogens of antibiotic resistant (ABR) bacteria to guide the development of effective treatments (WHO, 2017). The listed bacteria are Carbapenem-resistant (CR) *Acinetobacter baumannii*, CR *Pseudomonas aeruginosa*, CR *Escherichia coli*, and Methicillin-resistant *Staphylococcus aureus* (MRSA). These bacteria are often implicated in RTIs (Guitor and Wright, 2018). Respiratory tract infections (RTIs) are infections of body parts involved in breathing, such as the sinuses, throat, airways, or lungs (Oliva and Terrier, 2021). Transmission of RTIs is often through the coughs and sneezes of someone with an infection (Alsayari et al., 2021). Antibiotics treat many infections, and they are the most important due to their phenomenal impact on reducing human morbidity, mortality, and economic losses (Yayehrad et al., 2022). However, treating RTIs using antibiotics has become challenging because of the unprecedented rise of ABR bacteria (Huang, et al., 2023).

Medicinal plants and MNPs recently gained attention and emerged as promising candidates for antibacterial agents due to their ability to kill bacteria by targeting various cellular components such as cell walls, DNA, membranes, and proteins. Also, with the power of NPs to transport therapeutic agents to a specific site and reduce damage to healthy cells, their synergy may

provide alternative strategies to counter ABR of pathogenic bacteria. To the best of our knowledge, there is no study done on the synthesis of AgNPs and AuNPs using the extracts of the *S. africana*. Therefore, the present study focuses on the eco-friendly green synthesis of MNPs using medicinal plant extracts, characterisation, and evaluating their antimicrobial activities against ABR bacterial pathogens, antioxidant, cytotoxic, and anti-inflammatory effects. The impact of combining medicinal plant extracts with AgNPs and AuNPs on the WHO priority pathogenic bacteria accountable for RTIs is not fully known. Hence, this will help with further investigation of their impact on the pathogenic bacteria.

1.2 Rationale

Respiratory tract infections (RTIs) remain the deadliest communicable diseases in the world, and most people get infected once a year (Cock and Van Vuuren, 2020). Lower respiratory tract infections (LRTIs) continue to be the leading cause of death globally (Van Hecke et al., 2017; Ikuta et al., 2022). The population at risk of acquiring these infections are the elderly, immunocompromised, and children (Guitor and Wright, 2018). Antibiotics are preferred and used to treat bacterial respiratory tract illnesses because of their powerful outcomes (Wang et al., 2017; Duan et al., 2020). However, inappropriate, and excessive use of antibiotics has led to the development of ABR bacterial pathogens (Yang et al., 2020). The rise in ABR significantly contributes to worldwide morbidity and mortality, approximately 700,000 deaths occur annually due to antimicrobial resistance. The WHO estimates that by 2050 this number could increase to 10 million (Qing et al. 2019; Mancuso et al., 2021). In 2019, statistics also indicated that more than 1.2 million deaths occurred due to ABR bacterial infections, particularly bacterial RTIs (Tang et al., 2023; Murray et al., 2022) which highlights a serious concern to public health.

Hence, there is an urgent need to develop new strategies for treating ABR bacterial infections (Yang et al., 2020). Metallic nanoparticles (MNPs) have drawn attention due to their ability to transport therapeutic agents to a specific site and reduce damage to healthy cells (Gallo and Schillaci, 2021; Yayehrad et al., 2022). Moreover, the cost-effectiveness and environmentally friendly green synthesised nanoparticles have been considered an alternative way to combat antimicrobial resistance (Wintachai et al., 2019). There are several studies that have reported on the green synthesis of nanoparticles using medicinal plants (Yadav and Mendhulkar, 2018; Salayová et al., 2021), but no studies have been reported on medicinal plants conjugated nanoparticles to combat the challenge of antimicrobial resistance bacteria responsible for RTIs. Therefore, the present study aims to synthesise and characterise medicinal plant extracts-based MNPs and evaluate their activity against ABR bacterial pathogens causing RTIs.

1.3 Research questions

- Does the synthesis of NPs based on the *S. Africana* extracts increase the antibacterial efficacy against selected ABR bacterial pathogens?
- Does the combination of the different plant extracts increase their activity against highly resistant pathogens?
- What are the characteristics of NPs synthesized from silver and gold using *S. africana* extracts?
- What medicinal plant extracts and NP combinations would give better activity against selected bacterial pathogens?
- Do the synthesised NPs and crude extracts exhibit toxic effects against normal or cancer cells, and what does this mean for their potential use in medicine?
- Do the synthesised NPs and plant extracts exhibit any anti-inflammatory properties?

1.4 Objectives of the study

1.4.1 Primary objective

- To synthesise and characterise nanoparticles mediated by *Spirostachys africana* extracts, and subsequently investigate their biological activities.

1.4.2 Secondary objectives

- To synthesise AgNPs and AuNPs using the green synthesis method.
- To characterise the AgNPs and AuNPs using UV-Vis, XRD, DLS, and TEM.
- To characterise *Spirostachys africana* extracts using FTIR and LC/MS techniques.
- To determine the antimicrobial activity of *Spirostachys africana* extracts and its conjugated AgNPs and AuNPs against four selected bacterial strains.
- To test the cytotoxic activity of both plant extracts and nanoparticles on human breast cancer cell line (MCF7), normal human mammary epithelial cells (MCF10), and RAW 264.7 murine macrophage cells.
- To investigate the anti-inflammatory activity of plant extracts and nanoparticles by assessing their inhibition of nitric oxide production in lipopolysaccharide (LPS)-induced on stimulated macrophages (RAW 264.7).
- To evaluate the antioxidant activity of the plant extracts and nanoparticles by DPPH assay.

Chapter 2: Literature Review

2.1 Respiratory Tract Infections (RTIs)

Bacterial respiratory tract infections (RTIs) can affect the upper respiratory tract (rhinitis, sinusitis, pharyngitis, or tracheitis) and/or lower respiratory tract (mostly bronchitis and pneumonia) (Oliva and Terrier, 2021). The spread of RTIs often occurs through coughing and sneezing of an infected person (Alsayari et al., 2021). Children and adults with weakened immune systems are at higher risk of acquiring bacterial RTIs (Briaud et al., 2019).

A study by Duan et al. (2020) indicated that Gram-negative bacteria are more likely to cause RTIs than Gram-positive bacteria. According to Briaud et al. (2019), *Pseudomonas aeruginosa* (*P. aeruginosa*) was the most common bacteria found in adults hospitalised due to RTIs, while *Staphylococcus aureus* (*S. aureus*) was the most prevalent among children. Figure 2.1 provides a visual representation of the bacterial RTIs affecting the lower and upper respiratory tracts, illustrating the different types of infections that can occur in each region (Oliva and Terrier, 2021).

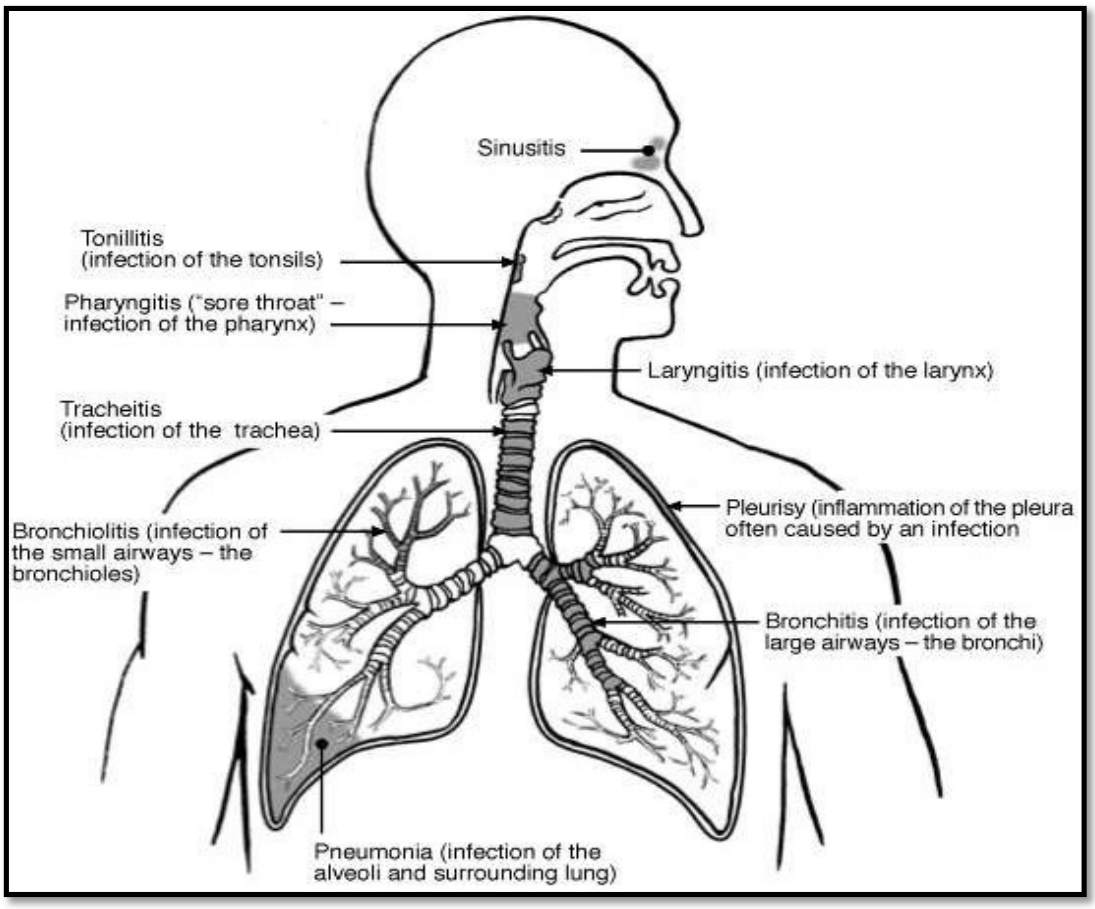

Figure 2.1: The diagram illustrates infections that target the respiratory tract system (Yana, 2014).

2.1.1 Carbapenem-resistant (CR) *Acinetobacter baumannii*

Acinetobacter spp. are glucose non-fermentative Gram-negative coccobacilli that have emerged as a major cause of healthcare-associated infections in critically ill patients and hospital outbreaks since the 1970s (Zarrilli et al., 2020). Among these, *Acinetobacter baumannii* (*A. baumannii*) is particularly responsible for causing RTIs, such as pneumonia, as well as other serious diseases like urinary tract infections (UTIs), septicaemia, and severe cases of necrotising fasciitis (Wintachai et al., 2019). It is one of the priority pathogens of urgent drug-resistant threats, listed by the World Health Organization to be the most dangerous

resistant bacteria (WHO, 2017). It has become resistant to multiple antibiotics, particularly carbapenems. Hence, it has turned into a human health threat (Ramirez et al., 2020).

2.1.2 Carbapenem-resistant (CR) *Pseudomonas aeruginosa*

P. aeruginosa is a Gram-negative bacteria, aerobic, non-spore-forming rod capable of causing a variety of infections in both immunocompetent and immunocompromised people (Wilson and Pandey, 2022). It is commonly found in water, plants, and soil (Alsayari et al., 2021). *P. aeruginosa* is the most common to infect humans and it causes many hospital-acquired infections, especially pneumonia (Iqbal and Rhee, 2020). It is very dangerous for patients suffering from chronic lung diseases. Additionally, *P. aeruginosa* has developed resistance to antibiotics that are used for treatment (Kim and Yang, 2018).

2.1.3 Carbapenem-resistant (CR) CR *Escherichia coli*

Escherichia coli (*E. coli*) are Gram-negative bacilli bacteria in the *Enterobacteriaceae* family (Makvana and Krilov, 2015). They are facultative anaerobes and nonsporulating organisms which are frequently present as pathogens in the gastrointestinal tracts of humans and animals. However, E. *coli* can also colonise to cause community and nosocomial-acquired infections leading to diseases such as meningitis, sepsis, UTIs, and pneumonia (Liang et al., 2018). It was recently reported that carbapenem-resistant *E. coli* has been a serious problem globally, generating a lot of interest and attention. To date, few cases of CR *E. coli* responsible for RTIs have been documented (Gong et al., 2020).

2.1.4 Methicillin-resistant *Staphylococcus aureus* (MRSA)

S. aureus are Gram-positive spherical (coccus) bacteria responsible for 1/3 of healthcare-acquired infectious diseases. They are the most common pathogens causing community-acquired pneumonia (Huang et al., 2021). *S. aureus* strains have shown resistance against one or more antibiotics and are becoming more and more difficult to treat with conventional

antibiotics. In the early 1940s, it was discovered that *S. aureus* bacteria had become resistant to penicillin. By the 1960s, over 80% of these bacteria had developed resistance. This growing issue of ABR led to the creation of semi-synthetic antibiotics like methicillin and cephalosporin, which were effective against the β-lactamase enzyme. However, over time, *S. aureus* bacteria also developed resistance to methicillin. A study in the United States found that approximately half of all identified methicillin-resistant *S. aureus* strains had also become resistant to other antibiotics (IDSA, 2004).

2.2 Treatment status of respiratory tract infections

Pathogens have developed new mechanisms that make them resistant to drugs, which is known as antimicrobial resistance (ABR). This poses a serious threat to our ability to treat common infections like RTIs (Sansone et al., 2022). Gram-negative bacteria that produce extended-spectrum β-lactamase enzymes have developed resistance to antibiotics like penicillin, cephalosporins, and monobactam (Trecarichi and Tumbarello, 2017).

Carbapenems are β-lactam antibiotics that are highly effective against severe and high-risk bacterial RTIs. They are typically used for Multi-Drug-Resistant (MDR) bacterial infections (Sansone et al., 2022). These antibiotics bind to penicillin-binding proteins, which prevents bacterial cell wall synthesis. Unfortunately, shortly after carbapenems were administered, the Gram-negative bacteria rapidly developed resistance to these antibiotics and spread throughout the world (Leylabadlo et al., 2015).

Carbapenem-resistant *Enterobacteriaceae* (CREs) and Carbapenemase-Producing Organisms (CPOs) are examples of these. Other CPOs include opportunistic bacteria like *P. aeruginosa* and *A. baumannii*, which can produce carbapenemase enzymes. Figure 2.2 illustrates the generic chemical structure of carbapenems (Ramirez et al., 2020).

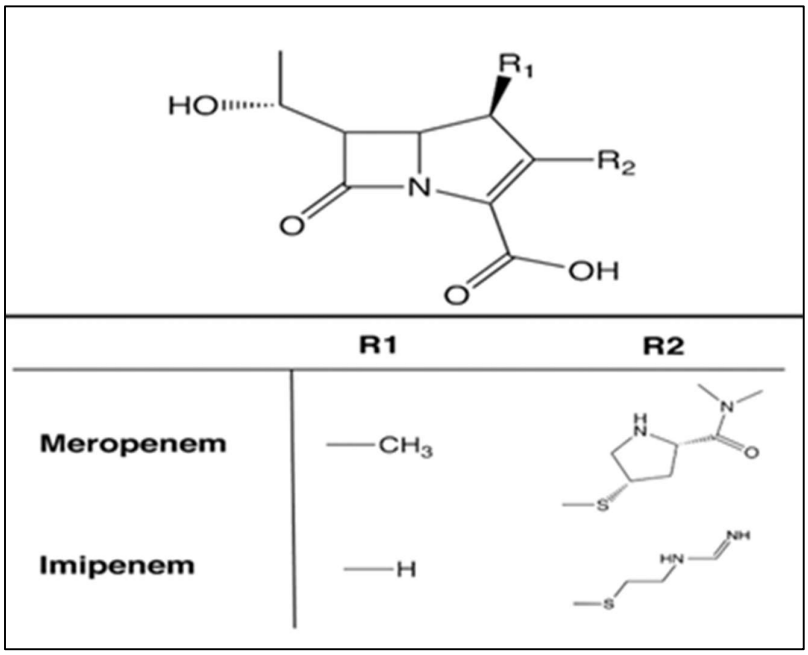

Figure 2.2: The generic chemical structure of carbapenems. The R1 and R2 groups for imipenem and meropenem (Ramirez et al., 2020).

An antibiotic known as Cefiderocol has been designed to treat carbapenem-resistant bacteria. In 2020, it was recommended that a certain treatment be used for Gram-negative bacteria that cause hospital-acquired bacterial pneumonia (HABP) and ventilator-associated bacterial pneumonia (VABP). This treatment has been shown to have significant in vitro activity against carbapenem-resistant bacteria. However, there is still a need for antibacterial agents that are both safe and effective against carbapenem-resistant organisms (Sansone et al., 2022).

Methicillin is a semisynthetic penicillinase-resistant β-lactam that was developed in response to the emergence and spread of penicillin-resistant *S. aureus* (Peacock and Paterson, 2015). However, by 1960, methicillin resistance emerged, leading to resistance against virtually all β-lactams, except for the latest generation of cephalosporins. Methicillin-resistant *S. aureus* (MRSA) can also develop resistance to a variety of antimicrobials, complicating treatment further. Vancomycin was introduced and used to treat MRSA pneumonia but has become less

effective over time, resulting in increased mortality rates (about 50 % and 47 % of deaths) (González et al., 1999). Linezolid is another antibiotic approved by the US Food and Drug Administration for the treatment of MRSA pneumonia and is a better treatment than vancomycin (Rubinstein et al., 2008).

2.3 Antibiotic resistance and plant-based nanoparticles

Antibiotics are substances that can either kill bacteria (bactericidal) or inhibit their growth (bacteriostatic) (Guitor and Wright, 2018). They can be produced synthetically in laboratories or obtained from natural sources like fungi and bacteria. Antibiotics primarily target essential cellular processes, including cell envelope synthesis, protein synthesis, DNA replication, and RNA production. However, their effectiveness is increasingly challenged by bacteria that have developed various resistance mechanisms. This issue is known as ABR, which poses a significant global health threat affecting both developed and developing countries (Littmann et al., 2015). The rising levels of ABR have raised concerns about entering a 'post-antibiotic era' where bacterial infections could become untreatable.

Antibiotic resistance (ABR) occurs when microorganisms such as bacteria, viruses, fungi, and parasites, develop resistance to antimicrobial agents like antibiotics (Moiketsi et al., 2023). Unfortunately, nearly all current antibiotics are no longer effective against many pathogenic bacteria, and even recently developed ones are likely to lose efficacy against the constantly evolving multidrug-resistant (MDR) bacterial strains. Clinically significant MDR bacteria include Vancomycin-resistant *Enterococci* (VRE), carbapenem-resistant *A. baumannii* (CRAB), carbapenem-resistant *Enterobacteriales* (CRE), extensively drug-resistant (XDR) *P. aeruginosa*, *Enterobacteriales* producing extended-spectrum β-lactamase (ESBL), and methicillin-resistant *S. aureus* (MRSA) (Jubair et al., 2021). Highly virulent MDR pathogens are termed ESKAPEE, which stands for *Enterococcus faecium* (*E. faecium*), *S. aureus*, *Klebsiella pneumoniae* (*K. pneumoniae*), *A. baumannii*, *P. aeruginosa*, *Enterobacter* species,

and *E. coli*. These bacteria are capable of escaping treatment from multiple antibiotics and traditional therapies (Bhatia et al., 2021). The World Health Organization (WHO) has identified these MDR strains as priority pathogens to guide the development of new drugs.

Multidrug-resistant (MDR) bacteria pose a serious One-Health threat, impacting people, animals, and the environment due to their rapid development and spread (Moiketsi et al., 2023). Control efforts are complicated by the potential for MDR bacteria and associated AMR genes to spread across various habitats. Projections suggest that antimicrobial resistance (AMR) could cause over 24 million people to live in poverty and result in 10 million deaths worldwide by the year 2050 (Kongkham et al., 2020). In Europe, AMR already accounts for approximately 25,000 deaths and €1.5 billion in medical costs each year, with even greater impacts anticipated in Africa due to limited data availability (Littmann et al., 2015). To reduce the overuse of antibiotics, the Africa Centers for Disease Control and Prevention (CDC) has advocated for collective action (Moiketsi et al., 2023). The widespread use of antibiotics in medicine and human activities like recycling wastewater accelerates the spread of these bacteria.

2.4 Mechanism of antibacterial resistance

Antibacterial resistance mechanisms are diverse and include various strategies, such as (i) altering the structure of bacterial porins to reduce permeability to antibiotic influx, (ii) hydrolysing antibacterial agents with hydrolytic enzymes, (iii) changing antibiotic binding sites, and (iv) accelerating antibiotic efflux through bacterial efflux pumps, which shortens the time it takes for medication to diffuse into bacteria. Understanding these resistance mechanisms is crucial for identifying potential targets for effective medication in the future (Jubair et al., 2021).

2.4.1 Alteration in the permeability of the membrane

The permeability of bacterial membranes plays a significant role in ABR, particularly in Gram-negative bacteria that have an outer membrane acting as an additional protective layer (Choi and Lee, 2019). Porins are proteins found in the outer membrane of bacteria that regulate the passage of various minerals and nutrients (Khameneh et al., 2019). Porins can be classified into two types based on their activity: specific and nonspecific. Specific porins are selective for certain compounds, such as LamB which is selective for maltose and maltodextrin. On the other hand, nonspecific porins are involved in membrane permeability and are linked to resistance against antimicrobial agents (Fernández and Hancock, 2012).

Porins can also be categorized based on their structure into monomeric, dimeric, and trimeric forms and based on their functions into specific porins for antibiotic transport (e.g., LamB, YddB), porins specific for membrane integrity (e.g., OmpA), and nonspecific porins that act on both antibiotic transport and membrane safety (e.g., OmpC, OmpF) (Khameneh et al., 2019). Changes in the structure of porins are associated with an increase in ABR bacteria. For example, a mutation in the OmpF porin leads to resistance in *E. coli* (see Figure 2.3) and *P. aeruginosa*. Additionally, bacteria like *A. baumannii* can resist carbapenems by reducing porin expression and changing outer membrane integrity (Breijyeh et al., 2020). *P. aeruginosa* employs mechanisms such as altering the structure of liposaccharides in its outer membrane to resist various antibiotics.

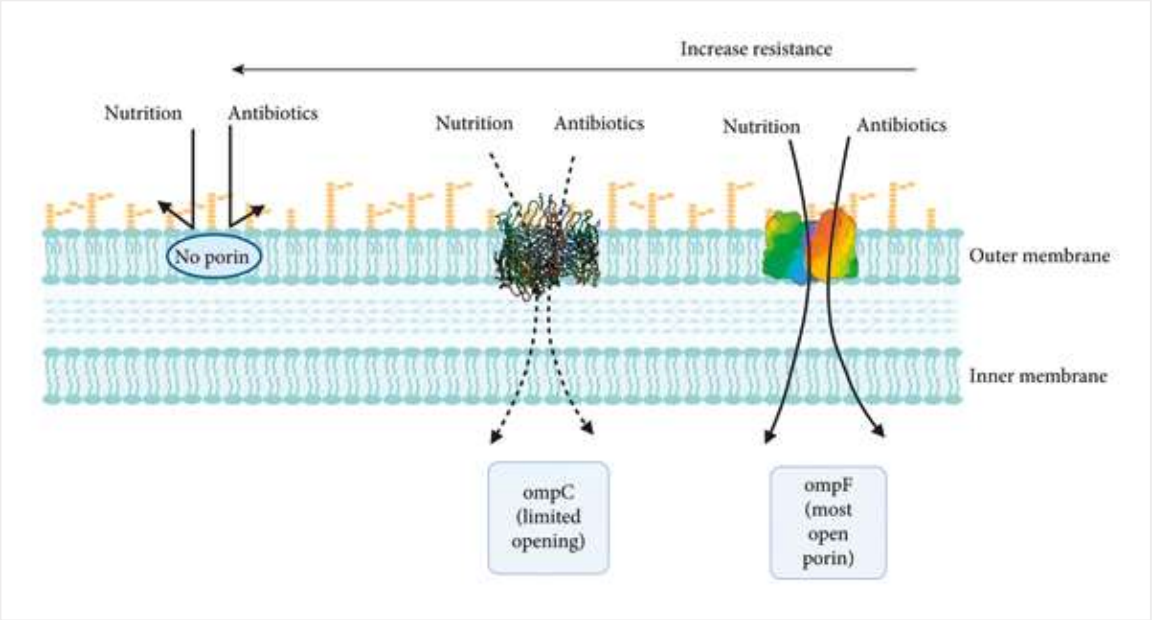

Figure 2.3: The impact of porins on membrane permeability in *Escherichia coli* (Jubair et al., 2021).

2.4.2 Destruction of Antibiotics by Enzymes

Bacterial enzymes play a crucial role in ABR by modifying or hydrolyzing antibiotic molecules, rendering them inactive. Some enzymes are involved in defence mechanisms against antibiotics, such as altering structural elements or changing the way drugs affect certain structural elements (Egorov et al., 2018). Methyltransferases, for example, can change the structure of ribosomes. Enzymes released by both Gram-positive and Gram-negative bacteria can hydrolyse or modify antibiotic molecules, making them inactive (Khameneh et al., 2019). By blocking the synthesis of bacterial proteins, most antibiotics are rendered inactive through this mechanism.

There are three main types of enzymes that contribute to ABR. First, β-lactamases hydrolyze the lactam ring found in penicillin, cephalosporins, and carbapenems, thus inactivating these antibiotics. Second, chloramphenicol acetyltransferase acetylates the hydroxyl group in

chloramphenicol, preventing it from binding effectively to its target site. Lastly, some enzymes modify antibiotic molecules to reduce their affinity for binding to the 30S ribosomal subunits (Jubair et al., 2021). Figure 2.4 below illustrates the bacterial enzymes involved in these mechanisms that enable bacteria to resist antibiotics.

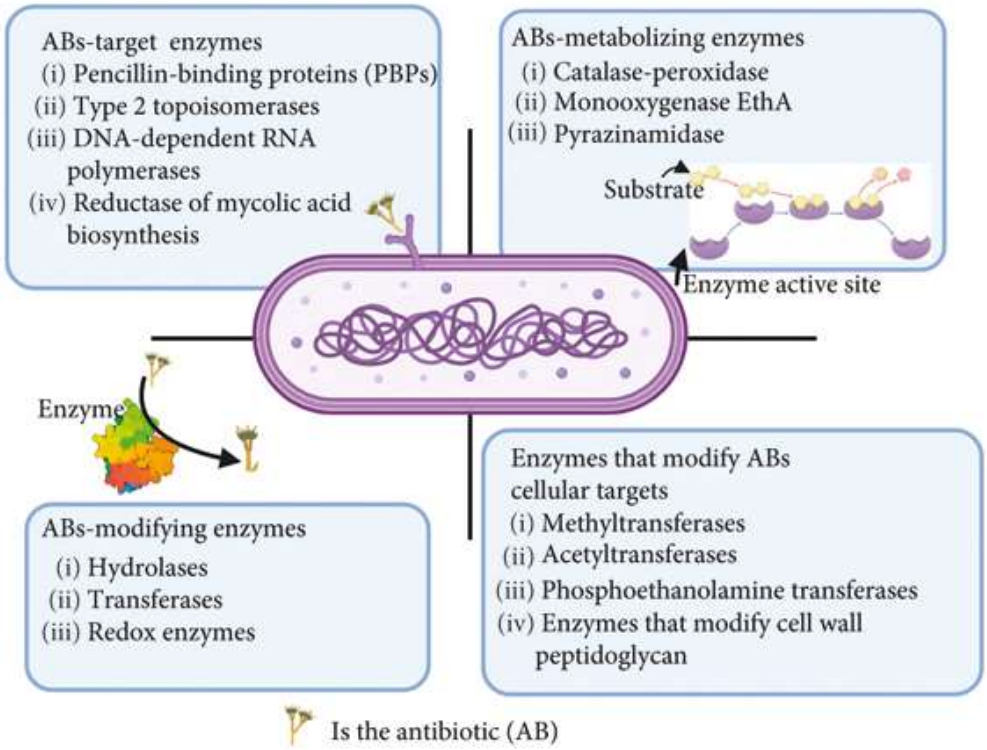

Figure 2.4: Enzymes produced by bacteria that are involved in different microbial resistance mechanisms (Jubair et al., 2021).

2.4.3 Alteration of bacterial binding site

Bacteria can develop resistance to antibiotics by modifying the antibiotic target site, which reduces the ability of the antimicrobial agent to bind effectively (Khameneh et al., 2019). For example, Methylation of the enzyme peptidyl transferase, which is responsible for erythromycin binding, significantly reduces binding interactions. Moreover, *Staphylococci* have developed resistance to methicillin and oxacillin by making mutational changes in the

penicillin-binding protein (PBP) (Goudarzi and Navidinia, 2019). Vancomycin-resistant *Enterococci* (VRE) resist antibiotics by changing the amide bond of the target enzyme to an ester bond, which results in a 1,000-fold lower binding affinity for the antibiotic (Akpaka et al., 2017). These mutations reduce the antibiotic's binding affinity for the bacterial target. Gram-positive bacteria can modify the ribosomal targets which causes antibiotics to be ineffective. This alteration of binding sites results in resistance to macrolides, lincosamides, streptogramins, tetracyclines, and aminoglycosides (Oliphant and Eroschenko, 2015). Figure 2.5 illustrates the mechanism of ABR by altering the binding site on the bacteria.

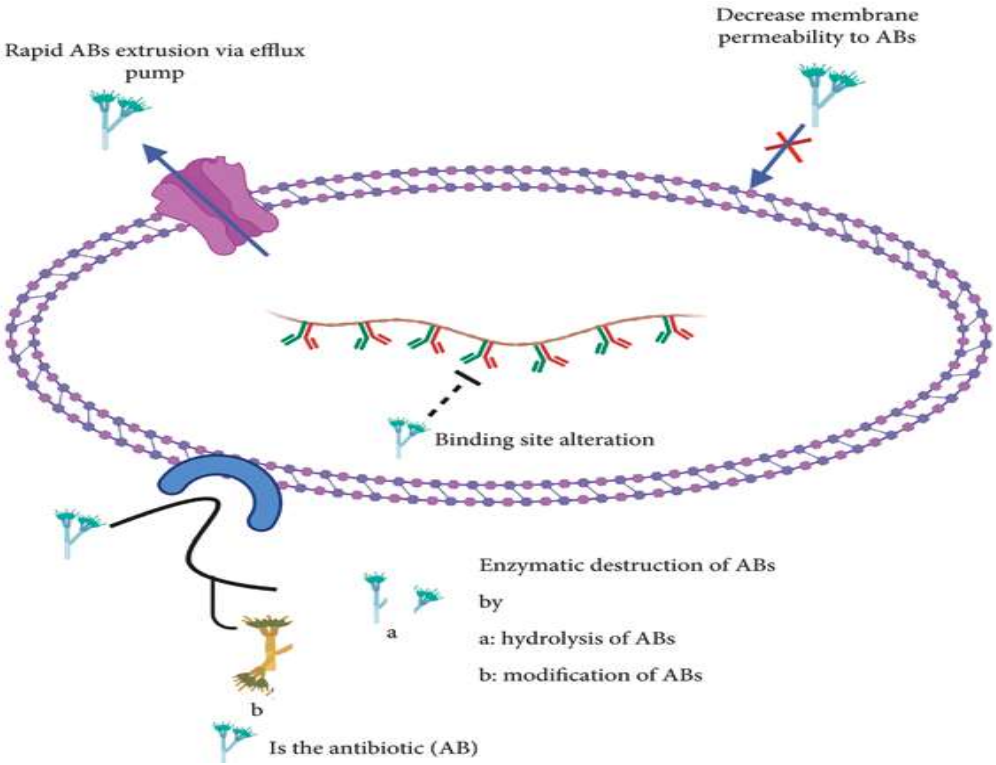

Figure 2.5: Diagrammatic depiction of antibiotic resistance (Jubair et al., 2021).

2.4.4 Efflux pump

Multidrug resistance (MDR) among bacteria is a critical issue that often occurs due to the efflux mechanism. This mechanism is facilitated by protein transporters known as efflux pumps. For

antibiotics to work effectively and combat bacterial infections, they must penetrate bacterial cells at sufficient concentrations and remain active for some time (Khameneh et al., 2019). However, efflux pumps expel antibiotics and toxins from the bacterial cell, rendering these drugs ineffective (Khameneh et al., 2019). A study highlighted the role of efflux pumps as a primary contributor to ABR, particularly in *E. coli* resistance to tetracycline (Blanco et al., 2016).

Bacterial efflux transporters are categorized into five main families, with the Resistance-nodulation-division (RND) family being prominent in Gram-negative bacteria. Other families, such as the ATP-binding cassette (ABC) superfamily, are found in both Gram-positive and Gram-negative bacteria. Approximately 20 genes encoding bacterial efflux pumps have been identified, many located within mobile genetic elements (MGEs) and bacterial chromosomes. These efflux pump genes significantly contribute to bacterial resistance, particularly in diverse Gram-positive bacteria (Sultan et al., 2018).

The MDR efflux pumps in *Enterobacteriaceae* and *P. aeruginosa*, which are categorized within the RND family, effectively expel tetracyclines and confer resistance to various antibiotics, including chloramphenicol, beta-lactams, fluoroquinolones, and fusidic acid. Additionally, efflux pumps, particularly those encoded in chromosomes belonging to the ABC family, are responsible for macrolide resistance in certain Gram-positive bacteria, with initial observations made in *Staphylococcus epidermidis* (Schroeder et al., 2016). Furthermore, *A. baumannii* demonstrates antibiotic resistance through efflux pumps like ABC and RND, which release antibiotics such as aminoglycosides, tetracyclines, beta-lactams, chloramphenicol, erythromycin, and cyclines from cells. This process leads to decreased drug accumulation at the target site, resulting in elevated MICs of antibiotics and rendering them ineffective. The image below depicts major categories of efflux pump families identified in bacteria (Figure 2.6).

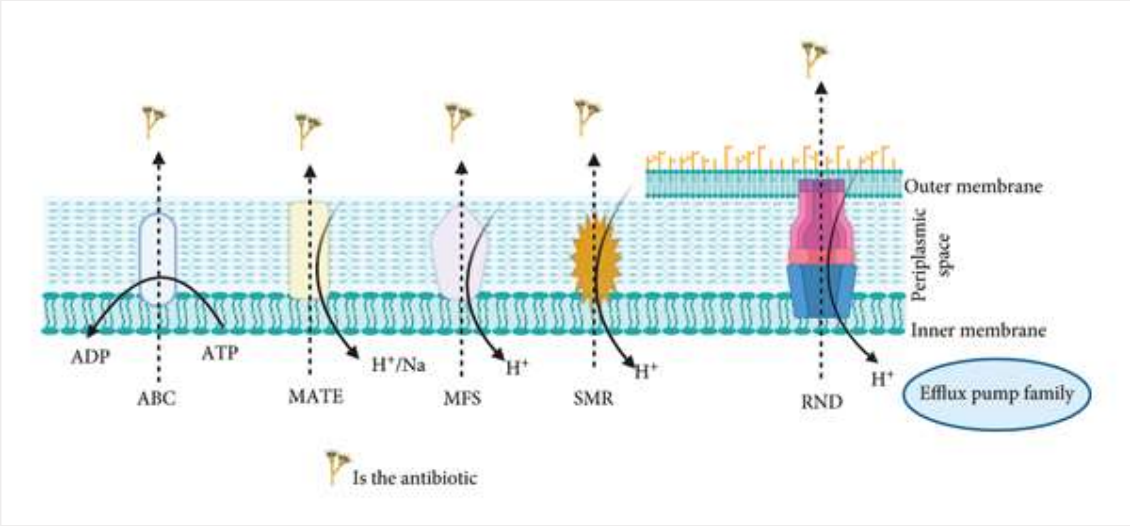

Figure 2.6: An illustration showing the primary types of efflux pump families discovered in bacteria. Gram-negative bacteria are characterised by the resistance-nodulation family (RND), while the small multidrug resistance (SMR), major facilitator superfamily (MFS), multidrug and toxin extrusion (MATE), and adenosine triphosphate-binding cassette (ABC) superfamily are all present in the inner membrane. These efflux pumps work together to move toxins and antibiotics using energy.

2.5 Background on medicinal plants

Medicinal plants have played a crucial role in healthcare across ancient civilizations for thousands of years. Their use in treating various diseases and promoting health is well-documented, with evidence dating back to 60,000 years ago (Fabricant and Farnsworth, 2001). These plants are highly valued for their numerous benefits to humans (Waylen, 2006). They have been integral to traditional medical practices, shaped by empirical knowledge inherited

from ancestors, passed down through healer-to-healer transfer, or developed through personal experiences over time (Khan, 2014).

Currently, the use of medicinal plants for disease treatment has become common worldwide, with developing countries employing them more extensively than developed countries (Singh et al., 2020). In South Africa, approximately 27 million people rely on medicinal plants to meet their primary healthcare needs (Kale, 1995; Mander, 1998; Richter, 2003; Mavundza and Mudau, 2010). The affordability, availability, and accessibility of traditional medicine, as well as the belief that it has no side effects, are some of the reasons why most Africans still depend on and prefer traditional medicine for managing their health.

Different solvents are utilized in the extraction of medicinal plants, with polar solvents like water and alcohols, intermediate polar solvents like acetone and dichloromethane, and non-polar solvents like n-hexane, ether, and chloroform being the most common (Abubakar and Haque, 2020). The selection of solvent is influenced by factors such as the type of plant, the specific plant part being extracted, the properties of the bioactive compounds, and the availability of the solvent. The use of plant extracts has been gaining considerable interest as a promising approach to combat the emergence of antibacterial resistance (Abbas et al., 2020; Safdar et al., 2021). Additionally, crude plant extracts have shown significant potential for antibacterial activity, which has prompted extensive research by scientists into purifying plant bioactive compounds (Romano et al., 2021).

2.6 Phyto-bioactive compounds in medicinal plants

Phyto-bioactive compounds are plant-derived substances that offer protection against various diseases but are not essential for dietary purposes (Riaz et al., 2023). Phyto-bioactive compounds are also referred to as secondary metabolites and phytochemicals of the plant (Fatima et al., 2021). These compounds are typically categorized into six major groups:

phenolics, terpenes, alkaloids, saponins, glycosides, and polysaccharides. Their classification is shown in a flow diagram (Figure 2.7).

These phytochemical compounds are part of the plant's defence mechanism, but they also exhibit remarkable potential for treating various diseases (Aanouz et al., 2021; Anjum et al., 2020). Phytochemical compounds of the plant encompass a wide range of effects, including anti-inflammatory, antimicrobial, antioxidant, analgesic, antipyretic, and immunomodulatory properties (Riaz et al., 2023).

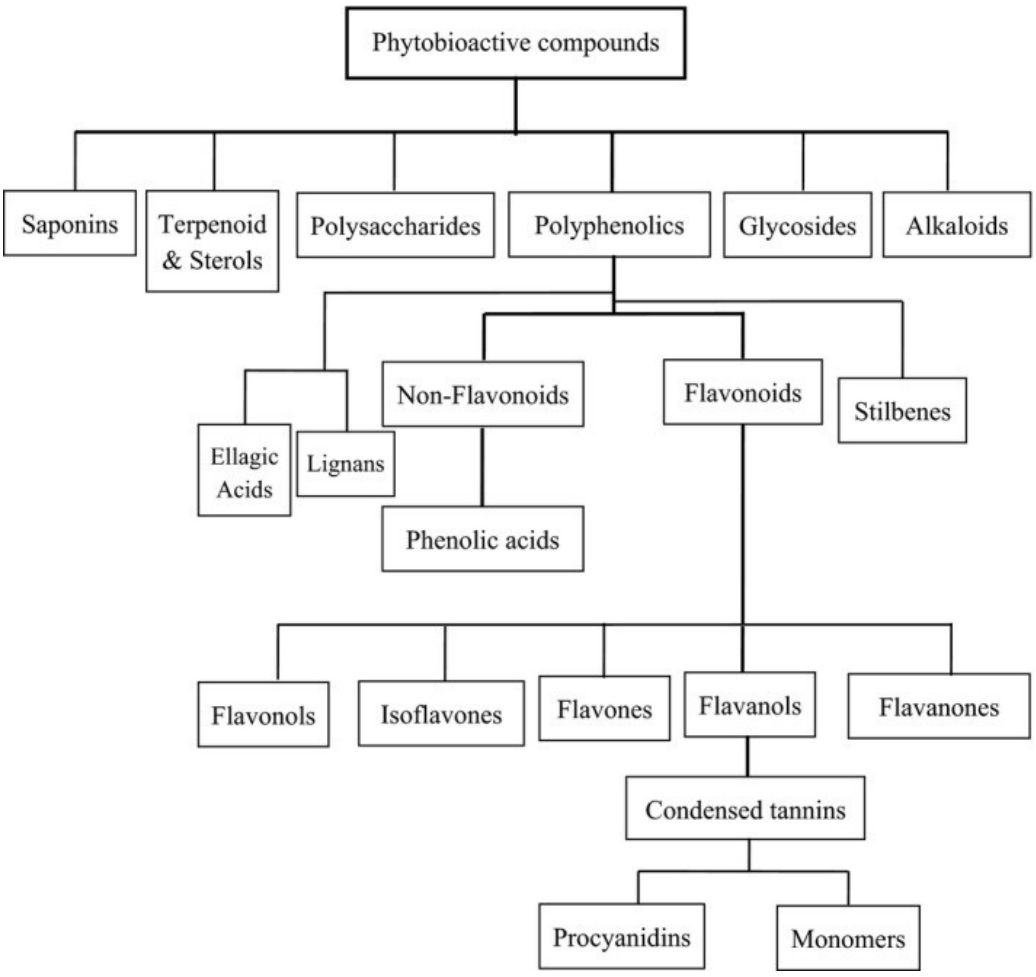

Figure 2.7: Schematic flow diagram illustrating the classification of phyto-bioactive compounds (Riaz et al., 2023).

2.6.1 Polyphenols

Polyphenols are natural compounds found in fruits, seeds, and vegetables, derived from secondary metabolism pathways in plants, particularly the phenylpropanoid pathway (Pandey and Rizvi, 2009). They exhibit diverse structures and include groups such as flavonoids, phenolic acids, lignans, stilbenes, tannins, and coumarins. These compounds contribute to the colour, aroma, and antioxidant properties of foods. Their importance is growing due to their numerous health benefits, such as preventing and treating diseases like cancer, cardiovascular diseases, inflammation, neurodegenerative disorders, and age-related degenerative diseases (Riaz et al., 2023).

Polyphenols play a crucial role in preventing carcinogenesis by interfering with cellular processes involved in tumour development, making them valuable chemo-preventive agents (Riaz et al., 2023). They mitigate damage caused by carcinogens and promote cell cycle regulation and apoptosis to inhibit cancer progression. Additionally, polyphenols combat oxidative stress by scavenging free radicals and regulating key cellular signalling pathways related to cancer development (Shen et al., 2017). Polyphenols combat oxidative stress by scavenging excess free radicals, thereby regulating key cellular signalling pathways involved in cancer development. Specific polyphenols, such as epigallocatechin gallate (EGCG), quercetin, curcumin, caffeic acid, and resveratrol, exhibit antioxidant effects and inhibit the activation of NF-kB, reducing the expression of inflammatory mediators.

2.6.1.1 Phenolic acids

Phenolic acids are a subset of polyphenols characterized by the presence of OH groups linked to benzene or aromatic rings. They play vital roles in plant colour development, pollination, and defence against pathogens (Riaz et al., 2023). Abundant in vegetables, fruits, wine, coffee, and tea. They are a key class of dietary polyphenols and natural antioxidants. They are

precursors to significant bioactive molecules regularly used in the therapeutic, cosmetics, and food industries.

Phenolic acids are mainly divided into two sub-groups: hydroxybenzoic acid (HBA) and hydroxycinnamic acid (HCA) (Zhang et al., 2022). They exhibit tremendous antioxidant activity and are recognized for their biological and pharmacological benefits, including anticancer, antimicrobial, antiallergic, antithrombotic, and hepatoprotective properties (Sharif et al., 2018)

2.6.1.2 Flavonoids

Flavonoids are a group of polyphenolic compounds widely distributed in plants, fruits, and beverages, with more than 8000 identified (Riaz et al., 2023). These compounds are subdivided into several subgroups, including anthocyanins and anthoxanthins (such as flavones, isoflavones, flavanols, and flavanones). Anthocyanins are responsible for plant and fruit colour, while anthoxanthins are colourless molecules. Numerous biological activities, including anti-inflammatory, anti-cancer, anti-allergic, and immunomodulatory qualities, are exhibited by flavonoids. Some of the most important flavonoids include kaempferol, hesperidin, naringenin, myricetin, and quercetin, which have significant impacts on human health due to their biological activities (Khairan et al., 2021).

2.6.2 Alkaloids

Alkaloids are a group of natural compounds that have at least one nitrogen atom. These nonpeptidic and nonnucleosidic compounds are primarily derived from amino acids and are classified into various groups based on their molecular precursors, structures, and origins (Hafiz et al., 2018, Fatima et al., 2020). Major classifications include diterpenoid, steroidal, quinazoline, indole, isoquinoline, quinoline, pyridine, and pyrrolidine (Hafiz et al., 2018; Fatima et al., 2020).

With around 5,500 known alkaloids, they represent the largest group of phyto-bioactive compounds and have a long history of medicinal use, serving as laxatives, astringents, and sedatives for various conditions, including snake bites and fever (Mehmood et al., 2012).

Alkaloids are known for their toxicity and bitterness, which help defend plants against pests and pathogens (Khadka et al., 2021). They exhibit a wide range of therapeutic effects, including cytotoxic, antifungal, antiviral, and antibacterial properties. For example, compounds like berberine are used in traditional medicine for their antiseptic and analgesic effects. Alkaloids such as songorine and berberine also show promise in treating neurodegenerative disorders and cancer due to their anti-inflammatory and neuroprotective properties (Fielding et al., 2020). Furthermore, approximately 40% of modern drugs are derived from natural sources, highlighting the significant role of alkaloids in drug development (Afzal et al., 2018).

2.6.3 Terpenoids

Terpenoids are the largest class of natural products, comprising over 55,000 known compounds (Noreen et al., 2020). They are formed as a result of the secondary metabolism of plant and animal species, which involves the connection of C5 isoprene units via mevalonic acid intermediates in a head-to-tail fashion (Yang, 2020). Terpenes are used extensively in the industrial sector, serving as spices, fragrances, flavours, scents, cosmetic products, and food additives. They are also active components in pharmaceutical drugs (Shahid et al., 2020).

Terpenes have numerous therapeutic applications, and some of the well-known terpene-based drugs are employed for antimalarial and anticancer purposes. Essential oils, which contain monoterpenes, have been found to possess the ability to damage microbial cells and inhibit microbial growth. Terpenes also exhibit remarkable antitumor, anti-inflammatory, antibacterial, and antiviral effects, promote transdermal absorption, and can prevent and treat cardiovascular diseases. They also have hypoglycemic activities (Yang, 2020).

Certain types of terpenoids have been shown to manage disorders caused by obesity by inhibiting the apoptosis of hepatic cells. Their antioxidant properties are linked to hepatoprotective activity, making them a safe and promising agent for treating diabetes (Chatterjee et al., 2019, Ielciu et al., 2021). Terpenes and terpenoids have a wide range of therapeutic applications, making them valuable compounds in various fields, including medicine, cosmetics, and food production.

2.6.4 Saponins

Saponins are natural compounds known for their surface-active properties and are widely distributed in the plant kingdom. They consist of both five-ring triterpene saponins and four-ring triterpene saponins, which have potential cardioprotective effects. These benefits are achieved through mechanisms such as regulation of calcium levels, modulation of energy metabolism, and suppression of inflammation and oxidative stress (Chen et al., 2017).

Polyphyllin I (PPI) is a steroidal saponin that can be extracted from *Paris polyphylla* roots and has been found to possess both anticancer and cardioprotective properties. It works by inhibiting tumour cell growth and activating NF-κB to mitigate oxidative stress and inflammation (Huang et al., 2020). Platycodin D is another saponin found in Platycodon grandiflorus that exhibits antioxidant, anti-inflammatory, and anti-atherosclerotic effects (Wang et al., 2018). Gypenoside A is derived from Gynostemma pentaphyllum and has been found to demonstrate anti-inflammatory, antioxidant, and antitumor activities (Chang et al., 2020). Ginsenoside Rb3, which is primarily found in Panax ginseng C. A. Meyer plants, has been found to exert antiapoptotic effects by inhibiting apoptosis through the activation of the NK/NF-κB signalling pathway (Ma et al., 2014).

2.6.5 Polysaccharides

Polysaccharides, commonly found in vegetables and fruits, exhibit significant cardioprotective potential. They operate through multiple mechanisms, including anticancer, antioxidative stress, anti-inflammatory, immunomodulatory, and metabolic regulation effects (Chen et al., 2021). Biologically important polysaccharides like gums and fucoidan, have garnered attention for their diverse health benefits. Gums, derived from plants, are classified into exudate and nonexudate gums (Naqvi et al., 2011; Hussain, Ali, et al., 2015; Hussain, Bakalis, et al., 2015). Exudate gums are synthesized by plants for protection against microbial attacks or in response to mechanical injury (a process known as gummosis), while nonexudate gums are artificially obtained from plants through suitable extraction methods (Munir et al., 2015).

These gums have extensive commercial applications, particularly in the food industry, where they enhance product quality (Munir et al., 2016). In addition to their functional roles, gums are recognized for their health benefits as dietary fibres with bioactive properties. Guar gum, a widely used natural gum, has applications in the pharmaceutical, textile, and food industries, with its utility enhanced through surface modification techniques. Modified guar gum exhibits improved thermal stability and crystallinity, making it valuable in various industrial applications (Anjum et al., 2014; Bukhari et al., 2014).

2.7 Description of *Spirostachys africana* plant

Spirostachys africana (*S. africana*) is a medicinal plant known as "*Muonze*" in Venda, within the *Euphorbiaceae* family (Singh et al., 2020). It is a deciduous tree of medium size, characterised by hardwood, and capable of reaching heights of up to 18 meters (Lennox and Bamford, 2015). Distinctive features of *S. africana* include a thick, rough bark neatly cracked into rectangular blocks, ranging from dark brown to black (Lennox and Bamford, 2015). Its leaves, measuring up to 70 x 35 mm, are simple, alternating, and finely toothed along the

margins. In spring, the young red leaves often stand out more prominently than the older green ones.

The *S. africana* has female flowers that are attached at the base of each spike, with the majority of the flowerheads, ranging from 15-30 mm in length, bearing male flowers. Flowers are produced before new leaves appear, typically in August and September. Male flowers exhibit a golden colouration due to pollen, while female flowers are crimson. The image below (Figure 2.8) shows the *S. africana* tree and its distinct features.

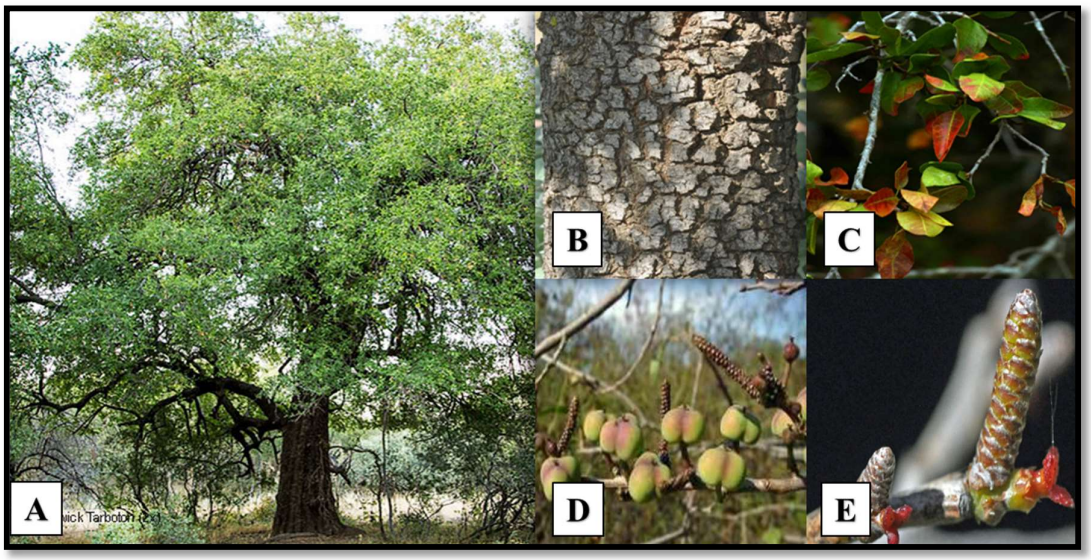

Figure 2.8: A) Picture showing the *Spirostachys africana* tree (Waterberg-bioquest.co.za., 2022), B) The bark of the tree (Becking, 2022), C) leaves and branches (Hyde et al., 2022), D) are the fruits (South African National Biodiversity Institute (SANBI), 2022) and E) flowers (Tree South Africa., 2022).

S. africana is widely distributed throughout southern and central Africa (Hutchings, 1996; The Plant List, 2018). It is commonly found in wooded grasslands and deciduous woodlands, and

in some cases, it forms pure woodland stands (Lennox and Bamford, 2015). The species is predominantly located in thickets along drainage lines and rivers in warm areas, and it is also prevalent in poorly drained brackish soils (Gandiwa et al., 2012; Lemmens et al., 2012; Lennox and Bamford, 2015). The *S. africana* plant is among Indigenous plant species that play a role in South African traditional medicine and is used to treat various diseases including respiratory illnesses.

This plant is among the indigenous plant species that play a role in South African traditional medicine, where it is used to treat various diseases, including respiratory illnesses. The stem bark and roots are utilized for treating colds, flu, fever, headaches, nosebleeds, and gum bleeding. Additionally, the bark is employed in the treatment of dysentery, diarrhoea, and stomach pains (Mabogo, 2012). Indigenous people boil the root or stem bark to make a soft porridge for individuals suffering from these ailments (Mabogo, 1990). It is used as an enema for blood purification and kidney cleansing. Moreover, it produces poisonous milky latex which is utilised as a purgative and emetic in small doses, typically one drop (Gelfand et al., 1985).

2.8 Nanoparticles

Nanoparticles (NPs) are materials with sizes ranging from 1 to 100 nm dimensions (Fatemeh Moradi et al., 2020). They can transport antimicrobials to the target site and may challenge the mechanisms of bacterial drug resistance with various mechanisms (Yayehrad et al., 2022). Several NPs are used as broad-spectrum antimicrobial agents and carriers of antimicrobial agents in consumer products (Adam and Khan, 2021). Among these, MNPs such as silver, gold, copper, zinc, titanium, and magnesium have gained attention because of their overabundance of unique properties and potential applications (Bharadwaj et al., 2021).

2.8.1 Silver nanoparticles

Silver nanoparticles (AgNPs) have attracted researchers toward various biomedical, biosensors, catalytic, optoelectronics, and food-related implications (Bharadwaj et al., 2021). AgNPs have unique physicochemical characteristics and display multiple modes of inhibitory action against microorganisms. Bharadwaj et al. (2021) found that green-synthesised AgNPs show significant antibacterial activity against *E. coli* and *S. aureus*. Due to their low cytotoxicity and high effectiveness against MDR bacteria, AgNPs are widely used in antibacterial treatment.

2.8.2 Gold nanoparticles

Gold nanoparticles (AuNPs) are becoming increasingly popular due to their optical and electrical properties, which vary significantly based on their size and shape. Research has shown that AuNPs can enhance the antimicrobial activity of drugs when loaded onto them. The modes of action include inhibition of microbial enzymes, reduction of cell permeability, and cell death (Aderibigbe, 2017). Studies have reported that AuNPs conjugated with antibiotics or drugs have better antibacterial or antiviral activity when compared to antibiotics or drugs alone (Tao, 2018).

Bare AuNPs, on their own, do not affect bacterial growth or functional activity. However, when AuNPs are conjugated with biomolecules, they can inhibit bacterial cell growth. This suggests that the antimicrobial properties of AuNPs are primarily due to their ability to act as carriers for antibiotics or drugs, rather than any inherent antimicrobial activity of the NPs themselves.

2.8.3 Method of synthesis of nanoparticles

Metallic nanoparticles (MNPs) are synthesized using various methods, including chemical approaches like sol-gel, polyol synthesis, chemical reduction, and precipitation, as well as physical methods such as combustion assisted by microwave, pulsed laser deposition, and laser

evaporation (Dhayalan et al., 2018; Shao et al., 2018). Additionally, biological methods also known as green synthesis, which uses plants, bacteria, and fungi are also employed for MNP production (see Figure 2.9).

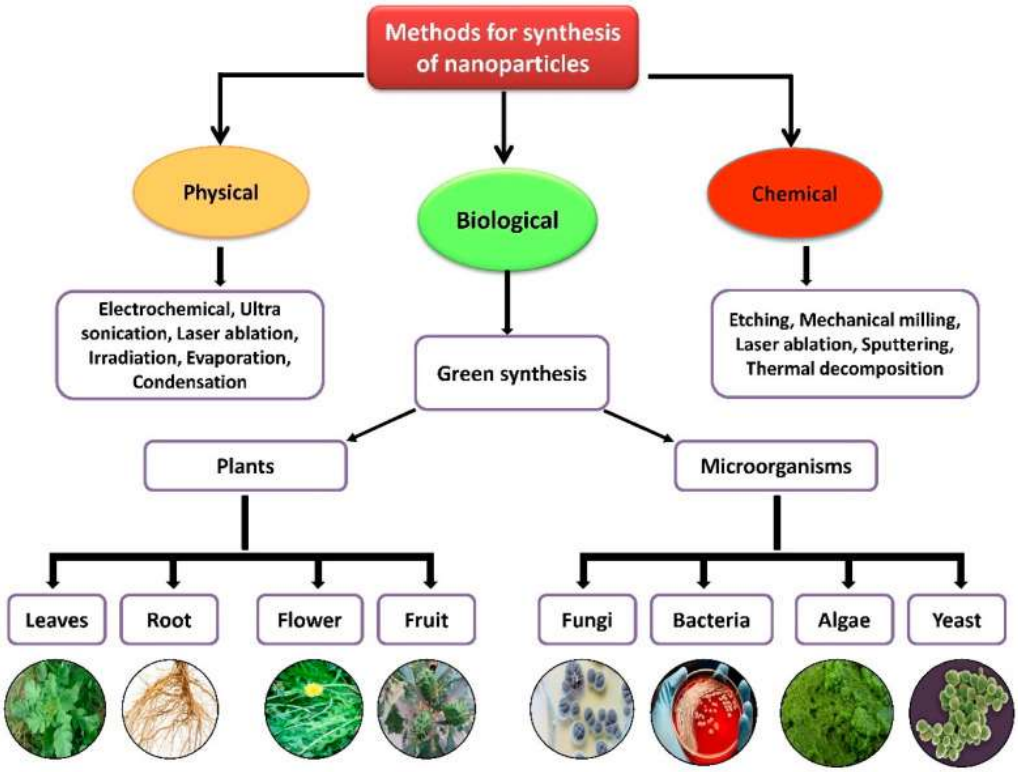

Figure 2.9: Different methods for the synthesis of nanoparticles (Khan et al., 2022).

Chemical and physical methods have disadvantages such as low yields, high costs, the production of hazardous byproducts, and reliance on toxic chemicals and solvents (Dhayalan et al., 2018). These drawbacks can compromise biocompatibility, require complex procedures, and result in environmentally unfriendly byproducts (Rehana et al., 2017; Selvan et al., 2018). In contrast, green synthesis offers several advantages, presenting itself as a safer, straightforward, eco-friendly, feasible, faster, and reliable method (Mukhopadhyay et al., 2018, Devasvaran and Lim, 2021).

Among all green synthesis methods, plant-based methods have attracted considerable attention as a more convenient option, since they produce stable NPs in a fast and efficient manner (Patil et al., 2018; Bharadwaj et al., 2021). Plant-based methods of synthesising NPs are more advantageous than microorganisms indicated (Table 2.1).

Table 2.1: The benefits and drawbacks of utilising nanoparticles synthesised through green methods involving plants and microorganisms (Zuhrotun et al., 2023).

Green synthesis method	Benefits	Drawbacks
Plant extracts-based biosynthesis	• Rapid production • Environmental friendliness • Absence of pollutants and toxicity • Cost efficiency • Ease of handling • Production of stable and unaggregated NPs • Scalability	• Lacks the capability for genetic manipulation
Microbial-based biosynthesis	• Environmental friendliness • Not toxic • Clean • Can be genetically manipula	• Slow production • Complex processes involving sampling, isolation, culturing, and storage of microorganisms • Difficulty in managing stability and aggregation • Time and cost-intensive culturing requirements • Potential presence of endotoxins.

Plant-based synthesis method involves extracting bioactive compounds from various plant parts. These compounds then play a crucial role in reducing and stabilizing metal ions, leading to the formation of NPs. Primary and secondary metabolites, among other complex biomolecules present in the plant extracts, are essential to the synthesis of MNPs. Alkaloids, terpenes, glycosides, and phenolic compounds are examples of secondary metabolites that are particularly significant in the reduction, stabilization, and capping of metal ions that result in the formation of MNPs (Paiva-Santos et al., 2021).

The synthesis process typically consists of two primary steps: the reduction of the metal precursor and the stabilization of the synthesized MNPs (Hernández-Morales et al., 2019). In this process, hydroxyl (OH) groups of phytochemical components and the metal form a chelate, initiating the synthesis of phyto-MNPs. Subsequently, the OH groups oxidize into corresponding carbonyl (CO) groups, leading to the reduction of metal ions. The plant extract then coats the MNPs to prevent their growth, serving as a stabilizing agent.

Plant-based production of MNPs is a single-step method that involves mixing and homogenizing the plant extract with the precursor metal salt solution, followed by purification and concentration of the extract (Paiva-Santos et al., 2021). The salt solution is typically aqueous and may be in the form of nitrate, acetate, chloride, or sulphate solution. Several critical parameters such as the type of plant, part of a plant to be extracted, type of metal salt, pH, temperature, and incubation time, can significantly impact the rate, production time, and properties of the synthesized NPs. Therefore, meticulous control and optimization of these parameters are essential to customize the green synthesis process and attain the desired NP properties (Makarov et al., 2014).

2.8.4 Mechanism of plant-based synthesis of AgNPs and AuNPs

The mechanism of plant-based synthesis of AgNPs is demonstrated in Figure 2.10, whereby the principal phytochemicals like antioxidant polyphenols and flavonoids play pivotal roles in reducing silver ions to silver metals (Ag^{+} to Ag^{0}) during the production of AgNPs. The produced AgNPs are stabilized by the presence of bioactive compounds, particularly phenolic compounds, which prevent their aggregation or coalescence (Jabeen et al., 2021).

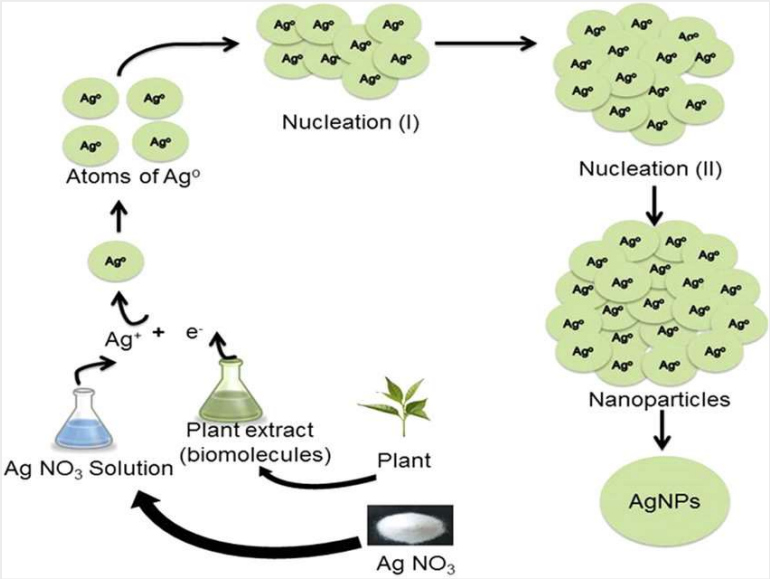

Figure 2.10: An example showing the mechanism of plant-based synthesised of AgNPs (Jabeen et al., 2021).

Phytochemical compounds not only aid in stabilising NP sizes but also serve as capping agents formed during the NP synthesis process. They tend to adhere to the NP surface, enhancing their stability and biological properties. Therefore, NP "capping" can carry out several key activities, including preventing NP agglomeration, lowering toxicity, and improving antibacterial properties. Moreover, these molecules can boost the potential of affiliation and the effect of

AgNPs on bacterial cells. Interestingly, plant "capping" compounds usually have inherent antibacterial properties that can increase NP activity (Mikhailova, 2020).

Likewise, the mechanism of biosynthesis of AuNPs involves mixing a biological extract derived from plants, with a solution containing gold salt ($HAuCl_4$). This mixture induces the reduction of gold ions (Au^{3+}) to gold atoms (Au^0), resulting in the formation of AuNPs (refer to Figure 2.11).

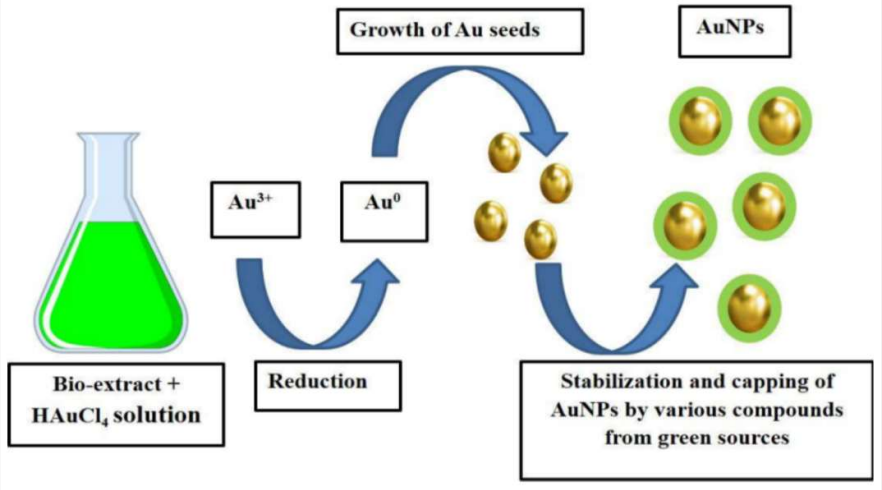

Figure 2.11: Mechanism of plant-based synthesised AuNPs (Santhosh et al., 2022).

2.8.5 Mechanism of AgNPs and AuNPs action on the cells of bacteria

Although a lot of research has been conducted in the field, the precise way in which AgNPs act on cells remains uncertain (Slavin et al., 2017). However, when working with plant extracts, there is substantial evidence to suggest that AgNPs can physically interact with the cell surfaces of various bacteria. The impact of AgNPs on cells is attributed to several mechanisms, including their attachment to the bacterial cell wall and membrane, penetration into the cell leading to disruption of intracellular organelles and biomolecules, induction of oxidative stress, and modulation of signal transduction pathways (Mikhailova, 2020). A recent study by Devasvaran and Lim (2021) demonstrated the antimicrobial activity difference of

polysaccharide pectin-AgNP on Gram-positive and Gram-negative bacteria due to differences in their cell walls (Figure 2.12).

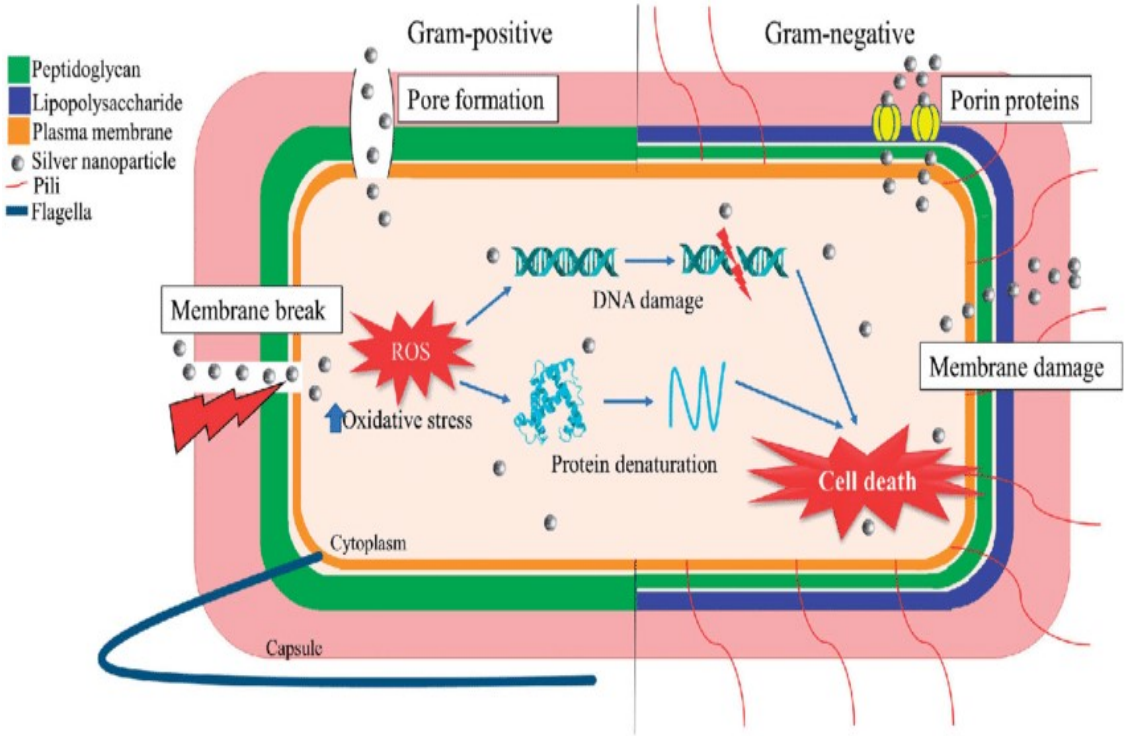

Figure 2.12: Mechanism of action of plant-synthesised AgNPs on Gram-positive and Gram-negative bacteria (Devasvaran and Lim, 2021).

The Gram-negative bacteria have a cell wall made of an outer membrane with lipopolysaccharide (LPS) and a thin layer of peptidoglycan (PG), whereas Gram-positive bacteria have a very thick layer of PG (Slavin et al. 2017). AgNPs are absorbed by the LPS in Gram-negative bacteria and directly damage the PG layer, increasing membrane permeability and killing the bacteria by diffusing released Ag ions into the cytosol. However, in Gram-positive bacteria, the AgNPs directly pass through the dense PG layer to generate an Ag ion leakage into the cytosol, increasing the bactericidal efficacy (Xu et al. 2019).

The mechanism underlying the effectiveness of plant-AuNPs is like that observed in AgNPs synthesized from plants. The antibacterial activity of synthesized AuNPs is primarily attributed to oxidative stress, Au ion release, and non-oxidative stress (Correa et al., 2020). For instance, biomolecules present in AuNPs obtained from *Nigella arvensis* leaf extract enhance their antibacterial efficacy by interacting with bacterial cell walls, leading to structural alterations and subsequent cell destruction (refer to Figure 2.13). Consequently, AuNPs interact with bacterial cell walls at the molecular level, highlighting the significance of their envelope composition in determining antibacterial activity, stability, and surface charge (Timoszyk and Grochowalska, 2022).

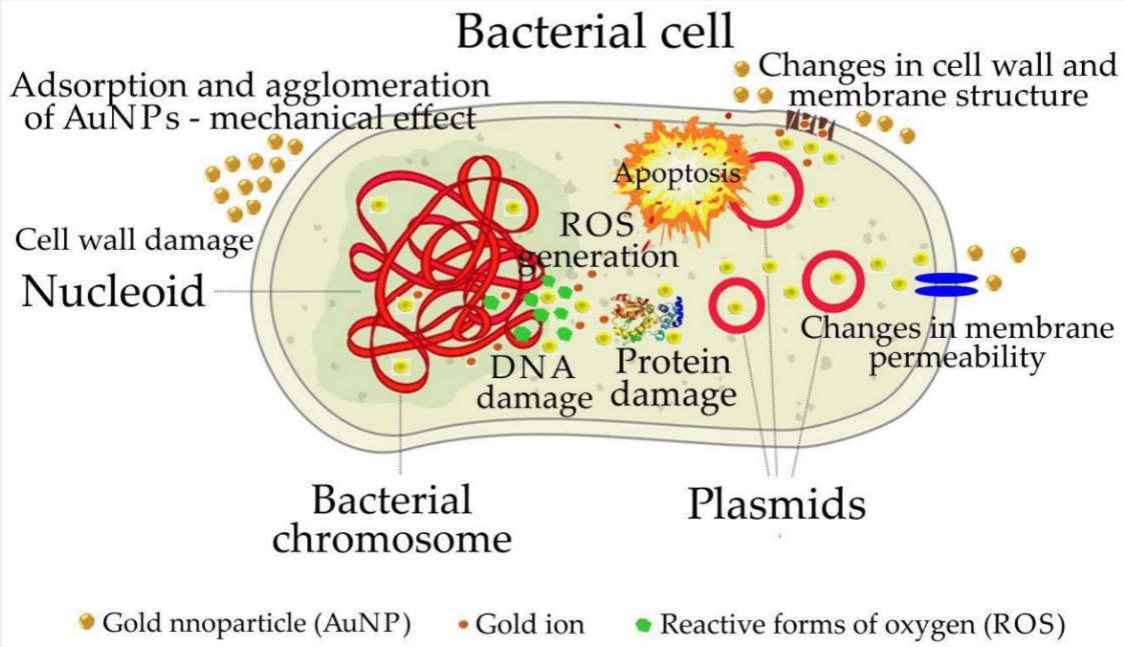

Figure 2.13: Mechanism of action of plant-synthesised AuNPs bacterial cell (Timoszyk and Grochowalska, 2022).

2.9 Characterisation of plant-mediated nanoparticles

Various methods are employed to characterize NPs, providing researchers with valuable insights into their properties (Figure 2.14) (Du et al., 2020). These methods include SPR, TEM, XRD, FTIR, DLS, Scanning Electron Microscopy (SEM), Atomic Force Microscopy (AFM), X-ray Photoelectron Spectroscopy (XPS) analysis, Energy-Dispersive X-ray Spectroscopy (EDS), Inductively Coupled Plasma Mass Spectrometry (ICP-MS), and High-Resolution Transmission Electron Microscopy (HRTEM).

By analysing these characteristics, researchers gain insights into how NPs interact with biological systems. This knowledge is crucial for various applications, including combating bacterial infections and inhibiting the growth of tumour cells.

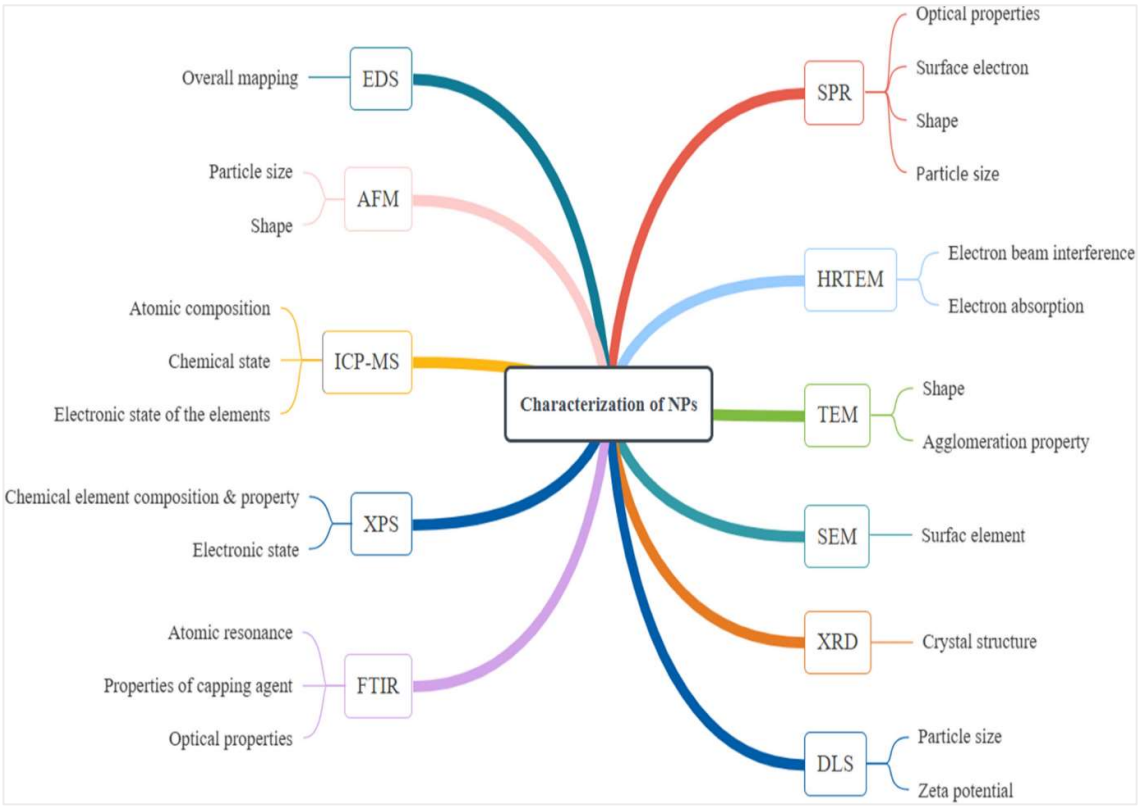

Figure 2.14: Distinct analytical techniques for nanoparticle characterisation (Du et al., 2020).

2.9.1 Structures and shapes of nanoparticles

The shapes of NPs can be identified through techniques of TEM and SEM. Common shapes include linear, spherical (or ellipsoidal), cubic, and plate-like (such as triangles or polygons), with spherical shapes being predominant. However, some studies have revealed unconventional shapes like clouds or petals (Anandan et al. 2019). This diversity in NP shapes in plant-based MNP synthesis may stem from the intricate structures of biological extracts, such as proteins and polysaccharides, which encase the nanomaterials in spherical or quasi-spherical forms (Barbinta-Patrascu et al., 2019). Additionally, AFM can be employed to investigate NP three-dimensional shape and elemental composition (Mourdikoudis et al., 2018).

The crystal structure and lattice dimensions of the NPs are analysed XRD, which is primarily aimed at determining NP three-dimensional architectures and crystallinity. The XRD analysis indicates that most plant nanomaterials possess face-centred cubic structures (Aadil et al., 2019; Dalal et al., 2019). The variation in shapes is closely linked to the reductants and preparation methods employed, with different shapes exhibiting distinct biological activities.

The FTIR spectroscopy is utilised to determine the structure and composition of NPs. This method measures the absorption of electromagnetic radiation and applies to both solid and liquid samples. FTIR analysis enables the identification of functional groups and metabolites present on NP surfaces, which can sometimes facilitate the reduction and stabilization of NPs (Nizamov et al., 2022).

2.9.2 The size of nanoparticles

Particle size is a critical factor influencing the biological activity and potential toxicity of nanomaterials. As particle size decreases, the surface area-to-volume ratio increases, impacting

the material's surface energy and reactivity (Oksel et al., 2015). Most nanomaterials are characterized with diameters ranging from 30 to 100 nm, but sizes can vary significantly, with minimum sizes as small as 3 to 6 nm and maximum sizes exceeding 100 nm (Rathi Sre et al., 2015; Du et al., 2019; Vijay et al., 2018).

To characterise the size of the NPs, techniques such as TEM, SEM, and AFM are commonly used (Susanti et al., 2022). Understanding the size of NPs is essential for assessing their interactions with biological systems and their potential applications in fields such as drug delivery and environmental safety.

2.9.3 Surface plasmon resonance of nanoparticles

The SPR of nanomaterials is typically characterised by the maximum absorption peak of NPs, which is commonly measured using a UV-Vis to demonstrate the SPR of the synthesised NPs (Khan et al., 2016). The SPR is produced due to the oscillation of electrons attracted to the positive charge of the nucleus, resulting in electron density waves known as surface plasmons on the surfaces of nanomaterials. The frequency of incident light, as measured by a UV-vis spectrophotometer, matches the frequency of these surface plasmons, allowing for photon absorption under resonance conditions. Particle size, shape, type, and surrounding environment of the NPs influence the SPR properties (Roque et al., 2019; Deepak et al., 2019).

2.9.4 Dispersion of the nanoparticles

Dispersion refers to the even distribution of NPs within a medium, minimizing the likelihood of particle aggregation. Well-dispersed nanoparticles are more stable as they are effectively separated and stabilized in the medium. The DLS techniques are frequently employed to assess NP size, size distribution, and aggregation levels (Susanti et al., 2022). Agglomeration, which occurs in both dry and suspended states of MNPs, impacts crucial physical and chemical properties such as particle size and distribution. Agglomerated nanomaterials may behave like

larger particles due to their increased hydrodynamic size, potentially affecting their biological effects and toxicity (Oksel et al., 2015).

Zeta potential (ZP), representing electrostatic repulsion between plant NPs, helps understand their surface state and predict long-term stability. Nanomaterials with zeta potentials below -30 mV or above 30 mV demonstrate extremely high stability, while those between -30 mV to -10 mV and +10 mV to +30 mV indicate low stability (Barbinta-Patrascu et al., 2019). Most plant-metal NPs prepared in experiments exhibit stability.

Under TEM, plant-AgNPs with a negative charge can induce depressions on bacterial cell walls, leading to damage, destabilization, or even collapse of the cell wall, resulting in internal material leakage and bacterial death (Deepak et al., 2019). Additionally, plant-based MNPs have shown similar effects in anticancer experiments (Mohamed et al., 2017). These findings underscore the importance of understanding dispersion and stability in NP applications for various purposes, including biomedical and environmental fields.

2.10 Application of plant-based nanoparticles

Plant-mediated NPs and their unique properties have facilitated a wide range of applications across various sectors including biomedical, environmental, and agricultural fields (Khan et al., 2022).

2.10.1 Biomedical application

Nanoparticles have been used in drug delivery, particularly hydrophilic (water-soluble) NPs like polyethylene oxide NPs, which serve as effective drug carriers. These NPs enhance therapeutic efficiency and improve patient compliance (Elahi et al., 2018). Additionally, plant-based AgNPs and AuNPs have shown significant promise in biomedical applications due to their antimicrobial properties and ability to encapsulate therapeutic agents. Their effectiveness

in targeting specific tissues further advances the potential of NP drug delivery systems in improving treatment outcomes (Long et al., 2015, Khan et al., 2022).

2.10.2 Environmental application

In environmental applications, NPs play a crucial role in purifying the environment by effectively binding with precipitates, debris, and heavy metals due to their high surface area-to-mass ratio (Khan and Malik, 2019). This binding capacity is influenced by factors such as the composition, morphology, and absorbency of the NPs. Nanoparticles are applied in the environmental sector in three primary ways. First, they contribute to the development of eco-friendly products through green chemistry approaches, aiming to mitigate pollution. Second, they aid in bioremediation efforts, assisting in the removal of environmental contaminants. Lastly, they serve as sensors, detecting shifts in environmental conditions (Khan et al., 2022).

2.10.3 Agricultural application

Nanoparticles (NPs) have numerous potential applications in agriculture due to their antimicrobial properties. They are utilized as nano-formulations of agrochemicals, acting as pesticides and fertilizers to enhance crop productivity. They serve as nano-sensors for disease detection in crops and nano-devices for genetic modification of plants. The AgNPs, have shown significant effectiveness against various pathogens, including *Bacillus cereus*, *S. aureus*, *Shigella flexneri*, and *E. coli* (Sharifi-Rad et al., 2020). Similarly, AuNPs antimicrobial effects have also been demonstrated antimicrobial effects (Muniyappan et al., 2021).

Currently, green-synthesised MNPs are recognized as potent tools for managing harmful soil-borne microbes. Numerous studies have explored the antimicrobial properties of these NPs, including those made of silver and gold. The use of plant-based NPs is increasingly promoted for managing plant-parasitic nematodes due to their multi-site mode of action and lack of phytotoxicity (Khan et al., 2022).

2.11 Limitations

Metal nanoparticles (MNPs) face various limitations and challenges that impact their safe and effective use. The physical and chemical properties, especially size, shape, and composition, significantly influence the attributes and potential health benefits of metal NPs (Lin et al., 2013; Nadaf et al., 2022). Smaller-sized spherical AgNPs are more prone to releasing silver and can easily penetrate bacterial cells, altering permeability and causing harm. The shape of NPs plays a crucial role in their therapeutic and biological activities, emphasizing the need for precise control over these parameters during AgNPs and AuNPs synthesis (Hong et al., 2016). Additionally, the toxicity associated with MNPs poses a significant risk, with adverse effects on human health and the environment observed due to chronic exposure to silver. Some bacteria have shown resistance or reduced susceptibility to AgNPs, further complicating their use across industries (Guo et al., 2020).

2.12 Conclusion

In conclusion, MNPs such as AgNPs and AuNPs have significant applications in biomedical, agricultural, food, and herbal sectors, with extensive research interest (Burlec et al., 2023). The "green" synthesis route shows promise due to its eco-friendliness, cost-effectiveness, and feasibility compared to traditional methods. The market for MNPs is projected to grow significantly by 2027, with plants playing a crucial role, particularly in healthcare applications. Plant-mediated NPs offer a promising alternative for combating pathogens and addressing issues related to mutation and drug resistance (Chandrakala et al., 2022). However, before their therapeutic use, toxicity assessment, and scalability need to be addressed as primary concerns. Understanding the transport, distribution, and interactions of metal NPs with biological systems is crucial for clinical translation. Future research should prioritize unravelling the intricate mechanisms of metal NP biogenesis, designing engineered NPs with minimal toxicity and enhanced health benefits, controlling their size and shape, and expanding the utilization of

plant-based MNPs in various fields. Additionally, plant-based silver and gold nanoparticles can combat antimicrobial resistance and RTIs, making them a promising alternative to traditional antibiotics (Burlec et al., 2023).

Chapter 3: Methodology

3.1 Plant material preparation

Stem bark and leaves of *S. africana* were harvested in Ha-Matsa village (Figure 3.1) in the Nzhelele region (Limpopo province, South Africa). The residents of Ha-Matsa helped to identify this valuable medicinal plant accurately. The stem bark and leaves were washed with tap water to eliminate contaminants and soil residues, then cut into smaller pieces and left to dry for two weeks at room temperature. Once the plant materials had dried, they were ground into a fine powder using an electric grinder model FZ102 (Tianjin Taisite Instruments, Tianjin, China) and stored in a sealed glass jar in the dark at ambient temperature for further use (Appendix A.1).

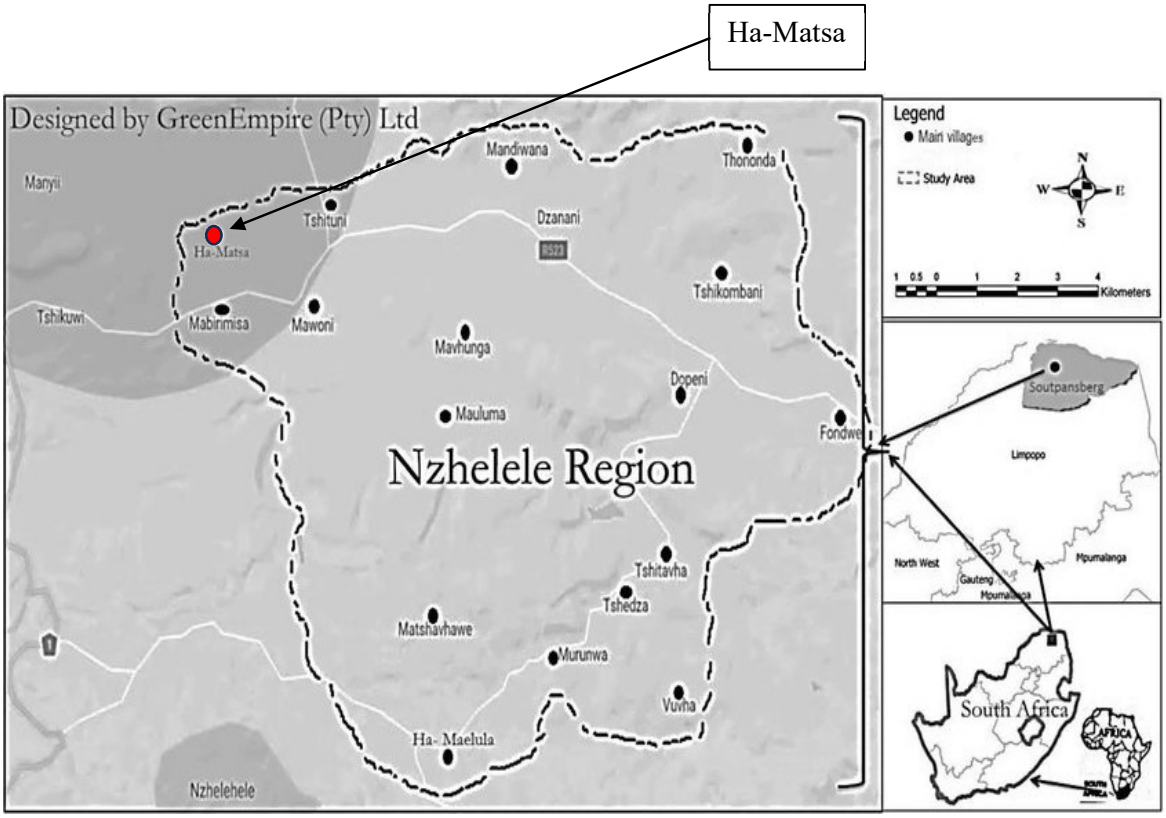

Figure 3.1: A map illustrating the location of Ha-Matsa village within the Nzhelele region of South Africa, situated in Limpopo province (Ramarumo et al., 2019).

The plant materials were extracted using different solvents, including methanol, ethanol, acetone (Rochelle Chemical, Gauteng, South Africa), and distilled water. Approximately 50 g of the ground bark and leaves were soaked in 500 mL of each solvent for 72 hours, with frequent shaking. The crude extracts were filtered using Munktell filter paper 3HW (Lasec, Gauteng, South Africa). The concentrated extracts were obtained by evaporating the solvents using a rotary evaporator (Buchi Rotavapor R-300, Cole-Parmer, Vernon Hills, IL, USA) under pressure at 40°C (Agyepong et al., 2014). The resulting concentrated extracts were then allowed to air-dry in a fume hood (Appendix A.2). For water extracts, the filtrate was first frozen at -80°C and then placed in a freeze dryer s (EPIC Freeze Dryer, Millrock Technology, Kinston, NY, USA) for 24 hours. All the plant extracts were stored at 4°C for future use.

3.2 Preparation of microorganisms

Four microorganisms used in this study are respiratory bacterial pathogens listed by the World Health Organization (WHO) as critical priority pathogens of antibiotic resistance. *Acinetobacter baumannii* (ATCC BAA-1605), *Pseudomonas aeruginosa* (ATCC 27853), *Escherichia coli* (ATCC BAA-2469), and *Staphylococcus aureus* (NCTC 12493). All bacterial strains used in this study were purchased from Anatech Instruments (Gauteng, South Africa). They were initially plated on their selective respective media and incubated at 37°C for 24 hours (Appendix A.3). The resulting colonies were preserved in the Muller-Hinton (MH) broth (Separations, Gauteng, South Africa) with 15% glycerol in Eppendorf tubes and stored at -20 °C. Before conducting the bioassays, inoculum suspensions were inoculated in 5 mL of MH broth and incubated for 24 hours at 37°C. The bacterial suspensions were then adjusted to 0.5 McFarland standard (1.5 x 10^8 CFU/mL) before antimicrobial testing.

3.3 Green synthesis of AgNPs and AuNPs mediated by *S. africana* extracts.

3.3.1 Preparation of AgNPs using *S. africana* extracts (*SA*-AgNPs)

The green synthesis of silver nanoparticles (AgNPs) was conducted following the methods outlined by Liaqat et al. (2022) and Khanal et al. (2023), with slight modifications. In a concise procedure, 10 mL from each *S. africana* (ethanol, methanol, acetone, and distilled water) extract (10 mg/mL) was introduced separately dropwise into a 250 mL sterile glass beaker containing 40 mL of silver nitrate (1, 2, and 5 mM) solution at the ratio (1:4 v/v) at room temperature, with shaking for few seconds. The reaction mixture was done in the dark to avoid photoactivation of silver nitrate ($AgNO_3$). Each sample was labelled, covered with aluminium foil, and incubated in the dark for 24 hours. After that, AgNPs were stored at different temperatures (at 4 and 25°C) to study the effect of temperature. The study also explored the impact of reaction time on SA-AgNP production at different time intervals (1 hour, 24 hours, seven days, month 2, and month 3). The confirmation of the reduction of Ag^+ to Ag^0 was primarily monitored by visual observation of colour change from light yellow to blackish-brown or yellowish-brown and from dark yellow to dark brown or reddish-brown and continuously assessed their UV-Vis spectral analysis to determine their stability state.

3.3.2 Preparation of AuNPs using *S. africana* extracts (*SA*-AgNPs)

Gold nanoparticles (SA-AuNPs) were synthesised using a microwave irradiation method (Ayinde et al., 2019). Initially, 2 mL of *S. africana* extracts were added to 8 mL of 1 mM $HAuCl_4$ solution in a 250 mL beaker at a ratio of 1:4 (v/v), and the mixture was thoroughly mixed. Various plant extracts (10, 50, and 100 mg/mL) concentrations were utilised in the synthesis process to optimise the nucleation intensity of the nanoparticles. Subsequently, the beaker with the solution mixture was placed on the turntable of a domestic microwave oven (Russell Hobbs 20L (RHEM 21L), operating at 700 W and a frequency of 2450 MHz. The exposure duration ranged from 30 to 90 seconds to achieve complete bio-reduction, with a

noticeable colour change from brown to deep purple or red wine, indicating gold nanoparticle formation. The produced SA-AuNPs samples were labelled accordingly and stored at 4 ℃ for subsequent characterisation and assessment of biological activities.

3.4 Characterisation of *S. Africana* crude extracts and its green synthesised AgNPs and AuNPs.

3.4.1 Ultraviolet-visible spectrophotometry analysis

The formation of *S. africana* silver nanoparticles (SA-AgNPs) and gold nanoparticles (SA-AuNPs) was further validated by measuring the absorbance of the reaction mixture using Ultraviolet-visible spectrophotometry (UV-Vis) (Baharara et al., 2018; Jalab et al., 2021). In a concise process, the SA-AgNPs or SA-AuNPs samples were diluted to a 1:24 ratio with the same solvent. Dilutions were performed in 2 mL centrifuge tubes, and then 200 µL of the diluent was transferred into a 96-well plate in triplicates. The plate containing the nanoparticle samples underwent scanning in a wavelength range from 200 to 800 nm using a SpectraMax M3 spectrophotometer (Molecular Devices, California, USA) at a resolution of 2 nm. However, this procedure was done for all the nanoparticle samples except for the acetone extracts-based nanoparticles, where 2 mL of the diluted solution was dispersed in a glass cuvette to read for absorbance, as acetone solvent was not suitable for the 96-well plate. Absorption peaks in the UV-Vis spectra confirming the production of nanoparticles were observed, and their values were recorded in Microsoft Excel. Subsequently, graphs were plotted using OriginPro 2023b software.

3.4.2 X-ray diffraction unit (XRD) analysis

The synthesised SA-AgNPs and SA-AuNPs were first filtered using a Munktell filter paper 3HW (Lasec, Gauteng, South Africa), and the pallets were analysed by an XRD (Pan Analytical, X-pert pro, Netherland). The XRD measurements of SA-AgNPs and SA-AuNPs

were conducted using a Cu-Kα radiation source (λ= 1.5406 Å) in the scattering range m (2θ) of 20 – 80 on an instrument operating at a voltage of 45 kV and a current of 40 mA. The XRD spectroscopy was employed to ascertain the synthesised nanoparticles' crystalline nature, phase variety, and grain size. The XRD data was analysed using the OriginPro 2023 software. The Debye-Scherrer formula was applied to calculate the average crystalline size:

$$D = \frac{0.9\lambda}{\beta cos\,\theta}$$

Where: D represents the crystallite size (measured in nm), k stands for the Scherrer constant, which has a fixed value of 0.9, λ denotes the wavelength of the X-ray source, θ signifies the peak position (measured in radians), and β represents the full width at half maximum (FWHM (Dubey et al., 2010).

3.4.3 Dynamic light scattering (DLS) particle analysis.

Dynamic light scattering (DLS) analysis was conducted using a Zetasizer instrument (Malvern, England) to determine the average particle size, distribution, and zeta potential (an indicator of nanoparticle stability) of SA-AgNPs and SA-AuNPs (Ghani et al., 2022). The technique measures NP hydrodynamic diameter in solution, yielding valuable information about their aggregation state. The DLS analysis played a crucial role in determining the size distribution and stability of the synthesised NPs. For this analysis, samples exhibiting the best antimicrobial activity (from silver and gold nanoparticles) were selected. Each sample underwent three runs, with all the results presented on a single graph for comprehensive representation.

3.4.4 Transmission electron microscopy

Transmission electron microscopy (TEM) with more excellent resolution and magnification was employed for studying SA-AgNPs and SA-AuNPs, as it allows direct visualisation of the particles and provides detailed information about their size, shape, and distribution (Cascio et al., 2015; Marinescu et al., 2022). The TEM analysis was conducted using an FEI Technai-12

electron microscope (FEI, Eindhoven, Netherlands) operated at an acceleration voltage of 120 kV. The samples were prepared by immersing a copper grid in the nanoparticle solution and quickly removed to enable drying, forming a thin film. Obtained images from TEM were analysed to determine particle sizes using ImageJ software by measuring the diameter (nm) of each particle. Following this, the acquired values were plotted using OriginPro 2023 software and subjected to statistical analysis to determine both the average size and standard deviation. Error was computed based on the obtained values. Notably, in this analysis, 100 nanoparticles from distinct regions were examined for each sample.

3.4.5 Fourier-transform infrared spectroscopy (FTIR) analysis.

The functional groups that were responsible for biological activities present in *S. africana* extracts, silver and gold nanoparticles were identified by FTIR using the Bruker ALPHA FT-IR Spectrophotometer (Bruker Scientific Private Limited, Mumbai, India). The analysis was done by placing 500 µL of the plant extracts or nanoparticle samples on top of the FTIR spectrophotometer chamber. Percentage transmittance measurements were recorded within the wavelength range of 400-4000 cm^{-1}, as outlined by Patel et al. (2020).

3.4.6 Liquid chromatography-mass spectroscopy (LC-MS) analysis of the plant extracts

Liquid chromatography-mass spectrometry (LC-MS) was used to analyse phytochemical compounds present in *S. africana*, to understand their potential contributions to antimicrobial activity, antioxidant activity, cytotoxicity, and anti-inflammatory properties. The analysis was conducted using the method developed by Moyo et al. (2022), with a few modifications. To prepare for the LC-MS analysis, 2 grams of the ground plant powder were extracted in 20 mL of each solvent (80% methanol, 80% ethanol, and distilled water) in a ratio of 1:10 m/v for 24 hours. The extraction was done by shaking on a digital rotisserie tube rotator (Dlab Scientific, Beijing, China) at 70 rpm at room temperature. The crude extracts were then centrifuged using

a benchtop fixed-angle centrifuge (Thermo Fischer Scientific, South Africa) at 5000 rpm for 15 minutes. The samples were filtered into HPLC glass vials through 0.22 µm nylon filters.

For the analysis, the prepared sample extracts were subjected to LC-MS quadrupole time-of-flight tandem (LC/MS-9030 q-TOF, Shimadzu Corporation, Japan). Chromatographic separation of phytochemical compounds was achieved using a Shim-pack Velox C18 column (100 × 2.1 mm, 2.7 µm) maintained at 55°C. An injection of 5 µL was used, and the compounds in the plant extracts were separated using a binary mobile phase gradient elution at a flow rate of 0.3 mL/min. The mobile phases, A and B, consisted of 0.1% (v/v) formic acid in ultra-high purity water and 0.1% formic acid in methanol, respectively. The mobile phase composition was 10% mobile B for 3 minutes and kept constant until 40 minutes. Between 40 and 43 minutes, mobile phase B increased to 30%, and between 45 and 49 minutes, it raised to 90%. The gradient was restored to 10% mobile phase B after about 50 minutes and remained there for 53 minutes.

The mass spectral acquisition utilized a q-TOF high-resolution MS with an electrospray ionization interface in negative ionization mode. Settings included a 400°C heat block temperature, 280°C DL temperature, 1.8 kV detector voltage, 300°C interface temperature, 3 L/min nebulization and dry gas flow (nitrogen), and 42°C flight tube temperature. Sodium iodide served as a calibration solution for high mass accuracy monitoring. MS1 and MS2 were acquired simultaneously for all ions within a m/z range of 100 to 1000 Da in data-dependent acquisition (DDA) mode. Argon was used as the collision gas for MS2 experiments at a collision energy of 30 eV and no spread.

Molecular networks were constructed using the Global Natural Product Social Molecular Networking (GNPS) website (http://gnps.ucsd.edu) based on the approach by Aron et al. (2020). Raw data from the Shimadzu LC-MS-9030 q-TOF instrument were first converted to

the open-source format (.mzML) before the analysis. Cytoscape software facilitated molecular network data integration, analysis, and visualization (https://cytoscape.org). Empirical formulas were derived from the precise mass of the compounds' MS/MS data to verify the putative annotation of both matched and unmatched nodes. Furthermore, a thorough evaluation was carried out to validate the accuracy of the identifications by comparing them with the findings from previous studies.

3.5 Antimicrobial activity of *S. africana* extracts and nanoparticles

3.5.1 Agar well-diffusion method

The antibacterial activities of both *S. africana* extracts, SA-AgNPs and SA-AuNPs, were determined using the agar well-diffusion method, as previously described by Bhakya et al. (2016) and Ghavam, (2021). Initially, Mueller-Hinton (MH) agar medium (Separations, Gauteng, South Africa) plates were prepared to culture bacterial strains. A 200 µL volume of the test organisms with turbidity adjusted to 0.5 McFarland standard was inoculated over the surface of MH agar using a sterile spreader and allowed to dry for 30 minutes. Six evenly spaced wells with a diameter of 8 mm were aseptically created by gently punching the agar with a tip. Each well was filled with 50 µL of each plant extract solution (10 mg/mL), silver (2.68 mg/mL), and gold (10.14 mg/mL) nanoparticles. The plates were left for 1 hour to allow diffusion of the treatment samples into the inoculated agar. Finally, the agar plates were incubated at 37°C for 24 hours. Antibiotic lomefloxacin hydrochloride (10 mg/mL) (Sigma-Aldrich, Darmstadt, Germany) was employed as a positive control, while 10 % dimethyl sulfoxide (DMSO) (Rochelle Chemical, Gauteng, South Africa) served as the negative control. To assess the efficacy of the experiment, the diameter of the clear zone, indicating the inhibition of bacterial growth, was meticulously measured in millimetres using a ruler. For the precision and reliability of the results, the experiment was repeated three times for each test organism. The growth inhibition zones were subsequently recorded and presented in graphs. This

experiment was also conducted for three months to investigate the effect of time and stability of the extracts on the extracts and AgNPs.

3.5.2 Microdilution assay

The minimum inhibitory concentrations (MICs) of the plant extracts against the priory pathogens (*A. baumannii*, *P. aeruginosa*, *E. coli*, and *S. aureus*) were determined using the microdilution assay (Eloff, 1998; Samie, 2005). The procedure was as follows: In a standard 96-well plate, each well was filled with 100 µl of Muller-Hinton (MH) broth as the growth medium. The plant extracts were initially dissolved in 10% DMSO (Rochelle Chemical, Gauteng, South Africa) to attain a final 20 mg/mL concentration. The plant extracts, negative and positive control, were added into the first row of the plate, starting with the negative control, which contained 10% DMSO, followed by the positive control, lomefloxacin hydrochloride at 10 mg/mL (Sigma-Aldrich, Darmstadt, Germany), and lastly the plant extracts to the rest of the remaining wells in the same row. A two-fold serial dilution was performed by mixing contents of the first raw and transferring 100 µL to the next well within the same column until reaching the last well within the same column, with the final 100 µL discarded. The resulting concentrations range from 10 to 0.078 mg/mL. Subsequently, 100 µL of the bacterial culture was added to the wells. The plates were then incubated for 24 hours at 37°C. The next day, 40 µL of a 0.2% Iodo Nitro Tetrazolium (INT) solution (Inqaba Biotech, Gauteng, South Africa) was added to each well and incubated at 37 ℃ for 30 minutes.

The MICs of Silver (SA-AgNPs) and gold (SA-AuNPs) nanoparticles were also acquired in the same way as the crude extracts, with slight differences in the concentrations of the nanoparticles. The SA-AgNPs concentrations after 50% serial dilution in the 96-well plate ranged from 2.68 to 0.03 mg/mL. Meanwhile, SA-AuNPs concentration ranged from 10.14 to 0.08 mg/mL. The entire assay was repeated three times in each case. The wells showing no colour change indicated that the plant extracts were active and inhibited the growth of bacteria,

whereas those which turned purple/pink exhibited bacterial growth. The stability testing was also conducted using the microdilution assay over three months on the plant extracts and AgNP samples. The trials were labelled Experiment 1, Experiment 2, and Experiment 3 for the first, second, and third months, respectively.

3.5.3 Determination of minimum bactericidal concentration (MBC)

For minimum bactericidal concentration (MBC), approximately 5 µL of each sample was taken from the wells with no observable bacterial growth during the MIC tests and subcultured onto Mueller-Hinton agar plates and subsequently incubated at 37°C for 24 hours. The MBC is defined as the minimum concentration at which no bacterial growth is observed on the agar (Quelemes et al., 2013).

3.5.4 Synergistic tests by microdilution method

The synergistic activity was only tested using the plant extract samples, and this was done to determine the synergistic effects of the crude extract combinations against antibiotic-resistant bacterial strains. The microdilution assay was employed as de Rapper et al. (2012) described. Briefly, extracts from leaves and bark, each with a concentration of 10 mg/mL, were combined in various ratios: 9:1, 7:3, 5:5, 3:7, and 1:9. The ratios were represented as mixture 1 up to 5 according to the corresponding order. A hundred microliters of MH broth were transferred to all wells of the 96-walled plate, followed by 100 µL of the plant mixture (ratio 9:1) in the first wells. Subsequently, 100 µL of mixture ratios (7:3, 5:5, 3:7 and 1:9) were in the consecutive wells of the first row. All the plant extract ratios were added in triplicate. After 50% serial dilutions, 100 µL of the culture was added to each well. Lomefloxacin hydrochloride (10 mg/mL) positive control and 10% DMSO negative control were used. The plates were placed in an incubator for 24 hours at 37°C, and the MICs of the plant combinations were visually determined using 0.2% INT.

All dual combinations of the plant extracts were tested, and the fractional inhibitory concentration index (FICI) was calculated for all synergistic assays. The FICI values were interpreted as follows: FICI < 0.5 (synergistic), 0.5 < FICI < 1 (additive), 1 < FICI < 4 (indifferent), and FICI > 4 (antagonistic), following the below formula (Odds, 2003; Donkor et al., 2023).

$$FICI = \frac{MIC\ of\ AB\ combination}{MIC\ of\ A} + \frac{MIC\ of\ AB\ combination}{MIC\ of\ B}$$

3.6 Cytotoxicity and Anti-inflammatory Assays

3.6.1 Cell lines

The cytotoxic and anti-inflammatory activity of the crude extracts and SA-AgNPs and SA-AuNPs were determined using samples that exhibited higher antimicrobial activity. These included acetone bark (SABA) and methanol leaf (SALM) plant extracts, *S. Africana* bark acetone-mediated AgNPs (SABA-AG) and leaf ethanol-mediated AgNPs (SALE-AG), as well as *S. Africana,* bark-ethanol-mediated AuNPs (SABE-AU). The mentioned samples were tested for cytotoxicity against human oestrogen-positive breast cancer cells (MCF7), normal human mammary epithelial cells (MCF10), and the RAW 264.7 murine macrophage cells. Meanwhile, for anti-inflammatory activity, RAW 264.7 cells were used. All cell lines were provided by the Department of Biochemistry, Genetics, and Microbiology at the University of Pretoria (Pretoria, South Africa).

3.6.2 Preparation of cell culture complete media

The Dulbecco Modified Eagles Medium F12 (DMEM F12)/Alpha Minimum Essential Medium (α-MEM) media (Thermo Fisher Scientific, Waltham, MA, USA) were prepared following the ScienCell^{MT} Research Laboratories manufacturer's protocol. The complete media were supplemented with 1% Penicillin-Streptomycin, Amphotericin B/ Fungizone, and 10% Fetal bovine serum (FBS) (Thermo Fisher Scientific, Waltham, MA, USA). Briefly, 500

µL was removed from 25 mL volume of the DMEM F12/ α-MEM media, followed by adding 250 µL of 1% Penicillin-Streptomycin and Amphotericin B/ Fungizone to make up a total volume of 25 mL. The supplemented media were pipetted up and down to ensure a complete mixture. Ten per cent (%) FBS media was prepared by transferring 2.5 mL FBS into 22.5 mL of the supplemented DMEM F12/ α-MEM media, mixed well, and stored at four degrees Celsius.

3.6.3 Cell culture

All the cells were first thawed for 2 minutes at 37 °C in a Steri-Cycle i160 humidified incubator (ThermoFisher, Forma^{TM} i160, USA) in 5% CO_2. Subsequently, 500 µL of the cells were transferred into a 2 mL Eppendorf tube and mixed with 500 µL of supplemented DMEM F12/ α-MEM media. The mixture was centrifuged at 1000 rpm for 5 minutes, and the supernatant was aspirated. One millilitre of the supplemented DMEM/ α-MEM media was added to the pallet and mixed carefully by pipetting up and down using a pasture pipette. The cells were gently transferred into a T25 flask containing 10 mL supplemented DMEM/ α-MEM media. After that, viewed under a light microscope at 20x magnification (Figure 3.2) and incubated at 37°C humidified incubator with 5% CO_2. The MCF7 cells were cultured in α-MEM, while MCF10 and RAW 264.7 cells were cultured in DMEM F12. The cultured cells were monitored daily and became confluent after seven days.

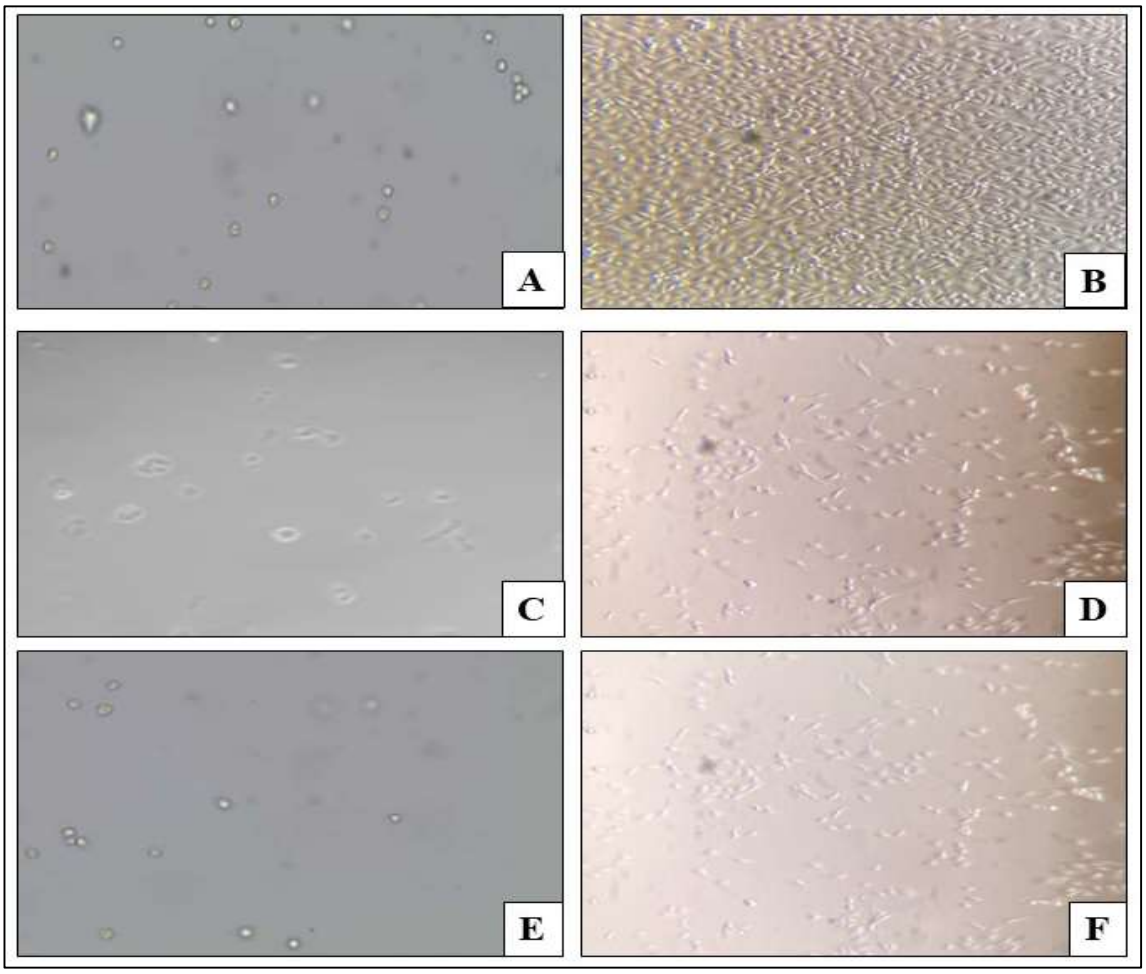

Figure 3.2: Cells under light microscopy at 20x magnification A= MFC7 day 0, B= MFC7 day 7, C= MCF10 day 0, D= MFC10 day 7, and E= RAW 264.7 day 0, F= RAW 264.7 day 7.

3.6.4 Cell count

Before counting the cells, the media was aspirated, and the flasks were rinsed twice with 2 mL of 1X Phosphate Buffered Saline (PBS) (Thermo Fisher Scientific, Waltham, MA, USA). Then, 2 mL of warm 0.25% Trypsin was added, and the cells were incubated for 2 minutes at 37ºC with 5% CO2 to detach them. After the cells detached, 4 mL of 10% FBS media was added to stop the trypsin digestion. The cell suspension was then transferred to a 2 mL Eppendorf tube and centrifuged at 1000xG for 5 minutes. The supernatant was decanted, and 1 mL of media was gently pipetted onto the resulting pellet to facilitate its dissolution. A

Scepter™ Cell Counter hemocytometer (Zeiss, Darmstadt, Germany) was used to count the cells. In brief, 100 µL cells were mixed with 500 µL of trypan blue dye (1:5 ratio). Approximately 10 µL of the mixture was pipetted into the chambers of the hemocytometer slide and counted manually by viewing under a Primovert light microscope (Zeiss, Gauteng, South Africa) at 10x magnification. The total number of viable cells was calculated by multiplying the average number of live cells by the dilution factor and 10^4. Following that, 1 mL aliquot of the cell suspension was diluted with an appropriate volume of complete media, yielding a final concentration of 1×10^5 cells/mL, which will be used for viability assay.

3.6.5 Cytotoxicity assay

The cytotoxicity of the plant extracts and nanoparticles was determined on the MCF7, MCF10, and RAW 264.7 cells using the 3-(4,5-dimethylthiazol-2-yl)-2,5-diphenyltetrazolium bromide (MTT) method (Vijayarathna and Sasidharan, 2012). Initially, 50 µL of media was added to all wells of a 96-well plate. Subsequently, 50 µL of the samples SABA, SALM, SABA-AG, SALE-AG and SABE-AU were added to the first row in triplicate, with three columns reserved for the negative control. A 50 µL two-fold serial dilution was performed by mixing the contents within each column across the 96-well plate, discarding 50 µL from the last well. The resulting sample concentrations ranged from 5 to 0.039 mg/mL, 1.34 to 0.01 mg/mL, and 10.14 to 0.08 mg/mL, respectively. Following this, 50 µL of cell suspension (5,000 cells) was seeded into all wells of the 96-well plate, bringing the final volume to 100 µL in each well. The negative control consisted of cells cultured with media alone. The plate was then incubated at 37°C in a humidified 5% CO_2 incubator for 48 hours. After incubation, 15 µL of MTT solution (Promega, USA) (5 mg/mL PBS) was added to each well and incubated for 4 hours. Subsequently, 100 µL of DMSO was added, and the plate was incubated overnight in a sealed container with a humidified atmosphere at room temperature to solubilise the formazan crystals completely. Absorbance was measured at 595 nm using a SpectraMax M3 multi-mode microplate reader

(Molecular Devices, California, USA), and the percentage cell viability was calculated using the following formula:

$$\%\ Cell\ viability = \frac{\text{Average absorbance of drug wells}}{\text{Average absorbance of control wells}} \text{ x } 100$$

The results were expressed as the mean ± standard error and further determined the half-maximal inhibitory concentration (IC50), defined as the concentration of the examined plant extracts that resulted in a 50% inhibition of cell growth compared to the control.

3.6.6 Anti-inflammatory activity

The anti-inflammatory activity of *S. Africana* extracts, silver, and gold nanoparticles was evaluated using RAW 264.7 macrophage cells. The cells were initially plated at a density of 5000 cells per well in a 96-well plate and left to incubate overnight. Subsequently, the cells were treated with the samples at varying concentrations ranging from 5 to 0.039 mg/mL, 1.34 to 0.01 mg/mL, and 10.14 to 0.08 mg/mL, respectively, after 50% serial dilution across the plate. The cells with the media alone served as negative control. After 4 hours of incubation, inflammation was induced by adding 1 µg/mL of lipopolysaccharide (LPS) (Promega, USA), and the cells were incubated for an additional 24 hours. The nitric oxide (NO) levels were then determined using the Griess reaction method (Promega). Approximately 50 µL of the cell supernatant was collected and mixed with 50 µL of sulfanilamide solution (1% sulfanilamide in 5% phosphoric acid) for a 10-minute reaction. Subsequently, 50 µL of NED solution (0.1% N-1-naphthylenediamine) (Promega, USA) was introduced for another 10-minute reaction period, and the absorbance was measured at 595 nm using SpectraMax M3 spectrophotometer. The concentration of nitrate released into the culture medium was then calculated from the slope of the standard curve (Bahrami et al., 2021; Kang et al., 2022).

3.7 Antioxidant activity

The free radical scavenging activity of the crude plant extracts, SA-AgNPs and SA-AuNPs was assessed by the 2,2-diphenyl-1-picrylhydrazyl (DPPH) method (Nemudzivhadi and Masoko, 2015). Briefly, 100 µL of deionised water was introduced into each well of a 96-well plate. Followed by 100 µL of plant extracts (1 to 0.007 mg/mL), silver (1.34 to 0,01 mg/mL) and gold (2.5 to 0.02 mg/mL) nanoparticles were dispensed into the first well of the 96-well plate in triplicate. Subsequently, 50% serial dilutions were performed. Vitamin C (1 mg/mL) was used as an antioxidant standard or positive control, and the solvents used to prepare these extracts were employed as the blanks. An additional 100 µL of a 0.1 mM DPPH methanolic solution (Inqaba Biotech, Gauteng, South Africa) was introduced into all the wells of the 96-microplate. The plate was then kept in the dark for 30 minutes. Following this incubation period, the absorbance was measured at 517 nm using VersaMax Microplate Reader (Molecular Devices, Sunnyvale, USA). The percentage scavenging activity (DPPH reduced) was calculated as follows:

$$\%\ \text{Scavenging activity} = \frac{\mathrm{A_{control}} - \mathrm{A_{sample}}}{\mathrm{A_{control}}} \times 100$$

Where $A_{control}$ is the absorption of the blank solution, and A_{sample} is the absorption of the extract solution. The IC_{50} values (the extract concentration at which 50% radical scavenging activity occurs) were determined from the graph using linear regression analysis and thereafter generated a table of DPPH scavenging activity using those values.

3.8 Statistical analysis

Data was recorded in Microsoft Excel, and the biological experiments conducted in triplicate were expressed as the average mean. One-way analysis of variance (ANOVA) was applied to assess the significance of individual differences at a $p<0.05$ level. Significant means were compared with Tukey's post hoc test via GraphPad Prism 8 software (GraphPad Software, San Diego, CA, USA). Graphs were plotted using Excel, GraphPad Prism, and OriginPro 2023b software.

Chapter 4: Results

4.1 Synthesis of *S. Africana*-AgNPs

The results indicated that the extracts from the *S. africana* plant effectively reduced $AgNO_3$ ions to AgNPs within 24 hours. This was evidenced by the colour change from yellow to blackish brown/yellowish-brown and from brown to dark brown/reddish-brown as depicted in Figure 4.1. The alteration in colour was attributed to the excitement of SPR in the AgNPs. It was also observed that the intensity of the colour increased over extended incubation time.

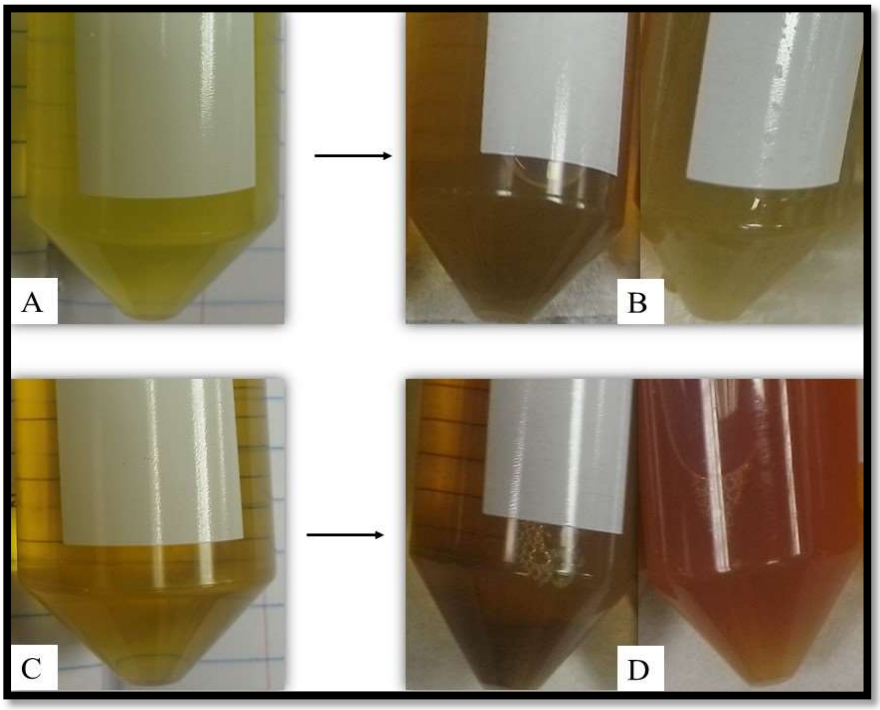

Figure 4.1: Image depicting the colour transformation of *S. africana* extracts when mixed with silver nitrate solution before (A and C) and after 24 hours (B and D) of incubation at room temperature.

The stability of SA-AgNPs was investigated by optimisation of various parameters such as reaction times, $AgNO_3$ concentrations, and temperatures. Initially, the colour intensity increased with reaction time, showing similar trends in methanol (SABM-AG/SALM-AG) and ethanol (SABE-AG/SALE-AG) samples, transitioning from light brown to blackish black or light yellow to yellowish brown. Acetone (SABA-AG/SALA-AG) samples changed from light yellow to dark brown/yellowish brown, while water (SABD-AG/SALM-AG) samples exhibited varying trends from dark yellow to dark brown over time. Subsequently, results revealed that increasing $AgNO_3$ concentration from 1 to 5 mM altered NP colour intensity, shifting from light yellow/brown at 1 mM to darker shades at 2 and 5 mM, accompanied by a shift in the SPR peak towards higher wavelengths. These stability test findings based on colour change are detailed in Appendix B1 and B2.

The study found that higher concentrations of $AgNO_3$ led to a quicker colour change. Furthermore, it was observed that SA-AgNPs incubated at 4℃ reacted slower than those at 25℃, with colour intensity increasing more over time at room temperature than in the fridge.

4.2 Synthesis of *S. africana*-AuNPs

The synthesis of SA-AuNPs was confirmed by a visible change in colour within the reaction mixture, transitioning from yellowish-brown to a deep purple within a few seconds, this colour is attributed to the excitation of SPR, as shown in Figure 4.2. The consistent nature of this colour change reliably indicates the successful reduction of Au^{3+} ions into NPs. Stable SA-AuNPs with enhanced activity were found after increasing the concentration of plant extracts and employing microwave-assisted synthesis for 30 to 90 seconds. However, the 90-second microwave synthesis yielded superior results as compared to reactions lasting 30 or 60 seconds.

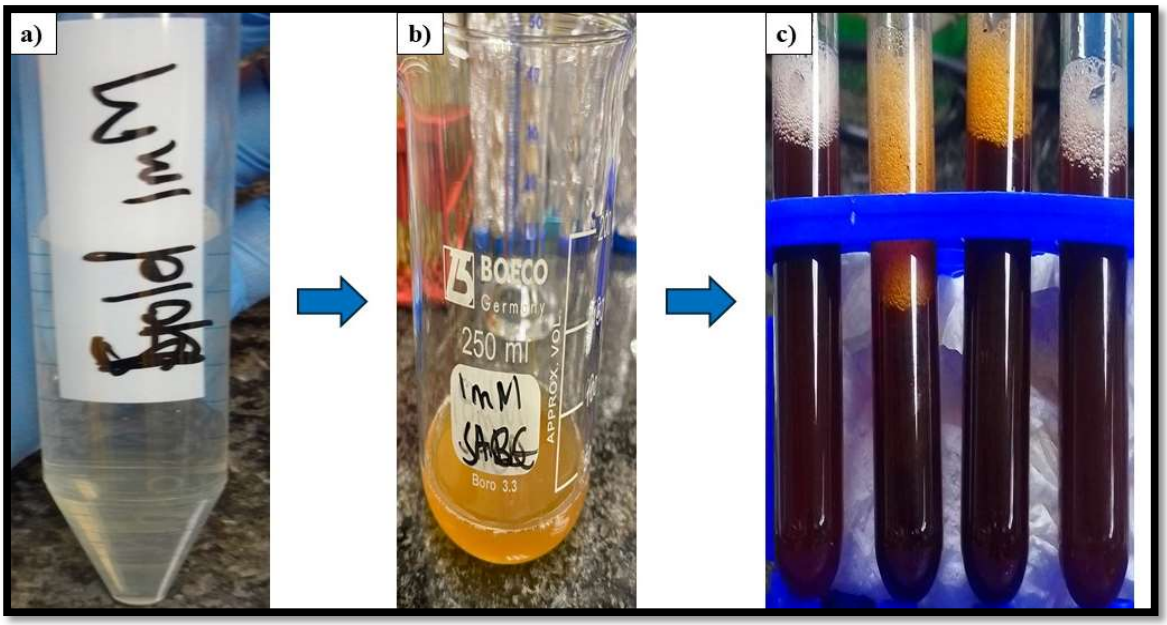

Figure 4.2: The colour change indicating the production of AuNPs: a) $HauCL_4$ solution, b) brown colour of *S. africana* plant extracts mixed with $HAuCL_4$ solution, c) complete transformation of the reaction mixture into deep purple shades.

4.3 Characterisation of *S. africana* extracts and its green synthesised SA-AgNPs and SA-AuNPs

4.3.1 Ultraviolet-visible spectrophotometry analysis

The utilisation of UV-Vis spectrophotometry, coupled with the integration of SPR, provided conclusive evidence for the successful synthesis of silver nanoparticles SA-AgNPs. The SPR of electrons within the SA-AgNPs solution led to an elevation in the peak of the ultraviolet spectrum. The results in Figure 4.3 show SPR peaks for SA-AgNPs produced by bark and leaf (methanol, ethanol, acetone, and water) extracts. Results presented were only considering SA-AgNPs samples prepared by 5 mM $AgNO_3$ concentration because they exhibited good antimicrobial activity.

The UV-Vis spectral analysis of SA-AgNPs derived from both bark and leaf samples unveiled distinct wavelength ranges. Bark samples exhibited SPR peaks ranging from 397 to 480 nm, while leaf samples displayed SPR peaks spanning 363 to 500 nm. Noteworthy variations were observed among specific SA-AgNPs samples: SABM-AG and SABE-AG revealed peaks at 397 nm and 454 nm, SABD-AG exhibited peaks at 397 nm and 470 nm, while SALM-AG and SALE-AG shared a peak at 363 nm (Figure 4.3A). Additionally, SABA-AG demonstrated a narrow SPR peak at 480 nm, and SALA-AG displayed absorption peaks at 370 nm and 500 nm (Figure 4.3B). Interestingly, SALD-AG did not exhibit any discernible absorption peak.

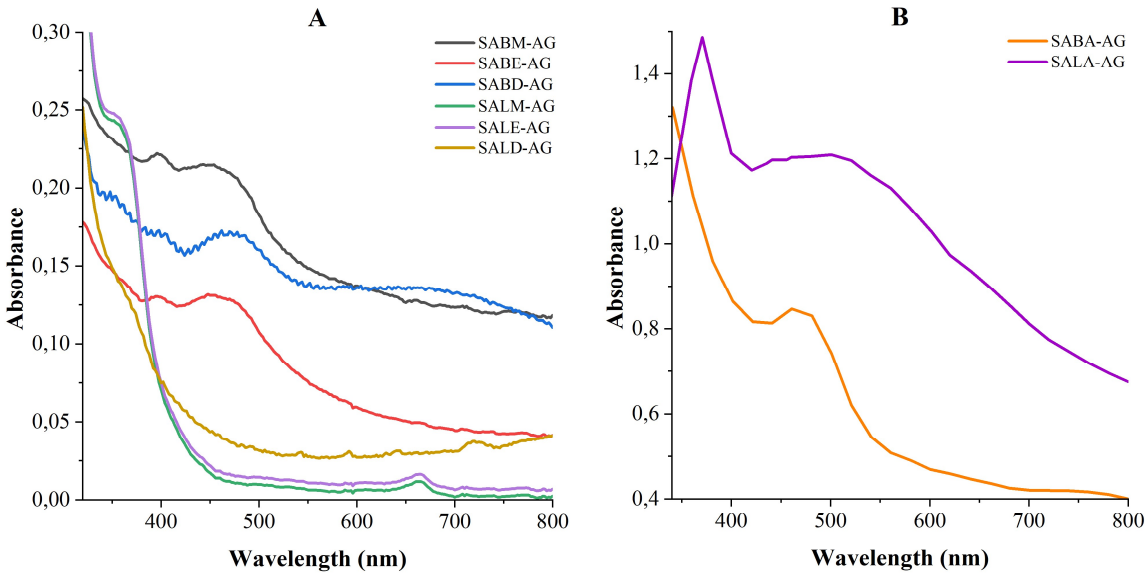

Figure 4.3: Ultraviolet-visible spectra of SA-AgNPs; SABM-AG (bark methanol AgNPs), SABE-AG (bark ethanol AgNPs), SABA-AG (bark acetone AgNPs), SABD-AG (bark distilled-water AgNPs), SALM-AG leaf methanol AgNPs), SALE-AG (leaf ethanol AgNPs), SALA-AG (leaf acetone AgNPs), SALD-AG (leaf distilled water AgNPs).

Additionally, stability testing of SA-AgNPs UV-Vis spectral analysis using various $AgNO_3$ concentrations, revealed that as concentrations increased from 1 to 5 mM increased colour intensity and caused the SPR peak to shift towards higher wavelengths, suggesting nanoparticle

aggregation (Appendix B3). While increasing $AgNO_3$ concentration from 1 to 2 mM resulted in higher absorbance values for SA-AgNPs, a decrease in absorbance was observed at 5 mM, indicating a transition point (Appendix B3). However, this trend was not consistent across all samples; bark methanol (SABM-AG) exhibited increased absorption at 5 mM, while bark acetone (SABA-AG) showed a decrease. These varied responses underscore the diverse effects of $AgNO_3$ concentrations on SA-AgNP synthesis across different samples.

The influence of reaction time on SABM-AG/SALM-AG indicated a decrease in the absorption peaks as the incubation time increased (Appendix B4). For 1 mM $AgNO_3$ concentration, SPR peak was observed after 24 hours at 404 and 439 nm on SABM-AG. The peaks became defined as the incubation period increased to month 3 with a peak at a wavelength of 450 nm. The concentrations of 2 and 5 mM had more intense and narrow peaks and the peaks indicated that the AgNPs were formed within an hour. The well-defined SPR peak at 470 was observed after 7 days at both 2- and 5-mM concentrations on the bark methanol sample. SALM-AG samples exhibited absorption peak after 1 hour and remained content till 24 hours (356 nm), thereafter decreasing as reaction time increased.

Ethanol (SABE-AG/SALE-AG) extracts, showing similar trends to those observed with methanol extracts, with SPR, decreased as reaction time increased (Appendix B5). SALE-AG exhibited strong peaks at 370 and 410 nm after 7 days at 1 mM concentration, while peaks at 364 nm were observed after 1 hour for 2- and 5-mM concentrations. Notably, 3rd month showed higher peaks compared to 2nd month 2 and seven days. In contrast, SA-AgNPs produced by bark-water (SABD-AG) extracts, formed after 24 hours with decreasing absorbance over time for 1- and 2-mM concentrations at both 356 and 468 nm (Appendix B6). At a 5 mM $AgNO_3$ concentration, the SPR peak appeared after 1 hour, intensifying by day 7 with peaks at 353, 404, and 485 nm. Leaf water (SALD-AG) samples exhibited no absorption peaks, indicating no AgNP formation at 1- and 2-mM concentrations.

Lastly, the influence of temperature on the synthesis of SA-AgNPs was studied and the findings were presented in Appendix B7, B8, and B9. Results showed that increasing temperature led to heightened SPR peaks. Narrower bands with higher absorbance values were consistently observed at 25°C compared to 4°C across most samples, except for the SABD-AG (1 mM), which exhibited a slightly higher peak at 4°C (Appendix B9).

The UV-Vis analysis of SA-AuNPs, as depicted in Appendix B10, B11, and B12, included only samples exhibiting optimal activity (AuNPs synthesised by 1 mM $HAuCl_4$ and 100 mg/mL extracts for 90 seconds in the microwave). Notably, the SPR bands for various samples. Specifically, sample SABM-AU exhibited an SPR peak at 533 nm, while samples SABE-AU and SABE-AU displayed peaks at 541 nm and 574 nm, respectively. These results confirmed that the synthesis of SA-AuNPs was successful.

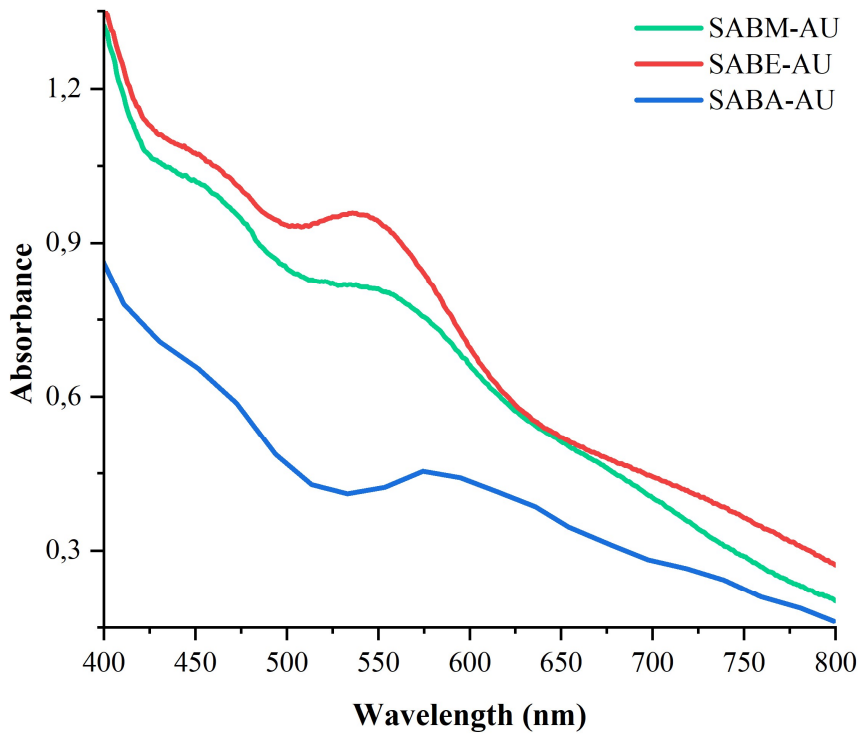

Figure 4.4: Ultraviolet-visible spectra of SA-AuNPs; SABM-AU (bark methanol AuNPs), SABE-AU (bark ethanol AuNPs), SABA-AU (bark acetone AuNPs).

4.3.2 X-ray diffraction unit (XRD) analysis of SA-AgNPs and SA-AuNPs

X-ray diffraction (XRD) spectroscopy was used to characterise the crystallinity and structures of the SA-AgNPs and SA-AuNPs. Four diffraction peaks with 2θ values were observed at 37º, 43º, 63º, and 76º with planes at (111), (200), (220), and (311), respectively (Figure 4.5) for SA-AgNPs samples using Bragg's law. An additional peak at 45° was also observed for sample SAMB-AG, while sample SABE-AG did not display a peak at 2θ angle 43°.

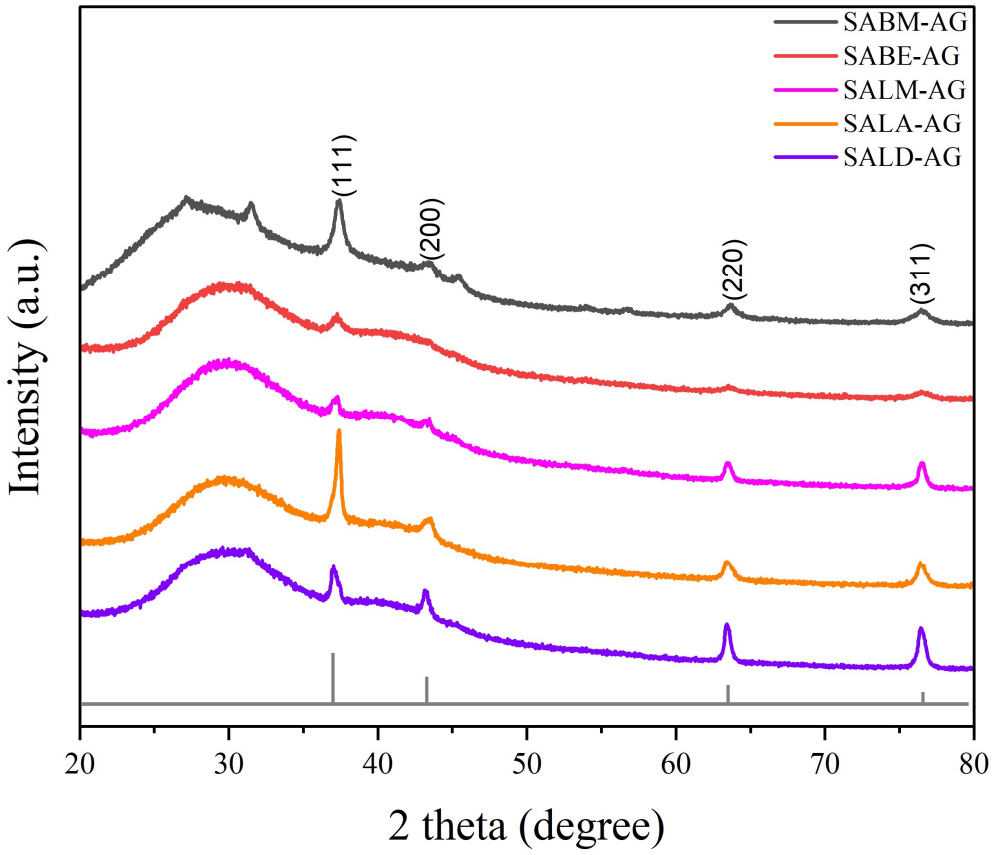

Figure 4.5: XRD spectrum of silver nanoparticles synthesised using *S. africana* extracts bark methanol-AgNPs (SABM-AG), bark ethanol-AgNPs (SABE-AG), leaf methanol-AgNPs (SALM-AG), leaf acetone-AgNPs (SALA-AG), and leaf water-AgNPs (SALD-AG).

The SA-AuNPs samples exhibited similar results to that of SA-AgNPs, with specific samples SABE30S100, SABE60S100, and SABA60S100 lacking peak at an angle of 43° (Figure 4.6). These diffraction indices align with the cubic face-centred (FCC) structure of silver and gold particles as specified by the Joint Committee on Powder Diffraction Standards (JCPDS) (JCPDS 01-1167).

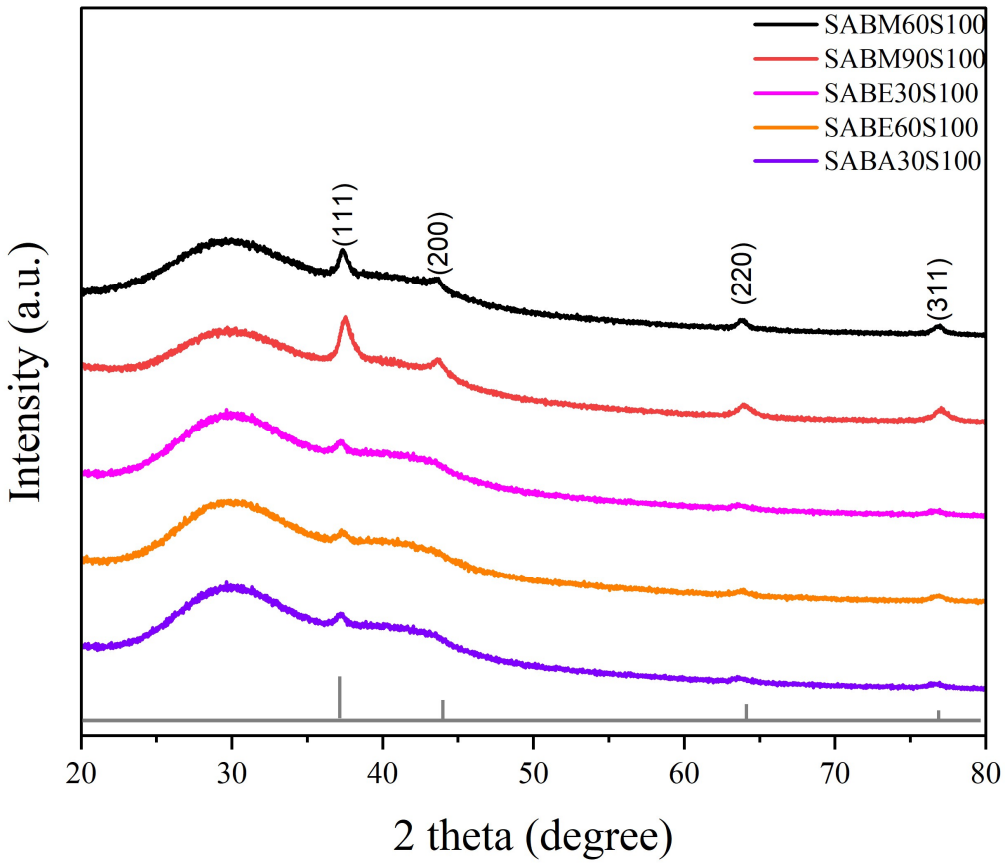

Figure 4.6: XRD spectrum of gold nanoparticles produced using *S. africana* extracts bark methanol-AuNPs at 60 seconds (SABM60S100), bark methanol-AuNPs at 90 seconds (SABM90S100), bark ethanol-AuNPs at 30 seconds (SABE30S90100), bark ethanol-AuNPs at 60 seconds (SABE60S100), and bark acetone-AuNPs at 30 seconds (SABA30S100).

The average crystalline size of SA-AgNPs samples varied across different experimental conditions ranging from 9 to 19 nm. Table 4.1 summarizes the average grain size values. Similarly, the average crystalline size of SA-AuNPs samples ranged from 9 to 10 nm (Table 4.2).

Table 4.1: Average crystalline size of silver nanoparticles (SA-AgNPs**)**

Sample	Average crystalline size (nm)
SABM-AG	9
SABE-AG	10
SALM-AG	19
SALA-AG	14
SALD-AG	14

Notes: SABM-AG= bark methanol conjugated AgNPs, SABE-AG= bark ethanol conjugated AgNP, SALM-AG= leaf methanol conjugated AgNP, SALA-AG= leaf acetone conjugated AgNP, SALD-AG= leaf water conjugated AgNP.

Table 4.2: Average crystalline size of gold nanoparticles (SA-AgNPs)

Sample	Average crystalline size (nm)
SABM60S100	9
SABM90S100	8
SABE30S100	9
SABE60S100	10
SABA30S100	9

Notes: SABM60S100= bark methanol conjugated AuNPs, SABM90S100= bark methanol conjugated AuNPs, SABE30S90100= bark ethanol conjugated AuNPs, SABE60S100= bark ethanol conjugated AuNPs, SABA30S100= bark acetone conjugated AuNPs, 60S/90S/30S= indicates the synthesis time in seconds, and 100= concentration of the plant extracts in mg/mL.

4.3.3 Dynamic light scattering (DLS) particle analysis of SA-AgNPs and SA-AuNPs

Dynamic light scattering (DLS) was utilized to assess the average particle size, particle size distribution and polydispersity index (PDI) of the synthesized silver (SA-AgNPs) and gold nanoparticles (SA-AuNPs). This method captures the dynamic alterations in light scattering intensity due to the Brownian motion of the nanoparticles. The findings revealed that the SA-AgNPs samples SABM-AG, SABE-AG, and SABA-AG average particle size diameters were around 132-409 nm, 994 nm, and 186 nm, respectively, along with corresponding PDI values of 1, 0.318, and 1. The intensity-weighted mean hydrodynamic size (Z-average) ranged from 1514, 1293, and 2511 d.nm for these AgNP samples (Figure 4.7A-C).

Figure 4.7: Dynamic light scattering (DLS) analysis for particle size of synthesised SA-AgNPs. A= SABM-AG (bark methanol conjugated AgNPs), B= SABE-AG (bark ethanol conjugated AgNP), and C= SABA-AG (bark acetone conjugated AgNP). Each sample underwent three runs.

In contrast, the AuNPs samples SABM-AU, SABE-AU, and SABA-AU displayed distinct average particle size distributions of 775 nm, 284 nm, and 1593-5560 nm, with PDI values of 0.253, 1, and 0.548, respectively. Z-average particle size for AuNPs ranged from 745.4 to 3353 d.nm (Figure 4.8A-C). Most of the synthesized AgNPs were polydisperse, except for sample SABE-AG, whereas the majority of AuNPs were monodisperse, except for sample SABE-AU.

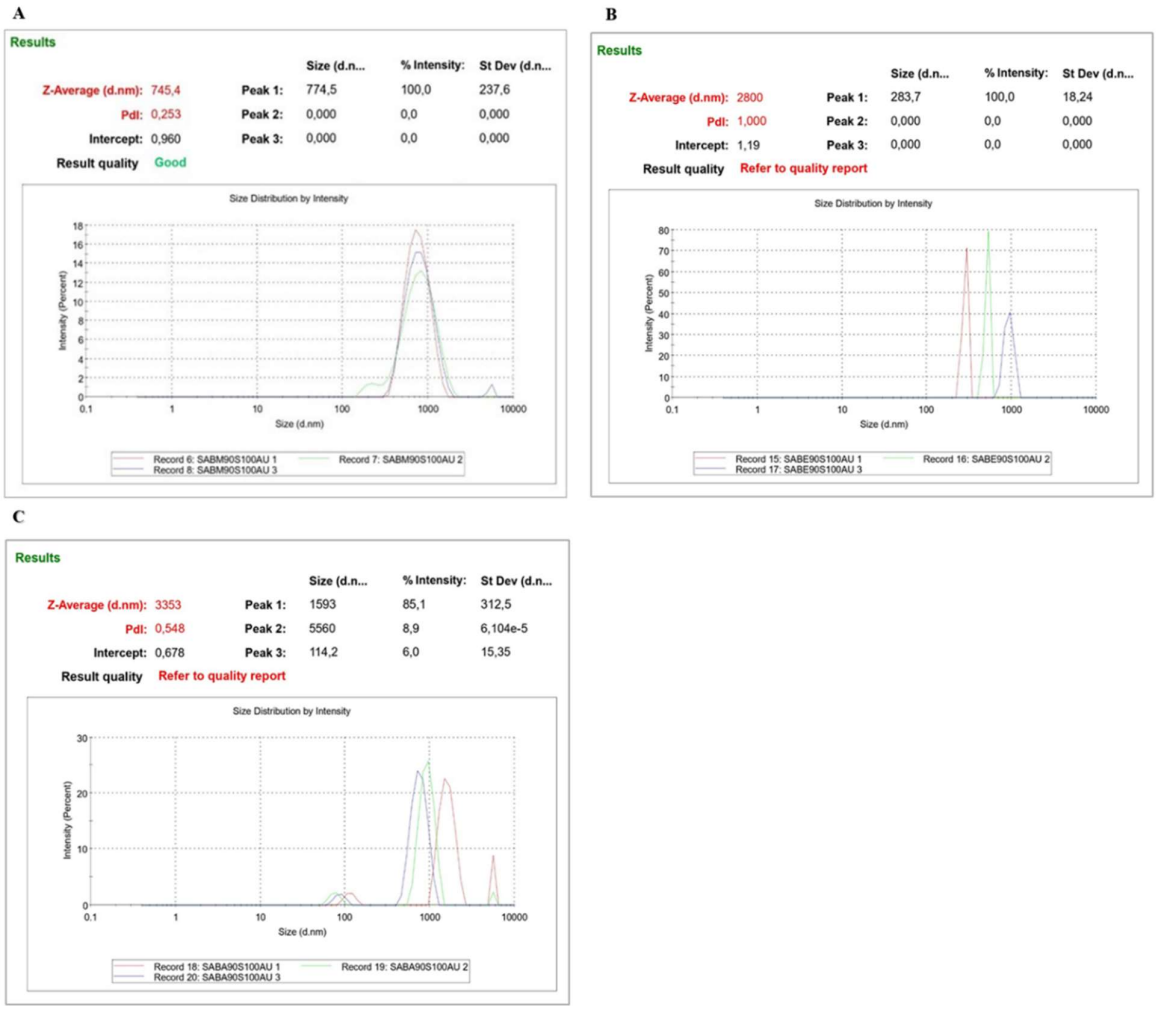

Figure 4.8: Dynamic light scattering (DLS) analysis for particle size of synthesised SA-AuNPs. A= SABM-AU (bark methanol conjugated AuNPs), B= SABE-AU (bark ethanol conjugated AuNP), and C= SABA-AU (bark acetone conjugated AuNP). Each sample underwent three runs.

The colloidal stability of the synthesized nanoparticles was assessed using zeta potential (ZP) measurements. For the SA-AgNPs samples SABM-AG, SABE-AG, and SABA-AG, ZP values were -27.7 mV, -16.5 mV, and -0.79 mV, respectively (Figure 4.9A-C). Similarly, for the SA-AuNPs samples SABM-AU, SABE-AU, and SABA-AU, ZP values were -10.9 mV, -0.822

mV, and -13.7 mV (Figure 4.10A-C). Nanoparticles typically exhibit stability when their ZP values fall within the range of +30 mV to -30 mV (Yadi et al., 2022). Based on this standard and the provided ZP values, it is evident that the SA-AgNPs sample SABM-AG exhibits the highest degree of stability. Conversely, the other nanoparticles, including SA-AuNPs, manifest varying degrees of instability or susceptibility to agglomeration over time.

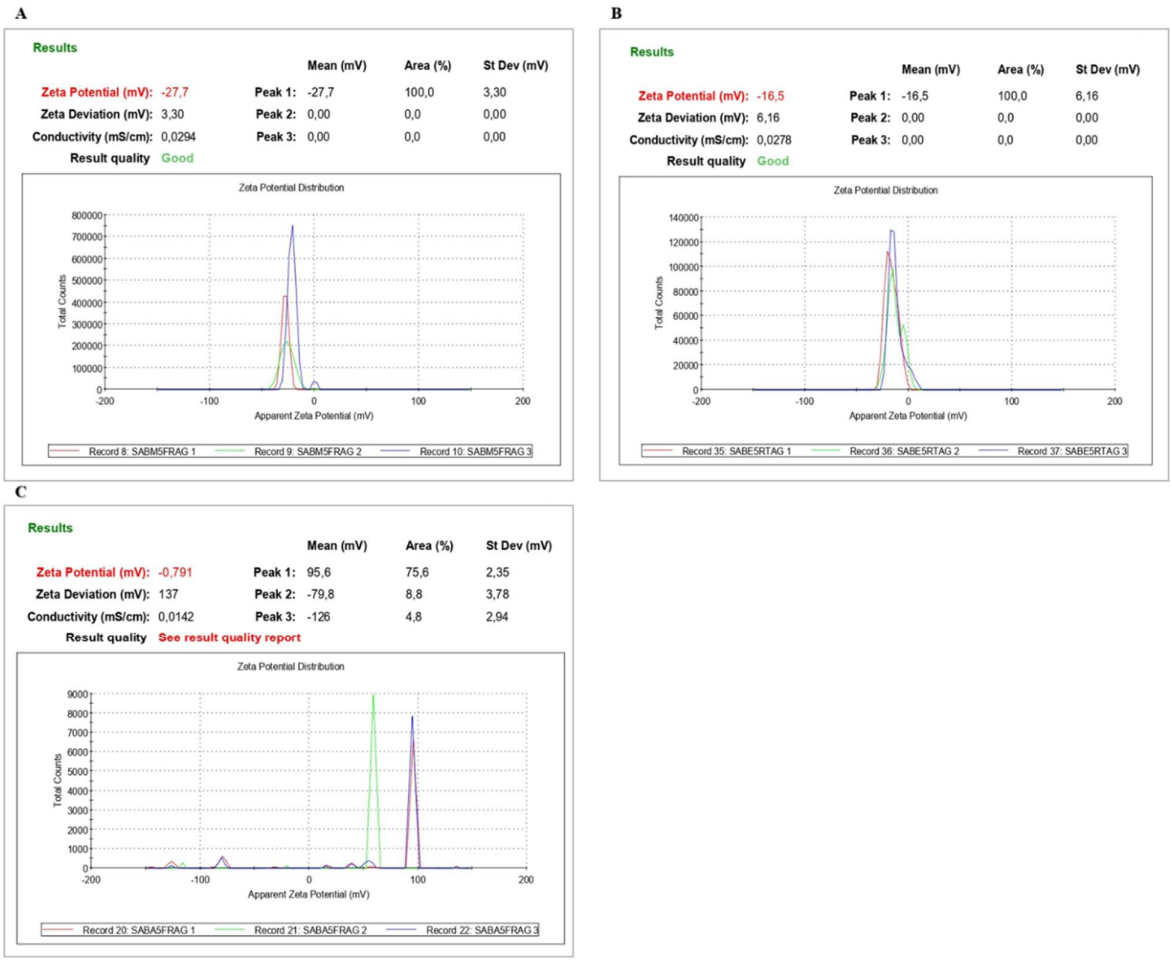

Figure 4.9: Zeta potential (ZP) stability analysis of the produced SA-AgNPs. A= SABM-AG (bark methanol conjugated AgNPs), B= SABE-AG (bark ethanol conjugated AgNP), and C= SABA-AG (bark acetone conjugated AgNP). Each sample was run in triplicates.

Figure 4.10: Zeta potential (ZP) stability analysis of the produced SA-AuNPs. A= SABM-AU (bark methanol conjugated AuNPs), B= SABE-AU (bark ethanol conjugated AuNP), and C= SABA-AU (bark acetone conjugated AuNP). Each sample was run in triplicates.

4.3.4 Transmission electron microscopy (TEM) analysis of SA-AgNPs and SA-AuNPs

Transmission electron microscopy (TEM) was used to investigate the shape and size of SA-AgNPs and SA-AuNPs. Figure 4.11 displays TEM micrograph images of SA-AgNPs at different magnifications (200, 100, and 20 nm), along with their corresponding particle size distribution portrayed in histogram graphs. The TEM analysis revealed diverse morphologies and sizes of both types of NPs. It was observed that SA-AgNPs consisted of smaller particles

predominantly exhibiting spherical shapes, along with larger particles displaying squash-spherical, hexagonal, and irregular forms.

The average core size of SA-AgNPs exhibited significant variation across the different samples. Specifically, the SABM-AG (A-C), SABE-AG (D-F), SABA-AG (G-I), and SALE-AG (J-L) samples showed particle size range of 13 to 53 nm, 4 to 35 nm, 2 to 9 nm, and 5 to 136 nm, respectively. With corresponding average particle size distribution of 23.2 ± 10.2, 17.7 ± 10.2, 5.9 ± 1.9, and 60.4 ± 49.5 nm, indicating a notable diversity in size among the various samples.

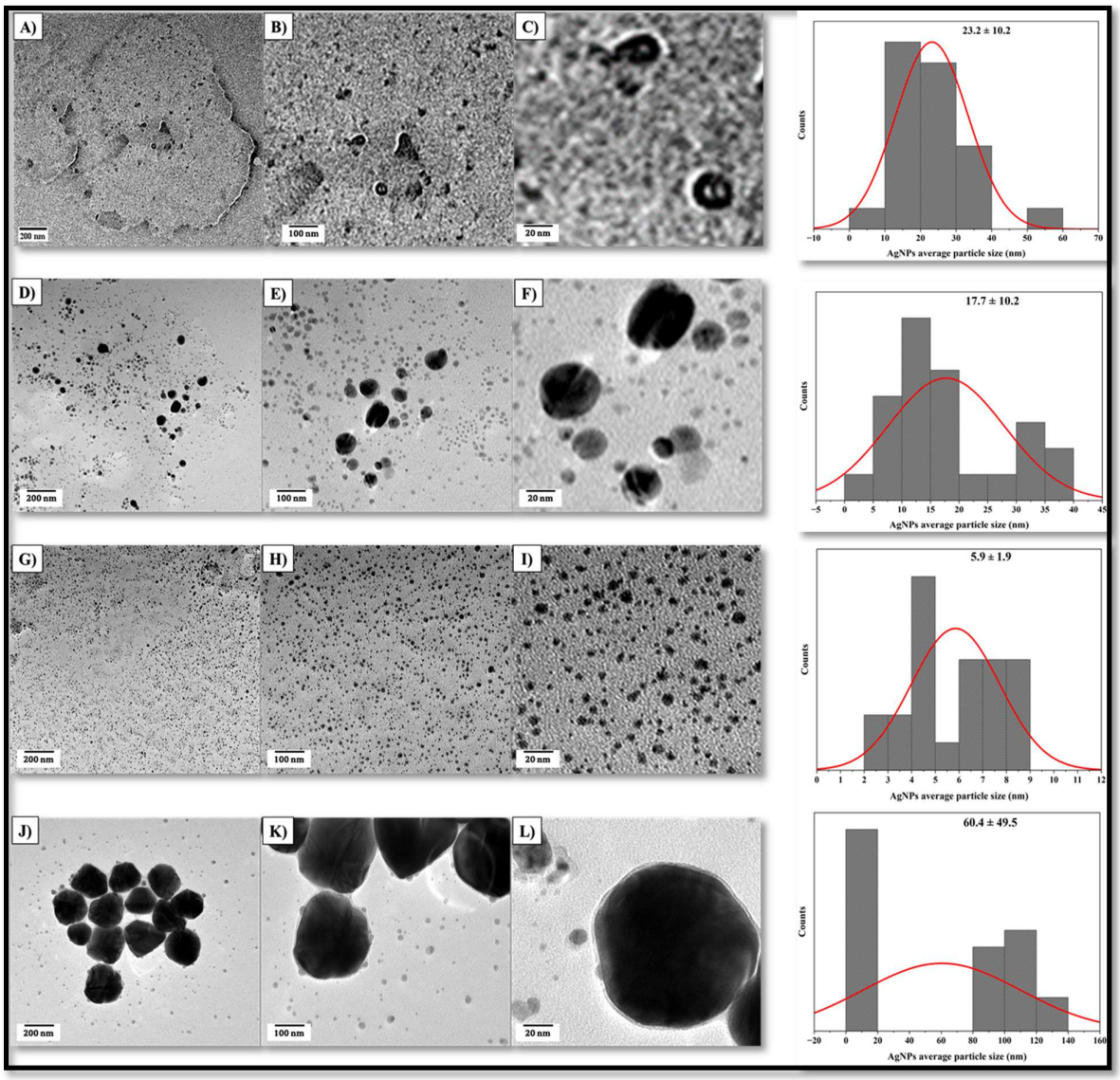

Figure 4.11: The TEM microgram images of various samples of SA-AgNPs at different magnifications (200, 100, and 20 nm) and their corresponding size distributions displayed in histograms. From A-C= SABM-AG (bark methanol conjugated AgNPs), D-F= SABE-AG (bark ethanol conjugated AgNP), G-I= SABA-AG (bark acetone conjugated AgNP), and J-L= SALE-AG (leaf ethanol conjugated AgNP).

Figure 4.12 presents TEM images of SA-AuNPs at magnifications 200, 100, and 20 nm, along with their corresponding particle size distribution shown in the histogram graph. The SA-AuNP (SABE-AU) have demonstrated various shapes such as spheroidal and star-shaped, with a core size range of 6 to 32 nm, and an average particle size distribution of 14.1 ± 6.4 nm.

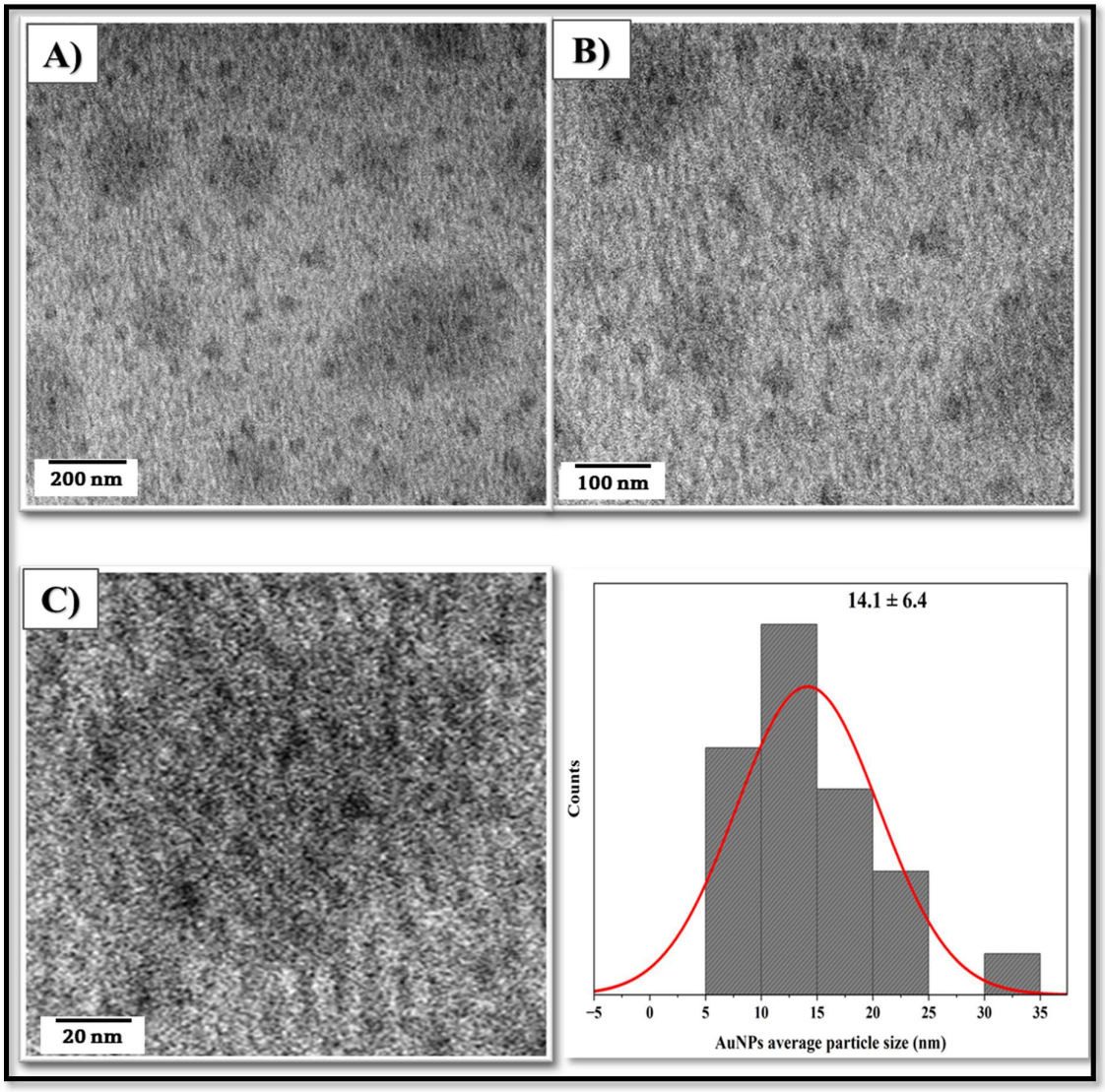

Figure 4.12: TEM micrograph images of SA-AuNPs sample SABE-AU (bark ethanol conjugated AuNP) shown at various magnifications (A= 200 nm, B=100 nm, C= 20 nm) along with their corresponding average particle size distributions.

4.3.5 Fourier-transform infrared spectroscopy (FTIR) analysis of the plant extracts and conjugated nanoparticles.

The FTIR spectral analysis results confirmed the functional groups and chemical compounds present in *S. africana* crude extracts (Figure 4.13). The bark extracts spectral analysis displayed

a broad peak at 3310 cm^{-1}, while leaf extracts had peat at 3301 cm-1, indicating the presence of O-H (hydroxy) groups. A narrow peak was observed at 1632 and 1639 cm^{-1} for bark and leaf, respectively, suggesting C=C stretching (alkenes) or N-H (amide) groups. Both extracts exhibited absorption peaks at 1011 cm^{-1}, which indicates C-O stretching (alcohols). Moreover, absorption at 950 cm^{-1} was also seen and is associated with C-H (aromatic) in-plane bending (Devi and Sathishkumar, 2017; Senthilkumar et al., 2018; Nandiyanto et al., 2019; Mickymaray, 2019; Wongsa et al., 2022).

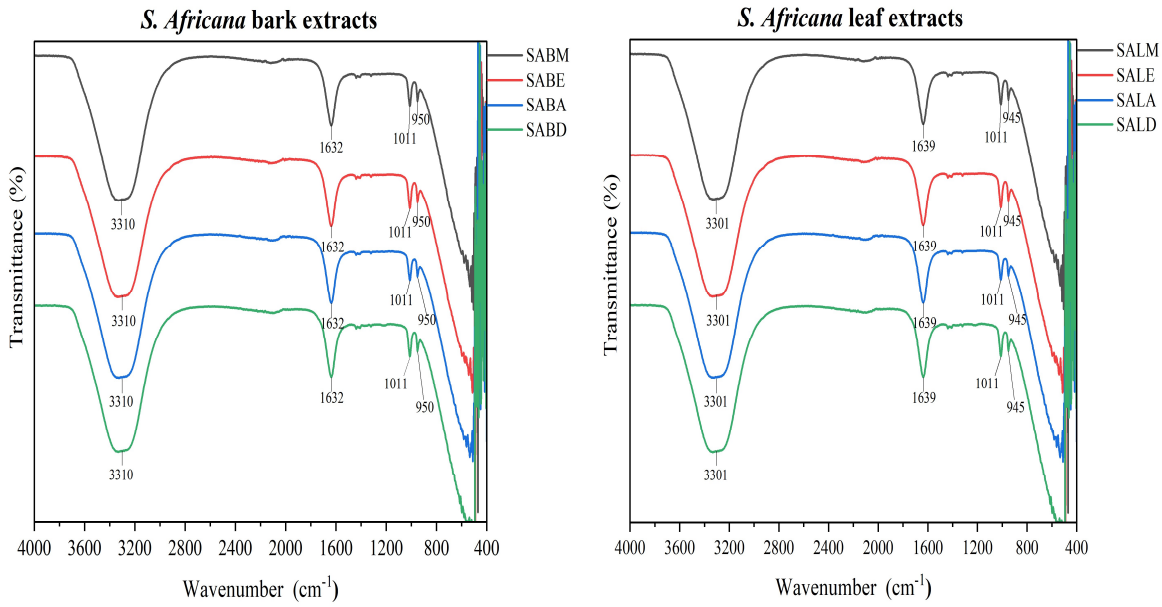

Figure 4.13: Fourier-transform infrared (FTIR) spectra for *S. Africana* crude extracts: bark methanol (SABM), bark ethanol (SABE), bark acetone (SABA), bark water (SABD), leaf methanol (SABM), leaf ethanol (SABE), leaf acetone (SABA), leaf water (SABD.

FTIR analysis of both SA-AgNPs and SA-AuNPs displayed similar results to those of the extracts, albeit with minor shifts in absorption bands. For this technique, samples with the best antimicrobial activity were presented in Figure 4.14. The results indicate the presence of functional groups such as hydroxyl (O-H), alkenes' C=C stretching or amide groups' N-H

stretch, alcohols' C-O stretch, and hydrocarbons' C-H stretch. Figures 4.14A-B depict SA-AgNP samples, while Figures 4.14C-E represent SA-AuNP samples.

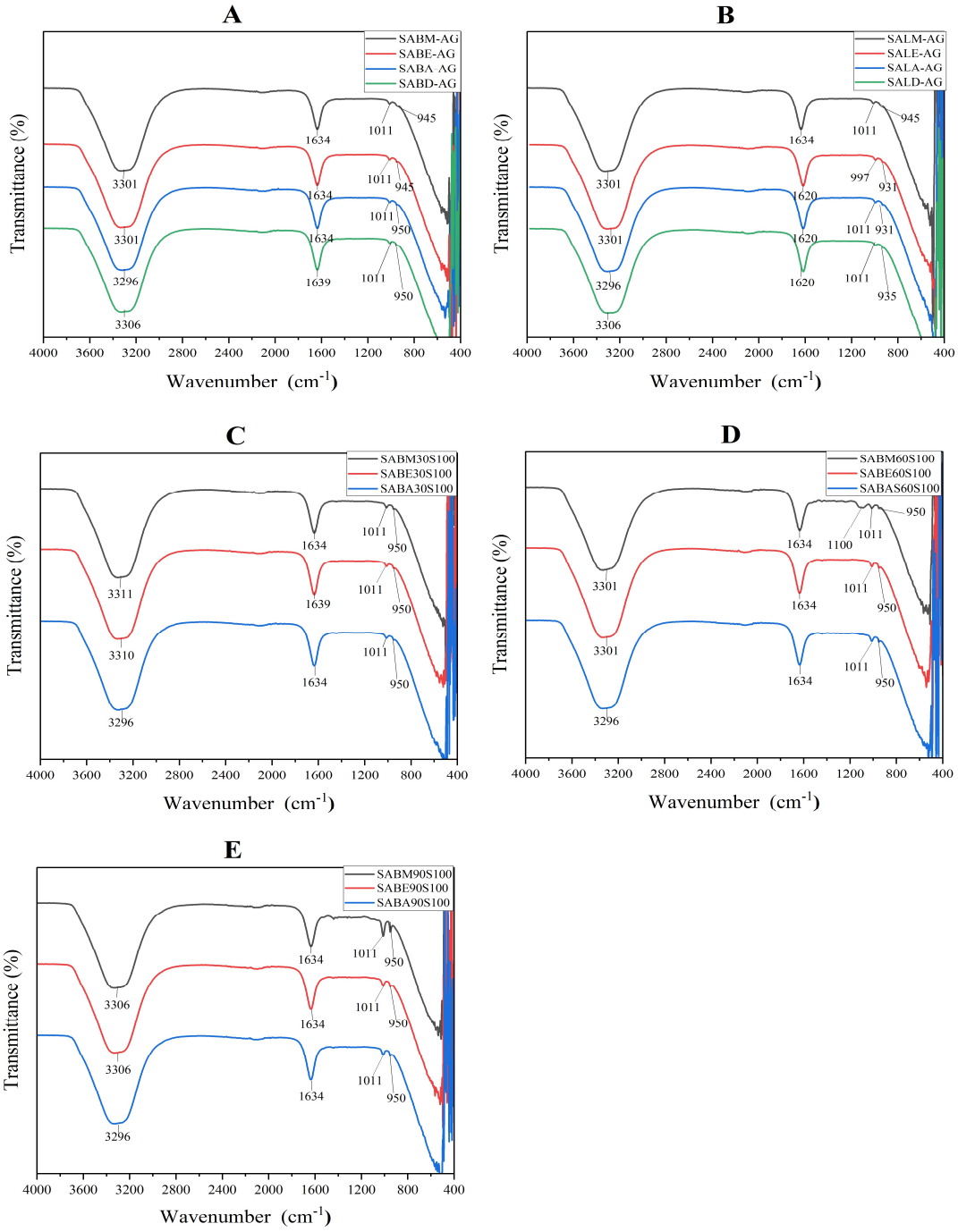

Figure 4.14: Fourier-transform infrared (FTIR) for SA-AgNPs and SA-AuNPs; SA-AgNPs produced by *S. africana* bark (A) and leaf (B) extracts at room temperature. SA-AuNPs

produced by *S. africana* bark extracts using microwave at reaction times 30 seconds (C), 60 seconds (D), and 90 seconds (E).

4.3.6 Liquid chromatography-mass spectroscopy (LC-MS) analysis of *S. africana* extracts

The LC-MS analysis of *S. africana* extracts was conducted in negative ion modes to identify phyto-compounds with biological activities such as antimicrobial, antioxidant, anti-inflammatory etc., based on their retention time and m/z ratio. The GNPS library was employed for the identification of potential compounds. The results revealed 23 bioactive compounds, each belonging to Flavonoids, Phenolic acids, Phenols, Tannins, Glycosphingolipids, Phospholipids, Terpenoids, Flavonoid glycosides, Ellagitannin, and Polyphenols. The analysis of phytochemical classes shows the presence of a diverse array of bioactive compounds within the samples. The findings are meticulously detailed in Table 4.3 and in Figure 4.15.

Table 4.3. Phytochemical compounds of *S. africana* extracts identified by LC-MS with their biological activities.

$[M-H]^-$ m/z	Rt (min, sec)	Molecular formula	Compound name	Class	Biological activity	Reference
305.136	3.380109	$C_{22}H_{18}O_{11}$	Gallocatechin - 30eV	Flavonoids	Antioxidant, antimicrobial, anti-inflammatory, and anticancer	Bae et al., 2020
609.161	8.591304	$C_{27}H_{30}O_{16}$	Rutin	Flavonoids	Antioxidant, anticancer, antimicrobial, anti-inflammatory, anti-diabetic, anti-arthritic,	Negahdari et al., 2021

					anti-allergic, and wound healing	
482.37	7.094063	$C_{20}H_{20}O_{14}$	[3,4,5-trihydroxy-6-(3,4,5-trihydroxybenzoyl)oxyoxan-2-yl]methyl 3,4,5-trihydroxybenzoate	Phenolic acids	Antioxidant, anti-inflammatory, antimutagenic, antimicrobial, antidiarrheal, and wound healing properties	Gomes et al., 2021
585.165	9.65913	$C_{15}H_{13}O_{11}$	Quercetin-O-(O-galloyl)-pentoside	Flavonoids	Anticancer, antioxidant, antibacterial, anti-inflammatory, anti-Alzheimer, antifungal, antiviral, anti-thalassemia, iron chelation, antiobesity, antidiabetic, antihypertension, and anti phospholipase A2 (PLA2) activities,	Alizadeh and Ebrahimzadeh, 2022
293.183	11.26365	$C_{17}H_{26}O_4$	6-Gingerol CollisionEnergy:205060	Phenols	anti-inflammation, antioxidant, and antitumor enhancing effect	Adetuyi, B.O. and Farombi, E.O., 2021.
895.216	9.199367	$C_{21}H_{20}O_{11}$	quercitrin	Flavonoids	antioxidant, anticancer,	David et al., 2016

					anti-inflammatory, and antiviral activities.	
951.076	7.16117	$C_{41}H_{28}O_{27}$	Geraniin	Tannins	antihypertensive, vasodilator effects, antiobesity, antihypercholesterolemic and antiatherosclerotic	Alizadeh and Ebrahimzadeh, 2022
635.109	6.814242	$C_{27}H_{24}O_{18}$	1,3,6-tri-O-galloylglucose	Tannins	Antioxidant, anti-inflammatory, and anti-tumor effects	Choi et al., 2019
712.556	14.23125	$C_{40}H_{75}NO_9$	Soyacerebroside I	Glycosphingolipids	anti-inflammatory, and antiviral activities.	Chiu et al., 2016
463.095	8.928814	$C_{21}H_{20}O_{12}$	Spiraeoside	Flavonoids	Anticancer	Nile et al., 2021
431.179	10.25675	$C_{21}H_{20}O_{10}$	afzelin	Flavonoids	Anticancer, antioxidant, anticholinergic, antidiabetic and antiglaucoma activities Antimicrobial	Durmaz et al., 2023
355.069	4.593492	$C_{16}H_{18}O_9$	5-caffeoylquinic acid	Phenolic acid	antioxidant, anti-inflammatory anticancer, antidiabetic, antibacterial, neuroprotecti	Mediani et al., 2023

					ve, and cardioprotective.	
480.097	9.07445	$C_{21}H_{20}O_{13}$	5,7-dihydroxy-3-[(2S,3R,4S,5R,6R)-3,4,5-trihydroxy-6-(hydroxymethyl)oxan-2-yl]oxy-2-(3,4,5-trihydroxyphenyl)chromen-4-one	Flavonoid	Antioxidant, anti-inflammatory, anti-cancer, neuroprotective, hepatoprotective, anti-obesity, anti-diabetic, anti-microbial, anti-viral, anti-hypertensive, anti-atherosclerotic, anti-aging, anti-angiogenic, and anti-mutagenic activities	Bajkoet al., 2016
289.079	5.567601	$C_{15}H_{14}O_6$	(-)-epicatechin	Flavonoid	Antioxidant, anti-inflammatory, anti-cancer, anti-diabetic, anti-microbial, and anti-viral activities.	Negahdari et al., 2021
473.105	4.664792	$C_{12}H_{16}O_4$	Triterpenoid, Olivetoric acid	Terpenoid	Antioxidant, anti-inflammatory, anti-cancer, anti-diabetic, anti-microbial,	Prakash et al., 2019

					and anti-viral activities.	
577.36	5.383894	$C_{30}H_{26}O_{12}$	Procyanidin B1	Flavonoid	Anti-inflammatory, anti-cancer, and anti-microbial activities.	Emsen et al., 2021
433.097	9.133299	$C_{20}H_{18}O_{11}$	Guajavarin	Flavonoid glycoside	Antioxidant, anti-inflammatory, anti-cancer, anti-diabetic, anti-microbial, and anti-viral activities.	Prabu et al., 2006
625.156	8.319383	$C_{28}H_{32}O_{16}$	Isorhamnetin-3-O-galactoside-6-rhamnoside	Flavonoid glycoside	Antioxidant, anti-inflammatory, anti-cancer, anti-diabetic, anti-microbial, and anti-viral activities.	Kim et al., 2013
865.22	5.165607	$C_{45}H_{38}O_{18}$	Procyanidin trimer	Flavonoid	Antioxidant, anti-inflammatory, anti-cancer, anti-diabetic, anti-microbial, and anti-viral activities.	Valencia-Hernandez et al., 2021
633.12	6.757082	$C_{27}H_{22}O_{18}$	Corilagin	Ellagitannin	Antioxidant, anti-inflammatory, anti-	Li Xuan et al., 2018

					cancer, anti-diabetic, hepatoprotective, and anti-microbial activities.	
939.135	7.470806	$C_{41}H_{32}O_{26}$	Beta-penta-O-galloyl-glucose	Polyphenol	Antioxidant, anti-inflammatory, anti-cancer, anti-diabetic, anti-microbial, and anti-viral activities.	Wen et al., 2023
302.01	9.306607	$C_{14}H_6O_8$	Ellagic acid	Polyphenol	Antioxidant, anti-inflammatory, anti-cancer, anti-diabetic, anti-microbial, and anti-viral activities.	Al-Harbi et al., 2021
343.204	2.284632	$C_{14}H_{16}O_{10}$	Theogallin	Flavonoid	Antioxidant, anti-inflammatory, anti-cancer, anti-diabetic, anti-microbial, and anti-viral activities.	Karwowska et al., 2023

Flavonoids, including rutin, quercetin-O-(O-galloyl)-pentoside, quercitrin, spiraeoside, afzelin, hyperoside, isorhamnetin-3-O-galactoside-6"-rhamnoside, procyanidin trimer, NCGC00385721-01, ellagic acid, and theogallin, were prominently detected. Furthermore,

phenolic acids, represented by [3,4,5-trihydroxy-6-(3,4,5-trihydroxybenzoyl)oxyoxan-2-yl]methyl 3,4,5-trihydroxybenzoate, were identified. Additionally, phenols like 6-gingerol, tannins such as geraniin and 1,3,6-tri-O-galloylglucose, glycosphingolipids like soyacerebroside I, phospholipids including 1-palmitoyl-2-linoleoyl-sn-glycero-3-phospho-(1'-rac-glycerol), triterpenoids such as olivetoric acid, ellagitannin like corilagin, and polyphenols such as beta-penta-O-galloyl-glucose were also observed.

The experimental LC-MS chromatograms of *S. africana* displayed more peaks in methanol extracts compared to other solvents, as depicted in Figure 4.15. This observation suggests that methanol extraction yields a higher diversity of compounds from the plant material. Furthermore, the chromatogram highlights the dominancy of flavonoids, which is evident from their prominent retention times.

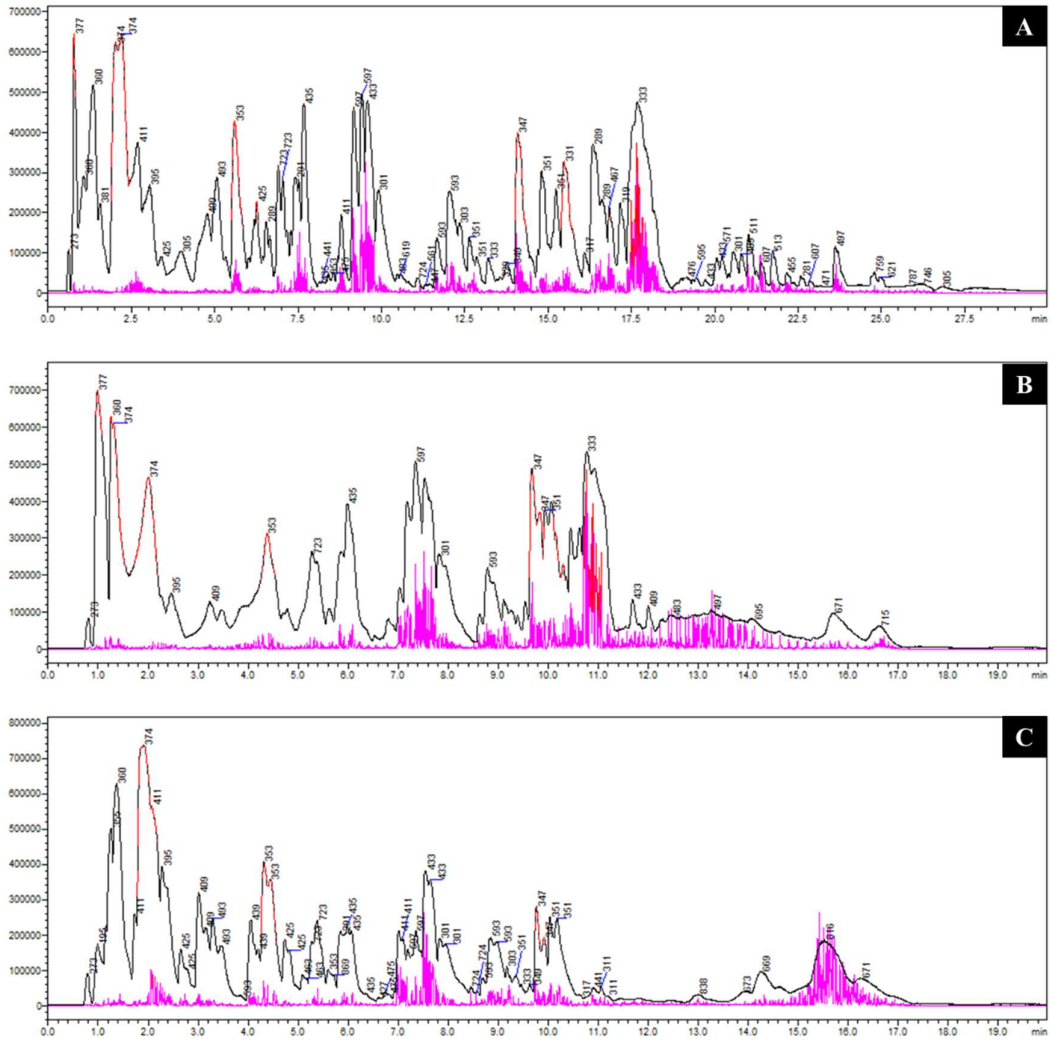

Figure 4.15: The LC-MS chromatograms of *S. africana* (A) methanol extracts, (B) ethanol extracts, and distilled water extracts (C) obtained using three different solvents.

4.4 Antimicrobial activity of *S. africana* extracts and nanoparticles

The antimicrobial activities of *S. africana* crude extracts and their synthesised SA-AgNPs/SA-AuNPs were tested against the WHO priority bacterial pathogens (*A. baumannii*, *P. aeruginosa*, *E. coli*, and *S. aureus*) of ABR, responsible for RTIs. The antimicrobial efficacy was tested via agar-well and microdilution methods. For the crude extracts and SA-AgNPs, the effectiveness and stability were assessed for three months, and the results presented with

Experiment 1 corresponded to the activity exhibited in the first month, Experiment 2 in the second month, and Experiment 3 in the third month. Meanwhile, for SA-AuNPs results were done only for three trials, because SA-AuNPs samples had the lowest activity, even when the synthesis process had been optimised with different $HAuCl_4$ concentration, temperature, and plant extracts concentrations, better activity was only seen after increasing the concentration of the plant extracts and employing microwave for the synthesis.

4.4.1 Agar well-diffusion assay

There was a significant difference in the antimicrobial activity of the *S. africana* extracts compared to the positive control ($p=0.0395$), suggesting their potential as effective antimicrobial agents. Agar-well diffusion assay results revealed that *S. africana* plant extracts acted as antimicrobial agents all bacteria (Figure 4.16). Antimicrobial activity by agar-well assay was in contrast with that obtained by the microdilution methods because the plant extracts were more active against *P. aeruginosa*, followed by *A. baumannii*, *S. aureus* and *E. coli.* The highest inhibition effect was observed from sample SABM (24 mm) extract against *P. aeruginosa* for both Experiment 1 and 2, followed by SALE with zone of inhibition diameter of 19 mm on both *S. aureus* and *A. baumannii*.

All the bark extracts had 0 mm inhibition zones on *E. coli*, except for the leaf extracts, which had a high inhibition effect at sample SALM (18 mm). Sample SALD (0 mm) was not active against all three tested bacteria except for *S. aureus*. An increase in antimicrobial activity of the extracts as their incubation period increases was also observed. However, leaf extracts against *A. baumannii* and bark extracts against *S. aureus* had higher activity during Experiment 1(first month), and the inhibition activity dropped as time goes (Experiments 2 and 3).

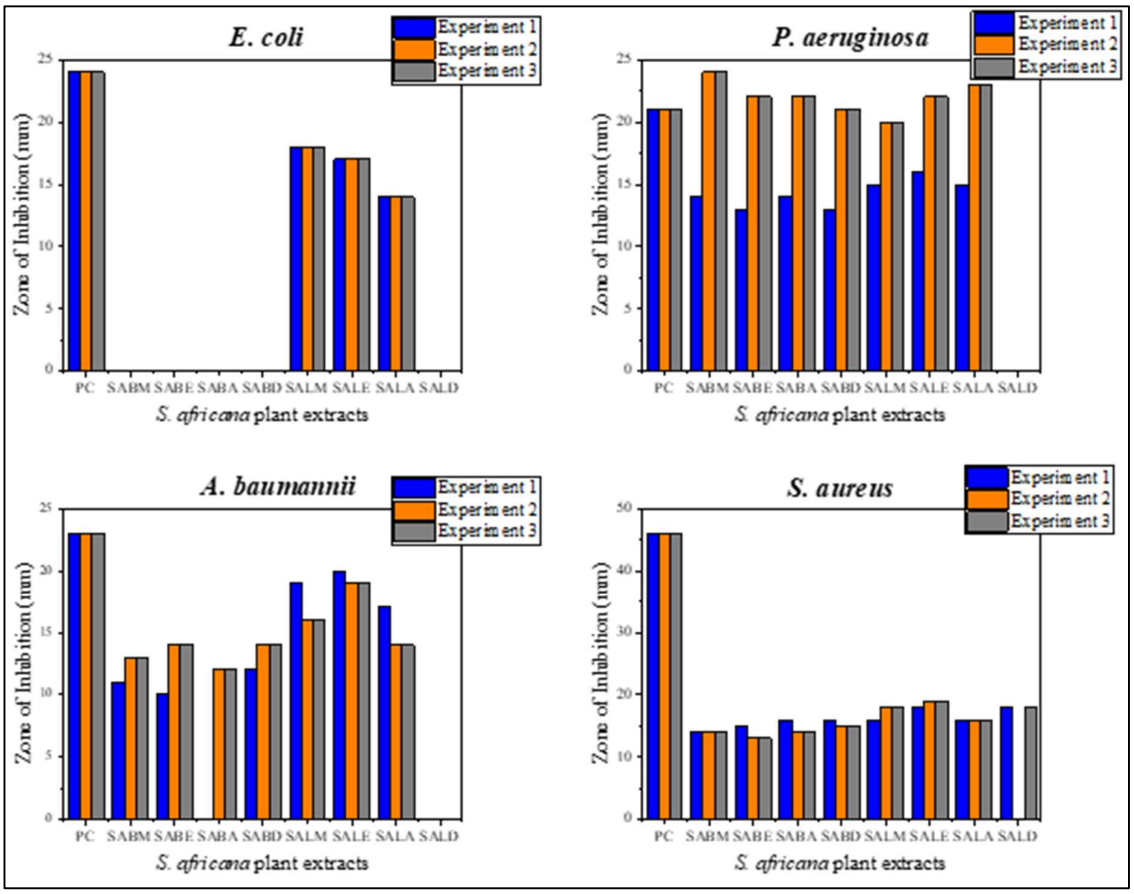

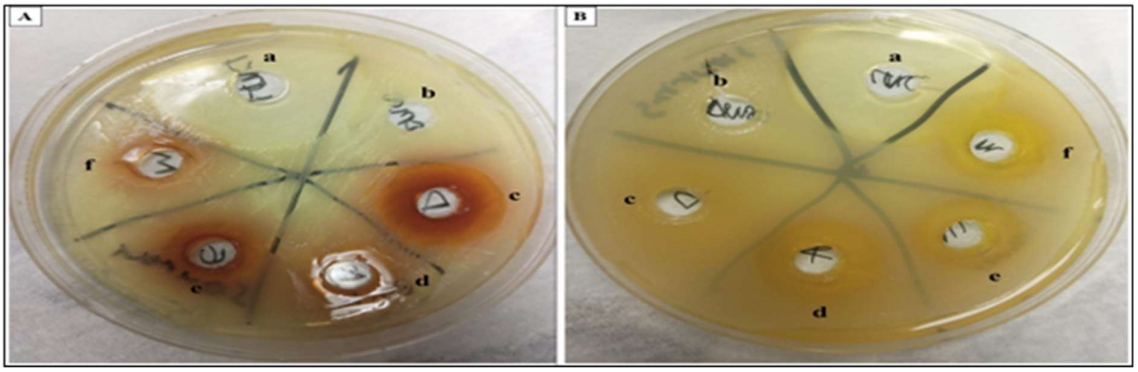

Figure 4.16: Zone of inhibition (mm) of *S. africana* plant extracts (10 mg/mL) against selected bacteria. PC= positive control (Lomefloxacin hydrochloride), SABM= bark methanol, SABE= bark ethanol, SABA= bark acetone, SABD= bark water, SABM= leaf methanol, SABE= leaf ethanol, SABA= leaf acetone, SABD= leaf water. A= bark extracts against *S. aureus*, B= leaf extracts against *S. aureus*, a= positive control, b= negative control (10% Dimethyl sulfoxide),

c= water extracts, d= acetone extracts, e= ethanol extracts, f= methanol extracts (One-way ANOVA, Tukey's post hoc test, $p<0.05$).

The overall results for SA-AgNPs are illustrated in Figure 4.17, showcasing the zone of inhibition in both a bar graph on the left and agar plates on the right. Among the tested strains, the SA-AgNPs exhibited greater efficacy against *P. aeruginosa*, followed by *S. aureus* and *A. baumannii*, and demonstrated relatively less activity against *E. coli*. Notably, samples SABA-AG and SALA-AG displayed the highest inhibition activity, achieving a substantial 22 mm diameter against *P. aeruginosa*. Furthermore, SABA-AG exhibited higher activity against *S. aureus*, with a 21 mm diameter zone of inhibition. In the case of *A. baumannii*, SALA-AG demonstrated greater effectiveness with an inhibition diameter of 18 mm, while *E. coli* proved more susceptible to SALM, displaying an 18 mm inhibition diameter. The findings were statistically significant, with a p-value of 0.0346, indicating a notable difference in the antimicrobial activity of SA-AgNPs compared to the positive control.

Conversely, SABD-AG exhibited lower activity, showing no inhibition against *E. coli* and minimal activity against *P. aeruginosa* and *S. aureus*. Additionally, SALE-AG displayed lower activity, particularly against *A. baumannii*. Overall, these findings highlight the varying degrees of antimicrobial activity observed among the tested samples, with SABA-AG and SALA-AG emerging as the most potent against the tested bacterial strains.

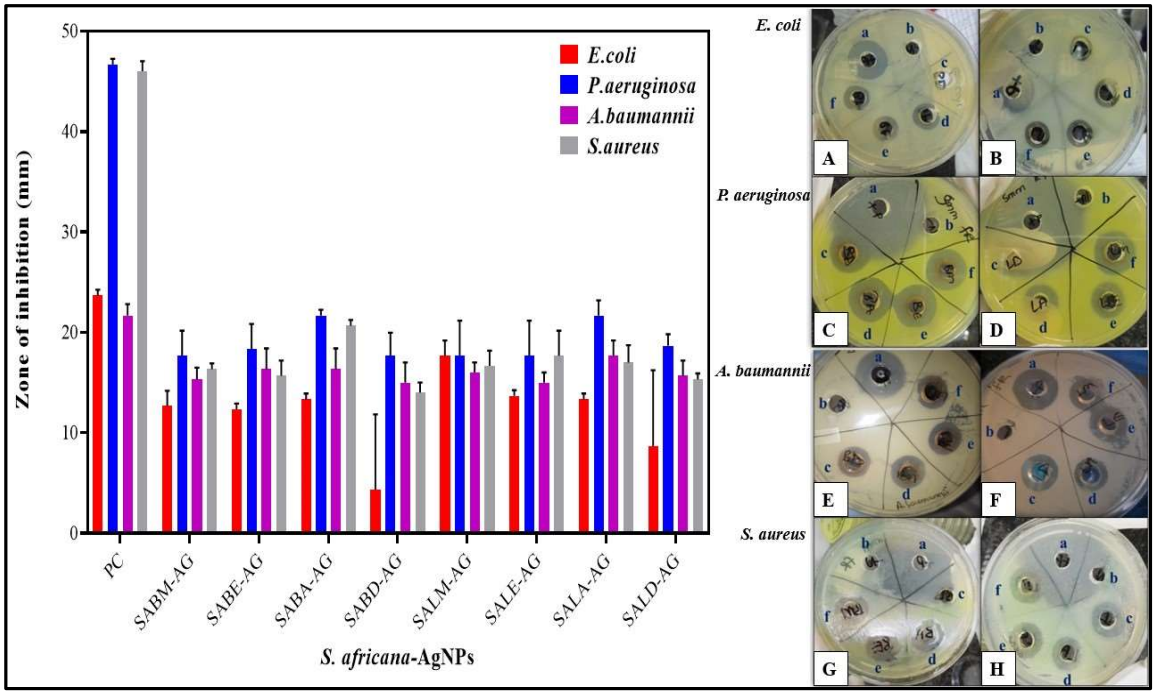

Figure 4.17: Antimicrobial activity SA-AgNPs (2.68 mg/mL) by zone of inhibition (mm) against *E. coli* (A-B), *P. aeruginosa* (C-D), *A. baumannii* (E-F), and *S. aureus* (G-H). SA-AgNPs synthesised by bark methanol (SABM-AG), bark ethanol (SABE-AG), bark acetone (SABA-AG), and bark water (SABD-AG) extracts. SA-AgNPs synthesised by leaf methanol (SALM-AG), leaf ethanol (SABE-AG), leaf acetone (SABA-AG), and leaf water (SALD-AG), PC is positive control (Lomefloxacin hydrochloride). One-way ANOVA followed by Tukey's post hoc test, $p<0.05$.

Antimicrobial activity of SA-AuNPs samples generally demonstrated lower activity compared to SA-AgNPs. However, it was notable that SA-AuNPs exhibited higher efficacy against *S. aureus*, followed by *P. aeruginosa*, with the lowest activity observed against *A. baumannii*. *E. coli* showed resistance to SA-AuNPs, as there was no inhibition observed.

The most significant activity was observed in samples SABM90S100 and SABE90S100, both showing a zone inhibition diameter of 25 mm against *S. aureus*. SABE90S100 is also seen to

have the highest activity against *P. aeruginosa* (16 mm). The difference in antimicrobial activity between SA-AuNPs and the positive control was statistically significant (p=0.0011), suggesting the potential of SA-AuNPs as antimicrobial agents. In contrast, lower activity was observed against *A. baumannii*, and none of the samples were effective against *E. coli*. The results are displayed in Figure 4.18.

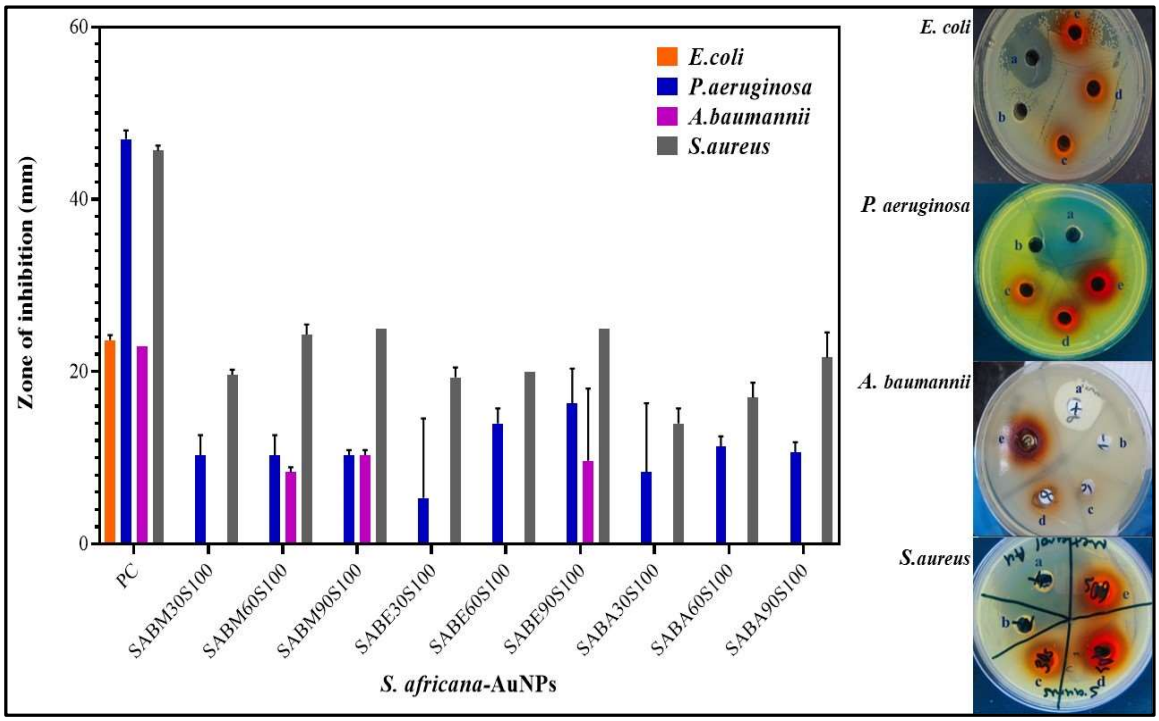

Figure 4.18: Antimicrobial activity of SA-AuNPs (10.14 mg/mL) against *E. coli*, *P. aeruginosa*, *A. baumannii*, and *S. aureus*, shown by the zone of inhibition (mm). SA-AuNPs synthesised by bark methanol-AuNPs for 30 seconds (SABM30S100), 60 seconds (SABM60S100), 90 seconds (SABM90S100), ethanol-AuNPs for 30 seconds (SABE30S100), 60 seconds (SABE60S90100), 90 seconds (SABE90S90100), and acetone-AuNPs for 30 seconds (SABA30S100), 60 seconds (SABA60S100) and 90 seconds (SABA90S100). PC is the positive control (Lomefloxacin hydrochloride) (One-way ANOVA, Tukey's post hoc test, $p<0.05$).

4.4.2 Microdilution assay

The microdilution assay evaluated the MIC of *S. africana* for three months. In general, inhibition activity was consistently increased over time for all extracts against all tested bacteria, with *S. aureus* being the most susceptible, followed by *E. coli*, *A. baumannii*, and *P. aeruginosa* (Figure 4.19). However, no statistically significant effect was observed for the *S. africana* extracts compared to the positive control (p=0.1214), indicating that the antimicrobial properties of the extracts may not be strong enough to warrant further investigation as effective agents against the tested bacteria.

In Experiment 1, SALA extract was the most active against *S. aureus,* with MIC value of 2.5 mg/mL. However, SALM, SALE, and SALA had lower inhibition effects against *E. coli* and *A. baumannii* with MIC values of 5 mg/mL and 10 mg/mL, respectively. Bark extracts were not active against these two bacterial strains. Additionally, *P. aeruginosa* was resistant to almost all the extracts except for SABD extract with the MIC of 10 mg/mL.

During Experiment 2; the sample with the highest antimicrobial activity was *S. africana* leaf-ethanol (SALE) extracts with an inhibition concentration of 1.25 mg/mL against *S. aureus*. An inhibition effect was also seen on SABM, SABE, SABA, SALM, and SALE against *E. coli* with the same MIC value of 5 mg/mL. The results displayed an increased inhibition activity on *A. baumannii* produced by SABM, SABE and SABA with MIC value of 5 mg/mL. On the contrary, all plant extracts were ineffective against *P. aeruginosa*. The samples SABD and SALD extracts had no activity against all tested bacteria.

Lastly, the results of Experiment 3 show the best antimicrobial activity at SALM and SALE plant extracts with the lowest MIC of 1.25 mg/mL against *S. aureus*. Followed by SABM, SABE, SALM and SALE with good inhibition activity for *E. coli* at MIC value of 2.5 mg/mL.

Despite increased extract activity as time progressed, a lower activity was observed against *A. baumannii* at SALM, SALE, and SALA with the MIC of 10 mg/mL. Notably, SALD extract consistently exhibited no activity against all bacterial strains, except for *P. aeruginosa*, which showed sensitivity with the lowest MIC of 1.25 mg/mL.

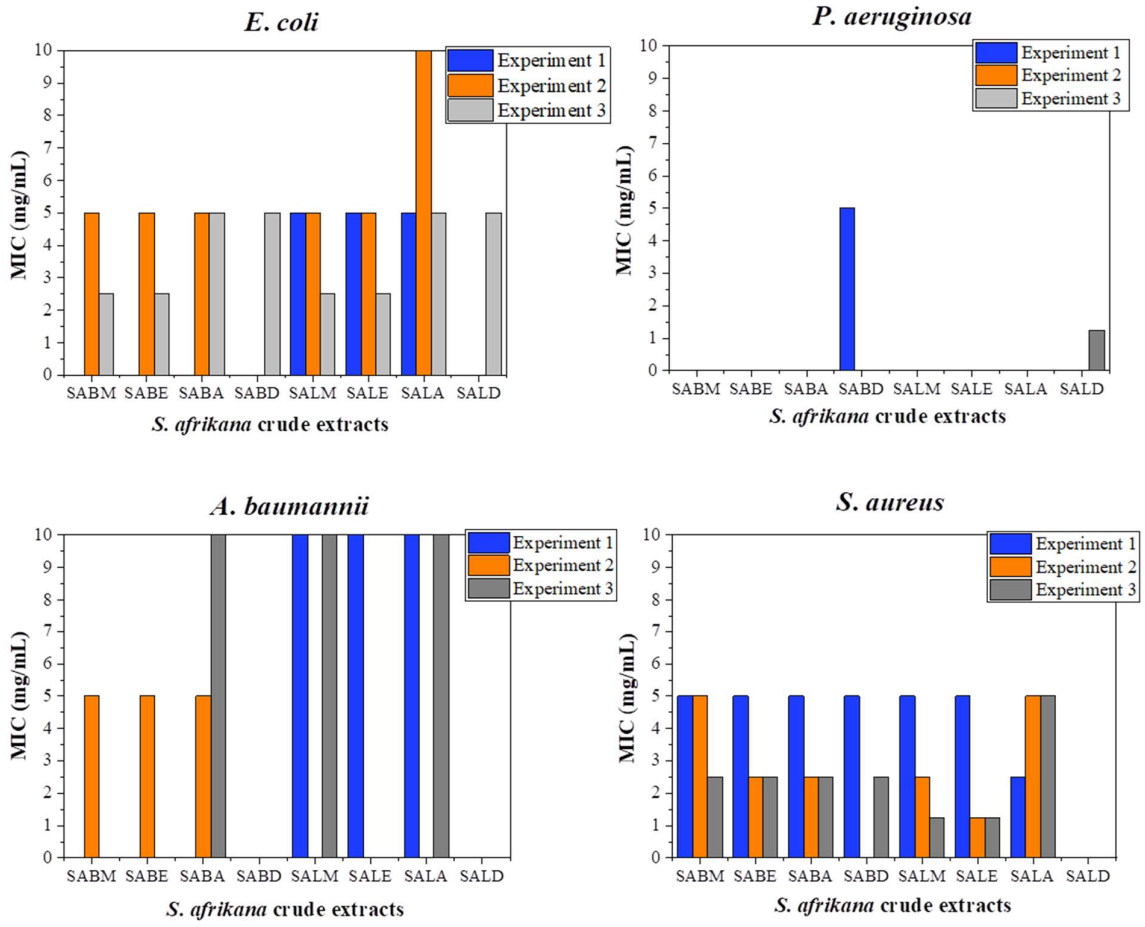

Figure 4.19: Minimum Inhibitory Concentration (MIC) in mg/mL of *S. africana* plant extracts. SABM (bark methanol), SABE (bark ethanol), SABA (bark acetone), SABD (bark distilled water), SALM (leaf methanol), SALE (leaf ethanol), SALA (leaf acetone), SALD (leaf distilled water), Experiment 1 (1st month), Experiment 2 (2nd month), Experiment 3 (3rd month) (One-way ANOVA, Tukey's post hoc test, $p>0.05$).

The MIC results from SA-AgNPs highlighted varying levels of activity among the samples against tested bacterial strains (Figure 4.20 and Figure 4.21). The SA-AgNPs activity was statistical significant when compared to the control (p=0.0287), indicating that their antimicrobial effects are likely reliable. Generally, *E. coli* was found to be the most susceptible to SA-AgNPs samples. Notably, SABM-AG, SABE-AG, and SALM-AG exhibited the lowest MIC value of 0.05 mg/mL against *E. coli*. SALM-AG also demonstrated a MIC of 0.05 mg/mL against *P. aeruginosa*, while SABE-AG displayed a MIC of 0.05 mg/mL against *A. baumannii*. Additionally, SABA-AG showed a MIC of 0.09 mg/mL against *S. aureus*. Conversely, SABD-AG and SALD-AG displayed the least activity against bacterial strains, particularly SALD-AG with MIC values of 0.67 mg/mL against *S. aureus* and *A. baumannii*. These results emphasise the differential antimicrobial efficacy of the samples, with some exhibiting potent inhibitory effects while others showed limited activity against certain bacterial strains.

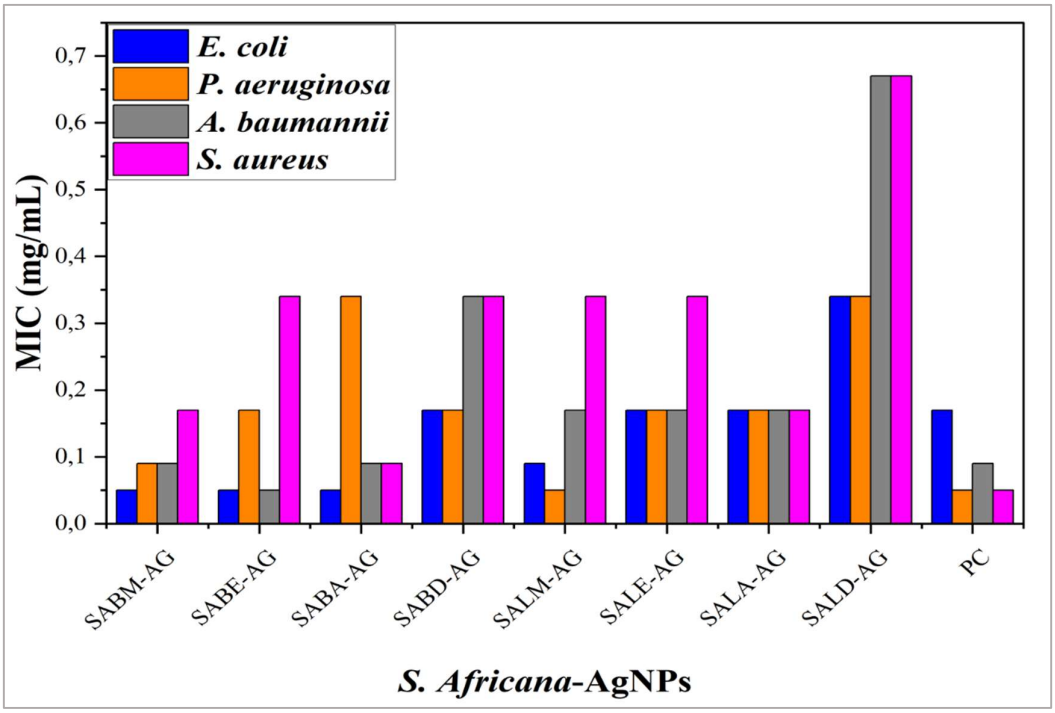

Figure 4.20: Minimum Inhibitory Concentration (MIC) in mg/mL of SA-AgNPs synthesised by bark methanol (SABM-AG), bark ethanol (SABE-AG), bark acetone (SABA-AG), and bark

water (SABD-AG) extracts. SA-AgNPs synthesised by leaf methanol (SALM-AG), leaf ethanol (SABE-AG), leaf acetone (SABA-AG), and leaf water (SALD-AG), PC= positive control (Lomefloxacin hydrochloride) (One-way ANOVA, Tukey's post hoc test, $p<0.05$).

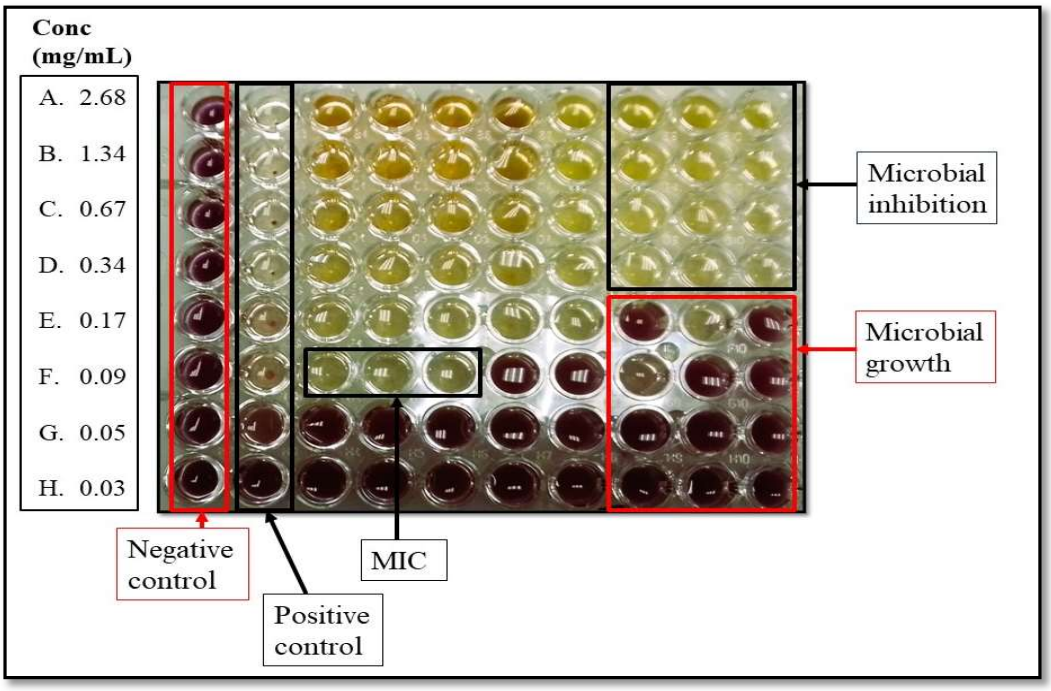

Figure 4.21: A 96 well plate depicting bacterial inhibition by microdilution assay for SA-AgNPs samples.

The MIC results for SA-AuNPs revealed varying levels of activity against the tested bacterial strains, with *S. aureus* emerged as the most sensitive among the strains examined (Figure 4. 22 and Figure 4. 23). Notably, samples SABM60S100 and SABE90S90100 exhibited the highest activity against *S. aureus*, with the lowest MIC value recorded at 0.64 mg/mL. Similarly, SABE90S90100 and SABA90S100 demonstrated notable efficacy against *E. coli*, both displaying a MIC value of 1.27 mg/mL. Additionally, SABA90S100 exhibited activity against *P. aeruginosa*, with a MIC value of 1.27 mg/mL. None of the tested SA-AuNPs samples

showed activity against *A. baumannii*. The antimicrobial activity of SA-AuNPs was not significantly different from the positive control (p=0.3154), indicating that the observed effects may be due to chance rather than a true antimicrobial effect. This suggests that while some activity was noted, the SA-AuNPs may not be effective enough to be considered reliable antimicrobial agents against the tested bacterial strains.

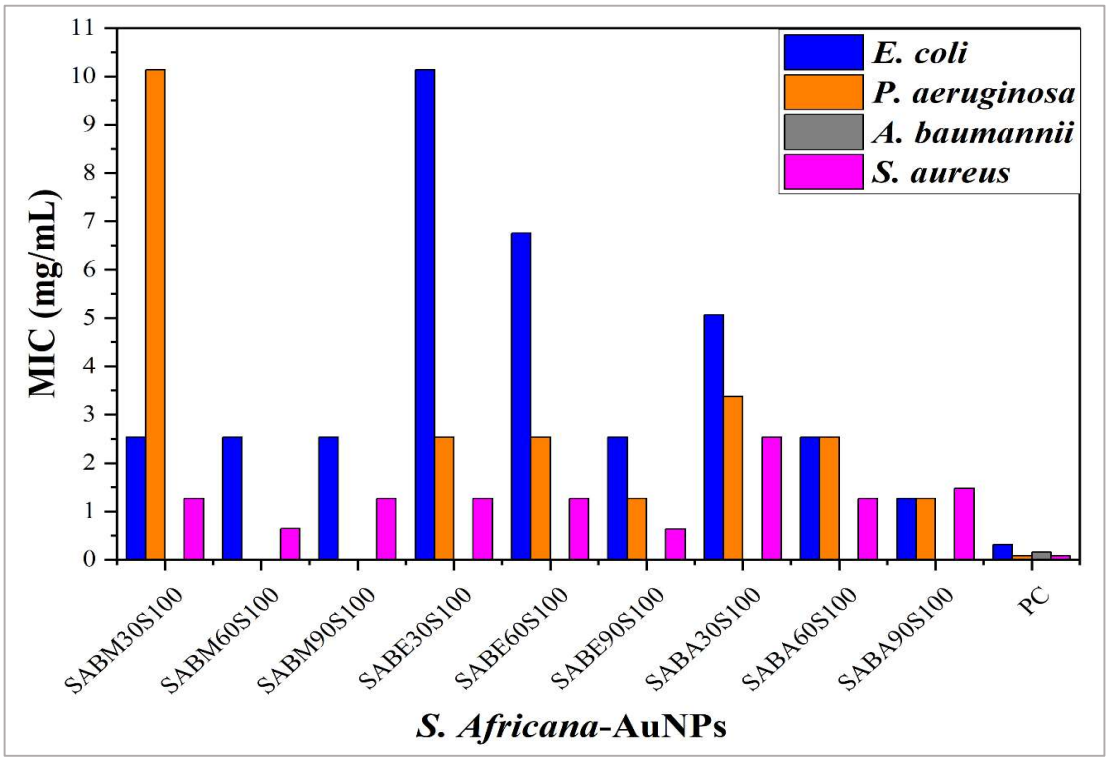

Figure 4.22: Minimum Inhibitory Concentration (MIC) in mg/mL of SA-AuNPs synthesised by bark methanol-AuNPs for 30 seconds (SABM30S100), 60 seconds (SABM60S100), 90 seconds (SABM90S100), ethanol-AuNPs for 30 seconds (SABE30S100), 60 seconds (SABE60S90100), 90 seconds (SABE90S90100), and acetone-AuNPs for 30 seconds (SABA30S100), 60 seconds (SABA60S100) and 90 seconds (SABA90S100). PC= positive control (Lomefloxacin hydrochloride) (One-way ANOVA, Tukey's post hoc test, p>0.05).

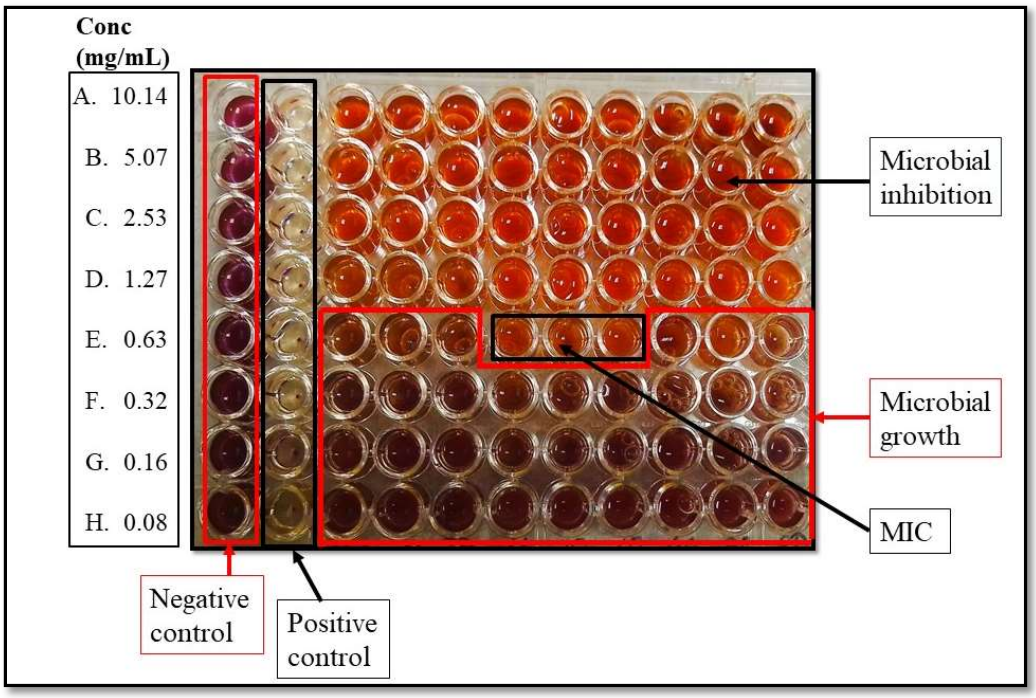

Figure 4.23: A 96 well plate depicting bacterial inhibition by microdilution assay for SA-AuNPs samples.

4.4.3 Minimum bactericidal concentration (MBC)

All the *S. africana* crude extracts were tested for their ability to kill bacteria by inoculating from all wells containing plant extracts or NPs with bacterial inhibition activity (no colure change) during the microdilution experiments. The results showed plant extracts had a bactericidal effect only on *S. aureus*. However, there was no statistically significant effect when compared to the positive control (p=0.3965), indicating that the antimicrobial properties of the extracts may not be strong enough to warrant further investigation as effective bactericidal agents against the tested bacteria. As shown in Figure 4.24, which displays the MBC of the plant extracts against *S. aureus*. The extract with the best killing activity was SALE, with the lowest MBC of 2.5 mg/mL. Sample SABM. SABD and SALD had no killing activity on *S.*

aureus. Additionally, none of the plant extracts also exhibited a bactericidal effect against *E. coli*, *P. aeruginosa* and *A. baumannii*.

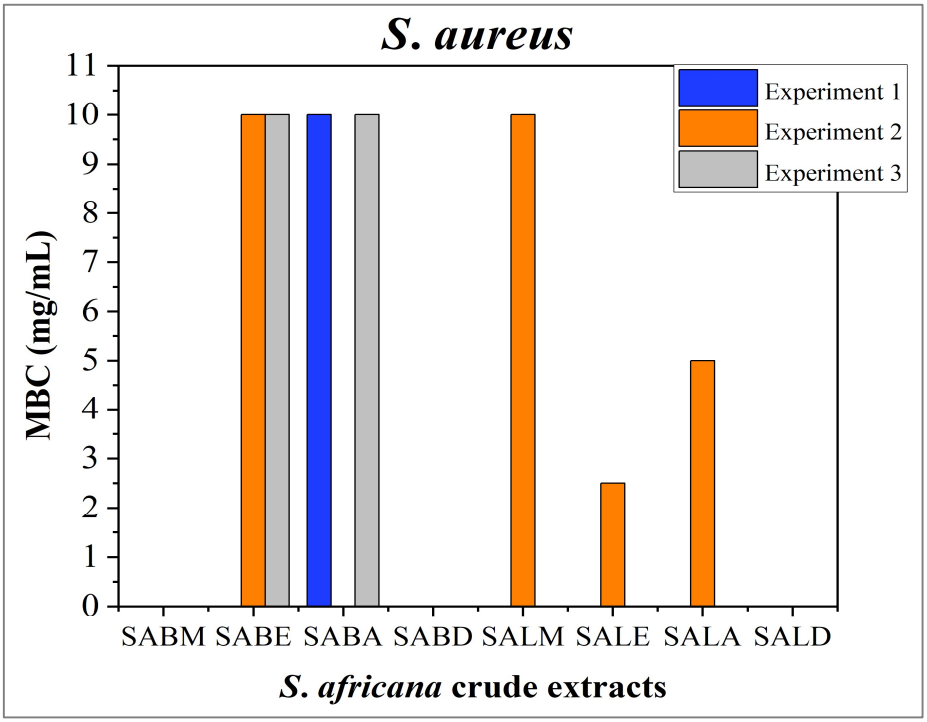

Figure 4.24: Minimum Bactericidal Concentration (MBC) in mg/mL of *S. africana* plant extracts. SABM (bark methanol), SABE (bark ethanol), SABA (bark acetone), SABD (bark distilled water), SALM (leaf methanol), SALE (leaf ethanol), SALA (leaf acetone), SALD (leaf distilled water). One-way ANOVA followed by Tukey's post hoc test ($p>0.05$).

The MBC results revealed varying levels of activity among the SA-AgNPs samples against the tested bacterial strains. Notably, samples SABM-AG and SABA-AG exhibited the lowest MBC value of 0.09 mg/mL against *A. baumannii*, indicating potent bactericidal activity. Additionally, SABA-AG demonstrated activity against *S. aureus*, also with an MBC of 0.09 mg/mL, SABM-AG displayed activity against *E. coli* and *P. aeruginosa*, with an MBC of 0.17 mg/mL. In contrast, SALD-AG showed the least activity, with MBC values ranging from 0.67 to 2.68 mg/mL. The p-value of 0.1547 suggests that the differences in MBC between the SA-

AgNPs samples and the positive control were not statistically significant, indicating that the observed bactericidal effects may have arisen from random variation rather than a true effect. The results of MBC of SA-AgNPs are presented in a graph below (Figure 4.25).

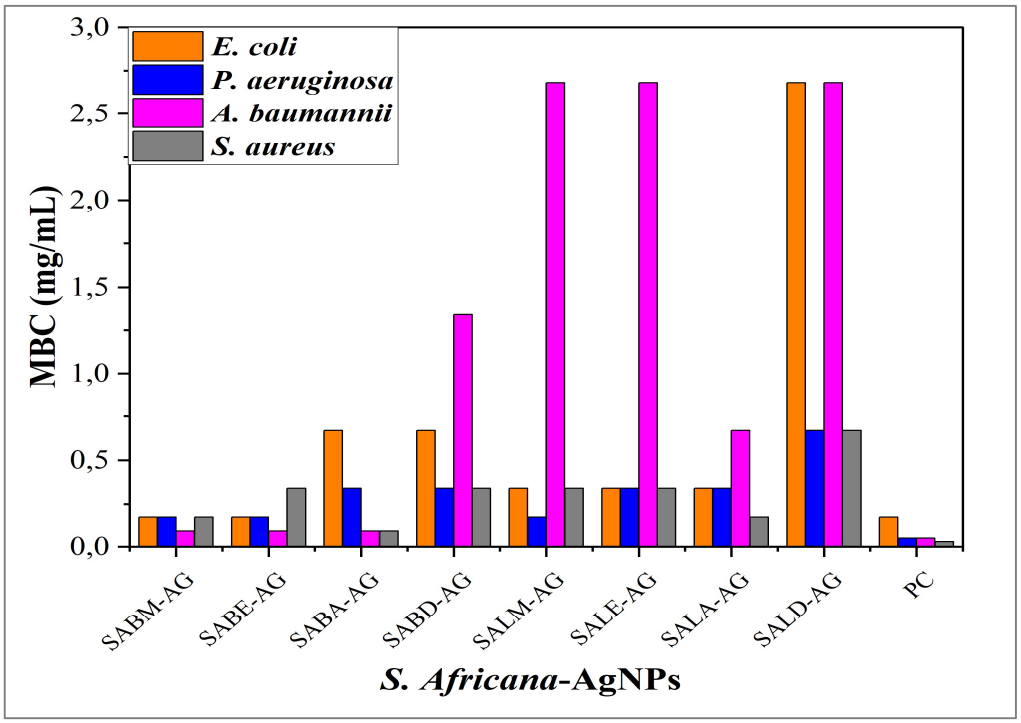

Figure 4.25: Minimum Bactericidal Concentration (MBC) in mg/mL of SA-AgNPs (One-way ANOVA, Tukey's post hoc test, $p>0.05$). SABM-AG= bark methanol, SABE-AG= bark ethanol, SABA-AG= bark acetone, SABD-AG= bark water, SALM-AG= leaf methanol, SABE-AG= leaf ethanol, SABA-AG= leaf acetone, SALD-AG= leaf water, and PC= positive control (Lomefloxacin hydrochloride).

The MBC results for SA-AuNPs indicated varying activity levels against the tested bacterial strains (Figure 4.26). Notably, sample SABE90S90100 exhibited the highest activity against both *S. aureus* and *E. coli*, with the lowest MBC values recorded at 0.63 mg/mL and 2.5 mg/mL, respectively. However, no killing activity was observed for *A. baumannii* and *P.*

aeruginosa. There was no significant difference when compared to the positive control (p=0.4196), suggesting the observed effects may be due to chance rather than a true antimicrobial impact. These findings underscore the differential bactericidal efficacy of SA-AuNPs against different bacterial strains, with some samples demonstrating potent bactericidal effects against specific pathogens while showing no activity against others.

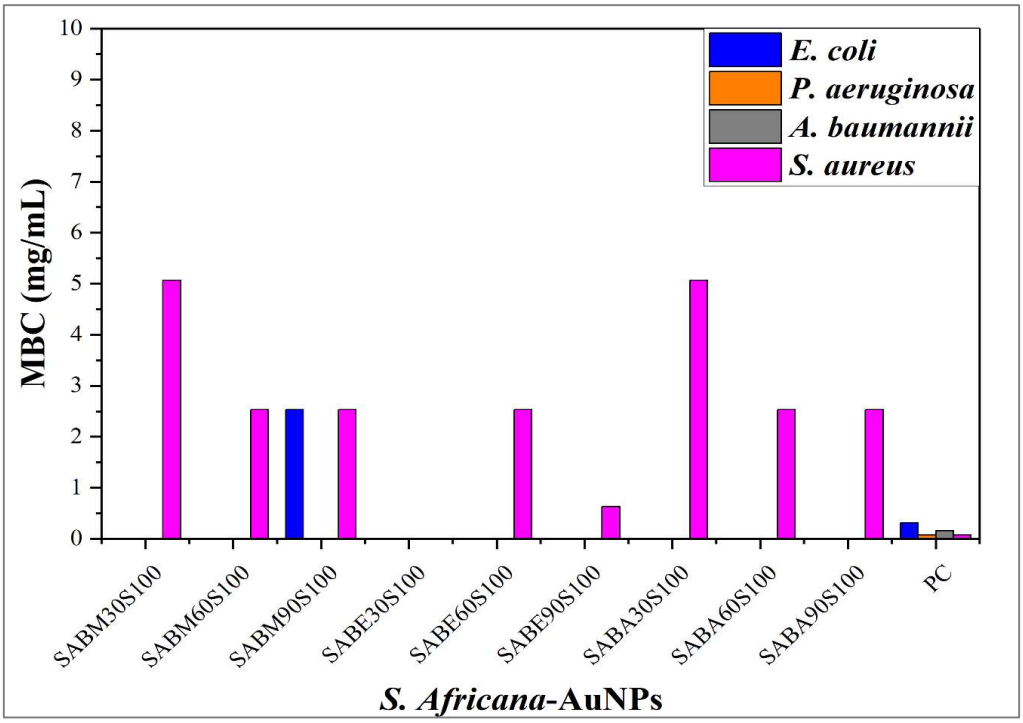

Figure 4.26: Minimum Bactericidal Concentration (MBC) in mg/mL of SA-AuNPs synthesised by bark methanol-AuNPs for 30 seconds (SABM30S100), 60 seconds (SABM60S100), 90 seconds (SABM90S100), ethanol-AuNPs for 30 seconds (SABE30S100), 60 seconds (SABE60S90100), 90 seconds (SABE90S90100), and acetone-AuNPs for 30 seconds (SABA30S100), 60 seconds (SABA60S100) and 90 seconds (SABA90S100). PC= positive control (Lomefloxacin hydrochloride) (One-way ANOVA, Tukey's post hoc test, p>0.05).

4.4.4 Synergistic tests of *S. Africana* plant extract combinations by microdilution method

The synergistic activity of *S. africana* methanol and ethanol extract combinations against resistant bacteria was evaluated using the microdilution assay. The overall inhibition activity of the plant extracts in combination was less effective than that of the individual plant extracts. However, ethanol mixtures showed the best antimicrobial activity against *S. aureus* with MIC values of 1.25 mg/mL. *E. coli* was susceptible to all the plant mixtures with a MIC value of 5 mg/mL. No inhibition activity was found in any of the mixtures against *P. aeruginosa* and methanol mixtures also showed no activity against *A. baumannii* (Table 4.4).

Table 4.4: The average mean of the minimum inhibitory concentrations (MIC) of the plant extracts combinations against antibiotic-resistant bacteria.

Plant extracts formulations	***E. coli***	***P. aeruginosa***	***A. baumannii***	***S. aureus***
Methanol bark and leaf extracts combinations				
Mixture 1	5	-	-	2.5
Mixture 2	5	-	-	2.5
Mixture 3	5	-	-	2.5
Mixture 4	5	-	-	1.25
Mixture 5	5	-	-	1.67
Ethanol bark and leaf extracts combinations				
Mixture 1	5	-	-	1.25
Mixture 2	5	-	5	1.25
Mixture 3	5	-	5	1.25
Mixture 4	5	-	5	1.25

Mixture 5	5	-	5	1.25

Note: (-) = No activity. Mixture 1 to 5 represent different bark to leaf ratio combinations tested agains antibiotic-resistant strains. Mixture 1 has a 9:1 bark to leaf ratio, Mixture 2 has a 7:3 ratio, Mixture 3 has a 5:5 ratio, Mixture 4 has a 3:7 ratio, and Mixture 5 has a 1:9 bark to leaf ratio.

Table 4.5 represents the fractional inhibitory concentration index (FICI) and their interpretations, and the results show that all plant extracts combinations had no synergistic effectivity on any of the bacteria but exhibited indifference and addictive effects. Mixture 1 to 5, from both methanol and ethanol extracts had indifference effects against *E. coli*. Meanwhile, mixture 4 of methanol extracts had an addictive effect against *S. aureus*. Ethanol mixture 2 to 5 also showed indifference effects on *A. baumannii*.

Table 4.5: The fractional inhibitory concentration index (FICI) of methanol and ethanol extracts combinations.

Bacterial strains	**Mixture 1**	**Mixture 2**	**Mixture 3**	**Mixture 4**	**Mixture 5**
Methanol bark and leaf extracts					
Escherichia coli	4(I)	4(I)	4(I)	4(I)	4(I)
Pseudomonas aeruginosa	-	-	-	-	-
Acinetobacter baumannii	-	-	-	-	-
Staphylococcus aureus	2(I)	2(I)	2(I)	1(A)	1.34(I)

Ethanol bark and leaf extracts					
Escherichia coli	4(I)	4(I)	4(I)	4(I)	4(I)
Pseudomonas aeruginosa	-	-	-	-	-
Acinetobacter baumannii	-	1.5(I)	1.5(I)	1.5(I)	1.5(I)
Staphylococcus aureus	1.5(I)	1.5(I)	1.5(I)	1.5(I)	1.5(I)

Key: A= Additive, I= Indifference, (-)= No activity.

4.5 Cytotoxicity assay

The cytotoxicity effects of *S. africana* extracts, SA-AgNPs, and SA-AuNPs on human estrogen-positive breast cancer cells (MCF7), normal human mammary epithelial cells (MCF10), and RAW 264.7 murine macrophage cells were investigated using the MTT method. Following the treatment with the samples, changes in cell morphology were observed under a light microscope after 24 hours of incubation at 37 ℃ (Figure 4.27). These observable changes in cell morphology, such as cell rounding or shrinkage, clearly indicate cytotoxicity.

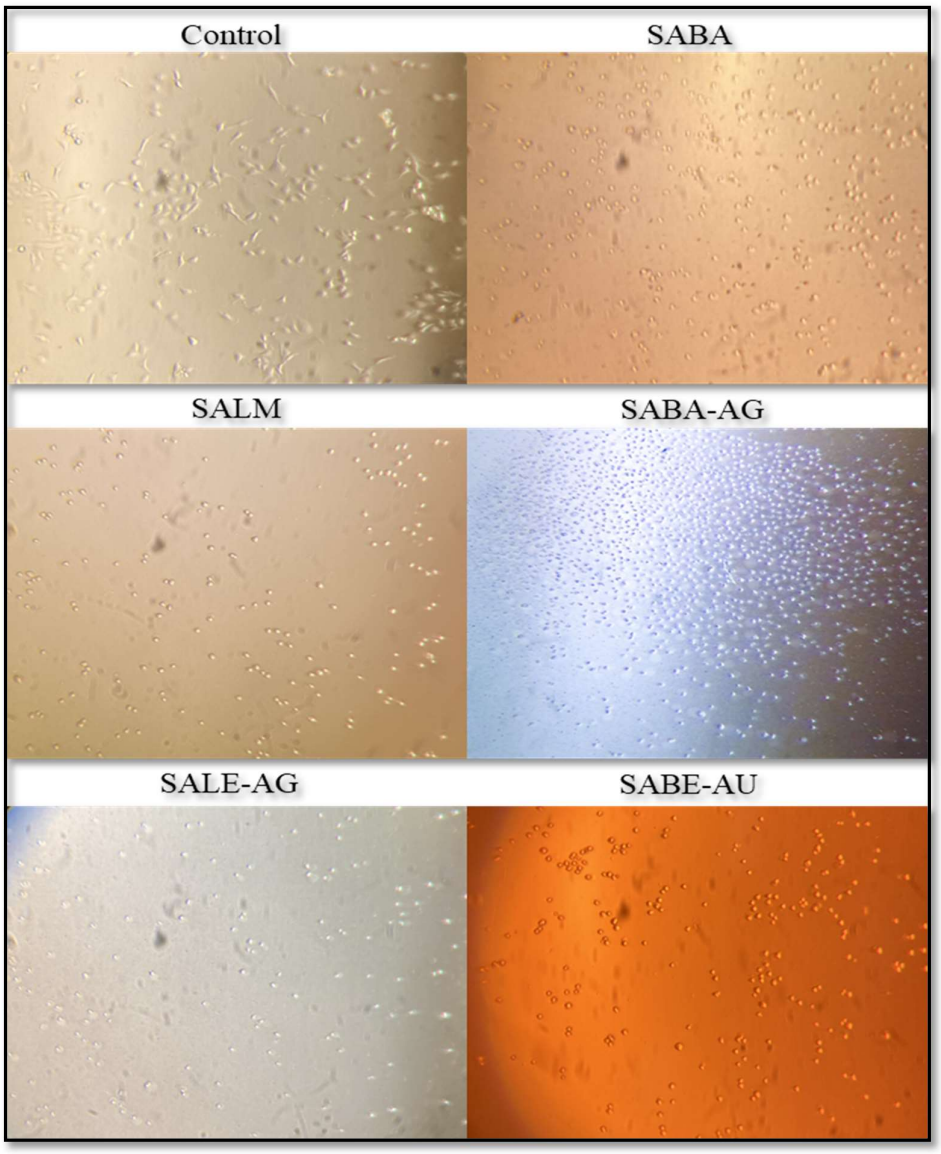

Figure 4.27: Changes in cell morphology caused by acetone bark extracts (SABA), leaf methanol extracts (SALM), bark acetone conjugated SA-AgNPs (SABA-AG), leaf ethanol conjugated SA-AgNPs (SALE-AG) and bark ethanol conjugated SA-AuNPs (SABE-AU) on the cells after 24 hours.

The cytotoxic activities were assessed using the MTT assay, with Figure 4.28 illustrating the cytotoxic effects against MFC-7 cancer cells and MCF-10 normal cells. Among the tested samples, plant extract SABA displayed no cytotoxic activity against all cell lines at

concentrations ranging from 5 to 0.156 mg/mL, with viability ranging from 214% to 154% for MCF-7 cells and 689% to 127% for MCF-10 cells. However, viability decreased to 41% at a lower concentration of 0.078 mg/mL MCF-7 cancer cells.

Following this, SA-AgNPs (SABA-AG and SALE-AG) demonstrated significant cytotoxicity across all tested cell lines. Specifically, SABA-AG inhibited MCF-7 cells by 12% and stimulated MCF-10 cells by 172% at the lowest concentration of 0.01 mg/mL. However, at concentrations ranging from 0.34 to 0.02 mg/mL, SABA-AG displayed toxicity against all cell types.

Lastly, SA-AuNPs sample SABE-AU exhibited cytotoxic effects on MCF-7 cells, with viability of 37% at concentrations at 0.08 mg/mL. Meanwhile, SABE-AU demonstrated higher viability in non-cancerous MCF-10 cell lines but also stimulated MCF-7 cancer cells at higher concentrations from 1.27 to 10.14 mg/mL.

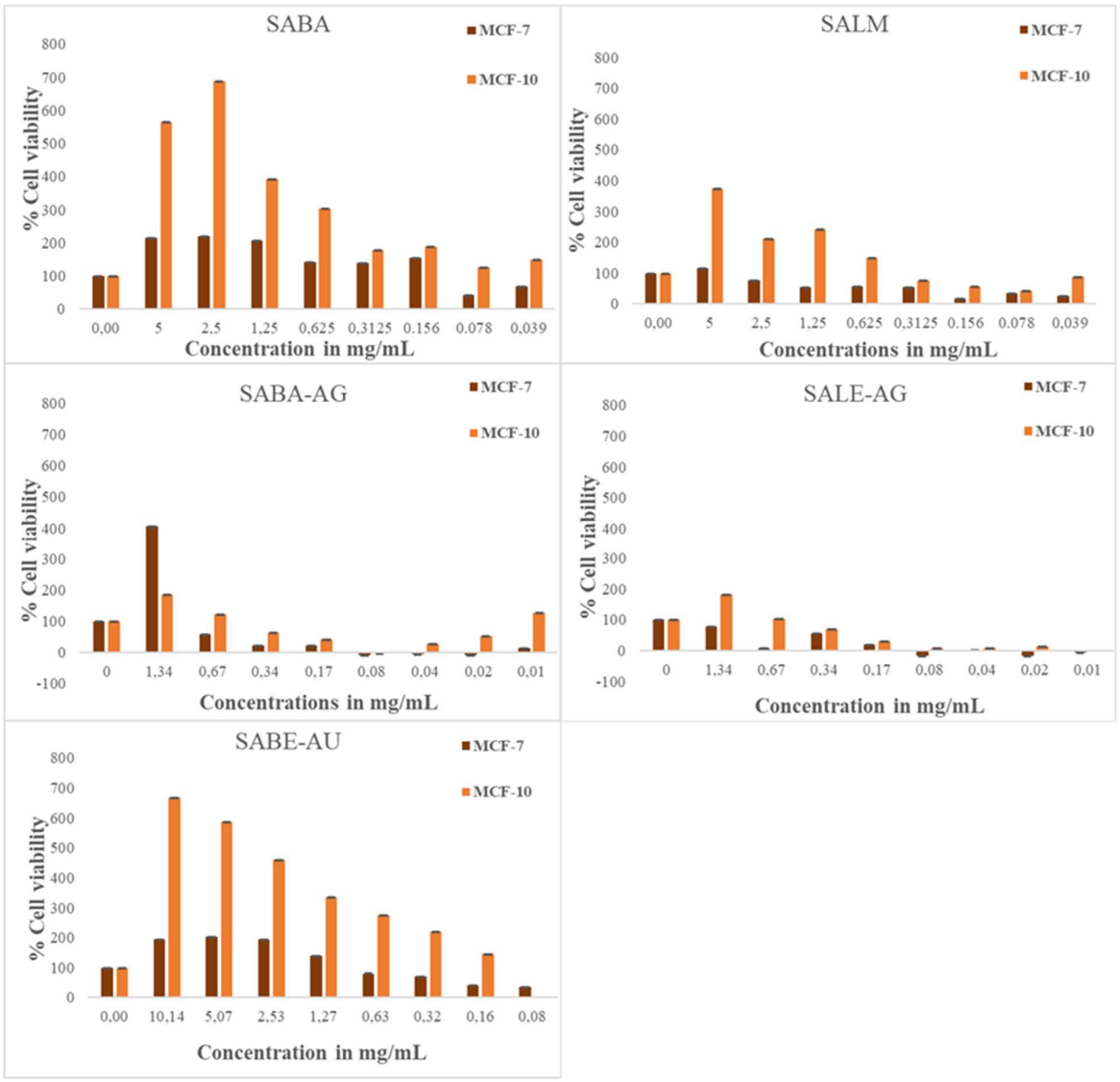

Figure 4.28: Cytotoxicity effects of *S. Africana* extracts (SABA and SALM), SA-AgNPs (SABA-AG and SALE-AG), and SA-AuNPs (SABE-AU) on A) MCF-7 and MCF-10 by MTT assay. SABA= acetone bark extracts, SALM= leaf methanol extracts, SABA-AG= bark acetone conjugated SA-AgNPs, SALE-AG= leaf ethanol conjugated SA-AgNPs and SABE-AU= bark ethanol conjugated SA-AuNPs. Two independent experiments portray results as means ± standard error of the means (SEMs).

The cytotoxic activity of RAW 264.7 macrophage cells was evaluated using the MTT assay (refer to Figure 4.29). The results revealed that the plant extract SABA exhibited no cytotoxic activity at concentrations ranging from 0.078 to 5 mg/mL. At these increased concentrations,

cell viability ranged from 105% to 605%. However, at the lowest concentration tested (0.039 mg/mL), the viability was reduced to 54%. In contrast, extract SALM displayed varying cell viabilities ranging from 62% to 387% at higher concentrations of 0.156 to 5 mg/mL, respectively. It showed cytotoxic effects at lower concentrations (0.039 to 0.078) mg/mL, with viabilities ranging from 25% to 28%.

The cytotoxicity results for SA-AgNPs (SABA-AG and SALE-AG) indicate the effects of these silver nanoparticles on cell viability at different concentrations. SABA-AG showed significant cytotoxic effects, especially at lower concentrations (0.34 to 0.01 mg/mL), where cell viability ranged from 42% to 5.7%. As the concentration increased to 0.67 and 1.34 mg/mL, the viability also increased to 79% and 117%, respectively. On the other hand, SALE-AG exhibited cytotoxicity at even lower concentrations, starting from 0.04 to 0.01 mg/mL, with cell viability ranging from 19% to -9%. However, at higher concentrations (0.08 to 1.34 mg/mL), the cell viability increased significantly, ranging from 78% to 228%.

Lastly, SA-AuNPs sample SABE-AU exhibited less cytotoxic effects at 0.08 mg/mL concentration, with 58% viability. An increased viability was observed from 0.32 to 10.34 mg/mL, ranging from 105% to 667%. These results demonstrate varying degrees of cytotoxicity among the tested samples, with some showing potent effects at low concentrations while others required higher concentrations to elicit significant cytotoxic responses.

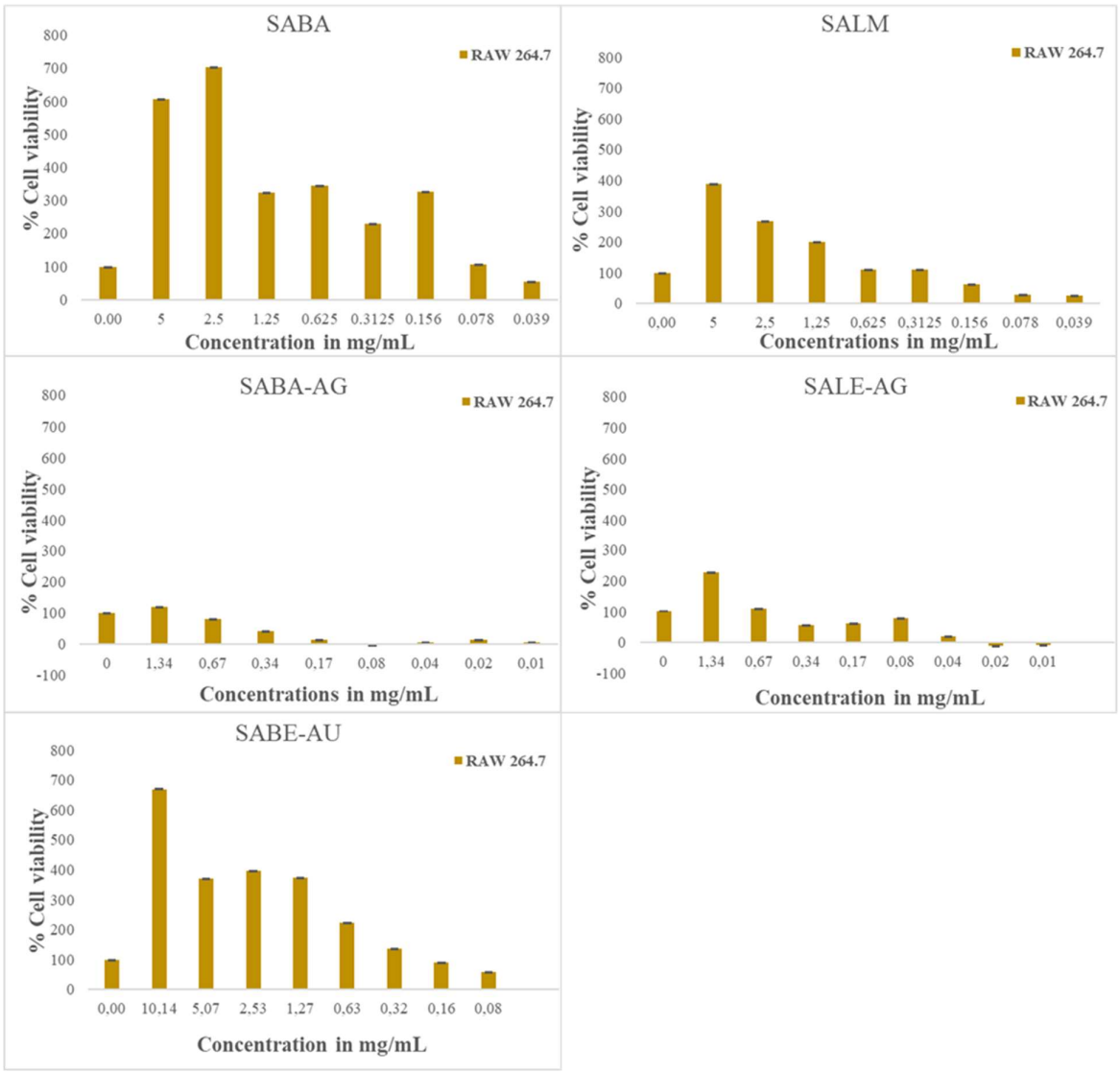

Figure 4.29: Cytotoxicity effects of *S. africana* extracts (SABA and SALM), SA-AgNPs (SABA-AG and SALE-AG), and SA-AuNPs on RAW 264.7 cells by MTT assay. SABA= acetone bark extracts, SALM= leaf methanol extracts, SABA-AG= bark acetone conjugated SA-AgNPs, SALE-AG= leaf ethanol conjugated SA-AgNPs and SABE-AU= bark ethanol conjugated SA-AuNPs. Two independent experiments portray results as means ± standard error of the means (SEMs).

4.6 Anti-inflammatory assay

The RAW 264.7 macrophage cells are known to play a critical role in regulating inflammatory diseases. In the current study, we aimed to investigate the potential effects of *S. africana* extracts, SA-AgNPs, and SA-AuNPs on the inflammatory response of macrophages when stimulated with LPS. The overall anti-inflammatory results of this study demonstrated that the treatment with tested samples efficiently inhibited the production and secretion of nitric oxide NO induced by LPS (Figure 4.30).

Sample SALM, SALE-AG, and SABE-AG exhibited a significant decrease in NO production across all concentration levels tested compared to the control (LPS treated solely). Conversely, SABA and SABA-AG demonstrated an elevated NO production, particularly at concentrations of 5, 0.156, and 0.078 mg/mL, as well as 0.08 and 0.02 mg/mL, respectively. These findings suggest that SALM, SALE-AG, and SABE-AU possess potential anti-inflammatory effects across all tested concentrations. In contrast, SABA and SABA-AG may contribute to a pro-inflammatory response, especially at specific concentrations.

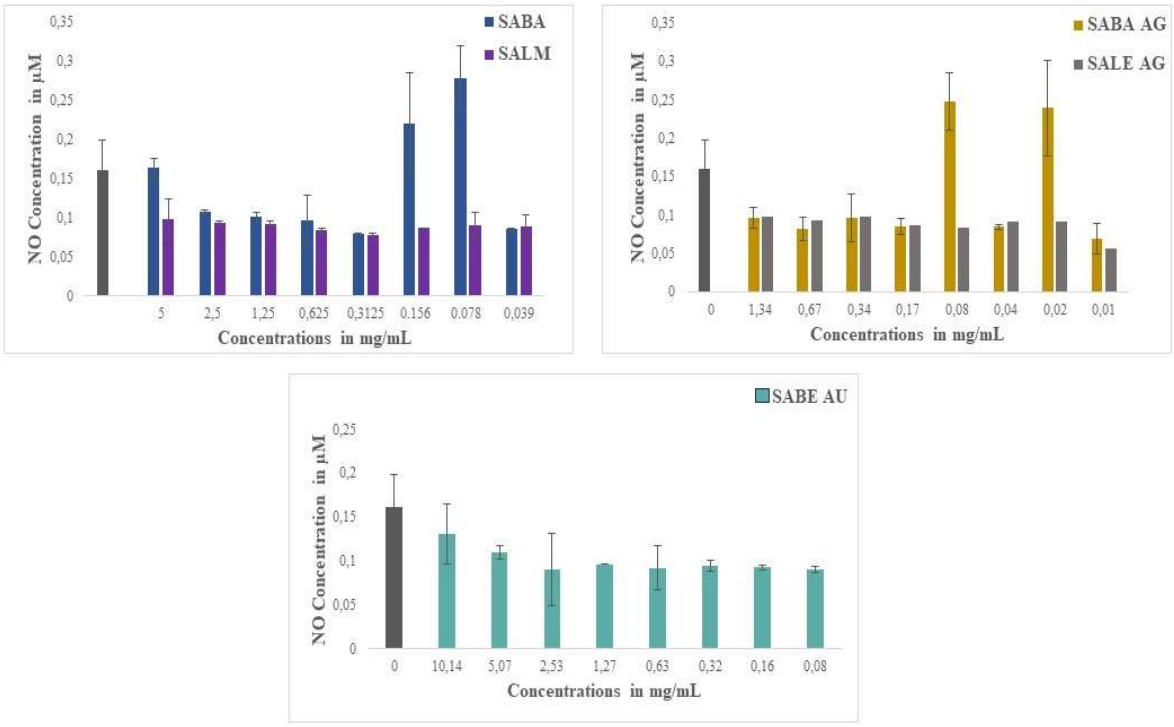

Figure 4.30: The inhibitory effects of different concentrations of plant extracts (SABA and SALA), silver (SABA-AG and SALE-AG), and gold (SABE-AU) nanoparticles on lipopolysaccharide (LPS) induced inflammatory response on nitric oxide (NO) production in RAW 264.7 macrophage cells. Two independent experiments portray results as means ± standard error of the means (SEMs).

4.7 Antioxidant activity

The antioxidant activities of different *S. africana* extracts, SA-AgNPs, and SA-AuNPs were evaluated using the DPPH assay, and the calculated IC_{50} values (mg/mL) of DPPH free radical scavenging activity are presented in Table 4.6. The antioxidant activity of the tested samples was primarily assessed by observing the colour change from purple (after the addition of the DPPH solution) to yellow (after a few minutes), as depicted in Figure 4.29. It is well-established that a lower IC_{50} value indicates higher antioxidant activity (Albanese et al., 2019). Among all the tested samples, the plant extract SALA exhibited excellent antioxidant activity

with the lowest IC_{50} value of 0.000335 mg/mL. Conversely, SALE exhibited weak antioxidant activity with an IC_{50} value of 183 mg/mL. Moving on to SA-AgNPs, SABA-AG demonstrated good antioxidant activity with an IC_{50} value of 0.89 mg/mL, compared to the positive control Ascorbic acid (0.1 mg/mL). For SA-AuNPs, SABM-AU exhibited good antioxidant activity with an IC_{50} value of 0.38 mg/mL.

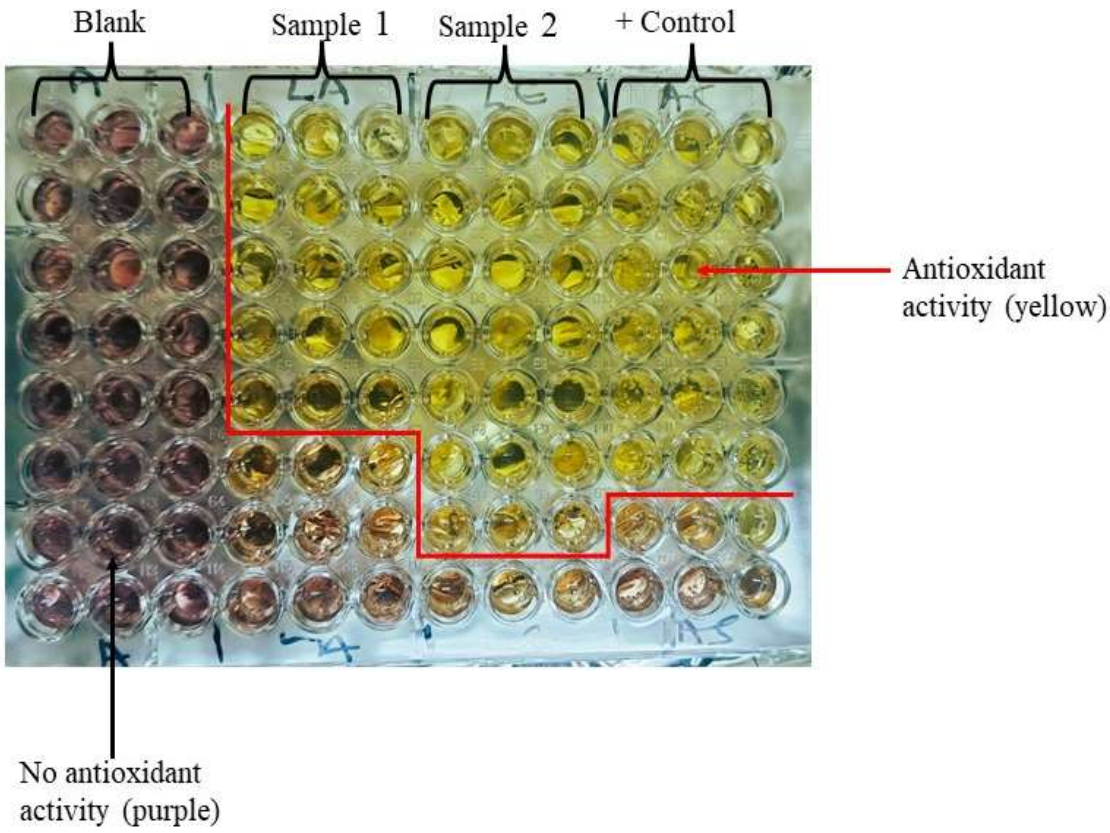

Figure 4.31: A 96 well plant depicting antioxidant activity of the tested samples via DPPH assay.

Table 4.6: Antioxidant activities of *S. africana* extracts, silver (SA-AgNPs), and gold (SA-AuNPs) by presented by DPPH scavenging activity IC_{50} values (mg/mL). Ascorbic acid was used a control for this assay.

Treatment	DPPH scavenging activity IC_{50} (mg/ml)
***S. africana* plant extracts**	
SABM	22,9954
SABE	7,22
SALA	0,000335
SALE	183,5641
Ascorbic acid	1,267336
Silver nanoparticles (SA-AgNPs)	
SABM-AG	19,28438
SABE-AG	2,46654
SABA-AG	0,898972
SALE-AG	1,216113
Ascorbic acid	0,103832
Gold nanoparticles (SA-AuNPs)	
SABM-AU	0,376778
SABA-AU	0,88046
Ascorbic acid	1,761042

Notes: SABM= *S. africana* bark-methanol, SABE= bark-ethanol., SALA= leaf-acetone, SABM-AG= bark-methanol conjugated AgNP, SABE-AG= bark-ethanol conjugated AgNP, SABA-AG= bark-acetone conjugated AgNP, SALE-AG= leaf-ethanol conjugated AgNP, SABM-AU= bark-methanol conjugated AuNP, SABA-AU= bark-acetone conjugated AgNP.

Chapter 5: Discussions

Medicinal plants have a long history of use against various diseases, including RTIs (Kavitha and Nadu, 2021). Their potential to inhibit microbial growth depends on the presence of different secondary metabolites (Asong et al., 2023). The emergence of ABR bacteria has led to a global crisis, and medicinal plants have gained attention as a promising source of new antibacterial drugs (Asong et al., 2023). Plant-based AgNPs and AuNPs have been recognized for their diverse applications and potential as eco-friendly solutions to combat ABR in bacteria (Anand et al., 2022).

In this context, the present study synthesised and characterised SA-AgNPs and SA-AuNPs using extracts from the *S. africana* plant, evaluating their antimicrobial activity against the ABR bacteria implicated with RTIs, which are listed as priority pathogens by the WHO. Additionally, the study assessed the cytotoxicity, anti-inflammatory, and antioxidant properties of the NPs and extracts. This study highlights the potential of plant-based NPs as a novel approach to combat ABR and treat RTIs.

The study successfully utilised methanol, ethanol, acetone, and water extracts of the *S. africana* plant to synthesise Ag^{+} and Au^{+} salt into NPs. Various parameters, such as concentration, reaction time, and incubation temperature, were optimised to achieve stable NPs with excellent activity. Our investigation revealed that SA-AgNPs synthesised with a 5 mM $AgNO_3$ concentration and incubated at 4°C exhibited favourable activity, parallel with findings by López-Miranda et al., (2016), who also reported positive outcomes under similar conditions. Htwe et al. (2020) reported that 5 mM led to more intense and narrow peaks, indicating quicker NP formation and a more uniform distribution.

The colour change observed during the synthesis of SA-AgNPs, from light yellow/brown at 1 mM to darker shades at 2 and 5 mM, suggests a correlation with NP agglomeration, as

previously reported by Mukaratirwa-Muchanyereyi et al. (2022). This phenomenon underscores the significance of concentration in controlling NP characteristics. Furthermore, our study supports the findings of Velgosova et al. (2017), who demonstrated that maintaining AgNPs at low temperatures and in darkness enhances their long-term stability, preventing agglomeration and preserving their spherical shape and narrow size distribution. Consequently, our study achieved stable SA-AgNPs when stored at 4°C for over three months.

In theory, the rate of conversion of ions into MNPs in the reaction depends on the initial concentration of metal ions, meaning that higher initial metal ion concentrations lead to faster conversion (Zhang et al., 2010; Htwe et al., 2020). This was also observed in the present study, samples with 5 mM SA-AgNPs changed colour within an hour.

For SA-AuNPs, the colour changed to deep purple within a few seconds when synthesised by microwave radiation, indicating a successful production of AuNPs (Singh and Mijakovic, 2022). The colour change is due to the surface plasmon vibrations and reduction of Au^{3+} ions by the phytoconstituents from extracts (Liaquat et al., 2022). Our study found optimal SA-AuNPs with good biological activity after synthesising with them using increased extracts' concentration and 1 mM $HAuCl_4$ through microwave synthesis for 90 seconds. The combination of phytochemicals and microwave heating facilitates the rapid synthesis of AuNPs, offering a novel method for medically relevant production (Yasmin et al., 2014). Saifuddin et al. (2009) also demonstrated that using plant extract-stabilized microwave radiation has shown that AuNPs can be formed quickly, in as little as one minute. Additionally, microwave radiation ensures uniform heating of aqueous solutions, preventing particle aggregation during synthesis.

The UV-Vis spectral analysis further confirmed the presence of SA-AgNP and SA-AuNP, revealing a variety of absorbance peaks indicative of the coherent oscillation of conduction

electrons within the NPs in response to visible light, known as SPR (B. Aziz et al., 2019). This SPR peak confirms the NPs and provides information about their size and shape (Noruzi, 2015).

In the SA-AgNP samples (SABM-AG/SABE-AG, SABD-AG, SALA-AG), the SPR peak exhibited maximum absorbance at 397 and 454 nm, 397 and 470 nm, and 370 and 500 nm, respectively. The presence of two distinct peaks suggests an anisotropic (non-uniform) morphology of the AgNPs, with the peak at 397 nm indicating the out-of-plane dipole resonance (Raza et al., 2016). This dual-peak phenomenon also suggests polydisperse size distributions of SA-AgNPs, with smaller NPs contributing to the narrow peaks at 360/390 nm and larger NPs contributing to the broad peak at 450/500 nm (Nakkala et al., 2014; Afreen et al., 2020; Sharma et al., 2020). These results are consistent with previous studies reporting SPR peaks within the range of 350-550 nm, which is indicative of AgNP formation (Babu and Gunasekaran, 2009).

Additionally, a single SPR peak at 363 nm was observed for SALM-AG and SALE-AG, indicating the presence of small spherical NPs with even distribution due to their narrow peak (Azwatul et al., 2023). Furthermore, sample SABA-AG displayed a narrow peak at 480 nm, indicating the presence of relatively homogeneous NPs in size and distribution, consistent with findings from previous studies by Ahmad et al. (2023). Several studies have reported SPR peaks around 480 nm (B. Aziz et al., 2019; Siakavella et al., 2020; Sharma et al., 2022).

Increasing $AgNO_3$ concentrations when synthesising SA-AgNP caused the SPR band to shift towards a higher wavelength region (red-shift) on samples SABM-AG, SALE-AG, SABA-AG, and SABD-AG. This shift is attributed to the aggregation of NPs, as higher concentrations of $AgNO_3$ are likely to lead to the formation of large AgNPs, causing the observed colour to change and peak shift (Ider et al., 2017; Mukaratirwa-Muchanyereyi et al., 2022). However,

contrasting results were observed in other studies that found a blue shift when the concentration is increased from 1 to 5 mM, portraying small monodispersed AgNPs (Zargar et al., 2014; Sharma et al., 2020).

The absorbance values of SA-AgNPs samples increased with $AgNO_3$ concentration up to 2 mM, then decreased at 5 mM, except for SABM-AG which had increased absorbance to 5 mM. In contrast, SABA-AG exhibited decreased absorbance as $AgNO_3$ concentrations increased. Decreased absorbance in this study resulted in SA-AgNPs with good activity (later described). These variations in the response to increasing $AgNO_3$ concentrations were observed across the different samples, indicating diverse effects on the synthesis of AgNPs.

The influence of reaction time on the synthesis of SA-AgNPs using methanol and ethanol extracts revealed decreased absorption peaks as the incubation time increased. Specifically, SABE-AG/SALE-AG demonstrated a decrease in SPR peaks as the reaction time progressed. These align with previous studies demonstrating that the appearance of characteristic SPR bands corresponds to the formation of AgNPs (Bamsaoud et al., 2021; Ider et al., 2017; Babu and Gunasekaran, 2009). We also observed red-shift with increased incubation, indicative of larger NP sizes (Ider et al., 2017; Babu and Gunasekaran, 2009). Additionally, the absence of absorption peaks in some cases suggests that AgNP formation does not occur under certain conditions, such as low concentrations of $AgNO_3$ and bark water extracts (Bamsaoud et al., 2021; Ider et al., 2017).

The impact of temperature on the production of SA-AgNPs revealed that increasing temperature led to heightened SPR peaks. Narrower bands with higher absorbance values were consistently observed at 25°C compared to 4°C across most samples. These findings are supported by previous reports which indicated that the rise of temperature causes the absorbance spectra to increase, further concluding that NPs synthesised at higher temperatures

produce larger particles that are aggregating (Liaquat et al., 2022; Mukaratirwa-Muchanyereyi et al., 2022). A study by Stavinskaya et al. (2019) demonstrated that high temperatures speed up the reduction of Ag ions, facilitating faster NP formation.

The SA-AuNPs samples resulted in SPR bands at wavelengths of 533 nm, 541 nm, and 574 nm for SABM-AU, SABE-AU, and SABA-AU samples, respectively, confirming the production of AuNPs (Tyagi et al., 2021; Perveen et al., 2021). This observation is consistent with the typical absorption spectrum of Au colloids, which exhibits a distinct absorption band in the visible region between 500-600 nm (Rastogi, 2013; Yadi et al., 2022). A study on *Hibiscus rosa-sinensis* stabilised AuNPs showed that changing plant extract concentration, synthesising with microwaves, and adjusting exposure time influenced absorption spectra. It was noted that increased plant extract concentration led to the formation of ideal AuNPs, while a 90-second exposure produced small NPs with a distinct peak around 520 nm (Yasmin et al., 2014). These results underscore the crucial role of plant extract concentration in controlling NP size and shape.

Additional peaks were also observed in the UV-Vis spectra of samples SABM-AU and SABE-AU before the 500 nm wavelength, possibly due to the presence of phytochemical compounds involved in Au^{3+} ion reduction. A study by Niranjan Dhanasekar et al. (2015) suggested that these peaks may arise from aromatic amino acids such as tryptophan, tyrosine, or phenylalanine, as well as peptide linkages, which help stabilise the NPs. A broad SPR band at wavelength 574 nm in SABA-AU represents the polydisperse nature of AuNPs (Perveen et al., 2021). These findings agree with earlier reports identifying a broad peak in the 550 to 600 nm range (Guadie Assefa et al., 2017). This is further validated because toward a higher wavelength (red-shift) where we find larger and aggregated NPs. Consistent with earlier reports that found the SPR peaks at 527, 541, and 543 nm, which suggested that AuNP size increases, as the SPR shifts to longer wavelengths (red-shift) (Nur and Nasir, 2008). Moreover, these

reports suggested that NPs with wavelengths around 500 to 550 nm exhibit a hexagonal shape. Overall, these findings emphasise the importance of optimising reaction parameters like extract type and concentration, metal salt concentration, reaction time, and temperature during the synthesis to achieve the desired properties of MNPs.

The X-ray diffraction (XRD) patterns observed in our study confirm the crystalline nature of the SA-AgNPs and SA-AuNPs synthesised. SA-AgNPs exhibited more well-resolved and intense diffraction peaks compared to SA-AuNPs, indicating a higher degree of crystallinity and structural order in the SA-AgNPs. This finding aligns with previous studies that reported similar results, where AgNPs demonstrated more pronounced crystallinity than their AuNPs counterparts (Arshi et al., 2011; Singh et al., 2012). Our results correlate with the calculated phases from the reference library JCPDS No. 01-1167, indicating a face-centred cubic (FCC) structure, which is consistent with the crystalline structures reported in other studies (Dilbar et al., 2023; Babu and Gunasekaran, 2009).

Interestingly, an additional peak at 45° was observed in the sample SAMB-AG, suggesting the presence of potential plant compounds or impurities (Kumkoon et al., 2023). This observation is supported by findings from Salayová et al., (2021), who also noted variations in peak characteristics that could be attributed to organic compounds from plant extracts. Conversely, SABE-AG and SABA60S100 lacked a peak at 43°, indicating possible variations in particle characteristics that may arise from differences in synthesis conditions, as previously highlighted by Raza et al., (2016).

The Bragg reflections observed propose that the X-ray scattering FCC nature of the NPs could act as capping agents, influencing NP structures (Qidwai et al., 2018). This is particularly relevant as other studies have shown that the presence of capping agents can significantly affect the crystallinity and stability of nanoparticles (Ashraf et al., 2016).

Another interesting observation in all samples is that the lattice planes corresponding to (200), (220), and (311) were noted to exhibit weak intensity and broadening peaks compared to the (111) Bragg's reflection. This suggests that the nanocrystals synthesised biologically display a high level of anisotropy, with the NPs predominantly oriented along the (111) direction (Singh et al., 2012). Which correlates with the UV-Vis results obtained. This finding is consistent with previous reports indicating that the (111) plane is often the most stable and energetically favourable orientation for MNPs (Zhang et al., 2017).

The average crystalline size of the SA-AgNPs samples varied between 9 to 19 nm under different experimental conditions, suggesting a range of particle sizes contributing to the observed XRD patterns. In contrast, the average crystalline size of the SA-AuNPs samples ranged from 9 to 10 nm, indicating relatively uniform particle sizes across different synthesis conditions (Dilbar et al., 2023). This discrepancy in crystalline size distribution between SA-AgNPs and SA-AuNPs may be attributed to variations in synthesis parameters affecting nucleation and growth processes, as noted in previous studies where different synthesis methods resulted in varying particle sizes (Bamsaoud et al., 2021; Ider et al., 2017).

The distinct XRD peak characteristics and crystalline size variations underscore the importance of precise control over synthesis conditions to tailor the structural properties of MNPs for specific applications. For instance, research by Ansari et al. (2016) demonstrated that altering the concentration of precursor materials can significantly influence the size and crystallinity of AgNPs. Similarly, the findings from this study highlight that optimising parameters such as reaction time, temperature, and precursor concentration is crucial for achieving desired NP characteristics, reinforcing the need for meticulous experimental design in NP synthesis.

Dynamic light scattering (DLS) was employed to analyse the average particle size distribution, polydispersity index (PDI), and zeta potential (ZP) of synthesised SA-AgNPs and SA-AuNPs,

which is crucial for assessing NP's stability and surface charge. By analysing the Brownian motion of NPs, it calculates the hydrodynamic diameter (representing particle size in solution, including the contribution surrounding hydration layers) (Karmaka, 2019; Noruzi, 2015). The results indicated that SA-AgNPs samples had an average particle size range of 132-994 nm, with a Z-average size range of 1514-2511 d.nm. Specifically, SABM-AG exhibited a broad particle size distribution consisting of 132 and 409 nm. The wide distribution was also seen in UV-Vis spectral analysis. The findings contradict several findings; Liaquat et al., (2022) found an average particle size range of 1-43 nm, and Karmakar, (2019) found 19 nm for plant extracts synthesised AgNPs by DLS analysis. Both studies further illustrated that smaller NPs around that range exhibit good stability, and they are monodispersed in nature.

The SA-AuNP samples exhibited average particle size distributions ranging from 775-5560 nm, with Z-average sizes ranging from 745.4-3353 nm. A broad particle size distribution range of 1593 and 5560 was also observed in SABA-AU. Different results were found in a study of *Salvia africana-lutea* extract-based AuNPs with a hydrodynamic size of 63 nm (Dube et al., 2020). It is known that a PDI value exceeding 0.7 suggests particle polydispersity, whereas a value below 0.7 indicates particle monodispersity (Honary et al., 2013). Most of the synthesised SA-AgNPs were polydisperse, while the majority of SA-AuNPs were monodisperse.

Monodisperse NPs are known to exhibit enhanced performance and distinctive applications in comparison to polydisperse NPs (Liaquat et al., 2022). However, plant-based NPs are generally polydispersed with different shapes, structures, and distribution of broad sizes (Noruzi, 2015). Zeta potential analysis of SA-AgNPs revealed a ZP value of -27 mV for sample SABM-AG, suggesting a high degree of electrostatic repulsion between the particles, leading to increased stability. Nanoparticles with ZP values greater than +30 mV or less than -30 mV exhibited the highest degree of stability (Yadi et al., 2022). The negative zeta potential observed could result from the biochemical compounds found in the plant extracts (Liaquat et al., 2022).

Analysis by TEM confirmed the presence of SA-AgNPs and SA-AgNPs with various particle core sizes, distribution, and morphology. The SA-AgNPs samples had a range of shapes, including smaller spherical particles and larger squash-spherical, hexagonal, and irregular shapes. Average particle size of 23.2 ± 10.2, 17.7 ± 10.2, 5.9 ± 1.9, and 60.4 ± 49.5 nm for SABM-AG, SABE-AG, SABA-AG, and SALE-AG, respectively. The observed smaller sizes made these samples have exquisite biological activities. The variation in geometry and size is a common observation in green synthesis of NPs, often linked to the phytochemical compound present in plants used to reduce $AgNO_3$ ions (Elbagory et al., 2016).

The SA-AuNP (SABE-AU) were smaller ranging from 6 to 32 nm, with an average particle size of 14.1 ± 6.4 nm. The SABE-AU had spheroidal and star-shaped morphology, suggesting that these NPs have a relatively small size and a narrow size distribution, which is desirable for many applications, including drug delivery, due to their increased surface area-to-volume ratio, which enhances their interaction with biological systems (Fouda et al., 2020; Zahra et al., 2023). The results are comparable to AuNP by active compounds in ginger aqueous extract, resulting in spherical NPs ranging from 5 to 53 nm, with an average size of 15.11 ± 8.5 nm (Fouda et al., 2020).

It was noted that the hydrodynamic particle size (Z-average) measured by DLS was larger than the core particle size observed under TEM. This is due to the interaction of the NP surface with the solvent in DLS analysis. Hence, DLS measures larger overall particle size, including the solvent layer, while TEM measures the dried particle core (Dube et al., 2020). The particle size distribution range observed in TEM validated the polydispersity nature in SA-AgNPs and supported the conclusions drawn based on the UV-Vis, XRD, and DLS analysis.

The FTIR analysis identified potential functional groups responsible for the reduction of Ag^+ and Au^+ ions into SA-AgNPs and SA-AuNPs, respectively. The crude extracts of *S. Africana*

bark and leaves revealed the presence of O-H (hydroxy) groups, C=C stretching (alkenes) or N-H (amide) groups, C-O stretching (alcohols), and C-H (aromatic) in-plane bending. These functional groups were also seen in SA-AgNPs and SA-AuNPs samples but with minor shifts in absorption bands. The observed frequency shift suggests that hydroxyl, alkenes, or amide groups, alcohols, and hydrocarbons played crucial roles in reducing and stabilizing metal ions in the synthesised SA-AgNPs/SA-AuNPs, thereby indicating successful synthesis (Hatipoğlu, 2022). This indicates that the phytochemicals present in the *S. africana* extracts, such as polyphenols, flavonoids, and terpenoids, are likely involved in the reduction and capping of the NPs (Mandal et al., 2013; Shafaghat, 2015).

Corresponding studies with other plant extracts, such as D. kaki and E. senticosus, have also shown the involvement of functional groups like hydroxyl, carboxyl, and amine groups in the reduction and capping of Ag^{+} and Au^{+} ions into nanoparticles (Keskin et al., 2023; Abbai et al., 2016). The shifting of the C=O peak in the FTIR spectra obtained from AgNPs indicates that carbonyl-containing functional groups may be responsible for the bio-reduction of Ag^{+} ions into AgNPs, while the shifting of stretching vibrations of O-H and N-H to lower wavelengths suggests binding of these functional groups with the surface of the AgNPs (Shafaghat, 2015). In addition, proteins and amino acids present in plant extracts also play a significant role in the capping, coating, and protection of MNPs (Ahn et al., 2019). The C-OH vibrations of proteins/polysaccharides observed in the FTIR spectra of the synthesized NPs support this notion.

The LC-MS results of *S. africana* extract confirmed the presence of phytochemical compounds with known biological activity, including flavonoids, phenolic acids, phenols, tannins, glycosphingolipids, phospholipids, triterpenoids, flavonoid glycosides, ellagitannins, and polyphenols. These compounds are associated with numerous health benefits and possess a wide range of biological activities, such as antimicrobial, antibacterial, antidiabetic,

antimalarial, antioxidant, larvicidal, cyanogenic, and anthelminthic properties (Singh et al., 2020).

The present study found that the *S. africana* extract is rich in flavonoids, including rutin, quercetin-O-(O-galloyl)-pentoside, quercitrin, spiraeoside, afzelin, hyperoside, isorhamnetin-3-O-galactoside-6"-rhamnoside, and procyanidin trimer. These flavonoids are known for their various health benefits, including anticancer, anti-inflammatory, antioxidant, and antibacterial properties (Abbai et al., 2016; Wendlocha et al., 2023).

Phenolic acids, represented by [3,4,5-trihydroxy-6-(3,4,5-trihydroxybenzoyl)oxyoxan-2-yl]methyl 3,4,5-trihydroxybenzoate, phenols such as 6-gingerol, tannins including geraniin and 1,3,6-tri-O-galloylglucose, glycosphingolipids like soyacerebroside I, phospholipids such as 1-palmitoyl-2-linoleoyl-sn-glycero-3-phospho-(1'-rac-glycerol), triterpenoids like olivetoric acid, ellagitannin like corilagin, and polyphenols such as beta-penta-O-galloyl-glucose, were also identified. These compounds exhibit a diverse range of biological activities (Mathabe et al., 2008; Molele et al., 2023), further emphasising the potential of *S. Africana* as a source of bioactive compounds.

In synthesising MNPs, flavonoids significantly reduce metal ions (Paiva-Santos et al., 2021). In the current analysis, they are believed to accelerate the reduction and capping of Ag^{+}/Au^{+} ions into AgNPs/AuNPs. Proteins, amino acids, alkaloids, tannins, phenolic acids, and flavonoids are identified as key components in the synthesis and stabilization of MNPs (Selvan et al., 2018). These plant components act as crucial capping and stabilizing agents, with proteins and flavonoids suggested to expedite the reduction of metal salt ions into MNPs.

Flavonoids, such as quercetin, have been shown to enhance the solubility and bioavailability of metallic ions, minimising their adverse side effects (Karuvantevida et al., 2022). The hydroxyl group on the C3 or C5 position of a flavonoid aids in the formation of metal

complexes, and the biological activities of a specific flavonoid are improved after developing a complex with metallic ions (Karuvantevida et al., 2022).

As far as we know, no previous study has synthesised AgNPs and AuNPs from *S. africana* or evaluated their biological activities. In this study, we investigated the antimicrobial activity of *S. africana* extracts and their conjugated SA-AgNPs/SA-AuNPs using the agar-well diffusion and microdilution assay. Agar-well diffusion results demonstrated that *S. africana* extracts exhibited significant inhibition activity against *P. aeruginosa*, *A. baumannii*, and *S. aureus*, with a notable lack of activity against *E. coli*. The highest inhibition zone recorded was 24 mm for bark-methanol extract (SABM) against *P. aeruginosa*, demonstrating the potential of this extract as an effective antimicrobial agent. Leaf-ethanol extract (SALE) exhibited significant inhibition (19 mm) against *S. aureus* and *A. baumannii*, underlining their broad-spectrum antimicrobial potential. Notably, the observed antimicrobial activity of the *S. africana* extracts was statistically significance when compared to positive control. This supports our hypothesis that *S. africana* possesses antimicrobial properties against resistant strains.

The effectiveness of *S. africana* extracts was demonstrated in previous studies, highlighting their consistent antimicrobial activity (Mulaudzi et al., 2013). The exceptional activity observed in SABM and SALM is attributed to their methanolic nature since they are extracted using methanol solvent; this underscores the solvent's ability to extract a maximum number of bioactive compounds (Awad et al., 2021; da Silva et al., 2020; Akhalwaya et al., 2018). This is supported by the present study's LC/MS experimental chromatograms, which showed more peaks in methanol extracts than other solvents, indicating a higher diversity of compounds.

A study reported that certain plant extracts of phenolic compounds disrupt bacterial cell walls and interfere with cellular processes, enhancing antimicrobial efficacy. Moreover, polyphenols and tannins can interfere with the membrane potential, affecting the transport of nutrients and

waste across the membrane. Hence, the medicinal plant *S. africana* exhibited good antimicrobial activity. It was also reported that phytochemical compounds present in plant extracts interact with *P. aeruginosa's* unique characteristics, such as its virulence factors and resistance mechanisms, leading to enhanced sensitivity (Innocent et al., 2022).

The antimicrobial activity of SA-AgNPs revealed notable trends in the effectiveness against a range of bacterial strains. It was observed that SA-AgNPs samples stored at 4℃ demonstrated higher activity compared to those stored at 25℃, suggesting the importance of storage conditions in preserving the efficacy of AgNPs. Moreover, the study found that increasing the concentration of $AgNO_3$ used to synthesise SA-AgNPs correlated with an increase in antimicrobial activity, indicating a concentration-dependent trend. Specifically, SA-AgNPs synthesised using 5 mM $AgNO_3$ had the best antimicrobial activity, while those synthesised using lower concentrations (1-2 mM) had lower activity (Salayova et al., 2021; Swolana and Wojtyczka, 2022). Suggesting that the concentration of $AgNO_3$ used in synthesising SA-AgNPs plays a significant role in determining their antimicrobial activity.

The SA-AgNPs (2.68 mg/mL) generally exhibited greater effectiveness compared to SA-AuNPs (10.14 mg/mL) and the extracts (10 mg/mL), consistent with previous reports attributing this to factors such as morphology and AgNP size (Franzolin et al., 2022). Notably, bark-acetone conjugated AgNPs (SABA-AG) and leaf-acetone conjugated AgNPs (SALA-AG) emerged as the most potent, achieving substantial inhibition zones of 22 mm against *P. aeruginosa*. The SABA-AG also demonstrated high activity against *S. aureus* (21 mm). SA-AgNPs showed significant effectiveness compared to the positive control ($p=0.0346$), indicating strong antimicrobial activity against the tested resistant bacteria. Meanwhile, bark-water conjugated AgNPs (SABD-AG), and leaf-ethanol (SALE-AG) exhibited lower activity, particularly against *E. coli* and *A. baumannii*, respectively. These findings underscore the

varying degrees of antimicrobial activity among the tested samples and highlight the potential of SABA-AG and SALA-AG as effective antimicrobial agents.

These findings align with earlier research on the antibacterial effects of plant-derived AgNPs by agar-well diffusion methods and revealed significant activity against *P. aeruginosa*, suggesting that the efficacy of these NPs depends on their 5 mM $AgNO_3$ concentration (Salayova et al., 2021). Contrastingly, Liaqat et al. (2022) observed that plant-based AgNPs exhibited a high zone of inhibition against Gram-positive bacteria, such as *S. aureus*, as compared to Gram-negative bacteria, suggesting that the reduced susceptibility of Gram-negative bacteria may be attributed to the positive charges of AgNPs being hindered or blocked by the presence of lipopolysaccharides in the outer membrane, thereby reducing their effectiveness as indicated by Loo et al. (2018).

The precise mechanisms by which AgNPs exert their antibacterial effects remain incompletely understood (Liaqat et al., 2022). However, several potential modes of action have been proposed. AgNPs are known to interact with bacterial membranes, leading to structural destabilization and increased permeability (Hameed et al., 2019). This disruption can result in the leakage of cellular contents and, ultimately, cell death. Studies indicate that AgNPs can bind to membrane phospholipids, causing damage consistent with the significant inhibition observed in our study against *P. aeruginosa* and *S. aureus*.

Another well-documented mechanism involves the generation of reactive oxygen species (ROS). AgNPs can induce oxidative stress, damaging various cellular components, including lipids, proteins, and nucleic acids, which contribute to cell death. The heightened sensitivity of *P. aeruginosa* to SA-AgNPs in our findings may be attributed to this oxidative damage, as supported by previous research demonstrating the role of ROS in nanoparticle-mediated antibacterial activity (Hameed et al., 2019).

Additionally, AgNPs may interfere with intracellular processes by engaging with cytosolic proteins and enzymes, altering their functions and disrupting essential metabolic pathways (Bruna et al., 2021). The release of silver ions from AgNPs further enhances their antibacterial efficacy by interacting with cellular components and disrupting metabolic pathways (More et al., 2023).

The SA-AuNPs showed higher effectiveness against *S. aureus* and *P. aeruginosa*. Lower activity was observed against *A. baumannii*, and resistance was noted in *E. coli*. Notably, bark-methanol conjugated AuNPs (SABM90S100) and bark-ethanol conjugated AuNPs (SABE90S100) displayed the most significant inhibition activity against *S. aureus* (25 mm). Sample SABE90S100 also exhibited the highest activity against *P. aeruginosa* (16 mm). These findings suggested that SA-AuNPs may have selective antimicrobial effects against specific bacterial strains, particularly *S. aureus* and *P. aeruginosa* while showing limited efficacy against others like *A. baumannii* and *E. coli*. Leaf-water extracts (SALD) and their conjugated SA-AgNPs/SA-AuNPs exhibited weaker activity against the tested bacterial strains.

Studies have shown that AgNPs and AuNPs synthesised via green approaches exhibit strong antimicrobial activities against both Gram-positive (*S. aureus*) and Gram-negative (*E. coli*) bacteria, including resistant strains (Sher et al., 2022; Rani et al., 2023). Researchers have discovered that plant-synthesised AgNPs/AuNPs generally possess superior antimicrobial activity due to factors such as morphology, surface area, particle size and shape, and surface polarity (Amina et al., 2020). The observed susceptibility of *P. aeruginosa* to both extracts and NPs underscores their promising antimicrobial potential, particularly against multidrug-resistant strains (Sher et al., 2022).

The microdilution assay was used to determine the MIC of *S. africana* extracts, SA-AgNPs, and SA-AuNPs. Notably, the antimicrobial activity was statistically significant for SA-AgNPs

when compared to the positive control. Among the tested bacterial strains, *S. aureus* exhibited the highest susceptibility to *S. africana* extracts, followed by *E. coli*, *A. baumannii*, and *P. aeruginosa*. The leaf-methanol (SALM) and leaf-ethanol (SALE) extracts demonstrated the most potent antimicrobial activity against *S. aureus*, with the lowest MIC value recorded at 1.25 mg/mL. For E. coli, the extracts SABM, SABE, SALM, and SALE exhibited the best activity, each with a MIC of 2.5 mg/mL. Conversely, leaf-distilled water (SALD) extracts were ineffective against all bacterial strains. These findings underscore the dynamic antimicrobial properties of the *S. africana* extracts over time, with varying effectiveness against different bacterial strains. However, all crude extracts lacked bactericidal effects against *E. coli*, *P. aeruginosa*, and *A. baumannii*. Except for *S. aureus*, with SALE revealing the best killing effect at MBC of 2.5 mg/mL. The results highlight the potential of specific extracts like SALE against *S. aureus* and shed light on the complex interactions between extracts and bacterial susceptibility patterns.

Previous studies have consistently demonstrated the significant antibacterial activity of *S. africana* against various pathogens. Mathabe et al. (2008) reported that ethanol extracts from *S. africana* exhibited higher antibacterial activity against *S. aureus* and *E. coli*, with a MIC of 50 µg/mL, suggesting that the plant's antimicrobial activity may be attributed to the presence of bioactive compounds, particularly triterpenoids. Similarly, Nielsen et al. (2012) noted the remarkable activity of *S. africana* against antibiotic-resistant strains, such as *E. coli*, *S. aureus*, and *M. tuberculosis*, with a MIC value of 39.06 µg/mL. Furthermore, Shirinda et al. (2019) found that *S. africana* extracts were effective against *S. aureus* at a lower MIC value of 0.78 mg/mL. Research indicates that different plant extracts exhibit varying antimicrobial activities against specific bacteria due to the complex composition of phytochemicals (Intorasoot et al., 2017).

The observed resistance of *E. coli* to the extracts tested in this study could be attributed to various factors, including the specific mechanisms of action of the plant compounds, the unique characteristics of the *E. coli* strains tested, and their resistance profiles (Intorasoot et al., 2017; Tayel et al., 2018). Additionally, the selective bactericidal activity of plant extracts against *S. aureus* underscores the complexity of plant-bacteria interactions and highlights the need for further research to elucidate the specific mechanisms underlying these observations.

Regarding the activity of SA-AgNPs against ABR bacterial strains, it was found that methanol and ethanol extracts conjugated with AgNPs were more active against *E. coli*, *P. aeruginosa*, and *A. baumannii*, with a MIC value of 0.05 mg/mL. In contrast, acetone extracts conjugated with AgNPs showed activity (MIC of 0.09 mg/mL) against *S. aureus*. However, water extracts conjugated with AgNPs displayed lower efficacy against all tested strains. The difference in activity against Gram-positive and Gram-negative bacteria may be attributed to structural differences in their cell walls. The thick peptidoglycan layer in Gram-positive bacteria acts as a barrier, while the thinner cell membrane of Gram-negative bacteria allows for easier penetration of nanoparticles, leading to structural changes and cell death (Gevorgyan et al., 2022).

The SA-AgNPs samples consistently inhibited bacterial growth at very low concentrations, indicating their high efficacy in combating ABR bacteria. Notably, these SA-AgNPs samples generally exhibited greater activity against Gram-negative bacteria (*E. coli*, *P. aeruginosa*, and *A. baumannii*) with lower MIC values than against Gram-positive bacteria (*S. aureus*), which is consistent with several studies (Bakht Dalir et al., 2020; Meikle et al., 2020; Gevorgyan et al., 2022). All SA-AgNPs samples were able to completely kill all tested antibiotic-resistant bacterial strains, with SABM-AG and SABA-AG displaying the highest MBC value of 0.09 mg/mL against *A. baumannii* and *S. aureus*. Additionally, SABM-AG exhibited an MBC value of 0.17 mg/mL against *E. coli* and *P. aeruginosa*. Mohammed (2015)

stated that the antibacterial efficacy of AgNPs is derived from their ability to disrupt microbial membranes containing adhesive substances like proteins and polysaccharides, as well as the bactericidal effects of Ag^+ ions. The antibacterial activity of SA-AgNPs against *E. coli* may be attributed to the inhibition of phosphate absorption and the penetration of small-sized NPs into the bacterial cell wall, leading to structural changes and cell death (Bakht Dalir et al., 2020; Gevorgyan et al., 2022; More et al., 2023). Silver particles have a high affinity for sulfur and phosphorus, which are abundant in the bacterial cell membrane (Bakht Dalir et al., 2020). In contrast, *S. aureus* has a thicker peptidoglycan cell wall, making it harder for AgNPs to penetrate and inhibit their growth (Malanovic and Lohner, 2016). Consequently, a higher concentration of AgNPs was necessary to achieve inhibition (Bakht Dalir et al., 2020).

The MIC results for SA-AuNPs were comparable to those of the crude extracts but with enhanced antimicrobial activity. We observed varying activity levels against the tested bacterial strains, with *S. aureus* emerging as the most sensitive among the strains examined. Notably, samples SABM60S100 and SABE90S90100 exhibited the highest activity against *S. aureus*, with the lowest MIC value recorded at 0.64 mg/mL. Similarly, SABE90S90100 and SABA90S90100 demonstrated notable efficacy against *E. coli*, displaying a MIC value of 1.27 mg/mL. Additionally, SABA90S100 exhibited activity against *P. aeruginosa*, with a MIC value of 1.27 mg/mL. Intriguingly, none of the tested samples showed activity against *A. baumannii*. The bactericidal activity of SA-AuNPs showed that sample SABE90S90100 killed *S. aureus* and *E. coli* with MBC of 0.63 mg/mL and 2.5 mg/mL. No bactericidal effect against observed in *P. aeruginosa*. The differential effectiveness of SA-AuNPs against various bacterial strains can be attributed to several factors, including the size, shape, and surface charge of the NPs. Other metal ions in the samples may also influence their antimicrobial activity (Dove et al., 2023). The lack of activity against *A. baumannii* may be due to the unique

characteristics of this bacterium, such as its ability to produce biofilms and its resistance to various antibiotics (Yakoup et al., 2024).

Even in the microdilution assays, SA-AgNPs revealed excellent antimicrobial activity compared to SA-AuNPs and the extracts. In accordance with our findings, plant-based AgNPs exhibited superior antimicrobial activities compared to AuNPs and extracts (Pannerselvam et al., 2022). Reports have indicated that the synthesis of biogenic AgNPs from plant extracts enhances their bioactivity compared to the antibacterial activity of the plant extracts alone (Ahmed, 2016). Additionally, combining AgNPs with plant extracts has shown synergistic effects in inhibiting bacterial growth, making AgNPs a promising alternative for combating ABR bacteria (Liaqat et al., 2022).

The synergistic activity of *S. africana* extracts against resistant bacteria was assessed using the microdilution assay. The overall inhibition of plant extract combinations was less effective than that of individual extracts. The reason for these synergistic results of *S. africana* extracts can be attributed to the complex interactions between the bioactive compounds present in the plant extracts. These compounds may have varying mechanisms of action that could lead to different effects when combined. Additionally, the specific concentrations and ratios of the compounds in the mixtures may influence their overall antimicrobial activity.

In summary, SA-AgNPs exhibited superior antimicrobial efficacy compared to SA-AuNPs and plant extracts. This enhancement in activity is attributed to the release of Ag ions by the AgNPs, which disrupt cell walls and secondary metabolites adsorbed onto the NPs (Elemike et al., 2017). Additionally, bioactive compounds within the organic matrix might contribute to the heightened antibacterial activity of AgNPs by potentially enhancing their interaction with the cell wall (Salayova et al., 2021). Smaller NPs have a greater bactericidal effect compared to larger ones because of their larger surface area, facilitating interaction and absorption more

easily. These findings collectively underscore the diverse antimicrobial effects of *S. africana* extracts and their conjugated MNPs, positioning them as promising candidates against ABR bacteria and treatment for RTIs.

The MTT assay is a fundamental method in cytotoxicity studies for assessing cell viability (Sylvester, 2011). This assay relies on the reduction of MTT, a yellow tetrazolium dye, by mitochondrial dehydrogenases, to form purple formazan crystals. Subsequently, these crystals are then solubilised into a coloured solution using reagents such as dimethyl sulfoxide. The amount of formazan produced correlates with the number of live cells, quantified by measuring absorbance between 500 and 600 nm wavelengths (Mosmann, 1983).

The overall cytotoxic results indicate that all tested samples significantly reduced the viability of MCF-7 cancer cells compared to normal MCF-10 cells and RAW 264.7 macrophage cells. Greater cytotoxic effect on cancer cells compared to normal cells, which is a desirable characteristic for potential anticancer agents. It was also observed that lower sample concentrations inhibited cell growth, while higher concentrations stimulated it, showcasing a paradoxical effect influenced by complex cellular mechanisms and compound characteristics.

Direko et al. (2019) reported similar outcomes, indicating that the *S. Africana* plant possesses anti-inflammatory and anti-cancer properties. Their findings revealed that extracts at concentrations below 10 µg/mL inhibited the growth of cancer cells (MCF-7) while simultaneously stimulating normal cells (MCF-10A) and nitric oxide (NO) production. Polyphenolic compounds, particularly ellagic acid, demonstrated safety towards healthy cells but toxicity towards cancerous cells, suggesting their pivotal role in observed toxicity (Constantinou et al., 1995; Lee et al., 2019). These results are corroborated by the LC/MS analysis of this study, which identified ellagic acid as a significant compound.

Plant compounds exhibit a dose-response relationship, whereby their effects on cells may vary based on the concentration (Fadeyi et al., 2013). At lower concentrations, these compounds may specifically target cellular processes or receptors, inhibiting cell growth or function (Jodynis-Liebert and Kujawska, 2020). On the other hand, at higher concentrations, certain dominant compounds may hinder the action of those with toxicity effects, potentially leading to increased cell viability. This phenomenon can be attributed to the presence of multiple bioactive compounds in the extracts, which can have different mechanisms of action and different dose-response relationships.

The study found that the leaf-methanol extract (SALM) selectively induced cell death in MCF-7 cancer cells while stimulating the growth of normal MCF-10 cells at a specific lower concentration of 0.039 mg/mL. On the other hand, SA-AgNPs such as bark-acetone conjugated AgNPs (SABA-AG) exhibited the best cytotoxic effects against both MCF-7 (12% viability) and MCF-10 (127%) cells at the lowest concentration of 0.01 mg/mL. This desirable trait suggests that the SALM extract and SABA-AG may be effective in cancer therapy, as they have the potential to selectively eradicate cancer cells without harming normal cells, indicating their potential use as anticancer agents in a concentration-dependent manner. However, bark-acetone extracts (SABA) and SA-AuNPs (SABE-AU) stimulated the growth of cells, including cancer cells, across all concentrations. This suggests that they are not suitable candidates for therapy.

The cytotoxic effects of plant extracts have been attributed to the presence of specific secondary metabolites, such as terpenoids, which also have exhibited antibacterial properties (Mathabe et al., 2008; Van Den Bout-van den Beukel et al., 2008). Devanesan et al. (2020), demonstrated that the cytotoxicity of *Asafoetida* extract-AgNPs depended on the concentration of the NPs, resulting in a higher number of MCF-7 cell deaths at lower concentrations. This effect could be attributed to the bioactive compounds of the plant used in the reduction of AgNPs

(Devanesan et al., 2020). Another explanation for the good AgNP cytotoxicity effect is the NP's large surface-to-volume ratio, which exhibits heightened activity by efficiently penetrating cells, interacting with cellular components, and disturbing cellular signalling pathways (Akter et al., 2018). The cytotoxicity of AuNPs synthesised using green tea extract was found to be dependent on the Au concentration, with higher toxicity observed at lower concentrations (Lee et al., 2019).

The observed cytotoxicity effect of SA-AgNPs and SA-AuNPs can be explained by the complex interplay between the surface properties of the NPs and their concentration-dependent behaviours. When NPs are not modified to prevent spontaneous agglomeration, higher concentrations can promote their aggregation, leading to the formation of nano aggregates where individual particles are closely packed together (Bagwe et al., 2006; Clark et al., 2010; Sur et al., 2012). This aggregation can hide or quench the originally hyperreactive surfaces of the smaller NPs (Mudunkotuwa and Grassian, 2011). Consequently, the specific larger agglomerated NP form appears to be less toxic at higher concentrations than a lower dose of smaller, but well-dispersed NPs (Bell et al., 2014). This phenomenon highlighted the importance of considering not only the concentration of the NPs but also their aggregation state and surface properties when assessing their toxicity in biological systems. Several studies support this concept, highlighting the need to assess thoroughly NP formulations and plant extracts to optimise their therapeutic efficacy and safety profiles (Majoumouo et al., 2020).

Recent studies have shown that AgNPs and AuNPs can be effective in inducing cytotoxic effects on cancer cells by interfering with the cellular electron transfer chain in mitochondria, leading to increased levels of reactive oxygen species (ROS) and oxidative stress, ultimately causing cellular toxicity (Grewal et al., 2022). Additional studies reported that AgNPs create an unfavourable environment for cancer cells by increasing ROS and malondialdehyde levels while decreasing catalase and glutathione peroxidase enzyme activity, resulting in cell death

(Motafeghi et al., 2023; Selvi et al., 2016). Liu and others discovered another pathway for inducing apoptosis using NPs, where the primary cause of cell death is the upregulation of endoplasmic reticulum stress-related messenger ribonucleic acid and protein expression (Liu et al., 2023).

The size and shape of NPs play a crucial role in their cytotoxicity, with smaller sizes and specific shapes impacting their effectiveness (Grewal et al., 2022). Biosynthesised AgNPs within a range of sizes (5 to 80 nm) and various shapes (spherical, cuboidal, pentagonal, and hexagonal) have shown toxic effects on MCF-7 cancer cells (Baharara et al. 2015; Sathishkumar et al. 2016). Similarly, AuNP with spherical and rod-shapes, are more efficient in inhibiting cancer cell proliferation. Furthermore, the oxidative tendency of AgNPs to form Ag^{+} ions can induce cell death (Simon-Deckers et al. 2008; Chernousova and Epple 2013).

The SABA extract did not induce cytotoxicity against RAW 264.7 macrophage cells within the tested concentration range. This means that the SABA extract may not have significant toxic effects on the immune cells like macrophage cells, which is a desirable trait for potential therapeutic agents. On the other hand, the SALM extract had cytotoxic effects at lower concentrations, which could limit its therapeutic potential.

For SA-AgNPs samples, both SABA-AG and leaf SALE-AG exhibited stronger cytotoxic effects on RAW 264.7 macrophage cell at lower concentrations, highlighting their potential to induce significant cell damage and reduce cell viability, particularly at lower doses (Jodynis-Liebert and Kujawska, 2020). Lower concentrations induce pronounced cytotoxic effects, possibly through oxidative stress or membrane damage, while higher concentrations may prompt cellular repair mechanisms (Matysiak-Kucharek et al., 2020; Majeed et al., 2020). The unexpected increase in viability at higher concentrations suggests potential cellular adaptation or protective responses against NP-induced stress.

The SA-AuNPs (SABE-AU) demonstrated mild cytotoxicity at the lowest concentration of 0.08 mg/mL, with 58% cell viability, suggesting a moderate impact on cell health. However, at higher concentrations, cell viability exceeded 100%, indicating potential activation of adaptive responses or cellular repair mechanisms within macrophage cells, implying a favourable safety profile compared to SA-AgNPs.

The minimal cytotoxicity of AuNPs may be attributed to the presence of bioactive functional groups in the plant extract, indicating a potential correlation between low toxicity and phytochemicals provided by the plant extract (Huo et al., 2018). Further investigation into the biocompatibility of these materials is recommended, as highlighted in previous studies on similar NPs and hydroxyapatite dispersions (Scheel, 2009). Oh et al., (2018) found that treatments with Cs-AuNPs and Cs-AgNPs synthesised from plants resulted in decreased cell viability, with MCF7 cells showing greater sensitivity compared to RAW 264.7 macrophage cells. Both NPs inhibited breast cancer cell proliferation without significantly affecting RAW 264.7 cell growth at lower concentrations (0.01 µg/mL) in a dose-dependent manner. These findings underscore the critical importance of considering both extract and NP concentrations when assessing cytotoxicity activities in biological systems.

The present study highlights the anti-inflammatory effects of various *S. africana* samples on NO production in RAW 264.7 macrophage cells stimulated with lipopolysaccharide (LPS), a typical inducer of inflammation. Nitric oxide (NO) is a critical inflammatory mediator released from activated macrophages during immune responses (Rod-In et al., 2021). Our findings indicate that samples such as SALM, SALE-AG, and SABE-AU significantly decreased NO production across all concentration levels, suggesting their potential as anti-inflammatory agents. Conversely, SABA and SABA-AG exhibited increased NO production at specific concentrations, indicating a pro-inflammatory response. This aligns with previous studies that have shown elevated NO levels can promote apoptosis (Tschugguel et al., 1999). Hence, we

observed higher toxicity of SABA-AG against the RAW 264.7 cell around the same concentration that elevated the NO production.

These findings underscore the complex interplay between different compounds and inflammation regulation (Rod-In et al., 2021). SALM, SALE-AG, and SABE-AG may hold promise for anti-inflammatory therapy, while caution should be exercised with SABA and SABA-AG due to their potential to exacerbate inflammation. Further research is essential to elucidate the underlying mechanisms and determine these samples' therapeutic potential and safety profiles in managing inflammatory conditions.

The observed anti-inflammatory effects are attributed to various compounds, including O-glycosides, quercetin, flavonoid-C-glycosides, tannins, and variations of cinnamic acid. These compounds have been shown to inhibit the production of inflammatory factors and interfere with LPS binding to Toll-like receptors, thereby activating the antioxidative nuclear factor erythroid 2-related factor 2 (Nrf2) and increasing the expression of antioxidant proteins (Nascimento et al., 2017). For instance, studies on *Kigelia africana* have demonstrated its ability to suppress inflammatory mediators by inhibiting nitric oxide synthase (iNOS) expression and NO release in LPS-induced macrophages, highlighting the role of specific compounds like verminoside in mediating these effects (Nabatanzi et al., 2020).

Respiratory tract infections (RTIs) can cause damage to lung tissue, particularly affecting epithelial cells, through microbial infection and the host's inflammatory response (Allard et al., 2018). Macrophages release pro-inflammatory chemicals, exacerbating tissue damage if the injury persists. Effective tissue repair requires inflammation reduction. Research suggests plant extracts and their bioactive compounds possess significant anti-inflammatory potential, offering promise in treating various inflammatory diseases, including RTIs (Matotoka et al., 2023). For instance, sorghum extracts inhibit nitric oxide (NO), interleukin-6 (IL-6), and

reactive oxygen species (ROS) production in activated macrophages, with ethanolic extracts showing superior anti-inflammatory activity due to their tannin content (Hong et al., 2020). Thus, reducing NO production with plant extracts may offer therapeutic benefits in diseases driven by excessive NO levels, including respiratory infections.

The antioxidant activities of *S. africana* extracts, SA-AgNPs, and SA-AuNPs by the DPPH assay showed that leaf-acetone extracts (SALA) had excellent antioxidant activity (IC_{50} value of 0.000335 mg/mL), indicating strong antioxidant properties (Nabatanzi et al., 2020). This is consistent with other studies that have reported good antioxidant activity of *S. africana* against DPPH with IC_{50} values of 0.23 mg/mL (Dikhoba et al., 2019). Conversely, leaf-ethanol extracts (SALE) showed weak antioxidant activity with an IC_{50} value of 183 mg/mL, suggesting lower antioxidant efficacy. Bark acetone extracts conjugated AgNPs (SABA-AG) demonstrated good antioxidant activity with an IC_{50} value of 0.89 mg/mL, which is promising and comparable to the positive control Ascorbic acid (0.1 mg/mL). Bark ethanol conjugated AuNPs (SABM-AU) exhibited good antioxidant activity with an IC_{50} value of 0.38 mg/mL, indicating significant antioxidant potential.

The mechanisms behind the observed antioxidant activities involve the ability of phytochemicals to scavenge free radicals and reduce oxidative stress. Oxidative stress occurs when there is an imbalance between ROS production and the body's ability to neutralize them, potentially leading to cellular damage. Antioxidative enzymes such as superoxide dismutase, glutathione peroxidase, and antioxidants like glutathione play a vital role in maintaining this balance (Chen et al., 2017). Free radicals, when not adequately regulated by antioxidants, can lead to oxidative stress, damaging lipids, proteins, and DNA, and contributing to various diseases (More and Makola, 2020). Plant compounds with antioxidative properties, such as flavonoids and polyphenols, are crucial in scavenging free radicals and preventing cellular damage (Wang et al., 2020).

Phytochemical compounds in *S. africana* reported to have anti-inflammatory and antioxidant properties are saponins, flavonoids, and glycosides (Nascimento et al., 2017; Direko et al., 2019). Flavonoids were notably abundant in the extracts of *S. africana* in the current study, potentially contributing to the observed antioxidant activity, consistent with findings by Huo et al. (2018). Additionally, terpenoids, specifically triterpenoids, were identified as key contributors to the antioxidant activities in the tested crude extracts (Mathabe et al., 2008; Direko et al., 2019; Singh et al., 2020). Total soluble phenolics in plant extracts may also contribute to their antioxidant properties (Kamatou, 2010). For example, the dichloromethane fraction of the brown seaweed *Sargassum siliquastrum* exhibited strong antioxidant activity, potentially due to the presence of phenolic compounds (Lim, 2002). The crude extract and ethyl acetate-soluble fraction of the red algae *Polysiphonia urceolata* also demonstrated high antioxidant activity, correlated with their total phenolic content and reducing power (Duan, 2006).

The difference in antioxidant activity between NPs was attributed to their biosynthesised nature, confirmed by FT-IR spectral results (Huo et al., 2018). This was evident in the current research, where SA-AgNPs exhibited fewer pronounced peaks than SA-AuNPs, indicating a higher concentration of phytochemicals in AuNPs, enhancing the antioxidant efficacy of SA-AuNPs against DPPH free radicals. These findings collectively suggest that the antioxidant properties of the *S. africana* extract, SA-AgNPs, and SA-AuNPs were likely due to their flavonoids, terpenoids, glycosides, phenolic content, and reducing power.

Chapter 6: Conclusions and Recommendations

6.1 Conclusion

The study proposed a novel approach to combating antibiotic-resistant (ABR) bacteria, implicated in RTIs, by synthesising MNPs from medicinal plants. The synthesis and characterisation of silver (SA-AgNPs) and gold nanoparticles (SA-AuNPs) using *Spirostachys africana* (*S. africana*) extract provided valuable insights into the NP formation process and their resulting properties. The study emphasised the importance of optimising reaction parameters, including extract type and concentration, metal salt concentration, reaction time, and temperature, to achieve desired NP characteristics.

Characterisation techniques such as UV-Vis, XRD, DLS, and TEM revealed distinct optimal properties for each type of NP. SA-AgNPs exhibited a narrow SPR peak at 480 nm, while TEM analysis showed that these SA-AgNPs consisted of smaller spherical particles and larger squash-spherical, hexagonal, and irregular shapes, with sizes ranging from 5 to 49.5 nm. In contrast, SA-AuNPs displayed an SPR peak at 541 nm and were characterised by spheroidal and star-shaped morphologies, with core sizes ranging from 6 to 32 nm.

XRD confirmed that both types of NPs possess a face-centred cubic (FCC) structure, with SA-AgNPs displaying a higher degree of crystallinity compared to SA-AuNPs. The average crystalline size ranged from 9-19 nm for SA-AgNPs and 9-10 nm for SA-AuNPs. DLS indicated that most synthesised SA-AgNPs were polydisperse, while the majority of SA-AuNPs were monodisperse. Zeta potential analysis revealed a high degree of stability among methanol extracts-conjugated SA-AgNPs, with a zeta potential value of -27 mV.

FTIR analysis identified key functional groups in the extracts and SA-AgNPs/SA-AuNPs. The functional groups included the hydroxyl, carboxyl, and amine groups, which play a role in reducing and capping Ag^{+} and Au^{+} ions. Additionally, LC-MS results of *S. africana* extract

confirmed the presence of various phytochemical compounds, such as flavonoids, phenolic acids, tannins, and polyphenols, which are known for their diverse biological activities. These compounds likely facilitated the reduction and stabilisation of metal ions into MNPs. Moreover, methanol proved to be the most efficient solvent for the extraction process.

The overall antimicrobial activity of the crude extracts and SA-AgNPs/SA-AuNPs demonstrated significant inhibition of both Gram-negative and Gram-positive bacteria. The results from agar well diffusion and microdilution methods revealed that SA-AgNPs possessed superior antimicrobial properties compared to SA-AuNPs and crude extracts, emphasising their potential as effective agents against ABR bacterial strains. Specifically, acetone bark/leaf-conjugated SA-AgNPs achieved the highest zone of inhibition (22 mm) against *P. aeruginosa*, while acetone bark-conjugated SA-AgNPs showed a 21 mm zone against *S. aureus*. Additionally, acetone leaf-conjugated SA-AgNPs were most effective against *A. baumannii* (18 mm), and methanol leaf-conjugated SA-AgNPs inhibited *E. coli* by 18 mm. Microdilution assays further confirmed the potent antimicrobial properties of SA-AgNPs, with methanol/ethanol-conjugated SA-AgNPs exhibiting lower MICs of 0.05 mg/mL against *E. coli*, *P. aeruginosa*, and *A. baumannii*. Acetone bark-conjugated SA-AgNPs had MIC of 0.09 mg/mL against *S. aureus*.

The cytotoxicity evaluation of *S. africana* extracts and their conjugated SA-AgNPs/SA-AuNPs demonstrated selective toxicity towards MCF-7 breast cancer cells compared to normal MCF-10 cells and RAW 264.7 macrophage cells at lower concentrations. This selective cytotoxicity highlights the potential of these extracts and NPs for targeted cancer therapy in a dose-dependent manner. Specifically, acetone extracts were toxic against MCF-7 cells while stimulating non-cancerous MCF-10 and RAW 264.7 cells at a concentration of 0.078 mg/mL. Additionally, ethanol extracts and their conjugated SA-AgNPs/SA-AuNPs significantly

reduced nitric oxide (NO) production, indicating anti-inflammatory potential. Lastly, acetone extract also exhibited exceptional antioxidant activity with an IC_{50} of 0.000335 mg/mL.

Overall, these findings indicate that the synthesis of SA-AgNPs and SA-AuNPs from *S. africana* extracts presents promising avenues for combating ABR bacteria responsible for RTIs. The antimicrobial properties of these NPs, combined with their potential for targeted cancer therapy and anti-inflammatory applications, highlighted their therapeutic potential. However, this study has several limitations. The long-term stability, potential toxicity, and clinical applicability of these NPs in therapeutic settings require further investigation. Additionally, in vivo evaluations and a deeper exploration of the mechanisms underlying the observed antimicrobial and anticancer activities are necessary to fully understand the efficacy and safety of these biogenic NPs.

6.2 Recommendations

Future research should focus on clarifying the mechanisms of NP formation to improve control over characteristics such as size, stability, and drug delivery efficiency. Isolating and identifying bioactive compounds in the *S. africana* plant is crucial, as these compounds can enhance NP efficacy. Further studies should investigate the complex mechanisms of NP formation, including nucleation, growth, stabilisation by capping agents, and the role of biomolecules in metal ion reduction. Additionally, exploring the synergistic effects of combining SA-AuNPs with existing antibiotics can enhance antimicrobial efficacy.

It is important to further investigate the dose-dependent nature of the cytotoxic and anti-inflammatory effects, as this underscores the significance of considering extract concentration in biological evaluations. Research should also examine how different phytochemicals influence NP formation kinetics to provide valuable insights. Finally, translating these findings into clinically relevant NP-based therapeutics and diagnostics is vital. This will enhance

applications in drug delivery, cancer therapy, and biosensing. By improving the understanding of NP formation processes, researchers can optimize synthesis to produce stable NPs with tunable properties for enhanced biomedical applications.

3.7 References

Abbai, R., Mathiyalagan, R., Markus, J., Kim, Y.J., Wang, C., Singh, P., Ahn, S., Farh, M.E.A. and Yang, D.C., 2016. Green synthesis of multifunctional silver and gold nanoparticles from the oriental herbal adaptogen: Siberian ginseng. *International journal of nanomedicine*, pp.3131-3143.

Abubakar, A.R. and Haque, M., 2020. Preparation of medicinal plants: Basic extraction and fractionation procedures for experimental purposes. *Journal of pharmacy & bioallied sciences*, *12*(1), p.1.

Adegbaju, O.D., Otunola, G.A. and Afolayan, A.J., 2020. Anti-inflammatory and cytotoxic evaluation of extracts from the flowering stage of Celosia argentea. *BMC complementary medicine and therapies*, *20*, pp.1-7.

Afreen, A., Ahmed, R., Mehboob, S., Tariq, M., Alghamdi, H.A., Zahid, A.A., Ali, I., Malik, K. and Hasan, A., 2020. Phytochemical-assisted biosynthesis of silver nanoparticles from Ajuga bracteosa for biomedical applications. *Materials Research Express*, *7*(7), p.075404.

Agyepong, N., Agyare, C., Adarkwa-Yiadom, M. and Gbedema, S.Y., 2014. Phytochemical investigation and antimicrobial activity of Clausena anisata (Willd), Hook. *African Journal of Traditional, Complementary and Alternative Medicines*, *11*(3), pp.200-209.

Ahmad, N., Ali, S., Abbas, M., Fazal, H., Saqib, S., Ali, A., Ullah, Z., Zaman, S., Sawati, L., Zada, A. and Sohail, 2023. Antimicrobial efficacy of Mentha piperata-derived biogenic zinc oxide nanoparticles against UTI-resistant pathogens. *Scientific reports*, *13*(1), p.14972.

Ahmed, S., 2016. Saifullah; Ahmad, M.; Swami, BL; Ikram, S. Green synthesis of silver nanoparticles using Azadirachta indica aqueous leaf extract. *J. Radiat. Res. Appl. Sci*, *9*, pp.1-7.

Akhalwaya, S., Van Vuuren, S. and Patel, M., 2018. An in vitro investigation of indigenous South African medicinal plants used to treat oral infections. *Journal of ethnopharmacology*, *210*, pp.359-371.

Akpaka, P.E., Kissoon, S., Wilson, C., Jayaratne, P., Smith, A. and Golding, G.R., 2017. Molecular characterization of vancomycin-resistant Enterococcus faecium isolates from Bermuda. *PLoS One*, *12*(3), p.e0171317.

Akter, M., Sikder, M.T., Rahman, M.M., Ullah, A.A., Hossain, K.F.B., Banik, S., Hosokawa, T., Saito, T. and Kurasaki, M., 2018. A systematic review on silver nanoparticles-induced cytotoxicity: Physicochemical properties and perspectives. *Journal of advanced research*, *9*, pp.1-16.

Albanese, L., Bonetti, A., D'Acqui, L.P., Meneguzzo, F. and Zabini, F., 2019. Affordable production of antioxidant aqueous solutions by hydrodynamic cavitation processing of silver fir (Abies alba Mill.) needles. *Foods*, *8*(2), p.65.

Aldbass, A., Amina, M., Al Musayeib, N.M., Bhat, R.S., Al-Rashed, S., Marraiki, N., Fahmy, R. and El-Ansary, A., 2021. Cytotoxic and anti-excitotoxic effects of selected plant and algal extracts using COMET and cell viability assays. *Scientific Reports*, *11*(1), p.8512.

Al-Harbi, S.A., Abdulrahman, A.O., Zamzami, M.A. and Khan, M.I., 2021. Urolithins: The gut based polyphenol metabolites of ellagitannins in cancer prevention, a review. *Frontiers in Nutrition*, *8*, p.647582.

Ali, H.R.K., Moawad, M.S. and Selim, S.A., 2016. In vitro study for comparing the cytotoxicity of silver and gold nanospheres on raw 264.7 murine macrophage cell line. *J Bacteriol Parasitol*, *7*, p.264.

Allard, B., Panariti, A. and Martin, J.G., 2018. Alveolar macrophages in the resolution of inflammation, tissue repair, and tolerance to infection. *Frontiers in immunology, 9*, p.380486.

Álvarez-Chimal, R. and Arenas-Alatorre, J.Á., 2023. Green synthesis of nanoparticles. A biological approach.

Amina, M., Al Musayeib, N.M., Alarfaj, N.A., El-Tohamy, M.F. and Al-Hamoud, G.A., 2020. Antibacterial and immunomodulatory potentials of biosynthesized Ag, Au, Ag-Au bimetallic alloy nanoparticles using the Asparagus racemosus root extract. *Nanomaterials*, *10*(12), p.2453.

Andrews, J.M., 2001. Determination of minimum inhibitory concentrations. *Journal of antimicrobial Chemotherapy*, *48*(suppl_1), pp.5-16.

Aron, A.T., Gentry, E.C., McPhail, K.L., Nothias, L.F., Nothias-Esposito, M., Bouslimani, A., Petras, D., Gauglitz, J.M., Sikora, N., Vargas, F. and van Der Hooft, J.J., 2020. Reproducible molecular networking of untargeted mass spectrometry data using GNPS. *Nature protocols*, *15*(6), pp.1954-1991.

Arshi, N., Ahmed, F., Anwar, M.S., Kumar, S., Koo, B.H., Lu, J. and Lee, C.G., 2011. Novel and cost-effective synthesis of silver nanocrystals: a green synthesis. *Nano*, *6*(04), pp.295-300.

Ashraf, J.M., Ansari, M.A., Khan, H.M., Alzohairy, M.A. and Choi, I., 2016. Green synthesis of silver nanoparticles and characterization of their inhibitory effects on AGEs formation using biophysical techniques. *Scientific reports*, *6*(1), pp.1-10.

Asong, J.A., Frimpong, E.K., Seepe, H.A., Katata-Seru, L., Amoo, S.O. and Aremu, A.O., 2023. Green Synthesis of Characterized Silver Nanoparticle Using Cullen tomentosum and Assessment of Its

Awad, A.M., Kumar, P., Ismail-Fitry, M.R., Jusoh, S., Ab Aziz, M.F. and Sazili, A.Q., 2021. Green extraction of bioactive compounds from plant biomass and their application in meat as natural antioxidant. *Antioxidants*, *10*(9), p.1465.

Ayinde, W.B., Gitari, W.M. and Samie, A., 2019. Optimisation of microwave-assisted synthesis of silver nanoparticle by Citrus paradisi peel and its application against pathogenic water strain. *Green Chemistry Letters and Reviews*, *12*(3), pp.225-234.

Azwatul, H.M., Uda, M.N.A., Gopinath, S.C., Arsat, Z.A., Abdullah, F., Muttalib, M.F.A., Hashim, M.K.R., Hashim, U., Isa, M., Uda, M.A. and Yaakub, A.R.W., 2023. Plant-based green synthesis of silver nanoparticle via chemical bonding analysis. Materials Today: Proceedings.

B. Aziz, S., Hussein, G., Brza, M.A., J. Mohammed, S., T. Abdulwahid, R., Raza Saeed, S. and Hassanzadeh, A., 2019. Fabrication of interconnected plasmonic spherical silver nanoparticles with enhanced localized surface plasmon resonance (LSPR) peaks using quince leaf extract solution. *Nanomaterials*, *9*(11), p.1557.

Babu, M.G. and Gunasekaran, P., 2009. Production and structural characterization of crystalline silver nanoparticles from Bacillus cereus isolate. *Colloids and surfaces B: Biointerfaces*, *74*(1), pp.191-195.

Baharara, J., Namvar, F., Ramezani, T., Mousavi, M. and Mohamad, R., 2015. Silver nanoparticles biosynthesized using Achillea biebersteinii flower extract: apoptosis induction in MCF-7 cells via caspase activation and regulation of Bax and Bcl-2 gene expression. *Molecules*, *20*(2), pp.2693-2706.

Baharara, J., Ramezani, T., Hosseini, N. and Mousavi, M., 2018. Silver nanoparticles synthesised coating with Zataria Multiflora leaves extract induced apoptosis in hela cells through p53 activation. *Iranian journal of pharmaceutical research: IJPR*, *17*(2), p.627.

Bahrami, M., Ghazavi, A., Ganji, A. and Mosayebi, G., 2021. Anti-inflammatory activity of S. Marianum and N. Sativa extracts on macrophages. *Reports of Biochemistry & Molecular Biology*, *10*(2), p.288.

Bakht Dalir, S.J., Djahaniani, H., Nabati, F. and Hekmati, M., 2020. Characterization and the evaluation of antimicrobial activities of silver nanoparticles biosynthesized from Carya illinoinensis leaf extract. *Heliyon*, *6*(3).

Bamsaoud, S.F., Basuliman, M.M., Bin-Hameed, E.A., Balakhm, S.M. and Alkalali, A.S., 2021, May. The effect of volume and concentration of AgNO3 aqueous solutions on silver nanoparticles synthesized using Ziziphus Spina–Christi leaf extract and their antibacterial activity. In *Journal of Physics: Conference Series* (Vol. 1900, No. 1, p. 012005). IOP Publishing.

Bamsaoud, S.F., Basuliman, M.M., Bin-Hameed, E.A., Balakhm, S.M. and Alkalali, A.S., 2021, May. The effect of volume and concentration of AgNO3 aqueous solutions on silver nanoparticles synthesized using Ziziphus Spina–Christi leaf extract and their antibacterial activity. In *Journal of Physics: Conference Series* (Vol. 1900, No. 1, p. 012005). IOP Publishing.

Bell, I.R., Ives, J.A. and Wayne, B.J., 2014. Nonlinear effects of nanoparticles: biological variability from hormetic doses, small particle sizes, and dynamic adaptive interactions. *Dose-Response*, *12*(2), pp.dose-response.

Bhatia, P., Sharma, A., George, A.J., Anvitha, D., Kumar, P., Dwivedi, V.P. and Chandra, N.S., 2021. Antibacterial activity of medicinal plants against ESKAPE: An update. *Heliyon*, *7*(2).

Blanco, P., Hernando-Amado, S., Reales-Calderon, J.A., Corona, F., Lira, F., Alcalde-Rico, M., Bernardini, A., Sanchez, M.B. and Martinez, J.L., 2016. Bacterial multidrug efflux pumps: much more than antibiotic resistance determinants. *Microorganisms*, *4*(1), p.14.

Breijyeh, Z., Jubeh, B. and Karaman, R., 2020. Resistance of gram-negative bacteria to current antibacterial agents and approaches to resolve it. *Molecules*, *25*(6), p.1340.

Bruna, T., Maldonado-Bravo, F., Jara, P. and Caro, N., 2021. Silver nanoparticles and their antibacterial applications. *International journal of molecular sciences*, *22*(13), p.7202.

Burlec, A.F., Corciova, A., Boev, M., Batir-Marin, D., Mircea, C., Cioanca, O., Danila, G., Danila, M., Bucur, A.F. and Hancianu, M., 2023. Current overview of metal nanoparticles' synthesis, characterization, and biomedical applications, with a focus on silver and gold nanoparticles. *Pharmaceuticals*, *16*(10), p.1410.

Cascio, C., Geiss, O., Franchini, F., Ojea-Jimenez, I., Rossi, F., Gilliland, D. and Calzolai, L., 2015. Detection, quantification and derivation of number size distribution of silver nanoparticles in antimicrobial consumer products. *Journal of Analytical Atomic Spectrometry*, *30*(6), pp.1255-1265.

Chandrakala, V., Aruna, V. and Angajala, G., 2022. Review on metal nanoparticles as nanocarriers: Current challenges and perspectives in drug delivery systems. *Emergent Materials*, *5*(6), pp.1593-1615.

Chen, T., Sheng, J., Fu, Y., Li, M., Wang, J. and Jia, A.Q., 2017. 1H NMR-based global metabolic studies of Pseudomonas aeruginosa upon exposure of the quorum sensing inhibitor resveratrol. *Journal of Proteome Research*, *16*(2), pp.824-830.

Chernousova, S. and Epple, M., 2013. Silver as antibacterial agent: ion, nanoparticle, and metal. *Angewandte Chemie International Edition*, *52*(6), pp.1636-1653.

Chiu, C.P., Liu, S.C., Tang, C.H., Chan, Y., El-Shazly, M., Lee, C.L., Du, Y.C., Wu, T.Y., Chang, F.R. and Wu, Y.C., 2016. Anti-inflammatory cerebrosides from cultivated Cordyceps militaris. *Journal of agricultural and food chemistry*, *64*(7), pp.1540-1548.

Choi, U. and Lee, C.R., 2019. Distinct roles of outer membrane porins in antibiotic resistance and membrane integrity in Escherichia coli. *Frontiers in microbiology*, *10*, p.953.

Constantinou, A., Stoner, G.D., Mehta, R., Rao, K., Runyan, C. and Moon, R., 1995. The dietary anticancer agent ellagic acid is a potent inhibitor of DNA topoisomerases in vitro.

da Silva, L.C., Souza, M.C., Sumere, B.R., Silva, L.G., da Cunha, D.T., Barbero, G.F., Bezerra, R.M. and Rostagno, M.A., 2020. Simultaneous extraction and separation of bioactive compounds from apple pomace using pressurized liquids coupled on-line with solid-phase extraction. *Food Chemistry*, *318*, p.126450.

Dada, A.O., Adekola, F.A., Dada, F.E., Adelani-Akande, A.T., Bello, M.O., Okonkwo, C.R., Inyinbor, A.A., Oluyori, A.P., Olayanju, A., Ajanaku, K.O. and Adetunji, C.O., 2019. Silver nanoparticle synthesis by Acalypha wilkesiana extract: phytochemical screening, characterization, influence of operational parameters, and preliminary antibacterial testing. *Heliyon*, *5*(10).

Desai, A.S., Ashok, A., Edis, Z., Bloukh, S.H., Gaikwad, M., Patil, R., Pandey, B. and Bhagat, N., 2023. Meta-Analysis of Cytotoxicity Studies Using Machine Learning Models on Physical Properties of Plant Extract-Derived Silver Nanoparticles. *International Journal of Molecular Sciences*, *24*(4), p.4220.

Devanesan, S., Ponmurugan, K., AlSalhi, M.S. and Al-Dhabi, N.A., 2020. Cytotoxic and antimicrobial efficacy of silver nanoparticles synthesized using a traditional phytoproduct, asafoetida gum. *International Journal of Nanomedicine*, pp.4351-4362.

Devi, G.K. and Sathishkumar, K., 2017. Synthesis of gold and silver nanoparticles using Mukia maderaspatna plant extract and its anticancer activity. *IET nanobiotechnology*, 11(2), pp.143-151.

Dikhoba, P.M., Mongalo, N.I., Elgorashi, E.E. and Makhafola, T.J., 2019. Antifungal and anti-mycotoxigenic activity of selected South African medicinal plants species. *Heliyon*, *5*(10).

Dilbar, S., Sher, H., Ali, H., Ullah, R., Ali, A. and Ullah, Z., 2023. Antibacterial Efficacy of Green Synthesized Silver Nanoparticles Using Salvia nubicola Extract against Ralstonia solanacearum, the Causal Agent of Vascular Wilt of Tomato. *ACS omega*, *8*(34), pp.31155-31167.

Direko, P., Mfengwana, H., Mashele, S. and Sekhoacha, M., 2019. Investigating the angiogenic modulating properties of Spirostachys africana in MCF-7 breast cancer cell line. *International Journal of Pharmacology*, *15*(8), pp.970-977.

Donkor, M.N., Donkor, A.M. and Mosobil, R., 2023. Combination therapy: synergism among three plant extracts against selected pathogens. *BMC Research Notes*, *16*(1), p.83.

Dos Santos, E.M.P., Martins, C.C.B., de Oliveira Santos, J.V., da Silva, W.R.C., Silva, S.B.C., Pelagio-Flores, M.A., Galembeck, A. and Cavalcanti, I.M.F., 2021. Silver nanoparticles–chitosan composites activity against resistant bacteria: tolerance and biofilm inhibition. *Journal of Nanoparticle Research*, *23*(8), p.196.

Dove, A.S., Dzurny, D.I., Dees, W.R., Qin, N., Nunez Rodriguez, C.C., Alt, L.A., Ellward, G.L., Best, J.A., Rudawski, N.G., Fujii, K. and Czyż, D.M., 2023. Silver nanoparticles enhance the efficacy of aminoglycosides against antibiotic-resistant bacteria. *Frontiers in Microbiology*, *13*, p.1064095.

Du, L., Zhang, R., Yang, H., Tang, S., Hou, Z., Jing, J., Lin, B., Zhang, S., Lu, Z. and Xue, P., 2020. Synthesis, characteristics and medical applications of plant nanomaterials. *Planta*, *252*, pp.1-16.

Egorov, A.M., Ulyashova, M.M. and Rubtsova, M.Y., 2018. Bacterial enzymes and antibiotic resistance. *Acta Naturae (англоязычная версия)*, *10*(4 (39)), pp.33-48.

Elbagory, A.M., Cupido, C.N., Meyer, M. and Hussein, A.A., 2016. Large scale screening of southern African plant extracts for the green synthesis of gold nanoparticles using microtitre-plate method. *Molecules*, *21*(11), p.1498

Fadeyi, S.A., Fadeyi, O.O., Adejumo, A.A., Okoro, C. and Myles, E.L., 2013. In vitro anticancer screening of 24 locally used Nigerian medicinal plants. B*MC complementary and alternative medicine*, *13*, pp.1-10.

Fernández, L. and Hancock, R.E., 2012. Adaptive and mutational resistance: role of porins and efflux pumps in drug resistance. *Clinical microbiology reviews*, *25*(4), pp.661-681.

Fouda, A., Eid, A.M., Guibal, E., Hamza, M.F., Hassan, S.E.D., Alkhalifah, D.H.M. and El-Hossary, D., 2022. Green synthesis of gold nanoparticles by aqueous extract of zingiber officinale: Characterization and insight into antimicrobial, antioxidant, and in vitro cytotoxic activities. *Applied Sciences*, *12*(24), p.12879.

Franzolin, M.R., Courrol, D.D.S., Silva, F.R.D.O. and Courrol, L.C., 2022. Antimicrobial activity of silver and gold nanoparticles prepared by photoreduction process with leaves and fruit extracts of Plinia cauliflora and Punica granatum. *Molecules*, *27*(20), p.6860.

Gelfand, M., Mavi, S., Drummond, R.B. and Ndemera, B., 1985. *Zambeziana: a new series on culture and society in Central Africa. 17. The traditional medical practitioner in Zimbabwe: his principles of pratice and pharmacopoeia*. Mambo press.

Gevorgyan, S., Schubert, R., Falke, S., Lorenzen, K., Trchounian, K. and Betzel, C., 2022. Structural characterization and antibacterial activity of silver nanoparticles synthesized using a low-molecular-weight Royal Jelly extract. *Scientific Reports*, *12*(1), p.14077.

Ghani, S., Rafiee, B., Bahrami, S., Mokhtari, A., Aghamiri, S. and Yarian, F., 2022. Green synthesis of silver nanoparticles using the plant extracts of vitex agnus castus L: An ecofriendly approach to overcome antibiotic resistance. *International Journal of Preventive Medicine*, *13*.

Ghavam, M., 2021. Relationships of irrigation water and soil physical and chemical characteristics with yield, chemical composition and antimicrobial activity of Damask rose essential oil. *PLoS One*, *16*(4), p.e0249363.

Gopinath, K., Kumaraguru, S., Bhakyaraj, K., Mohan, S., Venkatesh, K.S., Esakkirajan, M., Kaleeswarran, P., Alharbi, N.S., Kadaikunnan, S., Govindarajan, M. and Benelli, G., 2016. Green synthesis of silver, gold and silver/gold bimetallic nanoparticles using the Gloriosa superba leaf extract and their antibacterial and antibiofilm activities. *Microbial pathogenesis*, *101*, pp.1-11.

Goswami, S.R., Sahareen, T., Singh, M. and Kumar, S., 2015. Role of biogenic silver nanoparticles in disruption of cell–cell adhesion in Staphylococcus aureus and Escherichia coli biofilm. *Journal of Industrial and Engineering Chemistry*, *26*, pp.73-80.

Goudarzi, M. and Navidinia, M., 2019. Overview perspective of bacterial strategies of resistance to biocides and antibiotics. *Archives of Clinical Infectious Diseases*, *14*(2).

Grewal, J., Kumar, V., Rawat, H., Gandhi, Y., Singh, R., Singh, A., Babu, G., Srikanth, N. and Mishra, S.K., 2022. Cytotoxic effect of plant extract-based nanoparticles on cancerous cells: a review. *Environmental Chemistry Letters*, *20*(4), pp.2487-2507.

Guadie Assefa, A., Adugna Mesfin, A., Legesse Akele, M., Kokeb Alemu, A., Gangapuram, B.R., Guttena, V. and Alle, M., 2017. Microwave-assisted green synthesis of gold nanoparticles using Olibanum gum (Boswellia serrate) and its catalytic reduction of 4-nitrophenol and hexacyanoferrate (III) by sodium borohydride. *Journal of Cluster Science*, *28*, pp.917-935.

Guo, Z., Chen, Y., Wang, Y., Jiang, H. and Wang, X., 2020. Advances and challenges in metallic nanomaterial synthesis and antibacterial applications. *Journal of Materials Chemistry B*, *8*(22), pp.4764-4777.

Hatipoğlu, A., 2022. Green Synthesis of Silver Nanoparticles and Their Antimicrobial Effects on Some Food Pathogens. *Süleyman Demirel University Journal of Science and Technology*, *26*(1), pp.106-114.

He, Y., Du, Z., Ma, S., Liu, Y., Li, D., Huang, H., Jiang, S., Cheng, S., Wu, W., Zhang, K. and Zheng, X., 2016. Effects of green-synthesized silver nanoparticles on lung cancer cells in vitro and grown as xenograft tumors in vivo. *International journal of nanomedicine*, pp.1879-1887.

Hernández-Morales, L., Espinoza-Gómez, H., Flores-López, L.Z., Sotelo-Barrera, E.L., Núñez-Rivera, A., Cadena-Nava, R.D., Alonso-Núñez, G. and Espinoza, K.A., 2019. Study of the green synthesis of silver nanoparticles using a natural extract of dark or white Salvia hispanica L. seeds and their antibacterial application. *Applied Surface Science*, *489*, pp.952-961.

Heterogeneous size distributions of silver nanoparticles (AgNPs) refer to the presence of AgNPs with a wide range of sizes within a given sample.

Honary, S., Barabadi, H., Gharaei-Fathabad, E. and Naghibi, F., 2013. Green synthesis of silver nanoparticles induced by the fungus Penicillium citrinum. *Tropical Journal of Pharmaceutical Research*, *12*(1), pp.7-11.

Hong, S., Pangloli, P., Perumal, R., Cox, S., Noronha, L.E., Dia, V.P. and Smolensky, D., 2020. A comparative study on phenolic content, antioxidant activity and anti-inflammatory capacity of aqueous and ethanolic extracts of sorghum in lipopolysaccharide-induced RAW 264.7 macrophages. *Antioxidants, 9*(12), p.1297.

Hong, X., Wen, J., Xiong, X. and Hu, Y., 2016. Shape effect on the antibacterial activity of silver nanoparticles synthesized via a microwave-assisted method. *Environmental science and pollution research*, *23*, pp.4489-4497.

Htwe, Y.Z.N., Chow, W.S., Suda, Y. and Mariatti, M., 2019. Effect of silver nitrate concentration on the production of silver nanoparticles by green method. *Materials Today: Proceedings*, *17*, pp.568-573.

Huang, Y., Wei, W.I., Correia, D.F., Ma, B.H.M., Tang, A., Yeoh, E.K., Wong, S.Y.S., Ip, M. and Kwok, K.O., 2023. Antibiotic use for respiratory tract infections among older adults living in long-term care facilities: a systematic review and meta-analysis. *Journal of Hospital Infection*, *131*, pp.107-121.

Huo, Y., Singh, P., Kim, Y.J., Soshnikova, V., Kang, J., Markus, J., Ahn, S., Castro-Aceituno, V., Mathiyalagan, R., Chokkalingam, M. and Bae, K.S., 2018. Biological synthesis of gold and silver chloride nanoparticles by Glycyrrhiza uralensis and in vitro applications. *Artificial cells, nanomedicine, and biotechnology*, *46*(2), pp.303-312.

Hyde, M.A., Wursten, B.T., Ballings, P. & Coates Palgrave, M. (2022). Flora of Zimbabwe: Species information: individual images: Spirostachys africana. [Online] Available at: https://www.zimbabweflora.co.zw/speciesdata/imagedisplay.php?species_id=135700&imag_id=3 [Accessed 11 April 2022].

Ider, M., Abderrafi, K., Eddahbi, A., Ouaskit, S. and Kassiba, A., 2017. Silver metallic nanoparticles with surface plasmon resonance: synthesis and characterizations. *Journal of Cluster Science*, *28*, pp.1051-1069.

Ider, M., Abderrafi, K., Eddahbi, A., Ouaskit, S. and Kassiba, A., 2017. Silver metallic nanoparticles with surface plasmon resonance: synthesis and characterizations. *Journal of Cluster Science*, *28*, pp.1051-1069.

Ikuta, K.S., Swetschinski, L.R., Aguilar, G.R., Sharara, F., Mestrovic, T., Gray, A.P., Weaver, N.D., Wool, E.E., Han, C., Hayoon, A.G. and Aali, A., 2022. Global mortality associated with 33 bacterial pathogens in 2019: a systematic analysis for the Global Burden of Disease Study 2019. *The Lancet*, *400*(10369), pp.2221-2248.

Innocent, E., Marealle, A.I., Imming, P. and Moeller, L., 2022. An Annotated Inventory of Tanzanian Medicinal Plants Traditionally Used for the Treatment of Respiratory Bacterial Infections. *Plants*, *11*(7), p.931.

Intorasoot, A., Chornchoem, P., Sookkhee, S. and Intorasoot, S., 2017. Bactericidal activity of herbal volatile oil extracts against multidrug-resistant Acinetobacter baumannii. *Journal of intercultural ethnopharmacology*, *6*(2), p.218.

Jodynis-Liebert, J. and Kujawska, M., 2020. Biphasic dose-response induced by phytochemicals: experimental evidence. *Journal of Clinical Medicine*, *9*(3), p.718.

Jubair, N., Rajagopal, M., Chinnappan, S., Abdullah, N.B. and Fatima, A., 2021. Review on the antibacterial mechanism of plant-derived compounds against multidrug-resistant bacteria (MDR). *Evidence-Based Complementary and Alternative Medicine*, *2021*.

Kang, S.G., Lee, G.B., Vinayagam, R., Do, G.S., Oh, S.Y., Yang, S.J., Kwon, J.B. and Singh, M., 2022. Anti-Inflammatory, Antioxidative, and Nitric Oxide-Scavenging Activities of a Quercetin Nanosuspension with Polyethylene Glycol in LPS-Induced RAW 264.7 Macrophages. *Molecules*, *27*(21), p.7432.

Karmakar, S.A.N.A.T., 2019. Particle size distribution and zeta potential based on dynamic light scattering: Techniques to characterize stability and surface charge distribution of charged colloids. *Recent Trends Mater. Phys. Chem*, pp.117-159.

Karuvantevida, N., Razia, M., Bhuvaneshwar, R., Sathishkumar, G., Prabukumar, S. and Sivaramakrishnan, S., 2022. Bioactive flavonoid used as a stabilizing agent of mono and bimetallic nanomaterials for multifunctional activities. *J Pure Appl Microbiol*, *16*, p.1652

Karwowska, K., Kozłowska-Tylingo, K., Skotnicka, M. and Śmiechowska, M., 2023. Theogallin-to-Gallic-Acid Ratio as a Potential Biomarker of Pu-Erh Teas. *Foods*, *12*(13), p.2453.

Kavitha, R. and Nadu, T., 2021. Phytochemical screening and GC-MS analysis of bioactive compounds present in ethanolic extracts of leaf and fruit of Trichosanthesis dioica roxb. *International Journal of Pharmaceutical Sciences and Research*, *12*(5), pp.2755-2764.

Keskin, C., Ölçekçi, A., Baran, A., Baran, M.F., Eftekhari, A., Omarova, S., Khalilov, R., Aliyev, E., Sufianov, A., Beilerli, A. and Gareev, I., 2023. Green synthesis of silver nanoparticles mediated Diospyros kaki L.(Persimmon): determination of chemical composition and evaluation of their antimicrobials and anticancer activities. *Frontiers in Chemistry*, *11*, p.1187808.

Khameneh, B., Iranshahy, M., Soheili, V. and Fazly Bazzaz, B.S., 2019. Review on plant antimicrobials: a mechanistic viewpoint. *Antimicrobial Resistance & Infection Control*, *8*(1), pp.1-28.

Khan, H., 2014. Medicinal plants in light of history: recognized therapeutic modality. Journal of evidence-based complementary & alternative medicine, 19(3), pp.216-219.

Khanal, L.N., Dhakal, P.P., Kandel, M.R., Acharya, D., Baral, E.R., Chhetri, K. and Kalauni, S.K., 2023. Stem Bark-Mediated Green Synthesis of Silver Nanoparticles from Pyrus pashia: Characterisation, Antioxidant, and Antibacterial Properties. *Inorganics*, *11*(6), p.263.

Khorrami, S., Zarrabi, A., Khaleghi, M., Danaei, M. and Mozafari, M.R., 2018. Selective cytotoxicity of green synthesized silver nanoparticles against the MCF-7 tumor cell line and their enhanced antioxidant and antimicrobial properties. *International journal of nanomedicine*, pp.8013-8024.

Kim, T.H., Ku, S.K. and Bae, J.S., 2013. Anti-inflammatory activities of isorhamnetin-3-O-galactoside against HMGB1-induced inflammatory responses in both HUVECs and CLP-induced septic mice. *Journal of Cellular Biochemistry*, *114*(2), pp.336-345.

Kongkham, B., Prabakaran, D. and Puttaswamy, H., 2020. Opportunities and challenges in managing antibiotic resistance in bacteria using plant secondary metabolites. *Fitoterapia*, *147*, p.104762.

Kumkoon, T., Srisaisap, M. and Boonserm, P., 2023. Biosynthesized silver nanoparticles using Morus alba (white mulberry) leaf extract as potential antibacterial and anticancer agents. *Molecules*, *28*(3), p.1213.

Lee, Y.J., Ahn, E.Y. and Park, Y., 2019. Shape-dependent cytotoxicity and cellular uptake of gold nanoparticles synthesized using green tea extract. *Nanoscale research letters*, *14*, pp.1-14.

Li, X., Deng, Y., Zheng, Z., Huang, W., Chen, L., Tong, Q. and Ming, Y., 2018. Corilagin, a promising medicinal herbal agent. *Biomedicine & Pharmacotherapy*, *99*, pp.43-50.

Liaqat, N., Jahan, N., Anwar, T. and Qureshi, H., 2022. Green synthesised silver nanoparticles: Optimisation, characterisation, antimicrobial activity, and cytotoxicity study by hemolysis assay. *Frontiers in Chemistry*, *10*, p.952006.

Lin, C., Tao, K., Hua, D., Ma, Z. and Zhou, S., 2013. Size effect of gold nanoparticles in catalytic reduction of p-nitrophenol with NaBH4. *Molecules*, *18*(10), pp.12609-12620.

Littmann, J., Buyx, A. and Cars, O., 2015. Antibiotic resistance: an ethical challenge. *International Journal of Antimicrobial Agents*, *46*(4), pp.359-361.

Liu, H., Lai, W., Liu, X., Yang, H., Fang, Y., Tian, L., Li, K., Nie, H., Zhang, W., Shi, Y. and Bian, L., 2021. Exposure to copper oxide nanoparticles triggers oxidative stress and endoplasmic reticulum (ER)-stress induced toxicology and apoptosis in male rat liver and BRL-3A cell. *Journal of hazardous materials*, *401*, p.123349.

Lomelí-Rosales, D.A., Zamudio-Ojeda, A., Reyes-Maldonado, O.K., López-Reyes, M.E., Basulto-Padilla, G.C., Lopez-Naranjo, E.J., Zuñiga-Mayo, V.M. and Velázquez-Juárez, G., 2022. Green synthesis of gold and silver nanoparticles using leaf extract of Capsicum chinense plant. Molecules, 27(5), p.1692.

Loo, Y.Y., Rukayadi, Y., Nor-Khaizura, M.A.R., Kuan, C.H., Chieng, B.W., Nishibuchi, M. and Radu, S., 2018. In vitro antimicrobial activity of green synthesized silver nanoparticles against selected gram-negative foodborne pathogens. *Frontiers in microbiology*, *9*, p.1555.

López-Miranda, J.L., Vázquez, M., Fletes, N., Esparza, R. and Rosas, G., 2016. Biosynthesis of silver nanoparticles using a Tamarix gallica leaf extract and their antibacterial activity. *Materials Letters*, *176*, pp.285-289.

Madunić, J., Madunić, I.V., Gajski, G., Popić, J. and Garaj-Vrhovac, V., 2018. Apigenin: A dietary flavonoid with diverse anticancer properties. *Cancer letters*, *413*, pp.11-22.

Majeed, S., Binti Sekeri, S.H. and Tahir Ansari, M., 2020. In vitro cytotoxic effect of Aspergillus clavatus generated silver nanoparticles on RAW 264.7 cells. *Karbala International Journal of Modern Science*, *6*(4), p.2.

Majoumouo, M.S., Sharma, J.R., Sibuyi, N.R., Tincho, M.B., Boyom, F.F. and Meyer, M., 2020. Synthesis of biogenic gold nanoparticles from Terminalia mantaly extracts and the evaluation of their in vitro cytotoxic effects in cancer cells. *Molecules*, *25*(19), p.4469.

Makarov, V.V., Love, A.J., Sinitsyna, O.V., Makarova, S.S., Yaminsky, I.V., Taliansky, M.E. and Kalinina, N.O., 2014. "Green" nanotechnologies: synthesis of metal nanoparticles using plants. *Acta Naturae (англоязычная версия)*, *6*(1 (20)), pp.35-44.

Malanovic, N. and Lohner, K., 2016. Gram-positive bacterial cell envelopes: The impact on the activity of antimicrobial peptides. *Biochimica et Biophysica Acta (BBA)-Biomembranes*, *1858*(5), pp.936-946.

Marinescu, L., Ficai, D., Ficai, A., Oprea, O., Nicoara, A.I., Vasile, B.S., Boanta, L., Marin, A., Andronescu, E. and Holban, A.M., 2022. Comparative antimicrobial activity of silver nanoparticles obtained by wet chemical reduction and solvothermal methods. *International Journal of Molecular Sciences*, *23*(11), p.5982.

Mathabe, M.C., Hussein, A.A., Nikolova, R.V., Basson, A.E., Meyer, J.M. and Lall, N., 2008. Antibacterial activities and cytotoxicity of terpenoids isolated from Spirostachys africana. *Journal of ethnopharmacology*, *116*(1), pp.194-197.

Mathabe, M.C., Hussein, A.A., Nikolova, R.V., Basson, A.E., Meyer, J.M. and Lall, N., 2008. Antibacterial activities and cytotoxicity of terpenoids isolated from Spirostachys africana. *Journal of ethnopharmacology*, *116*(1), pp.194-197.

Matotoka, M.M., Mashabela, G.T. and Masoko, P., 2023. Phytochemical content, antibacterial activity, and antioxidant, anti-inflammatory, and cytotoxic effects of traditional medicinal plants against respiratory tract bacterial pathogens. *Evidence-Based Complementary and Alternative Medicine*, *2023*.

Matysiak-Kucharek, M., Czajka, M., Jodłowska-Jędrych, B., Sawicki, K., Wojtyła-Buciora, P., Kruszewski, M. and Kapka-Skrzypczak, L., 2020. Two sides to the same coin—cytotoxicity vs. potential metastatic activity of AgNPs relative to triple-negative human breast cancer MDA-MB-436 cells. *Molecules*, *25*(10), p.2375.

Meikle, T.G., Dyett, B.P., Strachan, J.B., White, J., Drummond, C.J. and Conn, C.E., 2020. Preparation, characterization, and antimicrobial activity of cubosome encapsulated metal nanocrystals. *ACS applied materials & interfaces*, *12*(6), pp.6944-6954.

Mickymaray, S., 2019. One-step synthesis of silver nanoparticles using Saudi Arabian desert seasonal plant Sisymbrium irio and antibacterial activity against multidrug-resistant bacterial strains. *Biomolecules*, *9*(11), p.662.

Mihailović, V., Srećković, N., Nedić, Z.P., Dimitrijević, S., Matić, M., Obradović, A., Selaković, D., Rosić, G. and Katanić Stanković, J.S., 2023. Green synthesis of silver nanoparticles using Salvia verticillata and Filipendula ulmaria extracts: Optimization of synthesis, biological activities, and catalytic properties. Molecules, 28(2), p.808.

Mishra, A., Pradhan, D., Halder, J., Biswasroy, P., Rai, V.K., Dubey, D., Kar, B., Ghosh, G. and Rath, G., 2022. Metal nanoparticles against multi-drug-resistance bacteria. *Journal of Inorganic Biochemistry*, p.111938.

Mishra, A., Pradhan, D., Halder, J., Biswasroy, P., Rai, V.K., Dubey, D., Kar, B., Ghosh, G. and Rath, G., 2022. Metal nanoparticles against multi-drug-resistance bacteria. *Journal of Inorganic Biochemistry*, p.111938.

Misra, R. and Sahoo, S.K., 2012. Antibacterial activity of doxycycline-loaded nanoparticles. In *Methods in enzymology* (Vol. 509, pp. 61-85). Academic Press.

Moiketsi, B.N., Makale, K.P., Rantong, G., Rahube, T.O. and Makhzoum, A., 2023. Potential of selected African medicinal plants as alternative therapeutics against multi-drug-resistant bacteria. *Biomedicines*, *11*(10), p.2605.

Molele, P.K., Makhafola, T.J. and Mongalo, N.I., 2023. GC-ToF-MS based phytochemical analysis and anti-mycotoxigenic activity of South African medicinal plants, Mystroxylon aethiopicum (Thunb.) Loes. and Spirostachys africana Sond. *South African Journal of Botany*, *153*, pp.11-20.

Mondéjar-López, M., López-Jiménez, A.J., Abad-Jordá, M., Rubio-Moraga, A., Ahrazem, O., Gómez-Gómez, L. and Niza, E., 2021. Biogenic silver nanoparticles from iris tuberosa as potential preservative in cosmetic products. *Molecules*, *26*(15), p.4696.

Mongalo, N.I., Opoku, A.R. and Zobolo, A.M., 2012. Antibacterial and antioxidant activity of the extracts of Waltheria indica Linn. collected from Capricorn District, Limpopo Province, South Africa. *Journal of Medicinal Plants Research*, *6*(43), pp.5593-5598.

Moosavy, M.H., de la Guardia, M., Mokhtarzadeh, A., Khatibi, S.A., Hosseinzadeh, N. and Hajipour, N., 2023. Green synthesis, characterization, and biological evaluation of gold and silver nanoparticles using Mentha spicata essential oil. *Scientific Reports*, *13*(1), p.7230.

More, G.K. and Makola, R.T., 2020. In-vitro analysis of free radical scavenging activities and suppression of LPS-induced ROS production in macrophage cells by Solanum sisymbriifolium extracts. *Scientific reports*, *10*(1), p.6493.

More, P.R., Pandit, S., Filippis, A.D., Franci, G., Mijakovic, I. and Galdiero, M., 2023. Silver nanoparticles: bactericidal and mechanistic approach against drug resistant pathogens. *Microorganisms*, *11*(2), p.369.

Motafeghi, F., Gerami, M., Mortazavi, P., Khayambashi, B., Ghassemi-Barghi, N. and Shokrzadeh, M., 2023. Green synthesis of silver nanoparticles, graphene, and silver-graphene nanocomposite using Melissa officinalis ethanolic extract: Anticancer effect on MCF-7 cell line. *Iranian Journal of Basic Medical Sciences*, *26*(1), p.57.

Moyo, B., Tavengwa, N.T. and Madala, N.E., 2022. Diverse chemical modifications of the chlorogenic acid composition of Viscum combreticola Engl.: A premise for the state of readiness against excessive sunlight exposure. *Journal of Photochemistry and Photobiology B: Biology*, *233*, p.112501.

Mukaratirwa-Muchanyereyi, N., Gusha, C., Mujuru, M., Guyo, U. and Nyoni, S., 2022. Synthesis of silver nanoparticles using plant extracts from Erythrina abyssinica aerial parts and assessment of their anti-bacterial and antioxidant activities. *Results in Chemistry*, *4*, p.100402.

Mulaudzi, R.B., Ndhlala, A.R., Kulkarni, M.G. and Van Staden, J., 2012. Pharmacological properties and protein binding capacity of phenolic extracts of some Venda medicinal plants used against cough and fever. *Journal of Ethnopharmacology*, *143*(1), pp.185-193.

Murray, C.J., Ikuta, K.S., Sharara, F., Swetschinski, L., Aguilar, G.R., Gray, A., Han, C., Bisignano, C., Rao, P., Wool, E. and Johnson, S.C., 2022. Global burden of bacterial antimicrobial resistance in 2019: a systematic analysis. *The lancet*, *399*(10325), pp.629-655.

Nabatanzi, A., Nkadimeng, S.M., Lall, N., Kabasa, J.D. and McGaw, L.J., 2020. Antioxidant and Anti-Inflammatory Activities of Kigelia africana (Lam.) Benth. *Evidence-Based Complementary and Alternative Medicine*, *2020*(1), p.4352084.

Nabatanzi, A., Nkadimeng, S.M., Lall, N., Kabasa, J.D. and McGaw, L.J., 2020. Antioxidant and Anti-Inflammatory Activities of Kigelia africana (Lam.) Benth. *Evidence-Based Complementary and Alternative Medicine*, *2020*.

Nadaf, S.J., Jadhav, N.R., Naikwadi, H.S., Savekar, P.L., Sapkal, I.D., Kambli, M.M. and Desai, I.A., 2022. Green synthesis of gold and silver nanoparticles: Updates on research, patents, and future prospects. *OpenNano*, p.100076.

Nakkala, J.R., Mata, R., Gupta, A.K. and Sadras, S.R., 2014. Biological activities of green silver nanoparticles synthesized with Acorous calamus rhizome extract. *European journal of medicinal chemistry*, *85*, pp.784-794.

Nandiyanto, A.B.D., Oktiani, R. and Ragadhita, R., 2019. How to read and interpret FTIR spectroscope of organic material. *Indonesian Journal of Science and Technology*, *4*(1), pp.97-118.

Nascimento, A.M., Maria-Ferreira, D., Dal Lin, F.T., Kimura, A., de Santana-Filho, A.P., Werner, M.F.D.P., Iacomini, M., Sassaki, G.L., Cipriani, T.R. and de Souza, L.M., 2017. Phytochemical analysis and anti-inflammatory evaluation of compounds from an aqueous extract of Croton cajucara Benth. *Journal of Pharmaceutical and Biomedical Analysis*, *145*, pp.821-830.

Nemudzivhadi, V. and Masoko, P., 2015. Antioxidant and antibacterial properties of Ziziphus mucronata and Ricinus communis leaves extracts. *African Journal of Traditional, Complementary and Alternative Medicines*, *12*(1), pp.81-89.

Nielsen, T.R., Kuete, V., Jäger, A.K., Meyer, J.J.M. and Lall, N., 2012. Antimicrobial activity of selected South African medicinal plants. *BMC complementary and alternative medicine*, *12*, pp.1-6.

Nile, A., Nile, S.H., Cespedes-Acuña, C.L. and Oh, J.W., 2021. Spiraeoside extracted from red onion skin ameliorates apoptosis and exerts potent antitumor, antioxidant and enzyme inhibitory effects. *Food and Chemical Toxicology*, *154*, p.112327.

Nimesh, S., Chandra, R. and Gupta, N., 2017. *Advances in nanomedicine for the delivery of therapeutic nucleic acids*. Woodhead Publishing.

Niranjan Dhanasekar, N., Ravindran Rahul, G., Badri Narayanan, K., Raman, G. and Sakthivel, N., 2015. Green chemistry approach for the synthesis of gold nanoparticles using the fungus Alternaria sp. *Journal of microbiology and biotechnology*, *25*(7), pp.1129-1135.

Noruzi, M., 2015. Biosynthesis of gold nanoparticles using plant extracts. *Bioprocess and biosystems engineering*, *38*(1), pp.1-14.

Nur, H. and Nasir, S.M., 2008. Gold nanoparticles embedded on the surface of polyvinyl alcohol layer. *Malaysian Journal of Fundamental and Applied Sciences*, *4*(1).

Odds, F.C., 2003. Synergy, antagonism, and what the chequerboard puts between them. *Journal of Antimicrobial Chemotherapy*, *52*(1), pp.1-1.

Oh, K.H., Soshnikova, V., Markus, J., Kim, Y.J., Lee, S.C., Singh, P., Castro-Aceituno, V., Ahn, S., Kim, D.H., Shim, Y.J. and Kim, Y.J., 2018. Biosynthesized gold and silver nanoparticles by aqueous fruit extract of Chaenomeles sinensis and screening of their biomedical activities. *Artificial cells, nanomedicine, and biotechnology*, *46*(3), pp.599-606.

Oh, K.H., Soshnikova, V., Markus, J., Kim, Y.J., Lee, S.C., Singh, P., Castro-Aceituno, V., Ahn, S., Kim, D.H., Shim, Y.J. and Kim, Y.J., 2018. Biosynthesized gold and silver nanoparticles by aqueous fruit extract of Chaenomeles sinensis and screening of their biomedical activities. *Artificial cells, nanomedicine, and biotechnology*, *46*(3), pp.599-606.

Oliphant, C.M. and Eroschenko, K., 2015. Antibiotic resistance, part 1: gram-positive pathogens. *The Journal for Nurse Practitioners*, *11*(1), pp.70-78.

Paiva-Santos, A.C., Herdade, A.M., Guerra, C., Peixoto, D., Pereira-Silva, M., Zeinali, M., Mascarenhas-Melo, F., Paranhos, A. and Veiga, F., 2021. Plant-mediated green synthesis of

metal-based nanoparticles for dermopharmaceutical and cosmetic applications. *International Journal of Pharmaceutics*, *597*, p.120311.

Pandey, K.B. and Rizvi, S.I., 2009. Plant polyphenols as dietary antioxidants in human health and disease. *Oxidative medicine and cellular longevity*, *2*, pp.270-278.

Pannerselvam, B., Durai, P., Thiyagarajan, D., Song, H.J., Kim, K.J., Jung, Y.S., Kim, H.J. and Rangarajulu, S.K., 2020. Facile synthesis of silver nanoparticles using Asian spider flower and its in vitro cytotoxic activity against human breast carcinoma cells. *Processes*, *8*(4), p.430.

Perveen, K., Husain, F.M., Qais, F.A., Khan, A., Razak, S., Afsar, T., Alam, P., Almajwal, A.M. and Abulmeaty, M.M., 2021. Microwave-assisted rapid green synthesis of gold nanoparticles using seed extract of Trachyspermum ammi: ROS mediated biofilm inhibition and anticancer activity. *Biomolecules*, *11*(2), p.197.

Phan, K. and Ferenci, T., 2013. A design-constraint trade-off underpins the diversity in ecologically important traits in species Escherichia coli. *The ISME Journal*, *7*(10), pp.2034-2043.

Prabu, G.R., Gnanamani, A. and Sadulla, S., 2006. Guaijaverin–a plant flavonoid as potential antiplaque agent against Streptococcus mutans. *Journal of Applied Microbiology*, *101*(2), pp.487-495.

Qidwai, A., Kumar, R. and Dikshit, A., 2018. Green synthesis of silver nanoparticles by seed of Phoenix sylvestris L. and their role in the management of cosmetics embarrassment. *Green Chemistry Letters and Reviews*, *11*(2), pp.176-188.

Quelemes, P.V., Araruna, F.B., De Faria, B.E., Kuckelhaus, S.A., Da Silva, D.A., Mendonça, R.Z., Eiras, C., dos S. Soares, M.J. and Leite, J.R.S., 2013. Development and antibacterial

activity of cashew gum-based silver nanoparticles. *International journal of molecular sciences*, *14*(3), pp.4969-4981.

Rabiee, N., Ahmadi, S., Akhavan, O. and Luque, R., 2022. Silver and gold nanoparticles for antimicrobial purposes against multi-drug resistance bacteria. *Materials*, *15*(5), p.1799.

Rahman, A. U.; Khan, A. U.; Yuan, Q.; Wei, Y.; Ahmad, A.; Ullah, S.; Khan, Z. U. H.; Shams, S.; Tariq, M.; Ahmad, W. Tuber Extract of Arisaema Flavum Eco-Benignly and Effectively Synthesize Silver Nanoparticles: Photocatalytic and Antibacterial Response against Multidrug Resistant Engineered E. Coli QH4. Journal of Photochemistry and Photobiology B: Biology 2019, 193, 31−38.

Rai, M.K., Deshmukh, S.D., Ingle, A.P. and Gade, A.K., 2012. Silver nanoparticles: the powerful nanoweapon against multidrug-resistant bacteria. *Journal of applied microbiology*, *112*(5), pp.841-852.

Ramarumo, L.J., Maroyi, A. and Tshisikhawe, M.P., 2019. Warburgia salutaris (G. Bertol.) Chiov.: An endangered therapeutic plant used by the Vhavenda ethnic group in the Soutpansberg, Vhembe Biosphere Reserve, Limpopo province, South Africa. *Research Journal of Pharmacy and Technology*, *12*(12), pp.5893-5898.

Random Harvest. (2022). South African Indigenous Plants - Spirostachys africana. [Online]. Available at: https://www.randomharvest.co.za/South-African-Indigenous-Plants/Show-Plant/PlantId/782/Plant/Spirostachys-africana [13 April 2022].

Rani, P., Varma, R.S., Singh, K., Acevedo, R. and Singh, J., 2023. Catalytic and antimicrobial potential of green synthesized Au and Au@ Ag core-shell nanoparticles. *Chemosphere*, *317*, p.137841.

Rastogi, L and Arunachalam, J., 2013. Green synthetic route for the size-controlled synthesis of biocompatible gold nanoparticles using aqueous extract of garlic (Allium Sativum). *Advanced materials letters*, *4*(7), pp.548-555.

Raza, M.A., Kanwal, Z., Rauf, A., Sabri, A.N., Riaz, S. and Naseem, S., 2016. Size-and shape-dependent antibacterial studies of silver nanoparticles synthesized by wet chemical routes. *Nanomaterials*, *6*(4), p.74.

Riaz, M., Khalid, R., Afzal, M., Anjum, F., Fatima, H., Zia, S., Rasool, G., Egbuna, C., Mtewa, A.G., Uche, C.Z. and Aslam, M.A., 2023. Phytobioactive compounds as therapeutic agents for human diseases: A review. *Food Science & Nutrition*.

Rod-In, W., Talapphet, N., Monmai, C., Jang, A.Y., You, S. and Park, W.J., 2021. Immune enhancement effects of Korean ginseng berry polysaccharides on RAW264. 7 macrophages through MAPK and NF-κB signalling pathways. *Food and Agricultural Immunology*, *32*(1), pp.298-309.

Saifuddin, N., Wong, C.W. and Yasumira, A.A., 2009. Rapid biosynthesis of silver nanoparticles using culture supernatant of bacteria with microwave irradiation. *Journal of Chemistry*, *6*, pp.61-70.

Salayová, A., Bedlovičová, Z., Daneu, N., Baláž, M., Lukáčová Bujňáková, Z., Balážová, Ľ. and Tkáčiková, Ľ., 2021. Green synthesis of silver nanoparticles with antibacterial activity using various medicinal plant extracts: Morphology and antibacterial efficacy. *Nanomaterials*, *11*(4), p.1005.

Sathishkumar, P., Preethi, J., Vijayan, R., Yusoff, A.R.M., Ameen, F., Suresh, S., Balagurunathan, R. and Palvannan, T., 2016. Anti-acne, anti-dandruff and anti-breast cancer efficacy of green synthesised silver nanoparticles using Coriandrum sativum leaf extract. *Journal of Photochemistry and Photobiology B: Biology*, *163*, pp.69-76.

Schroeder, M.R. and Stephens, D.S., 2016. Macrolide resistance in Streptococcus pneumoniae. *Frontiers in cellular and infection microbiology*, *6*, p.98.

Selvi, B.C.G., Madhavan, J. and Santhanam, A., 2016. Cytotoxic effect of silver nanoparticles synthesized from Padina tetrastromatica on breast cancer cell line. *Advances in Natural Sciences: Nanoscience and Nanotechnology*, *7*(3), p.035015.

Senthilkumar, P., Rashmitha, S., Veera, P., Ignatious, C.V., SaiPriya, C. and Samrot, A.V., 2018. Antibacterial activity of neem extract and its green synthesized silver nanoparticles against Pseudomonas aeruginosa. *Journal of Pure and Applied Microbiology*, *12*(2), pp.969-974.

Setha, B., Gaspersz, F.F., Idris, A.P.S., Rahman, S. and Mailoa, M.N., 2013. Potential of seaweed Padina sp. as a source of antioxidant. *International Journal of Scientific and Technology Research*, *2*(6), pp.221-224.

Sharma, K., Guleria, S. and Razdan, V.K., 2020. Green synthesis of silver nanoparticles using Ocimum gratissimum leaf extract: characterization, antimicrobial activity and toxicity analysis. *Journal of plant biochemistry and biotechnology*, *29*, pp.213-224.

Sharma, N.K., Vishwakarma, J., Rai, S., Alomar, T.S., AlMasoud, N. and Bhattarai, A., 2022. Green route synthesis and characterization techniques of silver nanoparticles and their biological adeptness. *ACS omega*, *7*(31), pp.27004-27020.

Sher, N., Alkhalifah, D.H.M., Ahmed, M., Mushtaq, N., Shah, F., Fozia, F., Khan, R.A., Hozzein, W.N. and Aboul-Soud, M.A., 2022. Comparative study of antimicrobial activity of silver, gold, and silver/gold bimetallic nanoparticles synthesized by green approach. *Molecules*, *27*(22), p.7895.

Shirinda, H., Leonard, C., Candy, G. and Van Vuuren, S., 2019. Antimicrobial activity and toxicity profile of selected southern African medicinal plants against neglected gut pathogens. *South African Journal of Science*, *115*(11-12), pp.1-10.

Siakavella, I.K., Lamari, F., Papoulis, D., Orkoula, M., Gkolfi, P., Lykouras, M., Avgoustakis, K. and Hatziantoniou, S., 2020. Effect of plant extracts on the characteristics of silver nanoparticles for topical application. *Pharmaceutics*, *12*(12), p.1244.

Simon-Deckers, A., Gouget, B., Mayne-L'Hermite, M., Herlin-Boime, N., Reynaud, C. and Carriere, M., 2008. In vitro investigation of oxide nanoparticle and carbon nanotube toxicity and intracellular accumulation in A549 human pneumocytes. *Toxicology*, *253*(1-3), pp.137-146.

Singh, C., K Baboota, R., Kr Naik, P. and Singh, H., 2012. Biocompatible synthesis of silver and gold nanoparticles using leaf extract of Dalbergia sissoo. *Advanced Materials Letters*, *3*(4), pp.279-285.

Singh, C., K Baboota, R., Kr Naik, P. and Singh, H., 2012. Biocompatible synthesis of silver and gold nanoparticles using leaf extract of Dalbergia sissoo. *Advanced Materials Letters*, *3*(4), pp.279-285.

Singh, K., Baijnath, H. and Street, R., 2020. Spirostachys Africana: a review of phytochemistry, traditional and biological uses and toxicity. *Indilinga African Journal of Indigenous Knowledge Systems*, *19*(2), pp.176-188.

Singh, P. and Mijakovic, I., 2022. Green synthesis and antibacterial applications of gold and silver nanoparticles from Ligustrum vulgare berries. *Scientific Reports*, *12*(1), p.7902.

Sofowora, A., Ogunbodede, E. and Onayade, A., 2013. The role and place of medicinal plants in the strategies for disease prevention. *African journal of traditional, complementary and alternative medicines*, *10*(5), pp.210-229.

Sofowora, A., Ogunbodede, E. and Onayade, A., 2013. The role and place of medicinal plants in the strategies for disease prevention. *African journal of traditional, complementary and alternative medicines*, *10*(5), pp.210-229.

South African National Biodiversity Institute (SANBI). (2022). Spirostachys Africana. [Online]. Available at: https://pza.sanbi.org/spirostachys-africana, [Accessed 11 April 2022].

Stavinskaya, O., Laguta, I., Fesenko, T. and Krumova, M., 2019. Effect of temperature on green synthesis of silver nanoparticles using Vitex agnus-castus extract. *Chemistry Journal of Moldova*, *14*(2), pp.117-121.

Sultan, I., Rahman, S., Jan, A.T., Siddiqui, M.T., Mondal, A.H. and Haq, Q.M.R., 2018. Antibiotics, resistome and resistance mechanisms: A bacterial perspective. *Frontiers in microbiology*, *9*, p.2066.

Swolana, D. and Wojtyczka, R.D., 2022. Activity of silver nanoparticles against Staphylococcus spp. *International Journal of Molecular Sciences*, *23*(8), p.4298.

Sylvester, P.W., 2011. Optimization of the tetrazolium dye (MTT) colorimetric assay for cellular growth and viability. *Drug Design and Discovery: Methods and Protocols*, pp.157-168.

Taciak, B., Białasek, M., Braniewska, A., Sas, Z., Sawicka, P., Kiraga, Ł., Rygiel, T. and Król, M., 2018. Evaluation of phenotypic and functional stability of RAW 264.7 cell line through serial passages. *PloS one*, *13*(6), p.e0198943.

Tang, K.W.K., Millar, B.C. and Moore, J.E., 2023. Antimicrobial resistance (AMR). *British Journal of Biomedical Science*, *80*, p.11387.

Tayel, A.A., Shaban, S.M., Moussa, S.H., Elguindy, N.M., Diab, A.M., Mazrou, K.E., Ghanem, R.A. and El-Sabbagh, S.M., 2018. Bioactivity and application of plant seeds' extracts to fight resistant strains of Staphylococcus aureus. *Annals of Agricultural Sciences*, *63*(1), pp.47-53.

Tree South Africa. (2022). Spirostachys Africana. [Online]. Available at: https://treesa.org/spirostachys-africana/ [Accessed 12 April 2022].

Tschugguel, W., Schneeberger, C., Unfried, G., Czerwenka, K., Weninger, W., Mildner, M., Gruber, D.M., Sator, M.O., Waldhör, T. and Huber, J.C., 1999. Expression of inducible nitric oxide synthase in human breast cancer depends on tumor grade. *Breast cancer research and treatment*, *56*, pp.143-149.

Tyagi, P.K., Quispe, C., Herrera-Bravo, J., Tyagi, S., Barbhai Mrunal, D., Kumar, M., Dablool, A.S., Alghamdi, S., Batiha, G.E.S., Sharifi-Rad, J. and Ramniwas, S., 2021. Synthesis of silver and gold nanoparticles: Chemical and green synthesis method and its toxicity evaluation against pathogenic bacteria using the toxtrak test. *Journal of Nanomaterials*, *2021*, pp.1-12.

Valencia-Hernandez, L.J., Wong-Paz, J.E., Ascacio-Valdés, J.A., Chávez-González, M.L., Contreras-Esquivel, J.C. and Aguilar, C.N., 2021. Procyanidins: From agro-industrial waste to food as bioactive molecules. *Foods*, *10*(12), p.3152.

Van Den Bout-van den Beukel, C.J., Hamza, O.J., Moshi, M.J., Matee, M.I., Mikx, F., Burger, D.M., Koopmans, P.P., Verweij, P.E., Schoonen, W.G. and Van Der Ven, A.J., 2008. Evaluation of cytotoxic, genotoxic and CYP450 enzymatic competition effects of Tanzanian plant extracts traditionally used for treatment of fungal infections. *Basic & clinical pharmacology & toxicology*, *102*(6), pp.515-526.

Velgosova, O., Čižmárová, E., Málek, J. and Kavuličova, J., 2017. Effect of storage conditions on long-term stability of Ag nanoparticles formed via green synthesis. *International Journal of Minerals, Metallurgy, and Materials*, *24*, pp.1177-1182.

Vijayan, R., Joseph, S. and Mathew, B., 2019. Anticancer, antimicrobial, antioxidant, and catalytic activities of green-synthesised silver and gold nanoparticles using Bauhinia purpurea leaf extract. *Bioprocess and biosystems engineering*, *42*, pp.305-319.

Vijayarathna, S. and Sasidharan, S., 2012. Cytotoxicity of methanol extracts of Elaeis guineensis on MCF-7 and Vero cell lines. *Asian pacific journal of tropical biomedicine*, *2*(10), pp.826-829.

Wang, D., Markus, J., Wang, C., Kim, Y.J., Mathiyalagan, R., Aceituno, V.C., Ahn, S. and Yang, D.C., 2017. Green synthesis of gold and silver nanoparticles using aqueous extract of Cibotium barometz root. *Artificial cells, nanomedicine, and biotechnology*, *45*(8), pp.1548-1555.

Wen, C., Dechsupa, N., Yu, Z., Zhang, X., Liang, S., Lei, X., Xu, T., Gao, X., Hu, Q., Innuan, P. and Kantapan, J., 2023. Pentagalloyl Glucose: A Review of Anticancer Properties, Molecular Targets, Mechanisms of Action, Pharmacokinetics, and Safety Profile. *Molecules*, *28*(12), p.4856.

Wendlocha, D., Krzykawski, K., Mielczarek-Palacz, A. and Kubina, R., 2023. Selected flavonols in breast and gynecological cancer: a systematic review. *Nutrients*, *15*(13), p.2938.

Wongsa, P., Phatikulrungsun, P. and Prathumthong, S., 2022. FT-IR characteristics, phenolic profiles and inhibitory potential against digestive enzymes of 25 herbal infusions. *Scientific Reports*, *12*(1), p.6631.

Wu, Q., Wang, Y. and Guo, M., 2011. Triterpenoid saponins from the seeds of Celosia argentea and their anti-inflammatory and antitumor activities. *Chemical and Pharmaceutical Bulletin*, *59*(5), pp.666-671.

Yadi, M., Azizi, M., Dianat-Moghadam, H., Akbarzadeh, A., Abyadeh, M. and Milani, M., 2022. Antibacterial activity of green gold and silver nanoparticles using ginger root extract. *Bioprocess and Biosystems Engineering*, *45*(12), pp.1905-1917.

Yakoup, A.Y., Kamel, A.G., Elbermawy, Y., Abdelsattar, A.S. and El-Shibiny, A., 2024. Characterization, antibacterial, and cytotoxic activities of silver nanoparticles using the whole biofilm layer as a macromolecule in biosynthesis. *Scientific Reports*, *14*(1), p.364.

Yang, W., Chen, X., Li, Y., Guo, S., Wang, Z. and Yu, X., 2020. Advances in pharmacological activities of terpenoids. *Natural Product Communications*, *15*(3), p.1934578X20903555.

Yasmin, A., Ramesh, K. and Rajeshkumar, S., 2014. Optimization and stabilization of gold nanoparticles by using herbal plant extract with microwave heating. *Nano convergence*, *1*(1), p.12.

Yasmin, A., Ramesh, K. and Rajeshkumar, S., 2014. Optimization and stabilization of gold nanoparticles by using herbal plant extract with microwave heating. *Nano Convergence*, *1*(1), p.12.

Zahra, S.T., Rasheed, S., Sajjad, S., Ali, M.A. and Sultan, B., 2023. Theranostics applications of plant-based nanoparticles. *Materials Chemistry and Mechanics*, *1*(2), pp.64-82.

Zargar, M., Shameli, K., Najafi, G.R. and Farahani, F., 2014. Plant mediated green biosynthesis of silver nanoparticles using Vitex negundo L. extract. *Journal of Industrial and Engineering Chemistry*, *20*(6), pp.4169-4175.

Zhang, Q.L., Yang, Z.M., Ding, B.J., Lan, X.Z. and Guo, Y.J., 2010. Preparation of copper nanoparticles by chemical reduction method using potassium borohydride. *Transactions of Nonferrous Metals Society of China*, *20*, pp.s240-s244.

Zhang, Y., Cai, P., Cheng, G. and Zhang, Y., 2022. A brief review of phenolic compounds identified from plants: Their extraction, analysis, and biological activity. *Natural Product Communications*, *17*(1), p.1934578X211069721.

Zheng, H., Li, J., Luo, X., Li, C., Hu, L., Qiu, Q., Ding, J., Song, Y. and Deng, Y., 2019. Murine RAW264. 7 cells as cellular drug delivery carriers for tumor therapy: a good idea?. *Cancer Chemotherapy and Pharmacology*, *83*, pp.361-374.

Zuhrotun, A., Oktaviani, D.J. and Hasanah, A.N., 2023. Biosynthesis of Gold and Silver Nanoparticles Using Phytochemical Compounds. *Molecules*, *28*(7), p.3240.

Appendix A

A1. Plant material collection and extraction process.

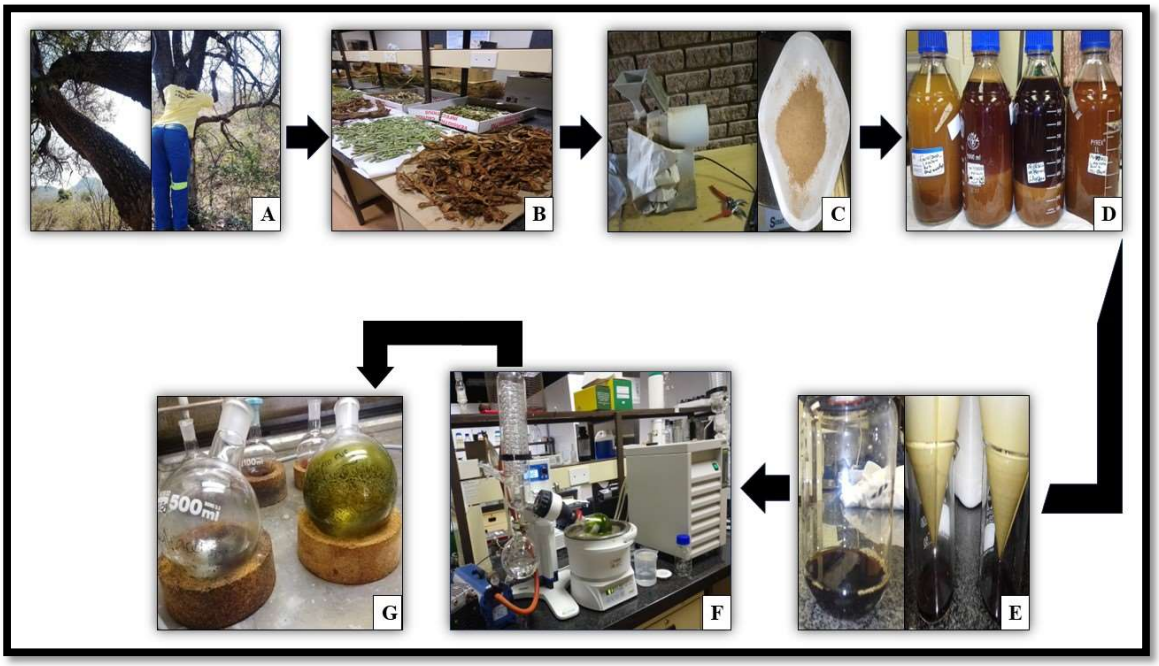

The process of collection and extraction of *S. Africana* plant material whereby A) bark and leaves were harvested, B) dried, C) ground, D) macerated, E) filtered, F) concentrated using a rotary evaporator, and finally G) dried concentrated plant extracts.

Appendix B

B1. Colour change of bark SA-AgNPs samples

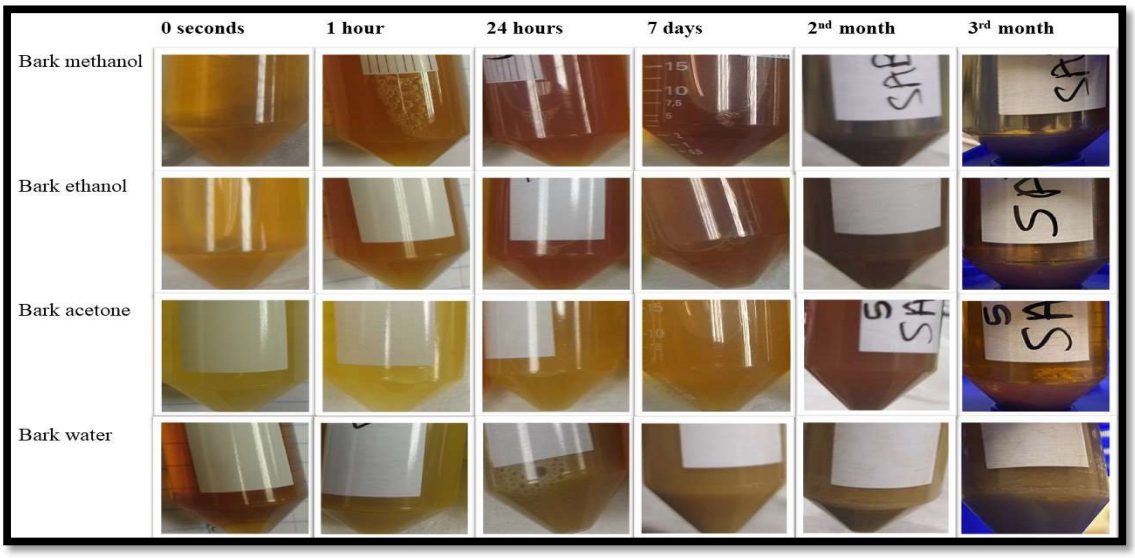

Colour change of *S. Africana* Bark-silver nanoparticles (SAL-AgNPs) at various incubation times.

B2. Colour change of leaf SA-AgNP samples

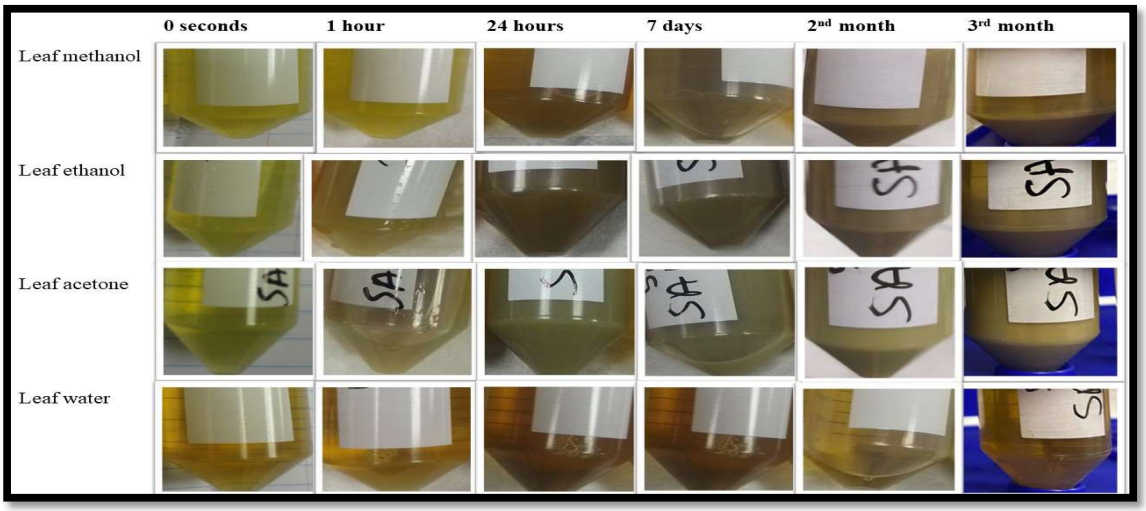

Colour change of *S. Africana* Leaf-silver nanoparticles (SAL-AgNPs) at various incubation times.

B3. UV-Vis analysis of SA-AgNPs and $AgNO_3$ effect

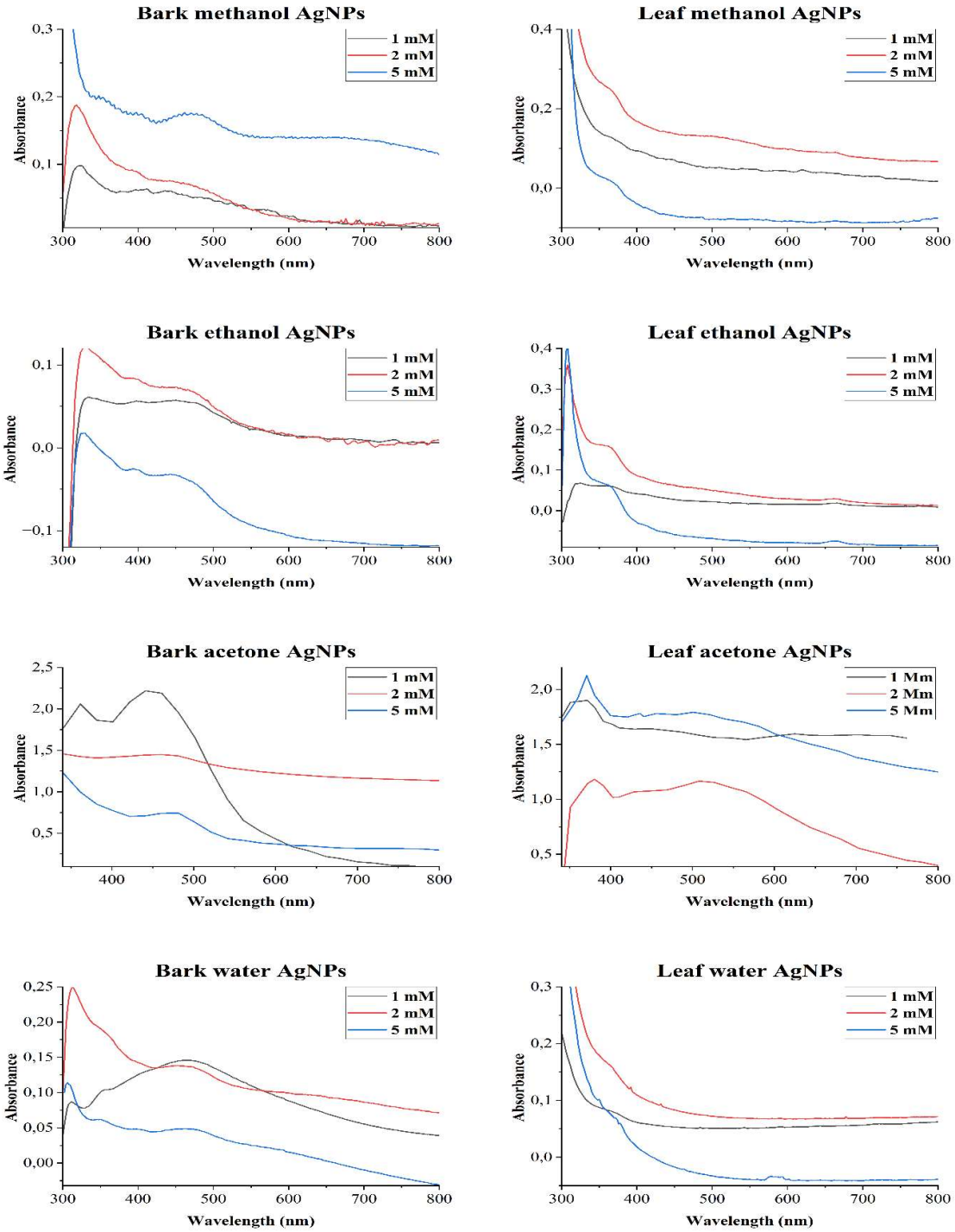

The effect of $AgNO_3$ concentration on the AgNP production by *S. Africana*-methanol, ethanol, acetone, and distilled water extracts.

B4. UV-Vis analysis of SABM-AG/SALM-AG and the impact of reaction

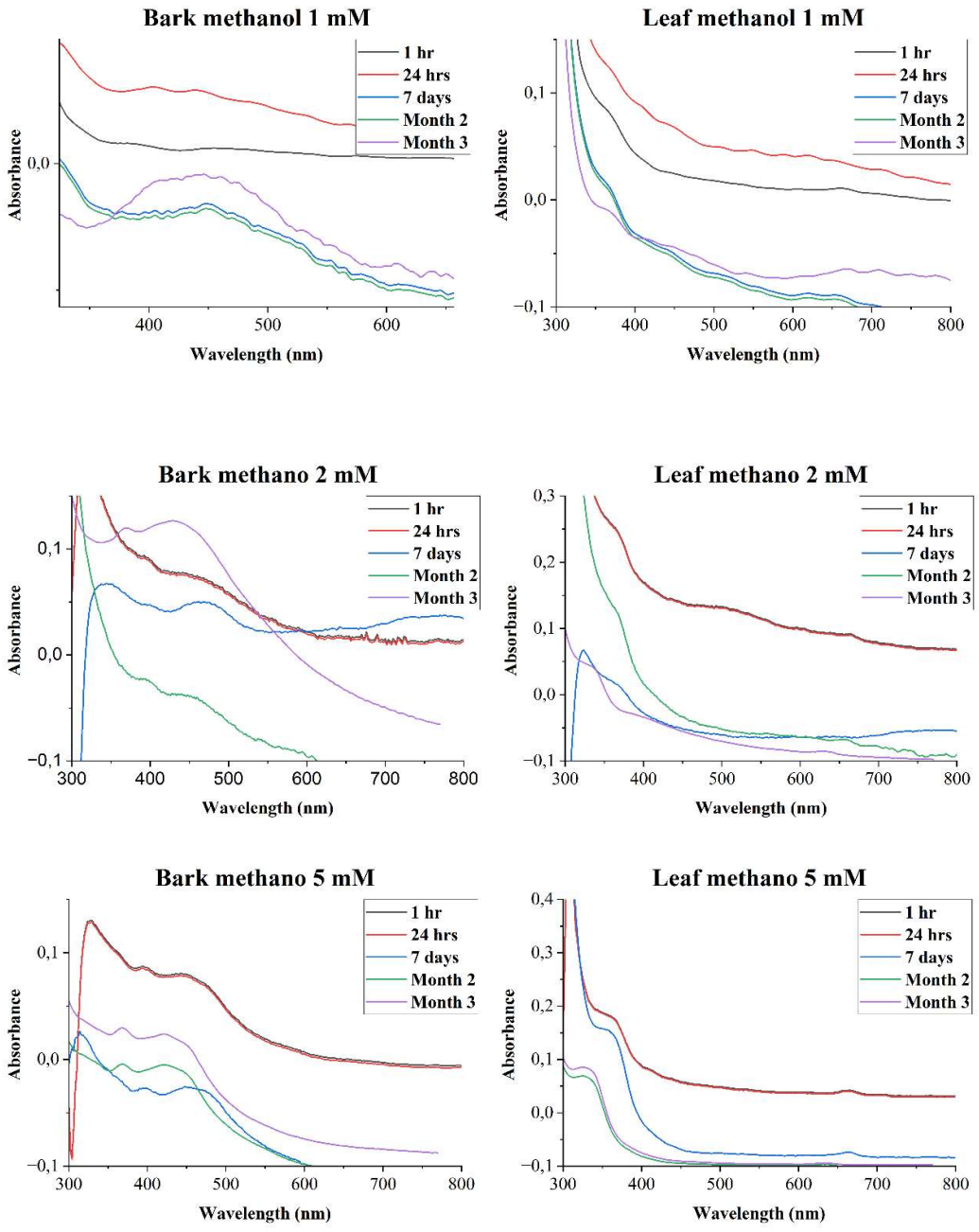

UV-Vis spectra of methanol extracts-based AgNPs showing the impact of reaction time on the synthesis.

B5. UV-Vis analysis of SABE-AG/SALE-AG and the impact of reaction

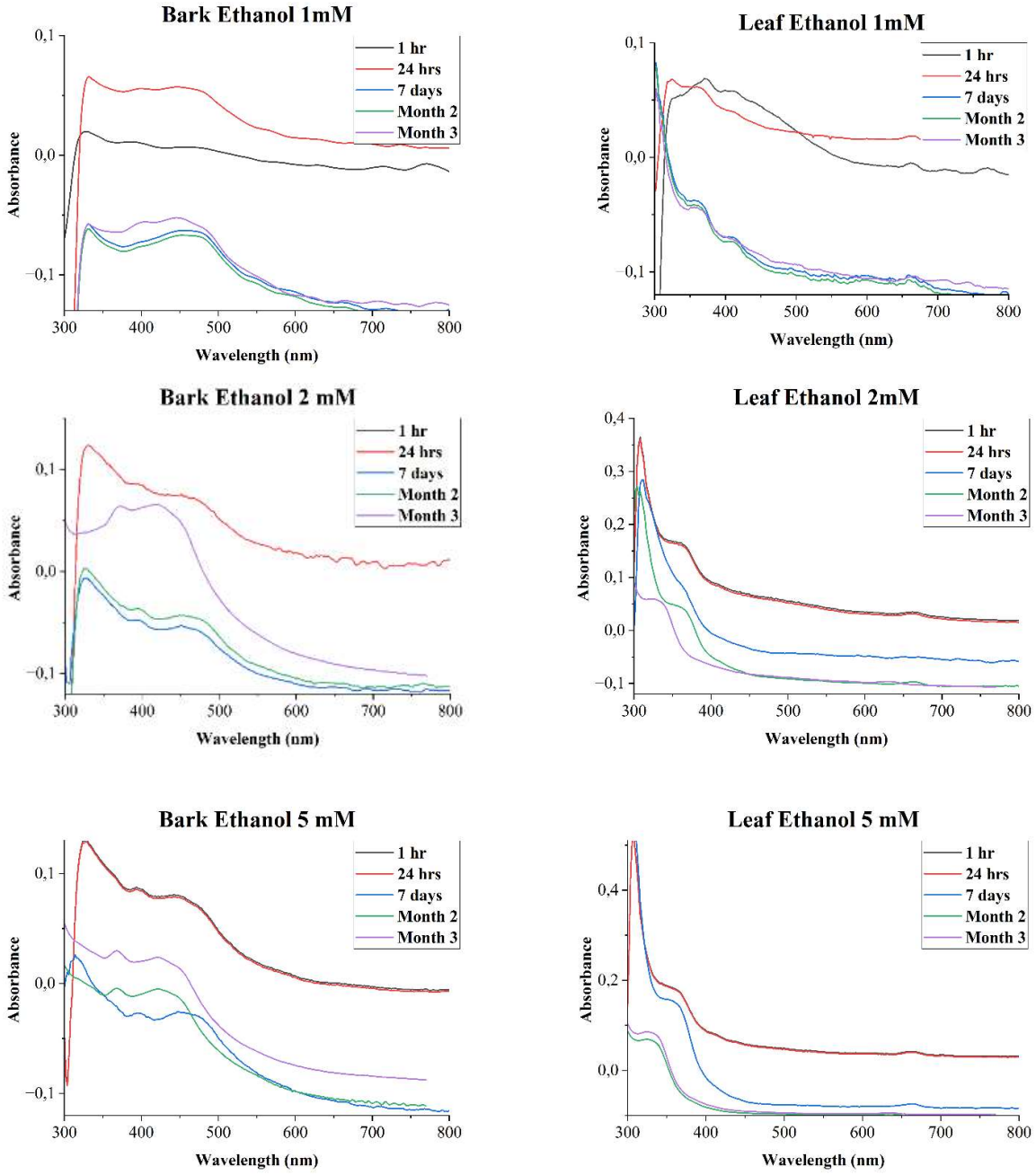

UV-Vis spectra of ethanol extracts-based AgNPs showing the impact of reaction time.

B6. UV-Vis analysis of SABD-AG/SALD-AG and the impact of reaction time

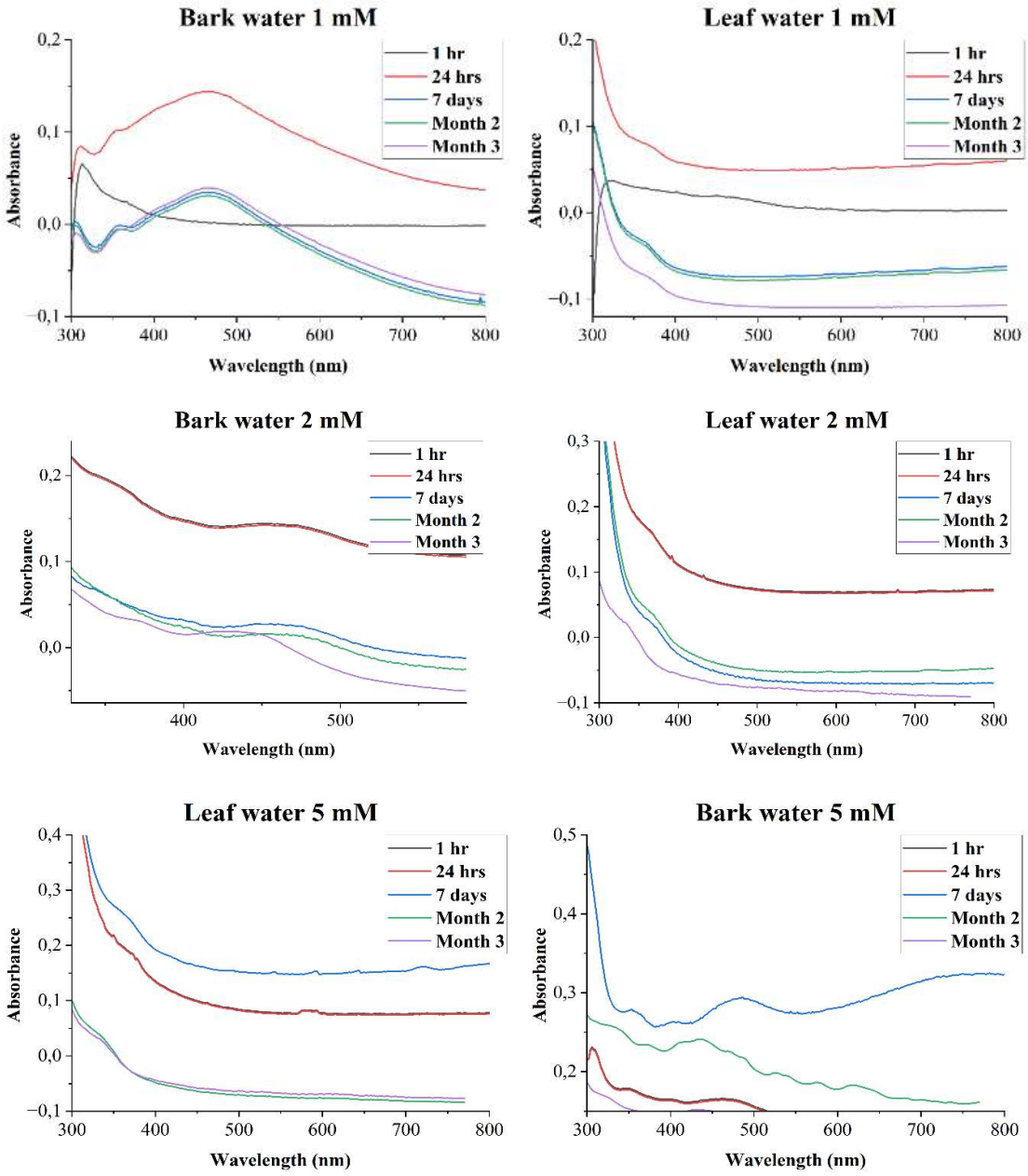

UV-Vis spectra of distilled-water extracts-based AgNPs showing the impact of reaction time.

B7. UV-Vis analysis of SABM-AG/SALM-AG and incubation temperature

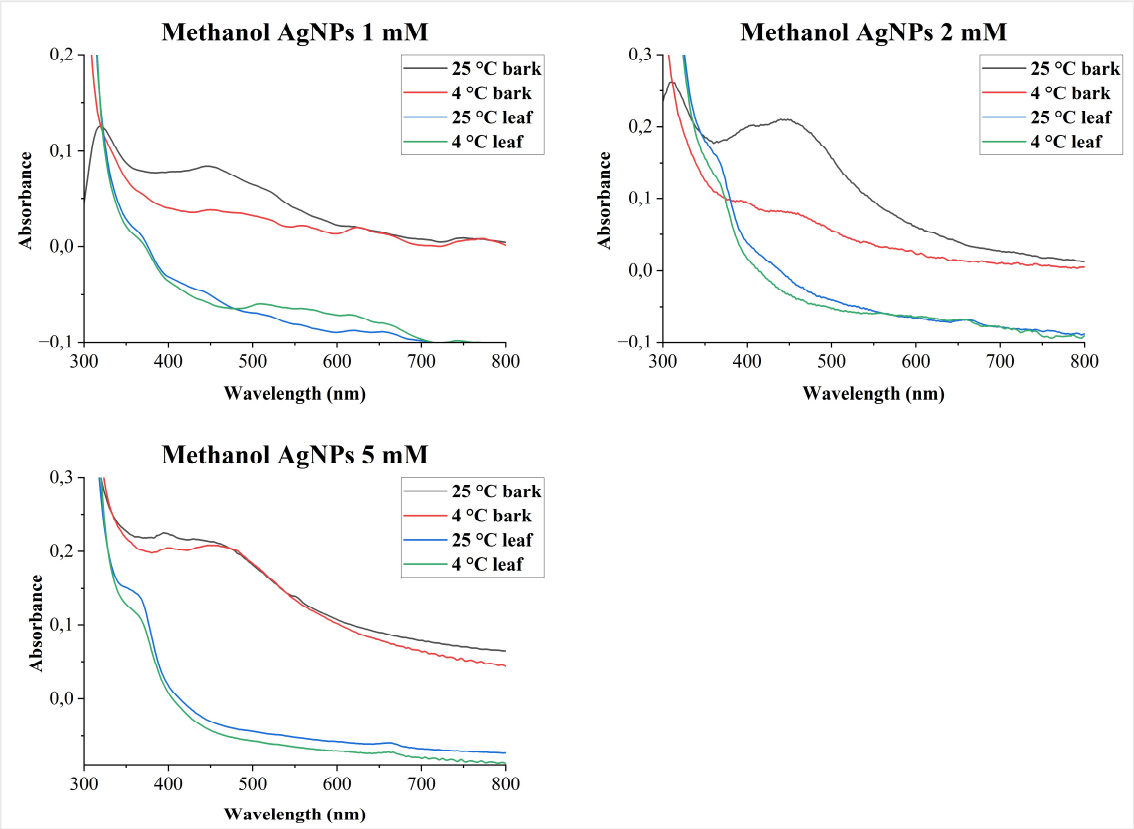

The influence of temperature on AgNPs synthesised by *S. Africana* methanol extracts.

B8. UV-Vis analysis of SABE-AG/SALE-AG and incubation temperature

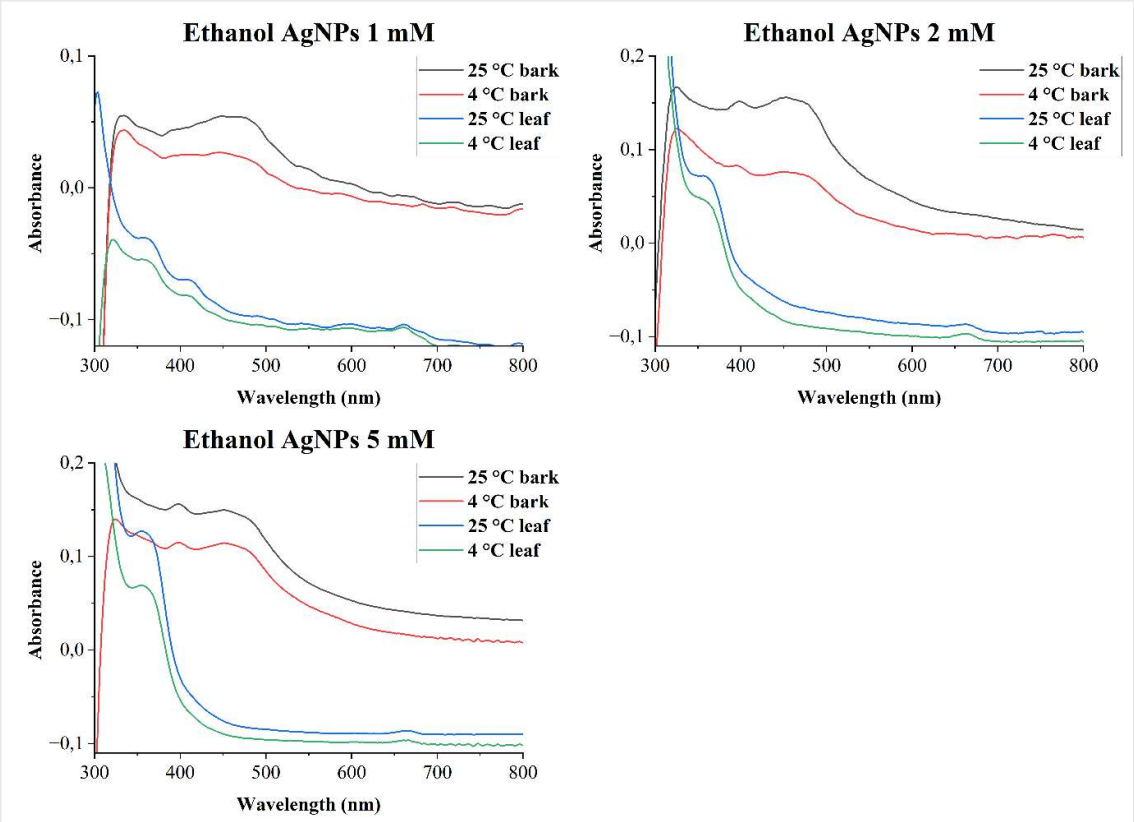

The influence of temperature on AgNPs synthesised by *S. Africana* ethanol extracts.

B9. UV-Vis analysis of SABD-AG/SALD-AG and incubation temperature

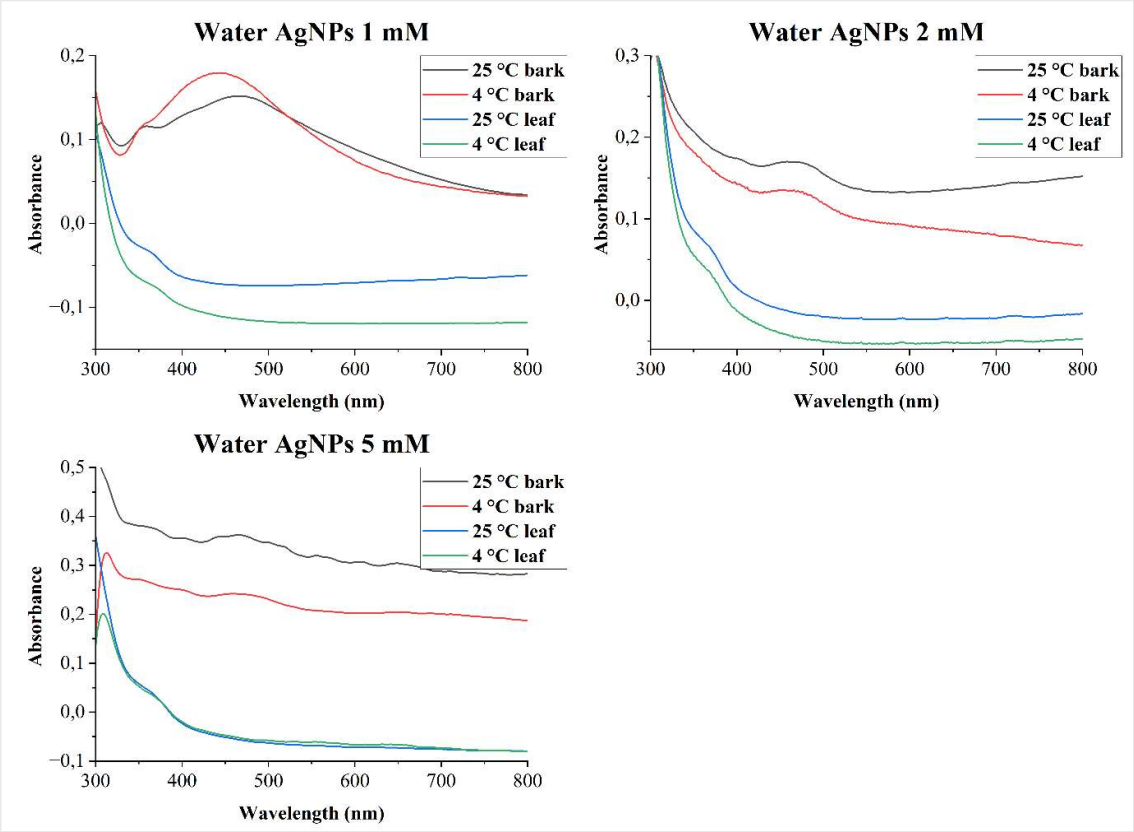

The influence of temperature on AgNPs synthesised by *S. Africana* distilled-water extracts.

B10. UV-Vis analysis of SABM-AU

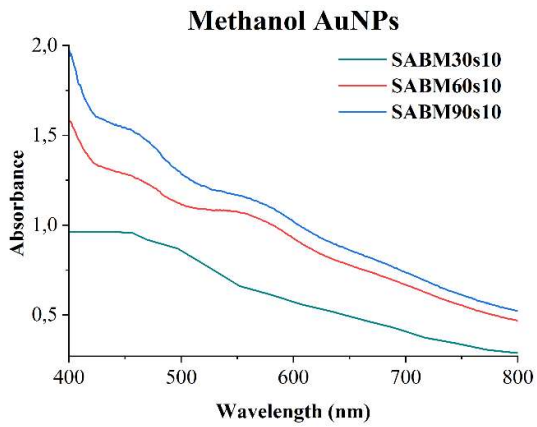

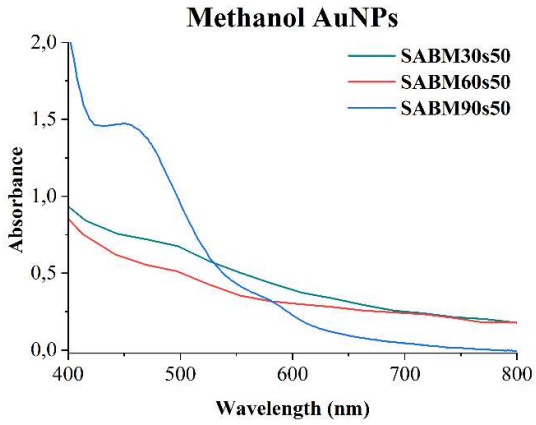

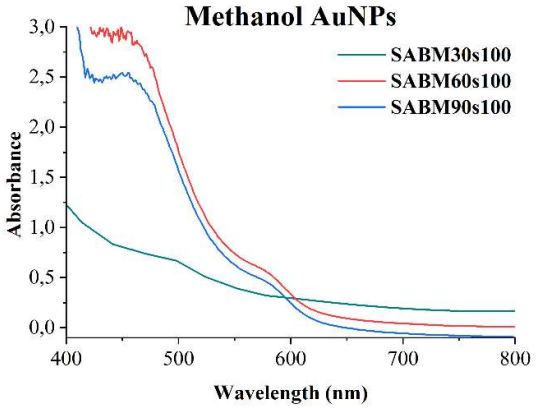

UV-Vis spectra of methanol extracts-based AuNPs at different reaction times and plant concentrations.

B11. UV-Vis analysis of SABE-AU

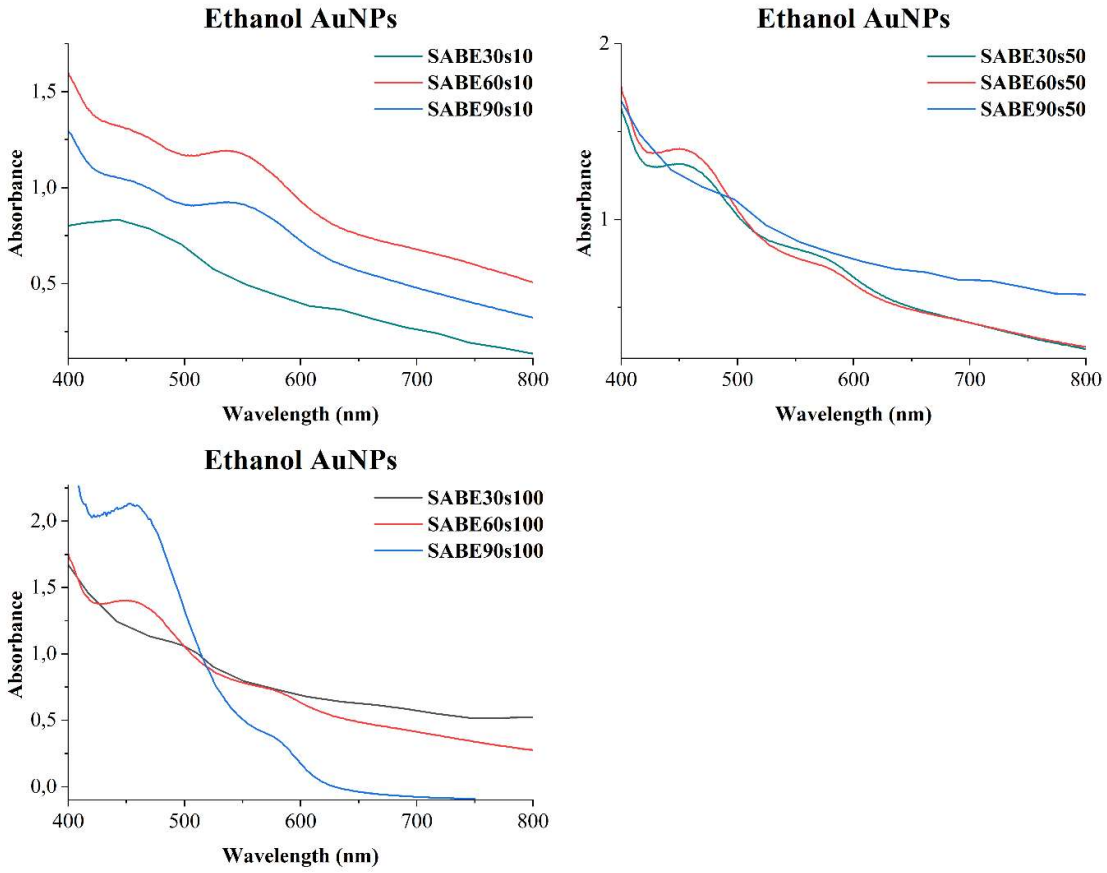

UV-Vis spectra of ethanol extracts-based AuNPs at different reaction times and plant concentrations.

B12. UV-Vis analysis of SABA-AU

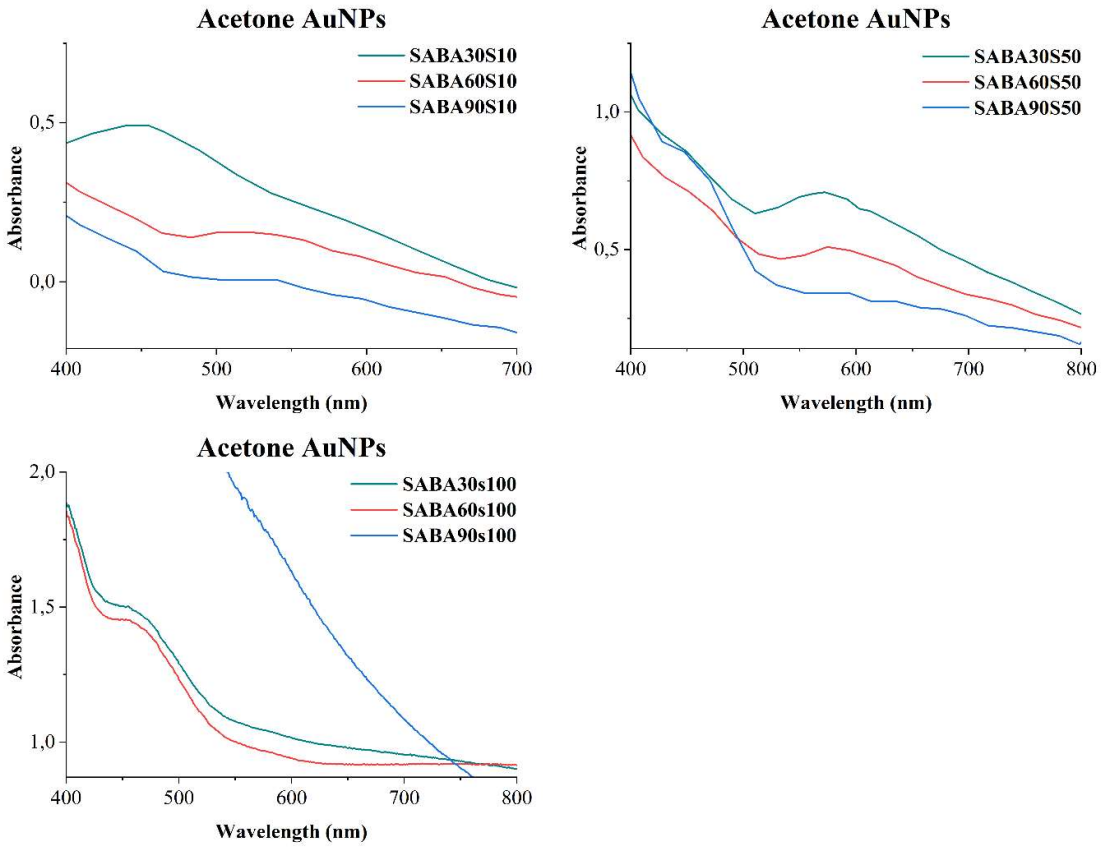

UV-Vis spectra of acetone extracts-based AuNPs at different reaction times and plant concentrations.

Appendix C

C.1 X-ray diffraction unit (XRD) analysis of SA-AgNPs and SA-AuNPs

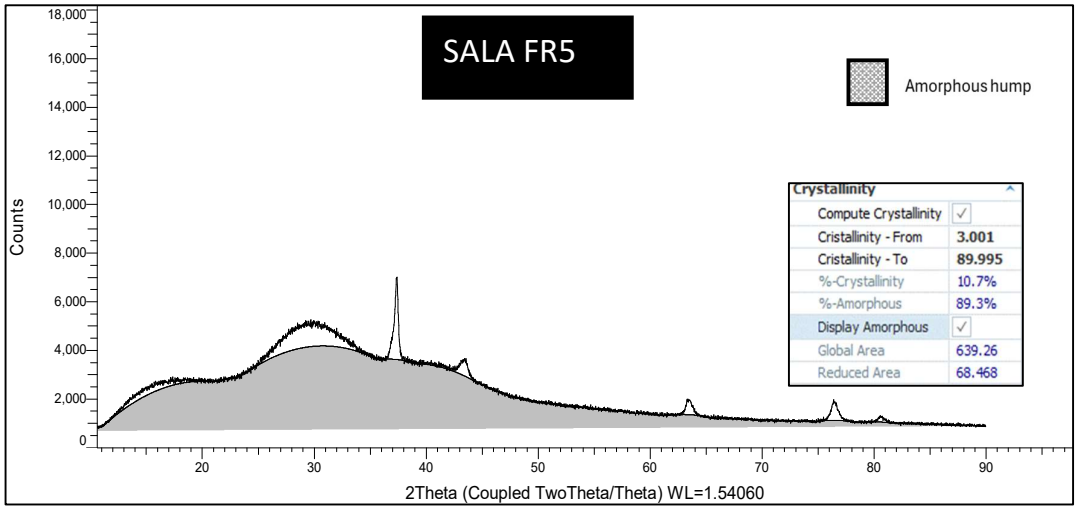

The experimental XRD spectrum of AgNPs synthesised using *S. africana* leaf-acetone extracts (SALA-FR5).

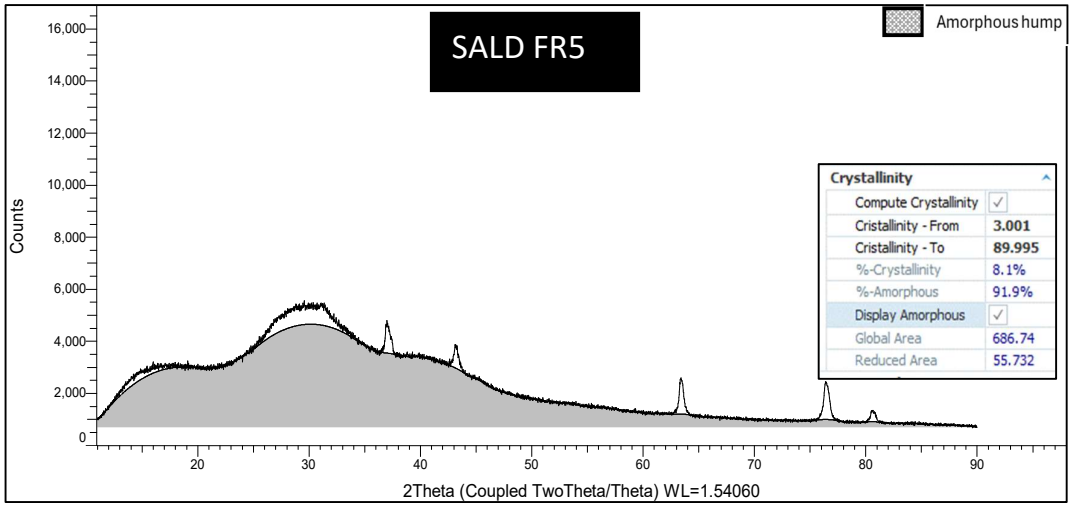

The experimental XRD spectrum of AuNPs synthesised by *S. africana* leaf-water extracts (SALD-FR5).

Appendix D

D.1 FTIR spectral of the plant extracts

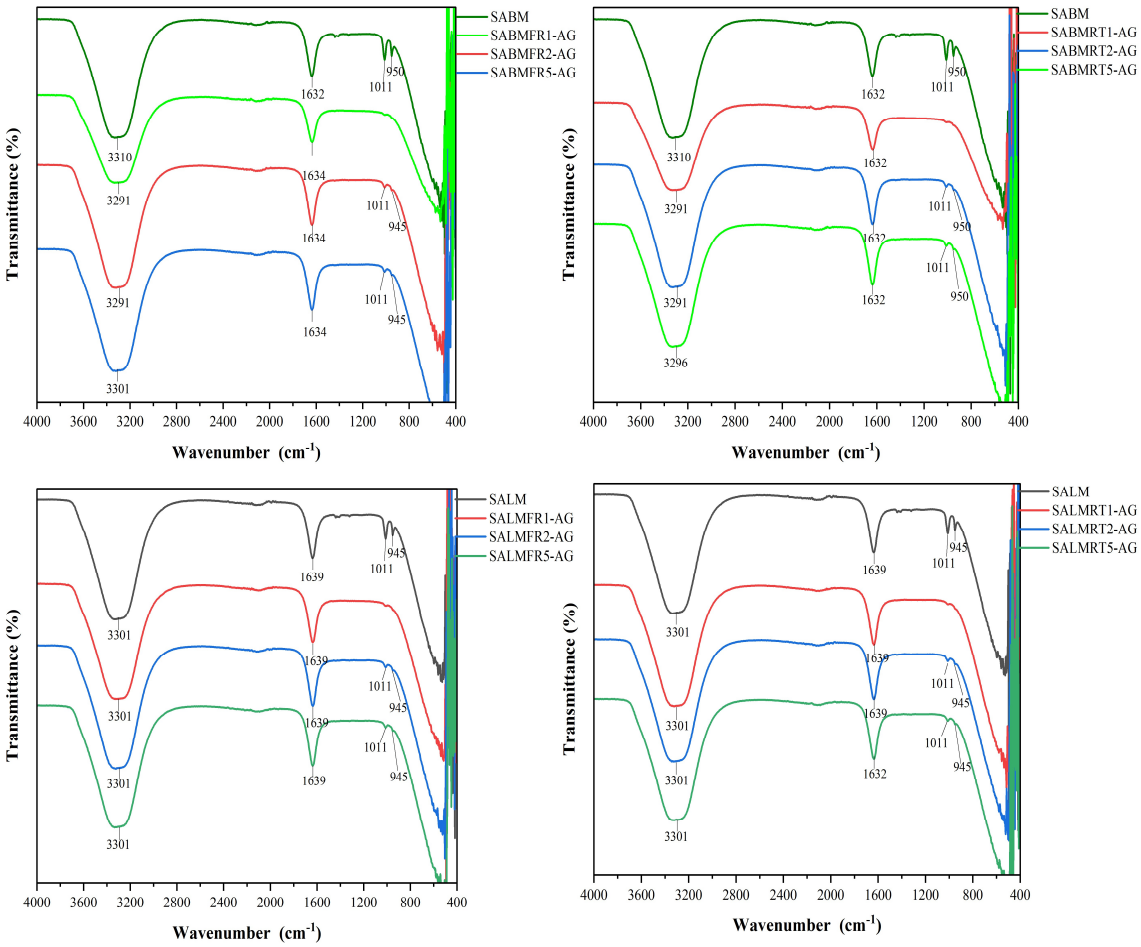

The FTIR specra of methanol extracts and their conjugated AgNPs at different $AgNO_3$ concentrations.

Appendix E

E.1. The MIC in mg/mL of SA-AgNPs and and SA-AuNPs

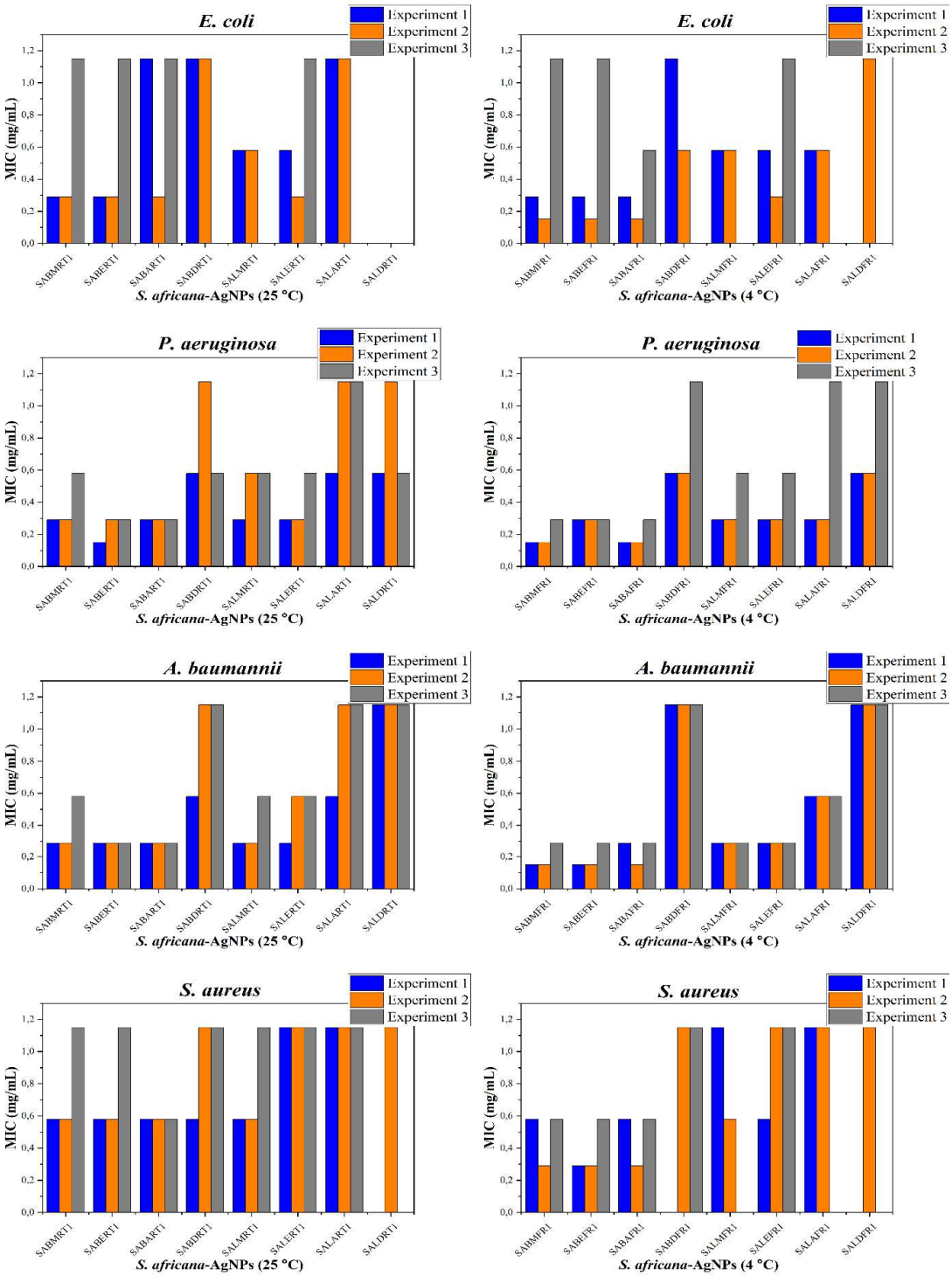

The MIC in mg/mL of SA-AgNPs synthesised at 1 mM $AgNO_3$ and stored at 25 or 4 ℃.

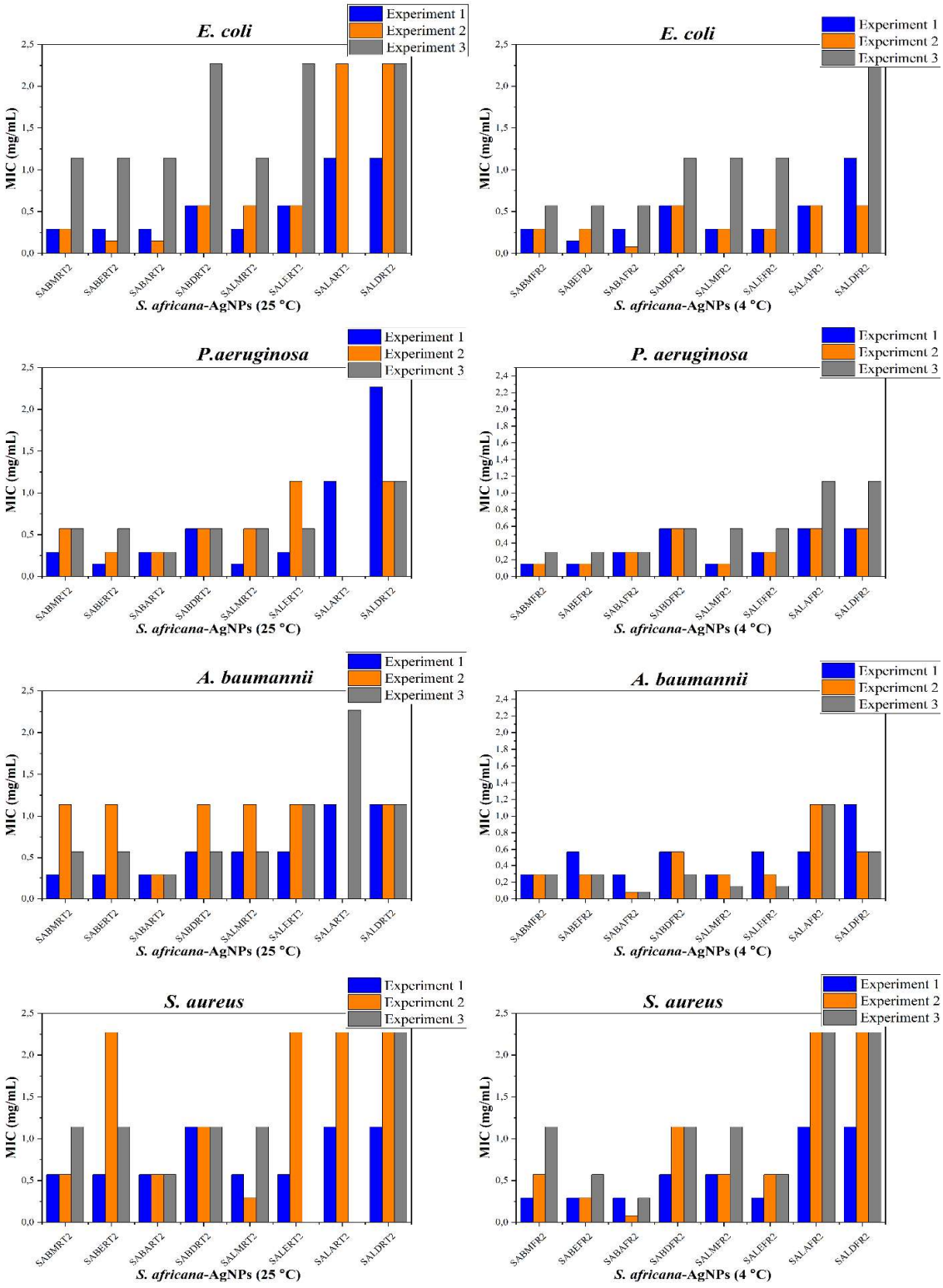

The MIC in mg/mL of SA-AgNPs synthesised at 2 mM $AgNO_3$ and stored at 25 or 4 ℃.

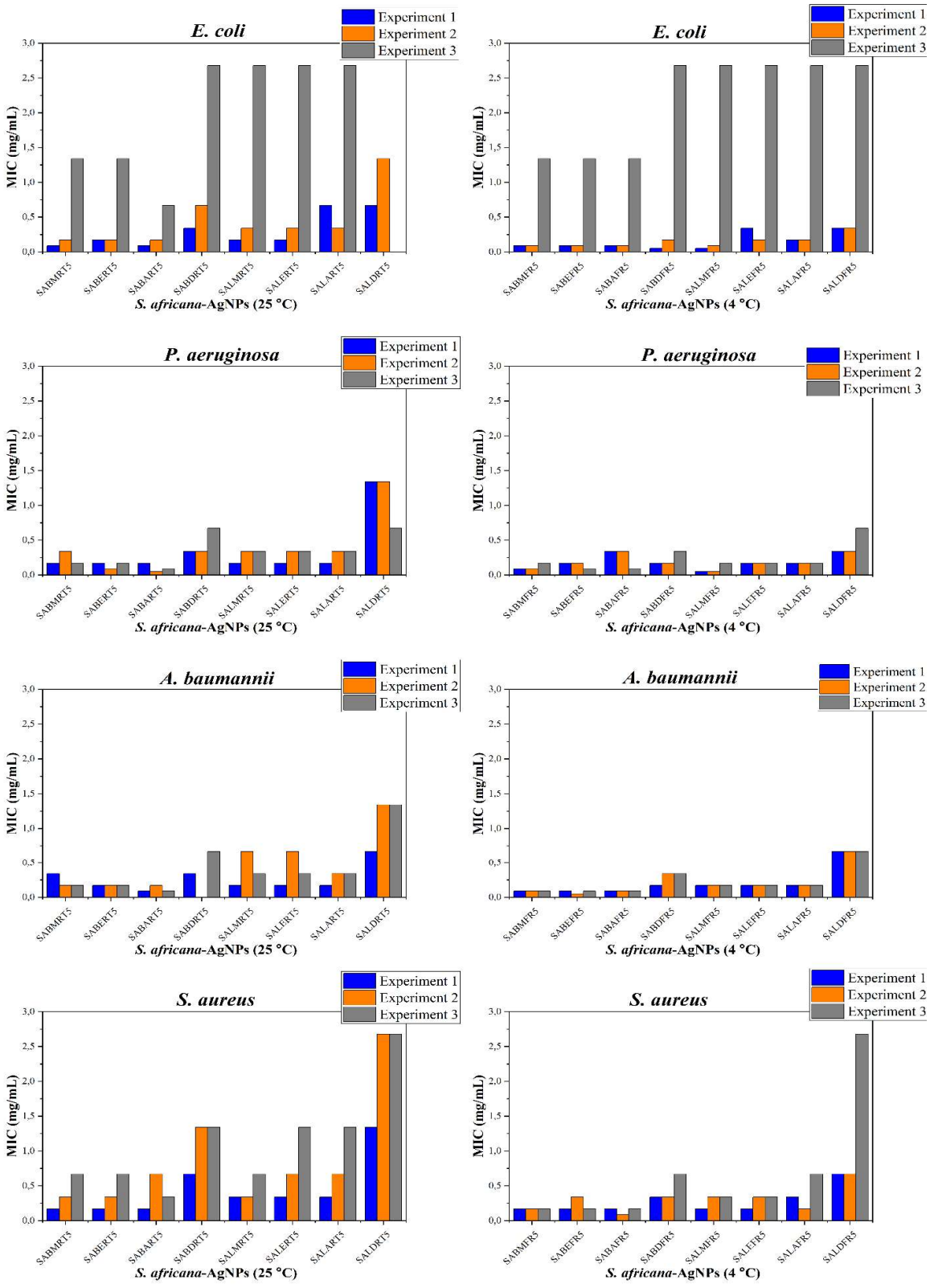

The MIC in mg/mL of SA-AgNPs synthesised at 5 mM $AgNO_3$ and stored at 25 or 4 °C.

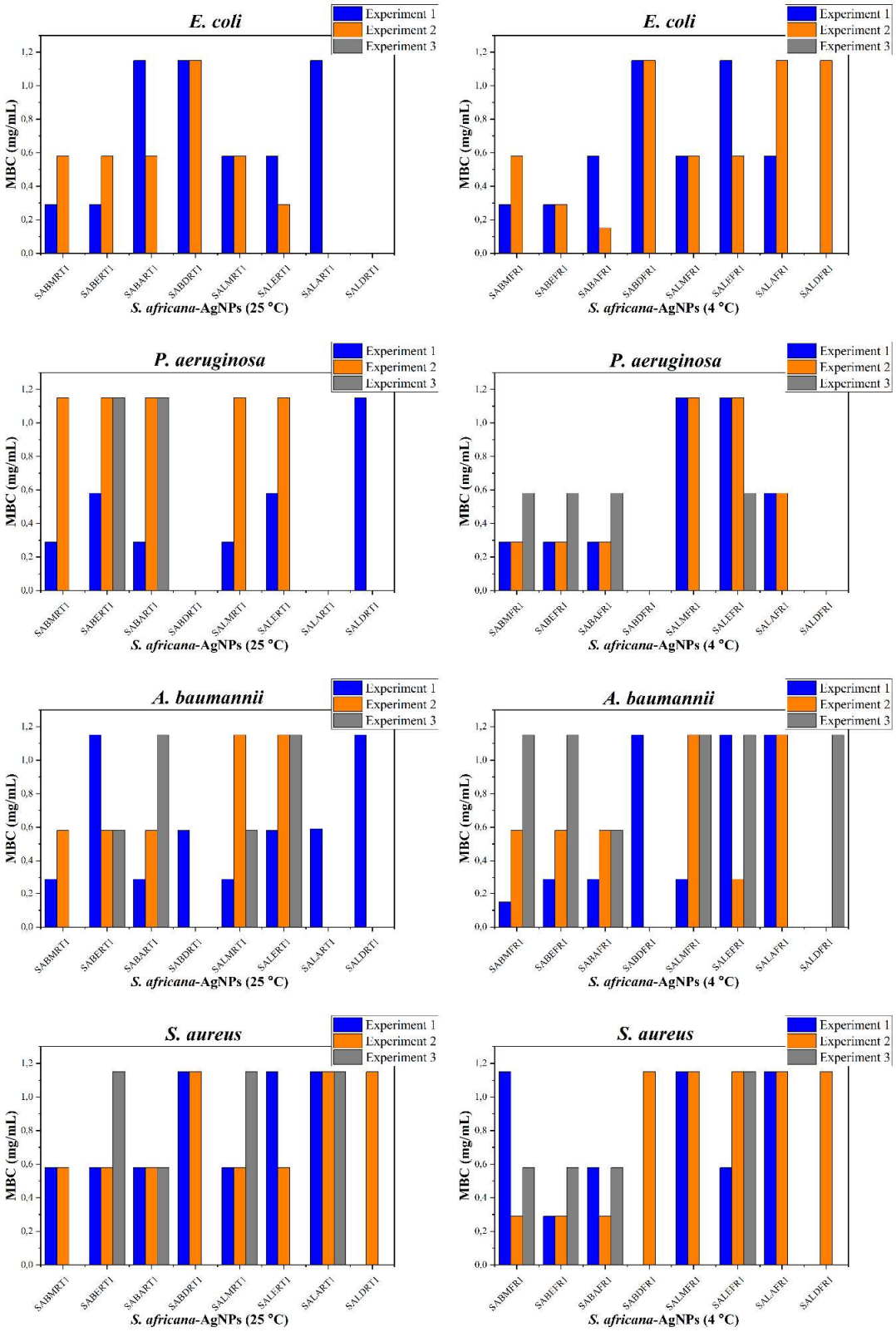

The MBC in mg/mL of SA-AgNPs synthesised at 1 mM $AgNO_3$ and stored at 25 or 4 °C.

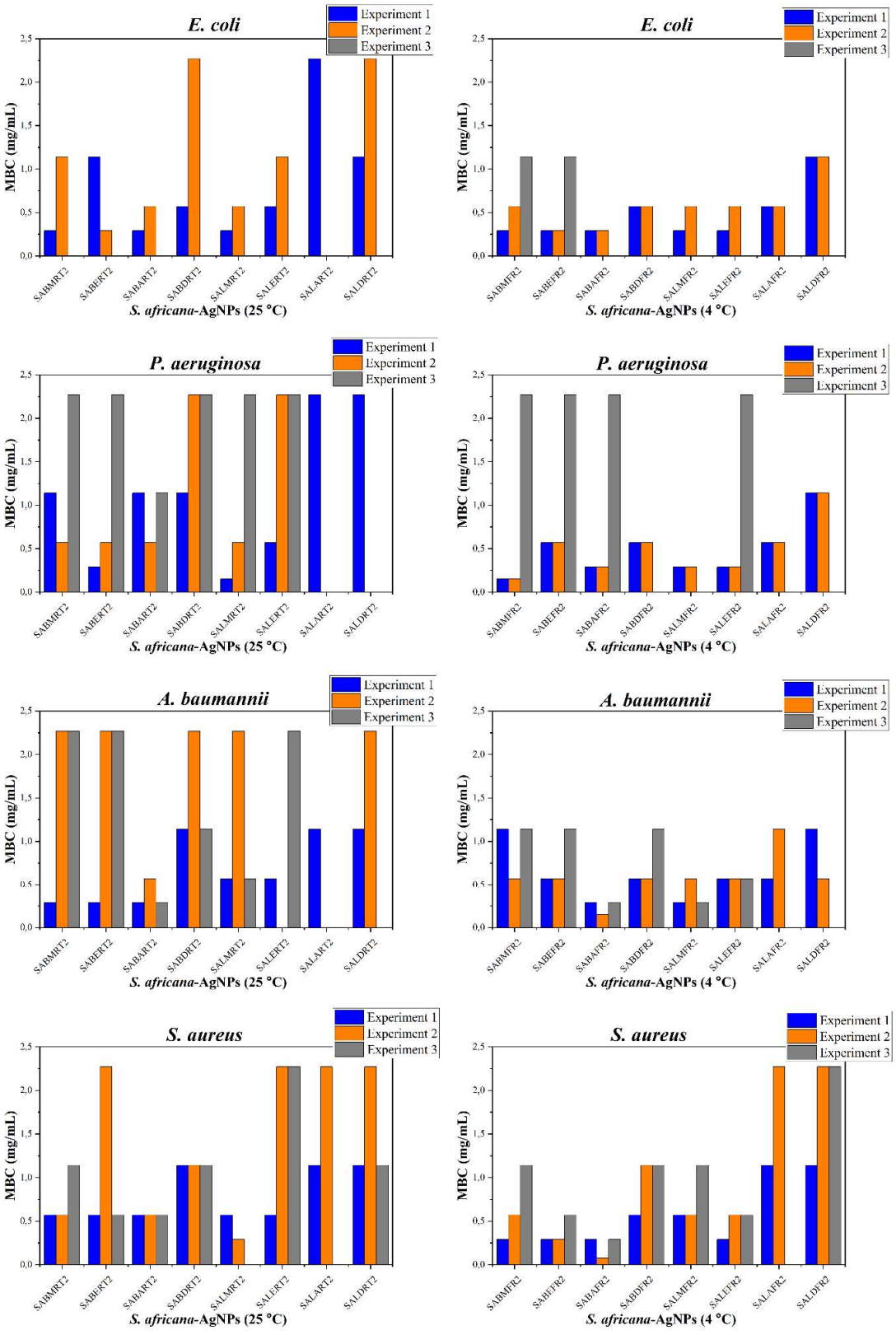

The MBC in mg/mL of SA-AgNPs synthesised at 2 mM $AgNO_3$ and stored at 25 or 4 °C.

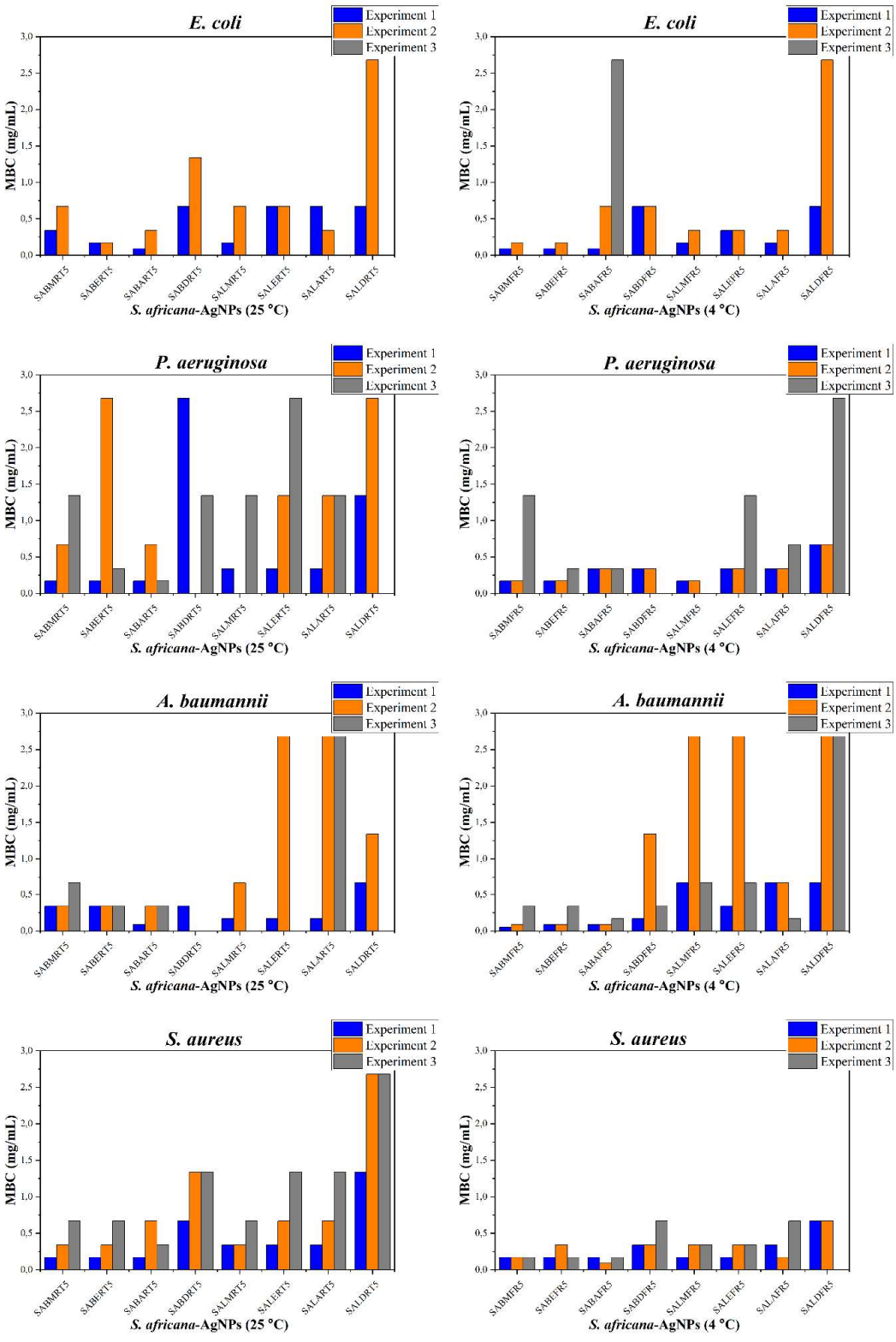

The MBC in mg/mL of SA-AgNPs synthesised at 5 mM $AgNO_3$ and stored at 25 or 4 °C.

E.2. Zone of inhibition (mm) of *S. Africana* extracts, SA-AgNPs, and SA-AuNPs against ABR bacterial strains.

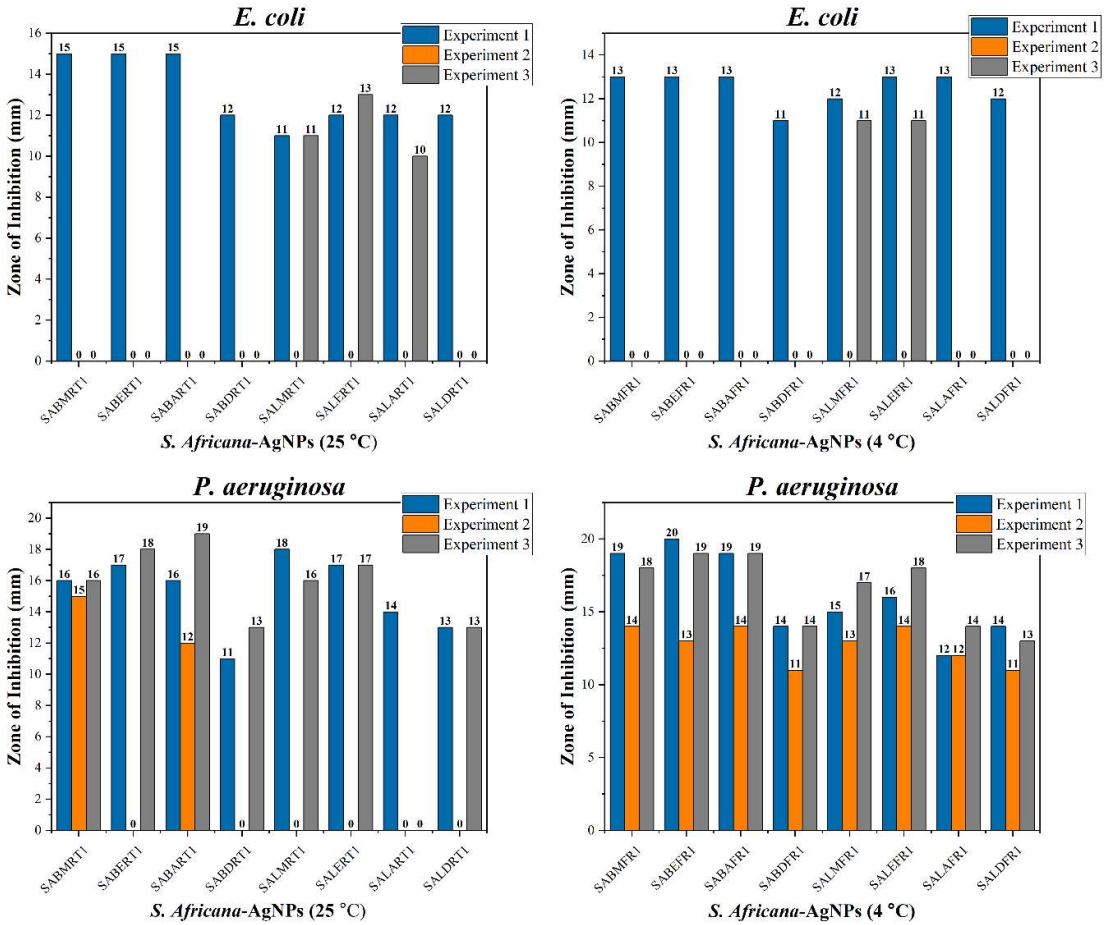

Zone of inhibition (mm) of of SA-AgNPs synthesised at 1 mM $AgNO_3$ and stored at 25 or 4 ℃ against *E. coli* and *P. aeruginosa*.

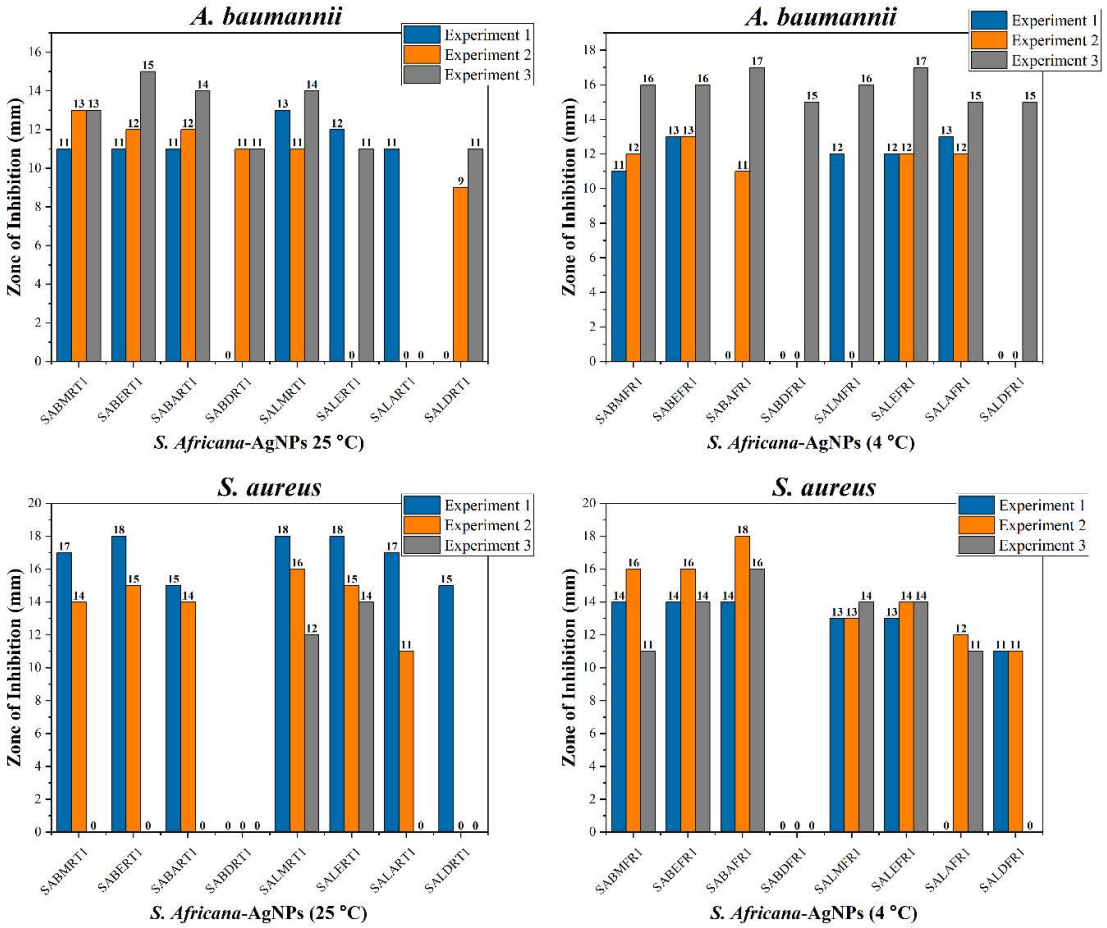

Zone of inhibition (mm) of of SA-AgNPs synthesised at 1 mM $AgNO_3$ and stored at 25 or 4 ℃ against *A. baumannii* and *S. aureus*.

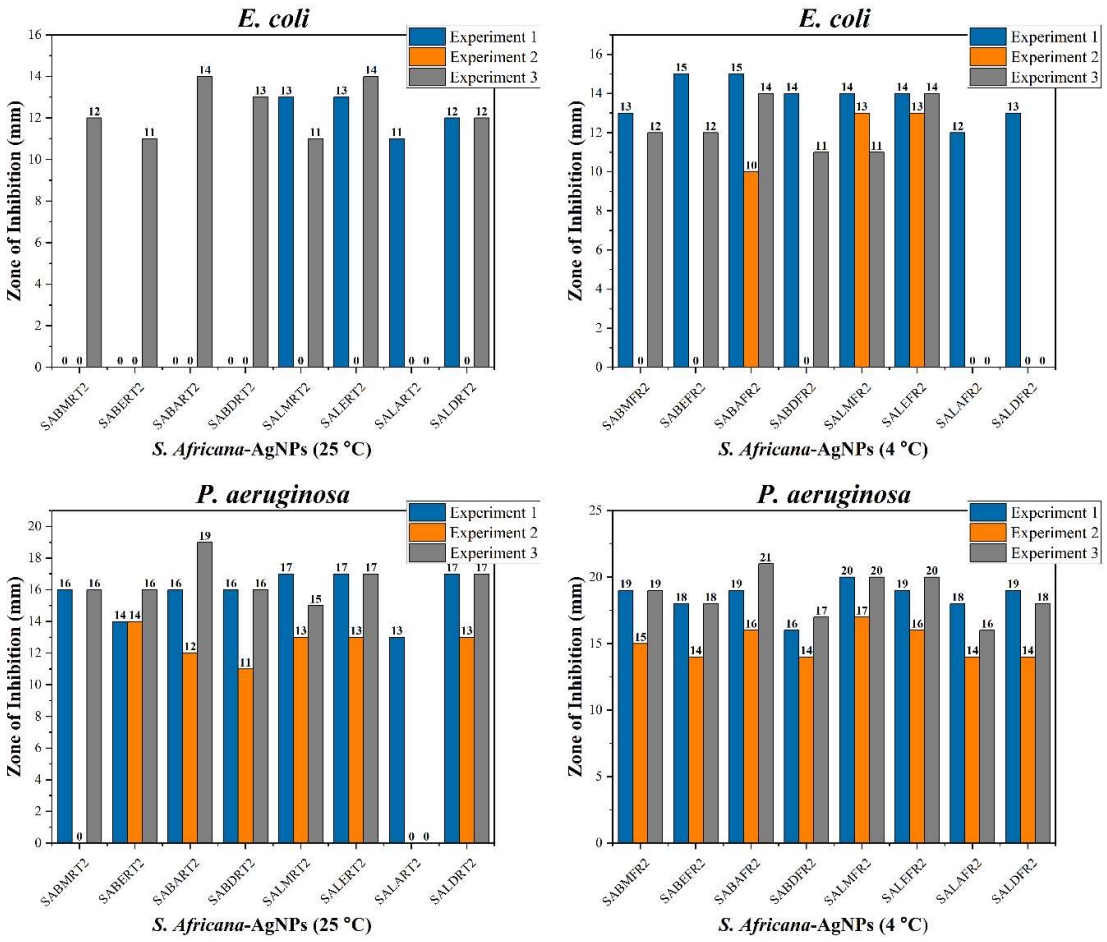

Zone of inhibition (mm) of of SA-AgNPs synthesised at 2 mM $AgNO_3$ and stored at 25 or 4 ℃ against *E. coli* and *P. aeruginosa*.

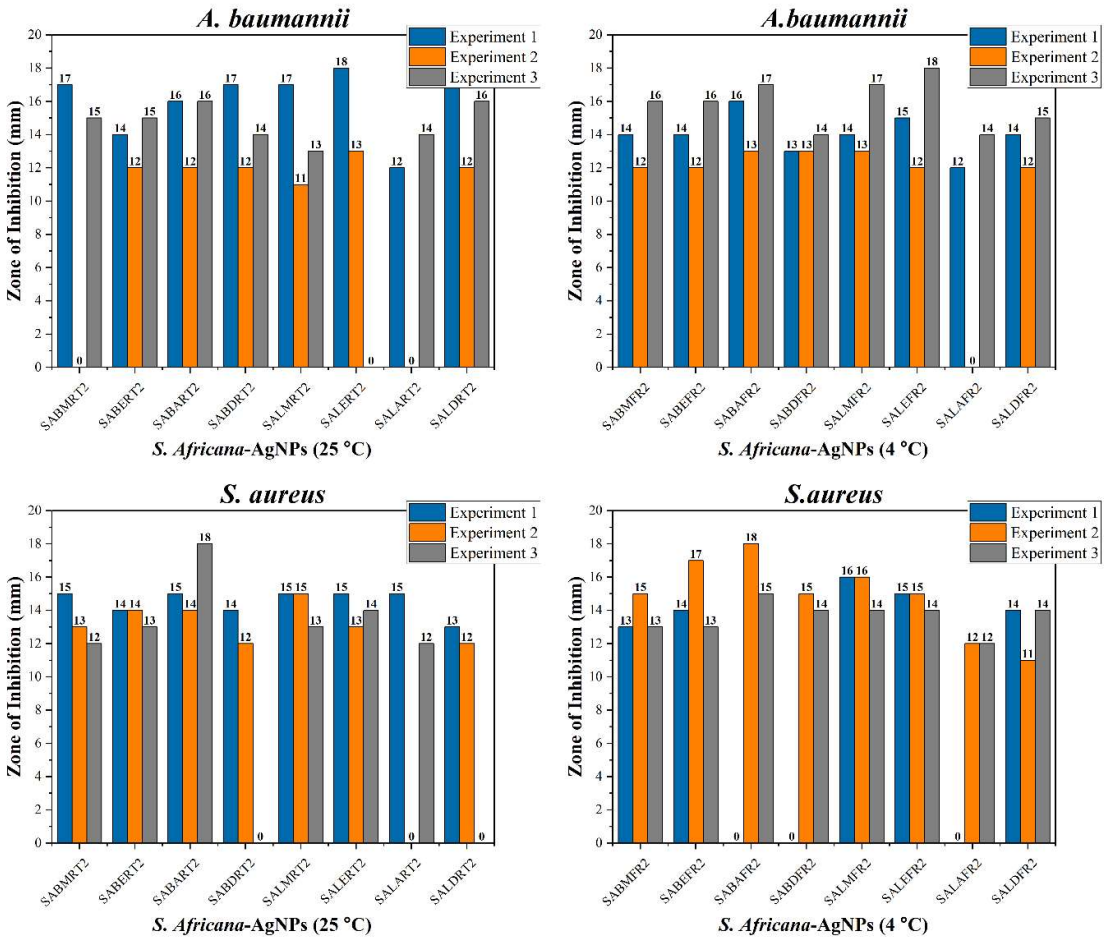

Zone of inhibition (mm) of of SA-AgNPs synthesised at 2 mM $AgNO_3$ and stored at 25 or 4 ℃ against *A. baumannii* and *S. aureus*.

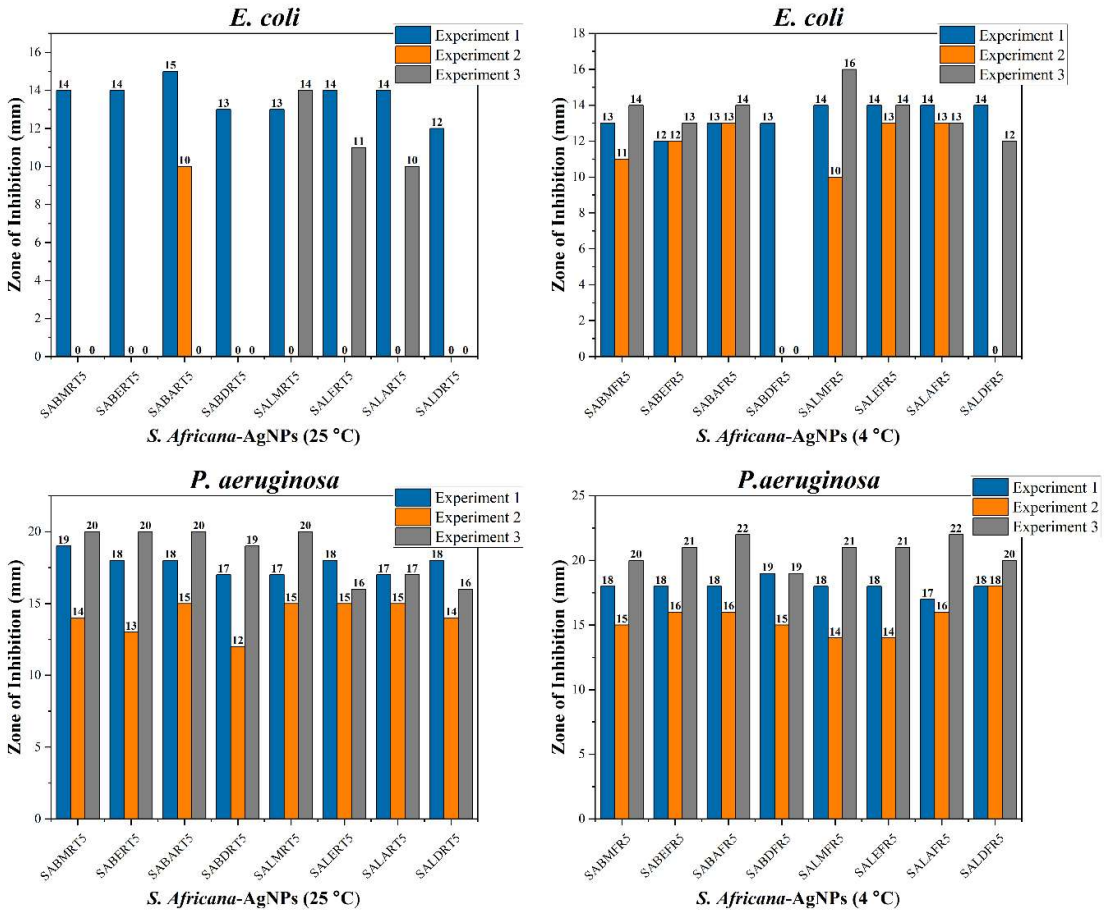

Zone of inhibition (mm) of of SA-AgNPs synthesised at 5 mM $AgNO_3$ and stored at 25 or 4 ℃ against *E. coli* and *P. aeruginosa*.

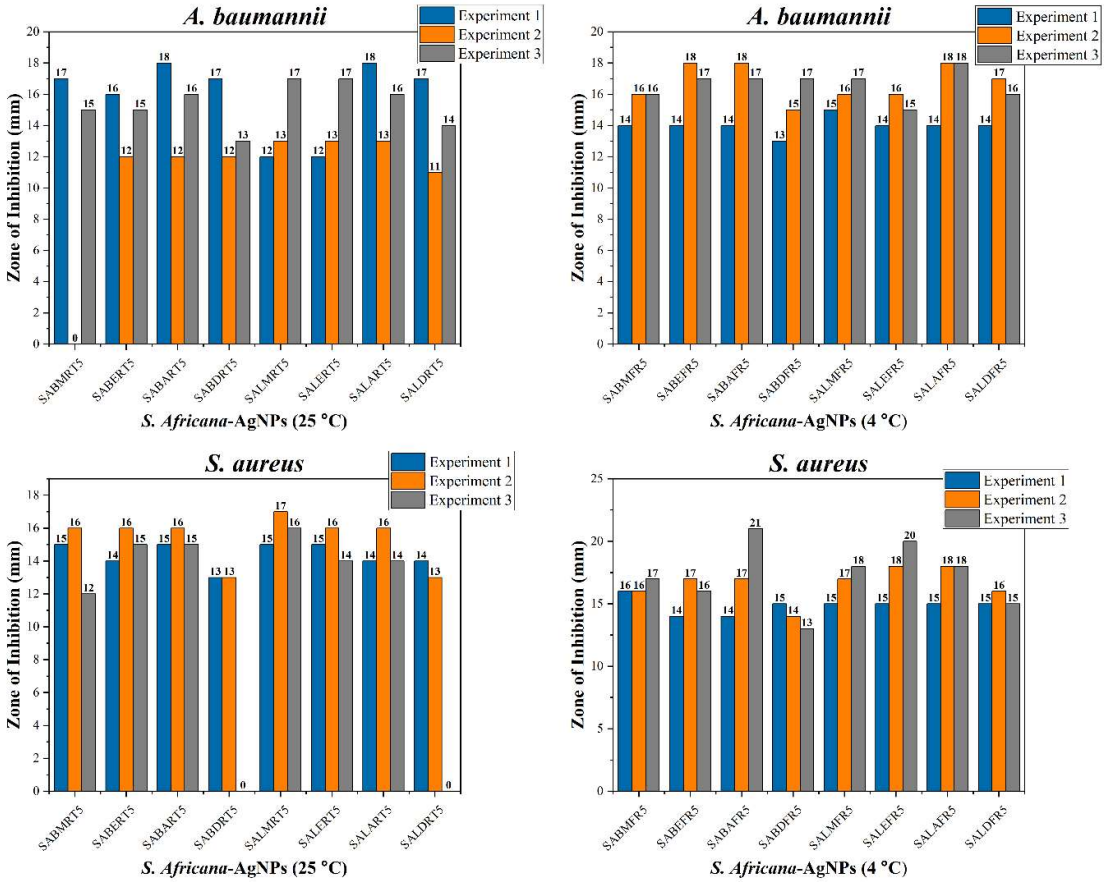

Zone of inhibition (mm) of of SA-AgNPs synthesised at 2 mM $AgNO_3$ and stored at 25 or 4 ℃ against *A. baumannii* and *S. aureus*.

Appendix D

D.1. Inhibition activity of *S. Africana* extracts, SA-AgNPs, and SA-AuNPs by MTT assay.

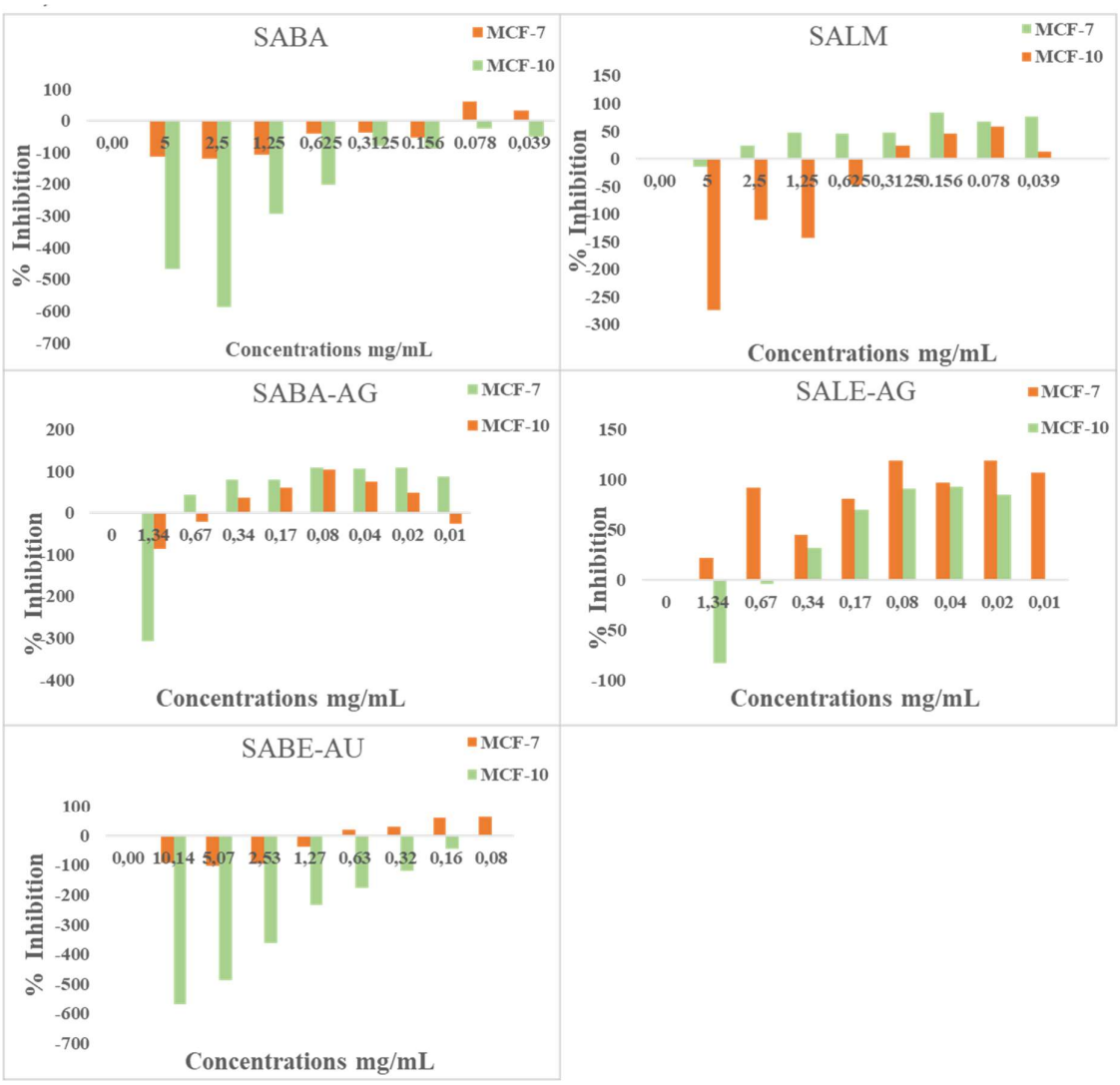

Inhibition activity of *S. Africana* extracts (SABA and SALM), SA-AgNPs (SABA-AG and SALE-AG), and SA-AuNPs (SABE-AU) on A) MCF-7 and MCF-10 by MTT assay.

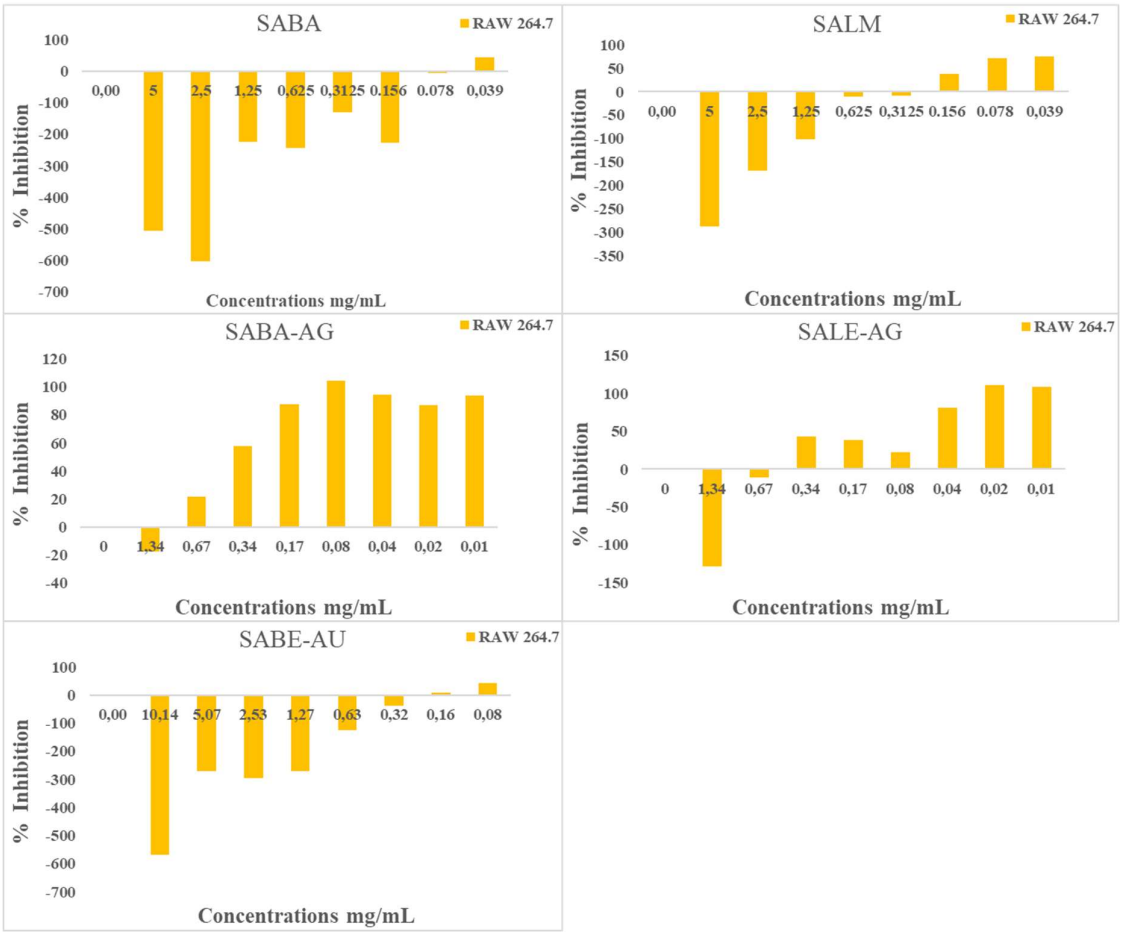

Inhibition activity of *S. Africana* extracts (SABA and SALM), SA-AgNPs (SABA-AG and SALE-AG), and SA-AuNPs (SABE-AU) on the RAW 264.7 cells.